Letter to the Editor

Dear Robert Harley,

you kindly accepted the editorship of our manuscript "Monitoring shipping emissions in the German Bight using MAX-DOAS measurements" and we would like to take the opportunity to thank you for the consideration of your work.

We individually answered point-by-point to all comments and questions of Referee #1 and Referee #2. We revised the original manuscript according to their suggestions and provided additional information the referees asked for. Below, you find again the answers to the referees that we also uploaded to the ACP web page. We also provide here a version of the revised manuscript in which changes in comparison to the initial version are marked color-coded. In addition to that, a version of the manuscript in the Copernicus two-column style (using the Copernicus Latex-Template) is attached. For this version, a few small changes have been applied to comply with the Copernicus Manuscript Preparation Guidelines (e.g. changing panel names from uppercase to lowercase letters, adjustments in figure sizes for the two column layout).

We hope that with the submission of the author's comments and the revision of the manuscript, our article will be accepted for publication in ACP.

Yours sincerely,

André Seyler

List of Attachments

- Author comments to Referee #1
- Author comments to Referee #2
- Revised manuscript
- Revised manuscript with color-coded changes
- Revised manuscript in Copernicus two-column style (Copernicus Latex-Template)

Interactive comment on "Monitoring shipping emissions in the German Bight using MAX-DOAS measurements" by André Seyler et al.

Anonymous Referee #1

Received and published: 23 February 2017

General comments

The manuscript entitled "Monitoring shipping emissions in the German Bight using MAX-DOAS measurements" presents remote sensing observations of NO2 and SO2 along a main shipping route towards the harbour of Hamburg. Ship emissions significantly contribute to the air pollution in these areas, and a monitoring of the air quality, in particular with respect to the impacts of the recent regulations of the fuel sulphur content, is of high scientific and political relevance. Therefore the topic of the manuscript is well suited for publication in ACP.

The paper is well structured and the scientific approach is clearly described. It provides a comprehensive introduction into the subject of ship emissions. The data is interpreted regarding the contribution of land- and seaborne emissions in a systematic way and the impact of the reduction of fuel sulphur content on atmospheric SO2 levels is discussed on the basis of statistical analyses. However, there are several aspects regarding the interpretation of the data which need to be revised. In particular, my impression is that the impact of horizontal inhomogeneities on the measurements and the fact that the remote sensing measurements average over a certain altitude range need to be considered more carefully. It appears to me that the latter is the main reason for the discrepancy between MAX-DOAS and in situ, which can and should be corrected for by accounting for the different vertical distribution of O4 and the target gases and thus different AMFs, as done during previous studies (e.g., Sinreich et al., AMT, 2013).

First, we would like to thank Anonymous Referee #1 for his/her helpful comments. Below, we reply point-by-point to the specific comments . As far as possible, we have considered the suggestions in the revised manuscript.

Specific comments

L56: Do you refer to fuel consumption and emission per vessel or in total (the latter would be obvious given the large increase in the number of ships).

We (and the cited studies) are referring to total fuel consumption and emissions. Following your suggestion, we included the word "total" to make this clearer:

"At the same time, *total* fuel consumption and emissions increased as well (Corbett and Koehler, 2003; Eyring et al., 2005a,b; Eyring et al., 2010b)."

Section 1.2:

Maybe the discussion of halogen chemistry should be removed since it is not of relevance for the present study. To my knowledge, the role of halogen radicals in polluted air is not well understood, and it is unclear whether the NO + XO reaction is of importance. In clean air, the conversion of XO to X proceeds either via self-reaction or reaction with HO2. In polluted air, reaction with NOx is likely to lead to a removal of halogen radicals by formation of halogen nitrates.

We removed the corresponding paragraph.

Section 3.1:

It could be mentioned that Equation (2) follows from (1) if the temperature and pressure dependence of the absorption cross section can be neglected.

Thank you very much for your thorough proof-reading, we had forgotten to include this important information. The corresponding paragraph now reads:

"Neglecting the temperature and pressure dependence of the absorption cross sections, polynomial and differential cross sections are fitted to the measured optical thickness ln (I/I0) in the linearized so-called DOAS equation:"

Section 3.2:
Please provide technical information on the fibre bundle (number of fibres, diameter, arrangement at both sides).
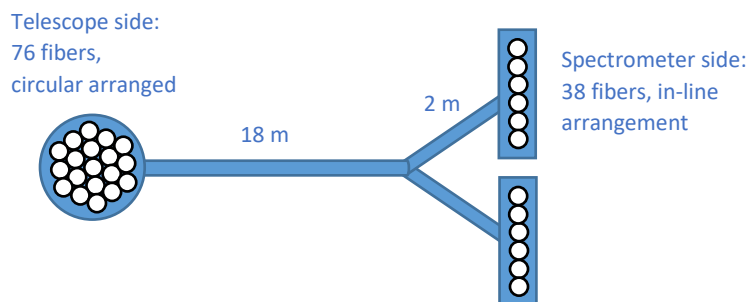
Type: Y-shaped quartz fiber bundle
Number of fibers: 2 x 38 = 76 single fibers
Diameter: 150µm each,
Length: 20m
Arrangement sketch:

Telescope side:
76 fibers,
circular arranged

18 m

2 m

Spectrometer side:
38 fibers, in-line
arrangement

We added this information to the text of the manuscript.

What are the wavelength ranges of both spectrographs?

We added the following sentence:

"The UV instrument covers the wavelength range 304.6-371.7 nm, the visible spectrometer covers 398.8-536.7 nm."

I am confused about the definition of the elevation angle. Usually, it should be the centre of the field of view, but here the definition is unusual and rather unspecific, being something like the lower edge of the field of view, which yields an offset to the common definition of 0.6_. Please specify the elevation angle as the centre of the field of view throughout the paper.

We changed the elevation angles to the actual values (center of field-of-view) throughout the paper.

Section 3.3:
It is important to include a discussion of the fit errors, detection limits and RMS residual for the target gases.

We added a paragraph on this in Section 3.3:

"Under good conditions, the typical fit RMS is around 1×10^4 for NO_2 in the visible, 2×10^4 for NO_2 in the UV and 5×10^4 for SO_2. By assuming that an optical density of twice the RMS can be detected (Peters, 2013), it is possible to estimate the detection limit of our instrument regarding the different trace gases. The differential absorption cross section of NO2 is in the order of $1 \times 10^{-19}\, cm^2/molec$, for SO_2 in the order of $2 \times 10^{-19}\, cm^2/molec$. Combining this yields a NO_2 detection limit of around $1 \times 10^{15}\, molec/cm^2$ corresponding to 0.05 pbb in the visible and $2 \times 10^{15}\, molec/cm^2$ corresponding to 0.1 pbb in the UV. The SO_2 detection limit is around $2.5 \times 10^{16}\, molec/cm^2$ corresponding to 0.2 pbb.

The typical absolute fit errors are $2\text{-}3 * 10^{14}\, molec/cm^2$ for NO_2 in the visible, $5\text{-}6 * 10^{14}\, molec/cm^2$ for NO_2 in the UV and $2 * 10^{15}\, molec/cm^2$ for SO_2, which is a factor of 5 to 10 smaller than the detection limit."

L345ff: Apart from the ozone absorption, a limitation for a retrieval window at shorter wavelengths is the lower light intensity.

This sentence was changed to the following:

"This results from the need to find a compromise between *the low light intensity caused by* the strong ozone absorption around 300nm on the one hand and the rapid decrease of the differential absorption of SO_2 at higher wavelengths on the other hand, limiting the choice of the fitting window."

Section 3.4:
The definition of the volume mixing ratio and its calculation from number concentration is well known and there is no need to discuss this here.

We removed the unnecessary explanation of volume mixing ratios and have completely rewritten this section focussing on the O_4 scaling approach and its limitations.

The uncertainties of the O4 scaling approach need to be discussed. For example, O4 usually has a profile shape very different from NO2 and SO2, which violates the basic assumption that the O4 dSCD is a good proxy for the light path through the NO2 and SO2 layers. Other studies use correction factors from radiative transfer calculations to account for this (Sinreich et al., AMT, 2013). Furthermore, the resulting near-surface volume mixing ratios will not be representative for the amount of trace gases directly at the surface, but for some kind of average over a certain height range in the boundary layer. There is also "light dilution", i.e. light scattered into the line of sight between the instrument and the trace gas plume (see e.g. Kern et al., Bulletin of Volcanology, 2010), which further reduces the measured SCDs . My impression is that these are the main reasons for the discrepancies between in situ and MAX-DOAS, and not horizontal inhomogeneities as speculated later in the paper by the authors (these would cancel out when averaging the data). The discussion of the data needs to be revised accordingly in order to account for the influence of these aspects.

We have completely rewritten this section discussing in detail the limitations of the O_4 scaling approach according to Sinreich et al. (2013)[1] and Wang et al. (2014)[2] as well as explaining the reasons why the suggested correction factors have not been applied to the data in this study: The height of the NO_2 and SO_2 layer is unknown and no additional measurements of the layer height exist. Furthermore, a comparison to our in-situ measurements indicates that the layer height and therefore the correction factors vary from day to day as well as over the course of individual days. In addition to that, an extensive RTM study like it was performed by Sinreich et al. (2013) and Wang et al. (2014) was out of the scope of this publication and the comparision to our in-situ instrument not the main point of the paper.

Equation 5: It should be mentioned that nO4 is the O4 concentration at the surface.

We added this information.

The remarks regarding the elevation angle from Section 3.2 are repeated at the end of this section. See my comments above. A deviation of 0.5_ in elevation angle is certainly not negligible at very low elevation angles.

---

[1] Sinreich, R., Merten, A., Molina, L., & Volkamer, R. (2013). Parameterizing radiative transfer to convert MAX-DOAS dSCDs into near-surface box-averaged mixing ratios. *Atmospheric Measurement Techniques*, *6*(6), 1521–1532. https://doi.org/10.5194/amt-6-1521-2013

[2] Wang, Y., Li, A., Xie, P. H., Wagner, T., Chen, H., Liu, W. Q., & Liu, J. G. (2014). A rapid method to derive horizontal distributions of trace gases and aerosols near the surface using multi-axis differential optical absorption spectroscopy. *Atmospheric Measurement Techniques*, *7*(6), 1663–1680. https://doi.org/10.5194/amt-7-1663-2014

We changed the elevation angles to the actual values (center of field-of-view) throughout the paper and removed the remarks. We also added a discussion on the limitations of the O4-scaling due to non-consideration of correction factors (see also above).

L474: It is not obvious to me why a thicker trace gas layer should lead to a reduction of the ratio between dSCDs near the horizon and in zenith. Wouldn't horizontal inhomogeneities, with more NO2 over the shipping lane than over the instrument, be a much more likely explanation for these findings?

This Paragraph is not about differences between SCDs near the horizon and in zenith sky direction, but about systematically higher NO_2 and SO_2 DSCDs in 0.5° Elevation compared to the 2.5° Elevation for wind from the shipping lane, indicating a low pollution layer over the shipping lane. For southerly winds, on average the NO_2 and SO_2 DSCDs in 0.5° and 2.5° Elevation are nearly equal. We have rephrased the paragraph to make it clearer:

"The highest NO_2 and SO_2 DSCD in the lowest elevation angle (0.5°, blue bars) in relation to DSCDs in higher elevations are measured especially for wind from all northern directions, in a sector ranging from WSW to ESE. These directions coincide with the course of the main shipping lane, which comes from the WSW direction (the English Channel, the Netherlands, East Frisian Islands), passes the island in the north and runs close to the city of Cuxhaven (ESE direction) into the river Elbe. This indicates that these enhanced columns in the 0.5° elevation angle is pollution emitted from ships in a surface-near layer.

For southerly wind directions, where no larger shipping lane is in the direct surrounding and land-based pollution sources dominate, the average DSCDs in 0.5° and 2.5° elevation are nearly the same for both NO_2 and SO_2."

Section 4.2:
The title of this section is too long and complicated. I suggest to replace it by something like "Volume mixing ratios of NO2 and SO2"

Done.

Section 4.5:
As already stated above, the fact that MAX-DOAS averages over a large horizontal distance should cancel out on temporal average when comparing to in situ measurements. Instead, a more probable explanation for the systematically lower mixing ratios is the fact that MAX-DOAS averages over a certain altitude range and that the differences in O4 and target gas profile shapes has not been considered. Light dilution will also play a certain role. The argument that MAX-DOAS yields lower values when the plume is orthogonal to the viewing direction does not seem convincing to me, because in this case the polluted air is also not transported towards the in situ instrument, which means that the in situ instrument might even miss particular plumes which are detected by MAX-DOAS.

This section has been completely rewritten discussing again the systematic deviations produced by the non-consideration of correction factors for the different profile shapes. Also a remark about light dilution as an uncertainty source reducing the actual measured SCDs was incorporated.

Section 4.6:
L655ff: NO2 concentrations at a particular location strongly depend on local sources, such as traffic, industry, domestic heating, etc., as well as on the distance to these sources and on the rate of vertical mixing. Therefore, the fact that amount of NO2 in background air observed in the Arctic is similar to the present study might be mere coincidence.

We have removed this paragraph.

Section 4.7:
L667: Detection limits are mentioned here for the first time. They should instead be discussed in Section 3.3.

We added a paragraph about detection limits in Section 3.3.

"By assuming that an optical density of twice the RMS can be detected (Peters et al., 2013), it is possible to estimate the detection limit of our instrument regarding the different trace gases. The differential absorption cross section of NO_2 is in the order of $1x10^{-19}$ cm²/molec, for SO_2 in the order of $2x10^{-19}$ cm²/molec. Combining this yields a NO_2 detection limit of around $1x10^{15}$ molec/cm² corresponding to 0.05 pbb in the visible and $2x10^{15}$ molec/cm² corresponding to 0.1 pbb in the UV. The SO_2 detection limit is around $2.5x10^{16}$ molec/cm² corresponding to 0.2 pbb."

Section 4.8:
An attempt is made here to separate shipping emissions from other sources by classifying the data according to the wind direction. The limitations of this approach need to be discussed more carefully. While I agree that northerly winds are little affected by background pollution, I strongly doubt that shipping emissions do not influence the measurements significantly when the wind is coming from the south. Data is filtered for light paths longer than 5 km, which means that for most observations the light path crosses the main shipping lane and probes air polluted by ship traffic. You reach this conclusion yourself in Section 4.1 (L438ff) in the context of the discussion of Figure 6, which shows that peaks from ship emissions clearly occur when air polluted by landbased sources is present. Thus, air masses classified as "Land" are likely to be partly affected by ship emissions.

You are right, air masses classified as "land" usually contain small fractions of shipping emissions as well. So the land source is slightly overestimated in these cases. How prominent ship emission peaks are in our measurements and how strong the contribution is compared to land based emissions depends on the wind direction. The wind sector classification is sketched in the following figure:


Blue sector: wind from open North Sea, shipping is the only pollution source

Green sector: mainly land-based air pollution (traffic, industry, …)
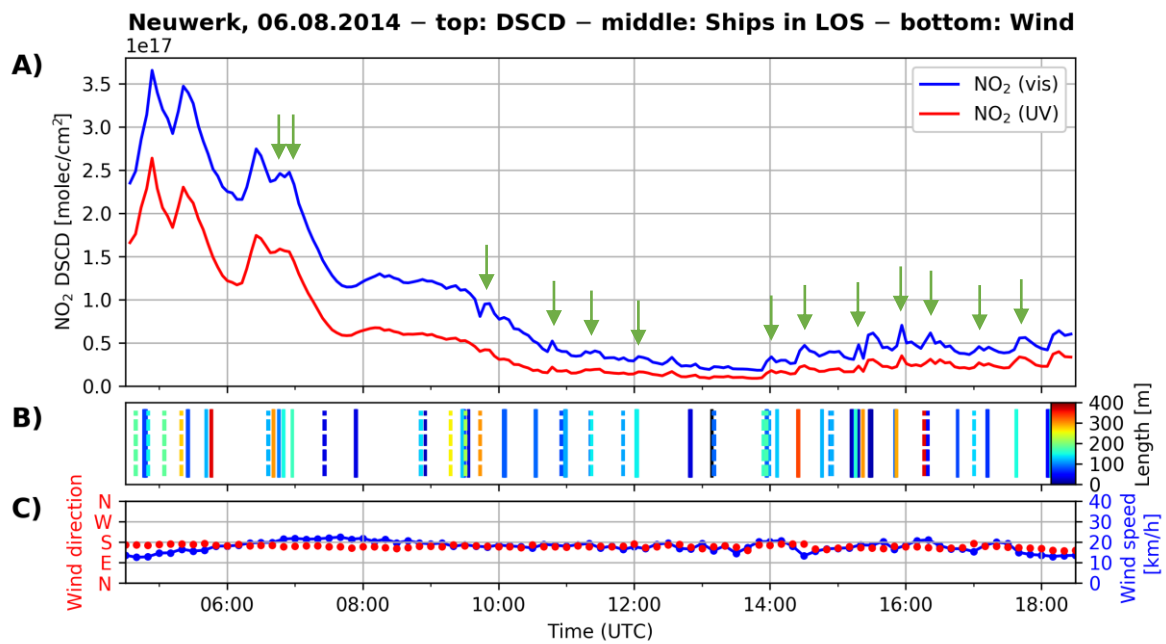
Yellow sector: air mass contains shipping emissions as well as land-based air pollution (mixed origin)

On 23 July 2014, the day in Figure 6 which you are referring to, in the morning the wind was coming from NE-ENE, and later turned towards NNE. Those wind directions are not included in the sector we chose for pollution coming from land. Wind from those directions clearly can contain large fractions of shipping emissions as well as pollution from land and are therefore classified as directions with "mixed" pollution origin in the study.
When the wind is coming from southerly directions, ship emission peaks are much less prominent in our measured time series of NO_2 or SO_2. A day which illustrates this nicely is 17 July 2014, shown in the plot below. Until noon, wind was coming from the south and later changed to northerly directions. Measurements were done in 0° elevation towards north. In the morning, although a lot of ships are present, as can be seen from the colored bars in Panel B, ship emission peaks are very small and hardly visible. A few are still visible, marked by the green arrows. As expected, the peaks are higher in the visible than in the UV, because wind is blowing the ship plumes away from the radar tower and our instrument. In the afternoon, ship emission peaks are higher and much more prominent. The contribution of shipping emissions to the overall NO_2 measured is certainly much higher in the afternoon than in the morning.

Neuwerk, 17.07.2014 − top: DSCD − middle: Ships in LOS − bottom: Wind
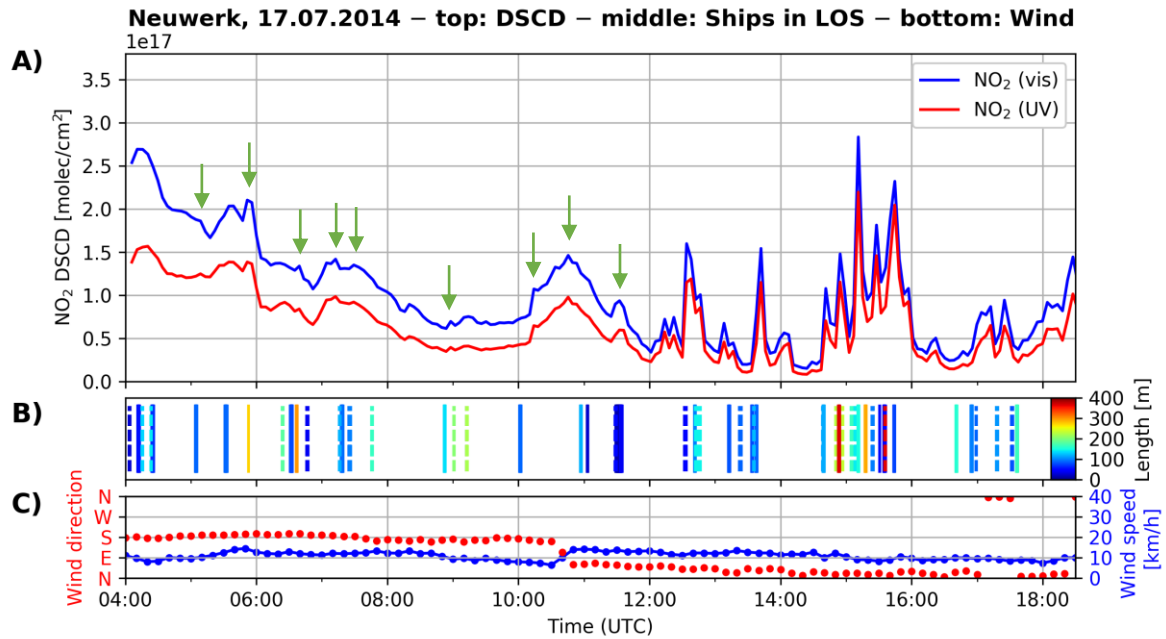
Another example is shown in the next plot for 6 August 2014.

Neuwerk, 06.08.2014 − top: DSCD − middle: Ships in LOS − bottom: Wind

To quantify the overestimation of the land source sector, the fraction of shipping emissions on the overall emissions on such a day has to be compared to the fraction of land sources. This is shown in the next plot: It is another example day with wind from southerly directions, 6 August 2014. Blue and red line show the NO₂ DSCD measured in the visible and UV. The cyan and magenta lines show the signal with removed ship emission peaks.

Neuwerk, 03.07.2014 – top: DSCD – middle: Ships in LOS – bottom: Wind
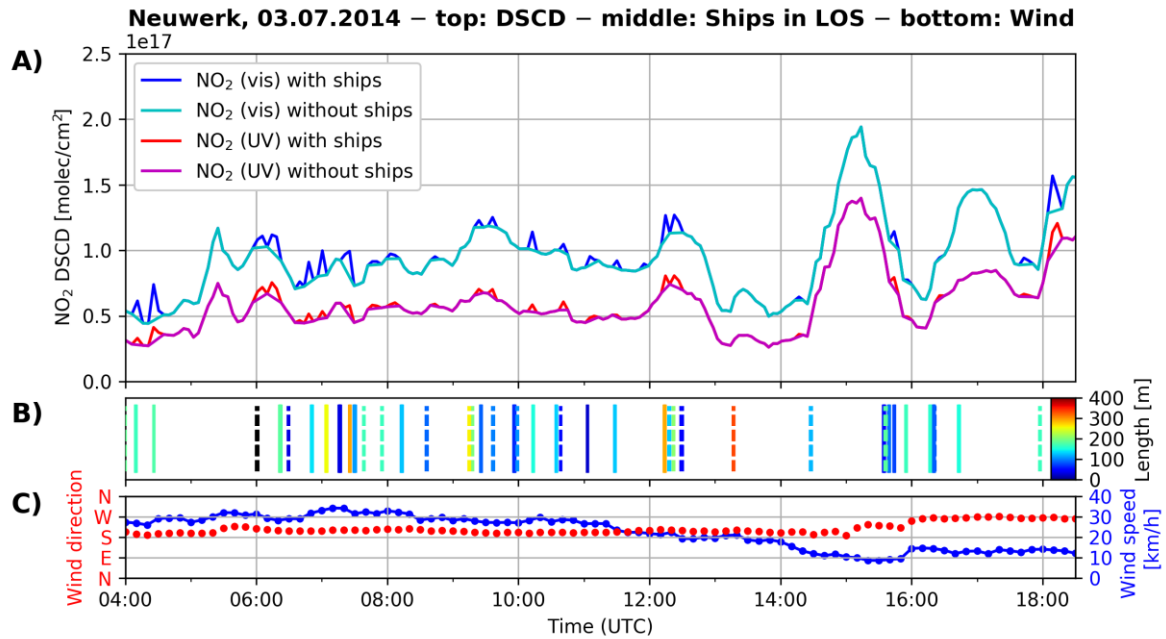
In the UV, the difference in the integral between "with ships" and "without ships" is around 1.4%, in the visible it is around 1.6%. So on this day, the NO_2 classified as "land source" is overestimated by around 1.5% due to shipping emissions which are still contained in the data set. In other measurement directions, to the NE or NW for example, this overestimation is be a bit higher, but never exceeds 3%.

So this overestimation is a small error and was therefore neglected in the study.

Section 4.9:
Given that SO2 scatters around a smooth (near-zero) background level, it is surprising to see that no negative SO2 to NO2 ratios were derived. It seems that negative values have been set to zero (Panel D of Fig. 20), which would significantly (and falsely) affect the statistics.

To address this shortcoming in our study we have completely redone the SO_2 to NO_2 ratio peak analysis. The baseline determination has improved substantially (using a second running median filter applied to the lower 50% quartile when necessary) and the positive bias in the measurements since 2015 is now gone. In addition to that, the section has been rewritten taking into account your comments. Also, the importance of NO to NO_2 titration especially for the comparison to other studies is now mentioned in this section.
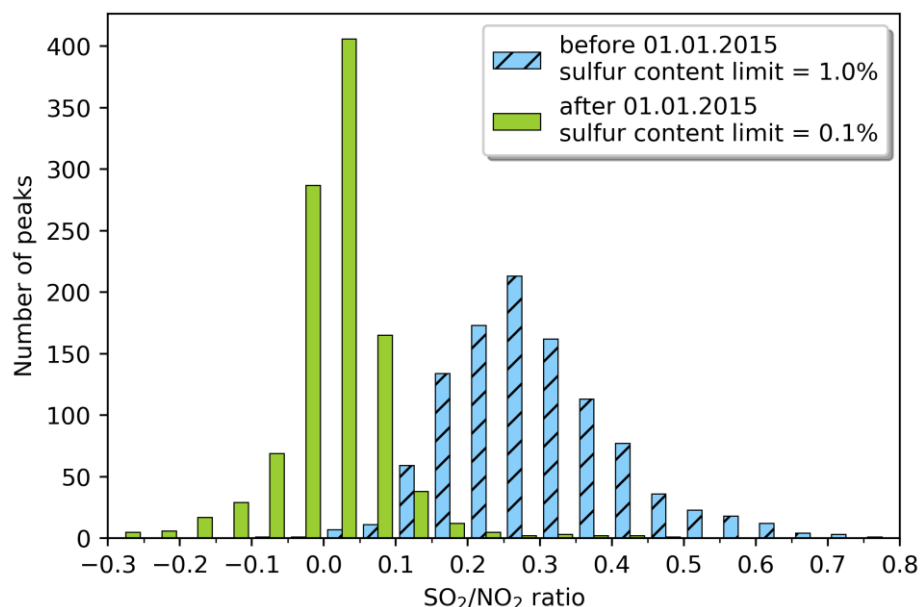
Updated plots:

For an example day (23.07.2014) before the change in regulations:
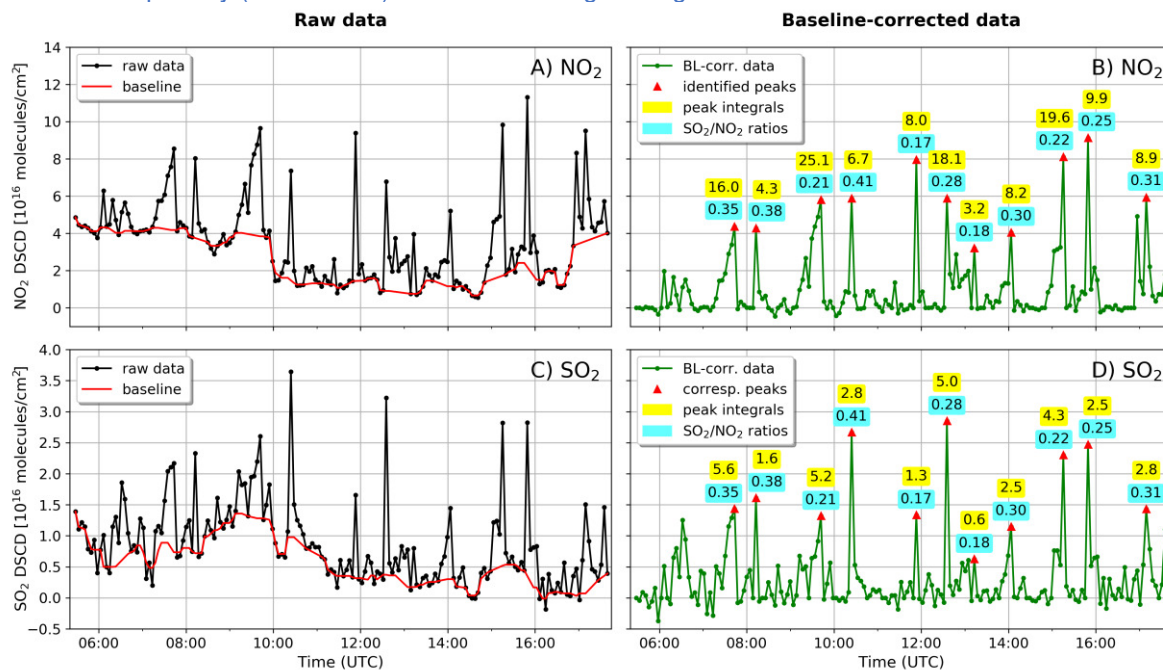
For an example day (03.07.2015) after the change in regulations:
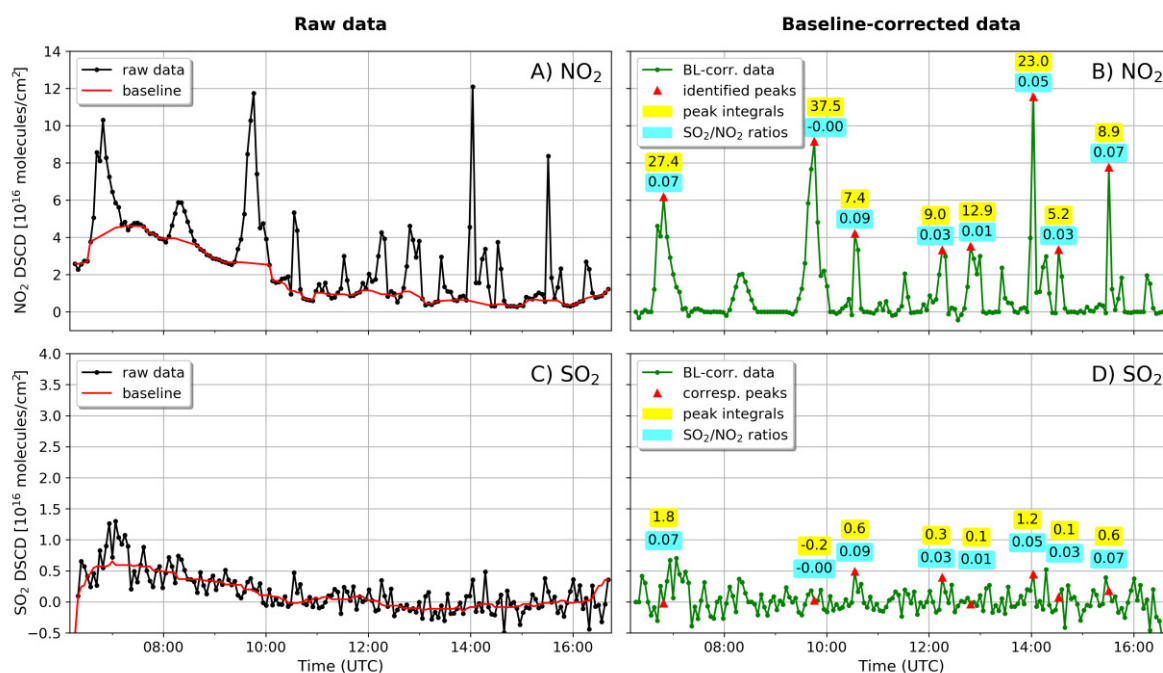
And the updated histogram:

Technical corrections
Equations: Please use single characters for variables (e.g., "S" instead of "SCD", "R" instead of "RESIDUAL", "H" instead of "MLH"). There is a difference between an abbreviation (e.g., "SCD" for slant column density) and the according mathematical symbol (e.g., "S").

This is a matter of personal taste. In the DOAS community, using variable names like "SCD" or "AMF" is quite common. Checking the most recent final revised papers in ACP and AMT containing "DOAS" in the title we found 20 papers using multi-letter variable names like "SCD", "AMF", "AOD", 1 paper using single letter variable names "S" and "M" etc. (and 8 papers without any such equations).

L11: Provide a number for the distance between measurement site and shipping lane

We added the distance:

"The island is located in the German Bight, close to the main shipping lane *(in a distance of 6-7 km)* into the river Elbe towards the harbor of Hamburg."

L13: The fact that the site is close to the shipping lane is repeated. Delete "which is a few kilometres from the shipping lane"

Done.

L17: "retrieved from NO2 retrievals" -> "determined from NO2 retrievals"

Done.

L54: ". . . from around 31 000 . . .. over 52 000 . . . to 89 000 . . ."

Done.

L68: ". . . molecular nitrogen (N2) and oxygen (O2) . . ."

Done.

L81: comma after "radicals"

This paragraph was removed.

L81: ". . . hydroperoxyl (HO2) or organic peroxy radicals (RO2) or halogen oxides (XO, were X = Cl, Br or I)

This paragraph was removed.

L84: "X atoms" -> "halogen atoms"

This paragraph was removed.

L85: "reacts" -> "react"; "reaction" -> "reaction rate"

This paragraph was removed.

L86: "Owing to the lack of photolysis, NO reacts rapidly . . .. during the night"

Done.

L87: "In addition, the nitrate radical (NO3) is formed. . ."

Done.

L110: Comma after "regions"

Done.

L112: "ecosystem" -> "ecosystems"

Done.

L121: Put "3" in "m3" into superscript

Done.

L162: Comma after "emissions"

Done.

L173: Comma after "example"

Done.

L206: Incomplete sentence. Replace, e.g., by ". . . first the measurement site is described, followed by a presentation of the wind statistics and data availability."

Done.

L215: ". . . were taken on Neuwerk, a small island in the North Sea with the size of . . ."

Done.

L221: "island of Neuwerk" or simply "Neuwerk" (here and anywhere else). Delete "where our measurement site is located" (repetition)

Done.

L225: Do you refer to a specific document from the "Statistische Ämter" or can you

provide an url to the data?

We are referring to a specific document/URL from the "Statistische Ämter…" from the year 2015. The URL to the document can be found in the bibliography under "Statistische Ämter… (2015)". The correct way how to cite this information is specified on the web page from the Statistische Ämter.

L224: Is this height above sea level?

No, this is height above ground. But the difference to height above sea level, as you can see from the photo, might be 1-2 meters and therefore negligible.

L248: "site for the measurements" -> "site"

Done.

L285: To "inject" light into the fibre sounds strange since this term suggests that the light is somehow transported actively. Replace by something like "focused on the entrance of the optical fiber"

Done.

L286: "opening angle" -> "field of view"

Done.

L307: Define what "SCD1" and "SCD2" refer to. Replace by variable names consisting of single letters.

We rephrased the sentence to make this more clear.

Regarding the single letter variable names: This is a matter of personal taste. In the DOAS community, using variable names like "SCD" or "AMF" is quite common. Checking the most recent final revised papers in ACP and AMT containing "DOAS" in the title we found 20 papers using multi-letter variable names like "SCD", "AMF", "AOD", 1 paper using single letter variable names "S" and "M" etc. (and 8 papers without any equations).

L316: It should be mentioned that a spatially limited plume directly over the instrument leads to an underestimation of the retrieved dSCDs.

Done.

Table 1: Only list the polynomial degree, not the number of coefficients.

I listed both since the definiton of the polynomial degree can be ambiguos, according to whether you count the lowest order linear term as index 0 or 1.

L399: "filtered" -> "discarded"

Done.

L439: Delete "the pollutant"

Done.

L441: ". . . difference between NO2 in the UV (red curve) and in the visible (blue curve). . ." (the discussion is about NO2 and not about the colors of the curves)

Done.

L442: "more intense" -> "stronger"

Done.

L445: "By comparing SO2 (black curve) with NO2 (red and blue curves), it can be seen. . ."

Done.

L447: Delete "A more dirty"

Done.

L454: "points in time" -> "times"

Done.
L497: "The difference between UV and visible peak values depends. . ."

Done.

L498: "A short distance of the plume to the instrument and its complete coverage by the shorter UV path leads to higher values in the UV. . ."

Done.

The title of section 4.3 does not make sense. It implies that the approach is statistically evaluated. Instead, the data is statistically evaluated. Replace with something like "Statistical evaluation of the NO2 and SO2 data"

This section is not about NO_2 and SO_2 but about NO_2 in UV and visible for DSCDs and VMRs. We changed the title to "Statistical evaluation of UV and visible NO_2 data"

L507: ". . .all single pairs of simultaneous measurements" -> "all single pairs of DSCD measurements. . ."

Done.

L508: "the left subplot in the upper row" -> "Panel A"

Done.

L509: "both measurements" -> "NO2 and SO2 DSCDs"

This section is not about NO_2 and SO_2 but about NO_2 in UV and visible. We changed „both measurements" to "NO_2 DSCDs in UV and visible".

L513: "The right subplot in the upper row" -> "Panel B"

Done.

L518: "the left subplot in the bottom row" -> "Panel C"

Done.

L523: "(right plot)" -> "(Panel D of Fig. 9)"

Done.

L533: "applied on mountains" -> "applied to mountain-based measurements"

Done.

L535: Delete "However"

L537: "This should lead" -> "This leads" (the enhancement in path length in a cleaner and less dense atmosphere is obvious)

L541: "various" -> "detailed" or "comprehensive"

L543: Delete "emitting"

Figure 10: Mark the three panels as "A", "B" and "C" (from top to bottom)

L544: "Measurements from Wednesday, 9 July 2014 are shown in Figure 10. Panel A shows. . ."

L545: "The middle one" -> "Panel B"

L549: "The lower sub-plot" -> "Panel C"

L563: "The differences of both measurement techniques need to be considered for such a comparison:"

L565: "at one point" -> "at a single location"

L568: Insert "the" before "line-of-sight"

L569: delete "line-of-sight" (it is already mentioned at the beginning of the sentence)

L579: Delete "From the Figure, it can be easily identified that"

L581: Delete "nicely"

L586: Delete "It is also clearly visible, that"

L591: "it's" -> "its"

Done.

L592: Delete the first sentence of this paragraph

Done.

L594: "the upper subplots" -> "Panel A"; Add ", respectively" to the end of the sentence.

Done.

L606: "makes no sense" -> "is of little use"

Done.

L603: "the lower subplot" -> "Panel B"

Done.

L613: Delete "As can be seen in the figures"; delete "usually"

Done. Done.

L614: What do you mean with "progression of both curves"?

We mean "curve shape" or "course of the curves". We changed the formulation to the latter.

L623: Insert comma after "combustion"

Done.

L643: "The mean NO2 volume mixing ratios for each weekday shown in Fig. 16 illustrate the influence of land-based road traffic."

Done.

L647: "There is only little weekly cycle for air masses coming from the open North Sea. Measurements . . ."

Done.

L665: "single day measurements" -> "Single day of measurements"

Done.

L704: Delete comma after "This implies"

Done.

L738: "like expected" -> "as expected"

Done.

L743: "It can be seen that this increase for the land source sector is only a relative increase by comparing. . ."

Done.

L765: "roll" -> "role"

Done.

L767: "A monitoring of emissions from single ships requires the analysis of individual plume peaks in the NO2 and SO2 data sets."

Done.

L780: I am not familiar with the term "emission factor". Do you mean "emission rate"?

Both terms mean more or less the same, in the sense of an emission intensity. However, in the community of shipping emission measurements, the term "emission factor" is more commonly used.

780: delete "both"

Done.

L796: "one can get rid of the background pollution" -> "the background pollution can be removed"

Done.

L801: "To achieve a better signal-to-noise ratio, the integrals . . .. in the last step"

Done.

L803: "one" -> "an"

Done.

L804: "In both the NO2 and SO2 signal" -> "Both the NO2 and SO2 signal show"

Done.

L805: delete "are visible"; delete "measured"; "The shape of the peaks is also often quite similar" -> "Most of the peaks are of similar shape"

Done. Done. Done.

L807: "The SO2 to NO2 ratio can vary strongly for different ships. For example, the plume of the ship passing the line of sight around 12:00 UTC has a high NO2 content, but is low in SO2, whereas the opposite is true for the ship passing at 12:30 UTC, indicating that the second ship. . ."

Done.

L811: Delete "In contrast to this,"

Done.

L813: "High NO2 peaks also occur on this day. However,. . ."

Done.

L818: "From this plot one can also see that" -> "As can be seen from this plot, "

Done.

L819: "overestimate" -> "overestimates"

Done.

L826: "retrieved" -> "analyzed"

Done.

L836: Insert comma before "indicating"

Done.

L839: "and for 2015 and 2016, one gets a mean value of . . . " -> ", and a mean value of . . . for 2015 and 2016"

Done.

L842: "leading to overestimation" -> "leads to an overestimation"

Done.

L850: "from" -> "by"

Done.

L851: "SO2 and NO2 emission ratios can also be derived from. . ."

Done.

L858: "the dependency of SO2 to NO2 ratio to fuels sulfur content"

Done.

L863: "Island Neuwerk" -> "Island of Neuwerk"

Done.

L865: "into" - > "and"

Done.

L871: Delete "also"

Done.

L882: "NO2" -> "daily averaged NO2"

This sentence is not about daily averages but about the weekly cycle (averages according to weekday) and diurnal cycle (averaged values according to the hour of the day) of NO_2.

L908: Insert "can" after "ratios"

Done.

Thanks again for your thorough proof-reading. This helped us a lot.

Interactive comment on Atmos. Chem. Phys. Discuss., doi:10.5194/acp-2016-1153, 2017.

Interactive comment on "Monitoring shipping emissions in the German Bight using MAX-DOAS measurements" by André Seyler et al.

Anonymous Referee #2

Received and published: 11 April 2017

General comment: This paper describes a 3 year series of multi axis DOAS measurements carried out from the German island Neuwerk, just south of the entry to the river Elbe. This is in the main ship channel of the port of Hamburg and the main aim of the measurements was to study these by observing UV and visible light horizontally towards the ship channel. The paper is well written, with good language and instructive graphs. The paper is a nice combination of measurements methodology and results paper. It shows the methodology to measure mixing ratios in a coastal places, together with ship plume measurements and some results about the effect of new IMO legislation. However, the OBJECTIVE and AIM should be declared more clearly in the text. The paper is also rather long, and I would recommend to shorten it, by removing sections which are outside the main scope of the paper. Forinstance merging and shortening sect 4.5 and 4.6 corresponding to mixing ratio measurements and comparisons. All in all, I believe the paper should be published, with some minor improvements, based on answering my specific comments below:

First, we would like to thank Anonymous Referee #2 for his/her helpful comments. Below, we reply point-by-point to the specific comments . As far as possible, we have considered the suggestions in the revised manuscript.
We tried to shorten the manuscript and omitted unnecessarily repeated information. Section 4.5 was shortened and two plots have been deleted and the remaining ones merged to a common figure. Also 40% of the pieplots in Figure 18 have been removed. At several places paragraphs have been rewritten to make the text more precise and shorter.

Specific comments:

Row 71, p 2: It is claimed that 25% of the NOx emerges as NO2 from the stack, but usually 10% is assumed from fluegas stacks; please give more details: I assume you also assume some titration?

The relevant text passage (Row 71) reads: "The emitted NO_x comprises mainly NO, with less than 25% of NO_x being emitted as NO_2 (Alföldy et al., 2013)." We are referring here to results from a study of Alföldy et al. from the year 2013[1]. In this study, the chemical composition of the plumes of 497 seagoing ships was measured in the port of Rotterdam in September 2008 and a statistical evaluation of emission factors was provided. For the scope of our study, especially the results shown in Figure 17 are interesting:
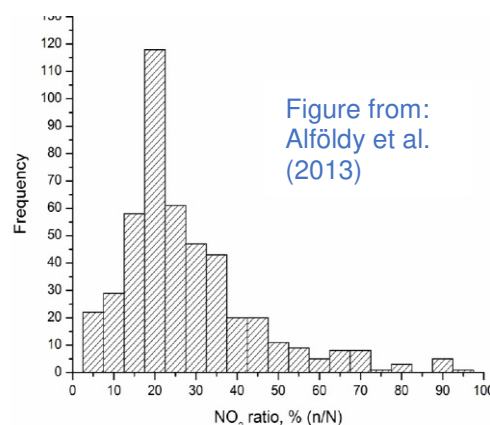

Figure from: Alföldy et al. (2013)

Fig. 17. Distribution of the NO_2/NO_x molar ratio among the studied ships. The total molar ratio range was divided into 19 bins. Frequen-

---

[1] Alföldy, B., Lööv, J. B., Lagler, F., Mellqvist, J., Berg, N., Beecken, J., … Hjorth, J. (2013). Measurements of air pollution emission factors for marine transportation in SECA. *Atmospheric Measurement Techniques*, *6*(7), 1777–1791. http://doi.org/10.5194/amt-6-1777-2013

The conclusion of the authors:

"The molar NO2-to-NOx emission ratio, calculated from the mixing ratios of the two components in the plume (%, n/N), is presented in Fig. 17. As can be seen, nitrogen oxides are mostly emitted as NO, the ratio of NO_2 emission is less than 25% at the majority of the ships."

In Row 71 we are simply referring to this result as background knowledge on the NO/NO_2 ratio in ship plumes, being important for our own study. We are not doing any assumptions here.

Row 278, p 9: IN the equation do you fit differential absorption cross sections or the absolute ones? Since you are using prime I assume you mean the differential ones; IN row 336 I however get the impression that you use the absolute ones.

We are fitting the differential absorption cross sections together with a low order polynomial to the measured optical depth. We have changed the sentence to make this point more clear:

"Multiple *(differential)* trace gas absorption cross sections obtained from laboratory measurements, as well as a low-order polynomial, are then fitted simultaneously to the optical depth."

Row 311, p 10: It is claimed that the vertical paths cancels out between path 1 and 2 in Fig 5; I agree with the stratospheric portion but for the tropospheric part there should be a cos (SZA) difference, even if NO2 is homogenously distributed in the troposphere?

That is a good objection. It is in fact true that this is only an assumption. To make things more clear we show a more detailed sketch below. The presented approach of using the O_4 column to estimate the effective horizontal light path length assumes single-scattering geometry. For the vertical paths in a layer of homogenously distributed NO_2 in the troposphere, like it is shown in the first sketch, to cancel out, the reference measurement must have the "assumed path". This means, it is assumed that the scattering point for the zenith reference is at the altitude of the instrument. In reality, of course, this is not the case. The real scattering altitude for light measured in zenith direction will be in an effective scattering height h, as it is shown in the sketch.
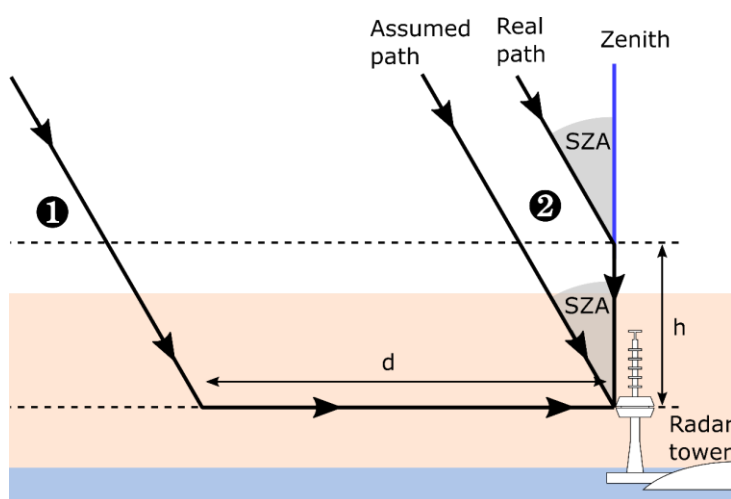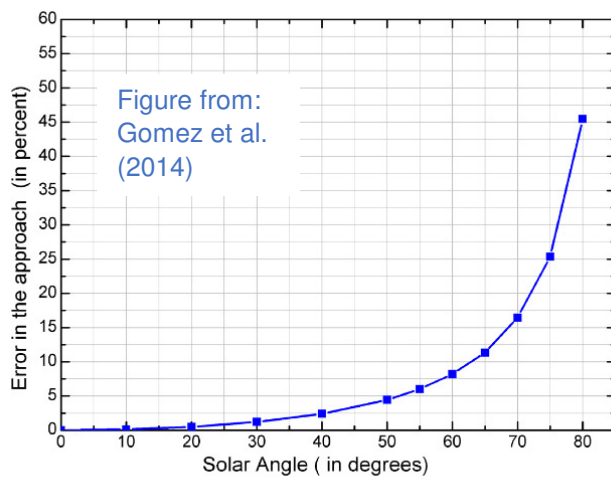

As can be seen from the figure, this leads to an underestimation of NO_2 in the reference and therefore to an overestimation of the NO_2 concentration. However, not only the NO_2 is overestimated, but also the O_4 path length is overestimated in a similar way.

Gomez et al. (2014)[2], applying this approach to MAX-DOAS measurements from a high mountain site, did a thorough error analysis in Section 3.2 of their publication. They showed that first, this scattering height h is nearly constant up to an SZA of 75°. Secondly, the path error depends only on the vertical distribution of the NO_2 (or SO_2) and on the differences in air mass factors (AMF) of NO_2 and O_4. By assuming a homogeneous layer, like it is shown in the sketch, the error comes from differences in the

[2] Gomez, L., Navarro-Comas, M., Puentedura, O., Gonzalez, Y., Cuevas, E., & Gil-Ojeda, M. (2014). Long-path averaged mixing ratios of O3 and NO2 in the free troposphere from mountain MAX-DOAS. *Atmospheric Measurement Techniques*, *7*(10), 3373–3386. http://doi.org/10.5194/amt-7-3373-2014

AMF. The SZA dependence of the error of the approach has been plotted by the authors in the following figure:

Figure 5. Estimated error of the MGA versus the SZA.

As can be seen from the figure, the error of the approach is less than 10 percent for typical daytime SZAs.

To keep the approach simple, this amount of uncertainty has to be accepted.

More important for this study is of course the measurement of ship emission plumes. When the wind is coming from the open North Sea, there is negligible background NO_2 and SO_2 in the lower troposphere. When a ship plume is in the horizontal path of the off-axis measurement, like it is sketched below, the difference between assumed and real reference path is irrelevant, introducing no additional error.
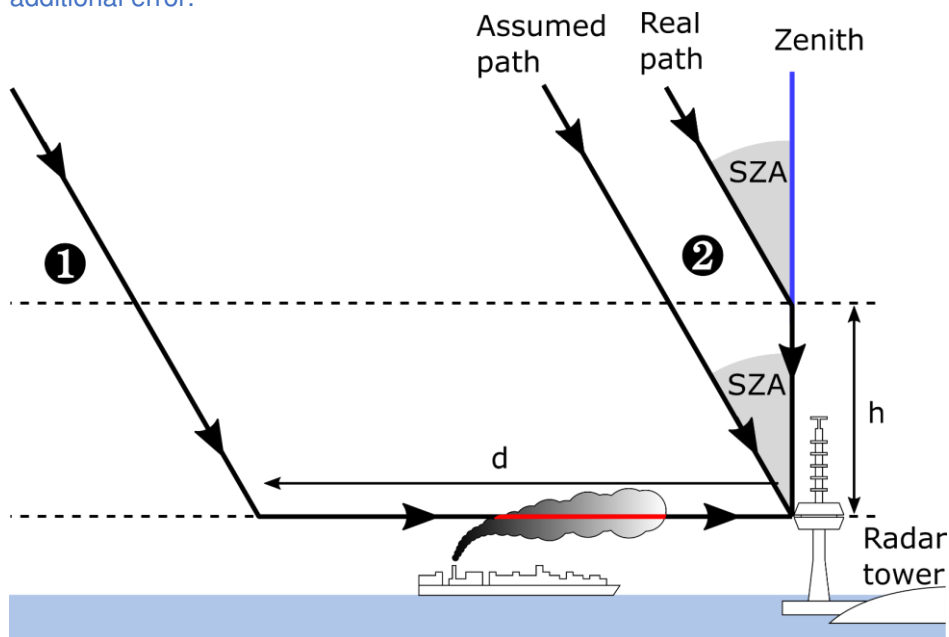
Row 387, p 13: Is it assumed that the wavelength difference in O4 signal is linear; if so what are the uncertainties involved?

We changed our method from a simple linear extrapolated scaling factor to using the empirically determined (from RTM simulations) formula from Wang et al. (2014)[3] to improve this source of uncertainty:

$$L_{310} = 0.136 + 0.897 \times L_{360} - 0.023 \times L_{360}^2. \qquad (6)$$

Which was determined from RTM simulations for a variety of aerosol conditions, which results are shown in the following figure:
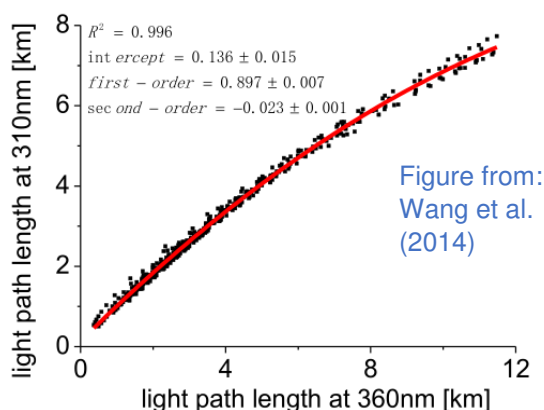

Figure from:
Wang et al.
(2014)

Figure 1. Scatter plot of light path lengths at 310 nm against light path lengths at 360 nm for 60 aerosol scenarios and combinations of three SZAs and RAAs. The statistical parameters derived from a second-order polynomial fitted to the simulation results are also shown.

Row 406, p 14: It is claimed that the conditions at the Neuwerk radar tower is similar to measurements from high mountains; please motivate better.

This section was completely rewritten to make our motivation clearer:

"This approach has been applied successfully by Sinreich et al. (2013) and Wang et al. (2014b) for measurements in urban polluted air masses over Mexico City and the city of Hefei (China) using MAXDOAS measurements in 1° and 3° (Sinreich et al., 2013) and only in 1° elevation (Wang et al., 2014b), respectively. Gomez et al. (2014) applied this approach to measurements on a high mountain site at the Izana Atmospheric observatory on Tenerife (Canary Islands), Schreier et al. (2016) at Zugspitze (Germany) and Pico Espejo (Venezuela). Due to the low aerosol amounts in such heights the latter two studies applied the approach without using correction factors. The fact that our instrument is located on a radar tower in a height of about 30m above totally at surroundings (the German Wadden Sea) allows an unblocked view to the horizon in all feasible azimuthal viewing directions. This led to theidea of trying to apply this approach to our shipping emission measurements on Neuwerk."

[3] Wang, Y., Li, A., Xie, P. H., Wagner, T., Chen, H., Liu, W. Q., & Liu, J. G. (2014). A rapid method to derive horizontal distributions of trace gases and aerosols near the surface using multi-axis differential optical absorption spectroscopy. *Atmospheric Measurement Techniques, 7*(6), 1663–1680. https://doi.org/10.5194/amt-7-1663-2014

Eq 4, p 13: It is difficult to follow how you get the expression in eq 4.

We deleted this equation and focus now on the approach which was actually applied to the data (the O4-scaling method).

Row 464 p 16: On this place, and some others, its is claimed that the differential slant columns are higher for SSE and ESE and (more elevated). But part of this should be wind speed effect since I would imagine that the wind speed will be higher from the sea and this will dilute the slant columns more. Has this been investigated ?

We have looked into this: The following polar plot shows the mean wind speed depending on wind direction. Wind speeds from the land sector (light green) are not substantially lower than wind speeds from the open Sea sector (light blue), so such a dependence has not been observed.
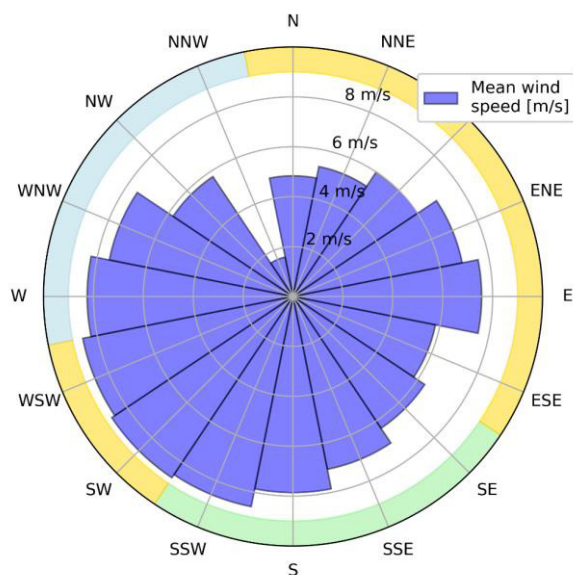
Row 470 p 16: Graph 7 is not totally clear. If I understand right the plot correspond to overlayed windroses for different elevation angles rather than that the area of each color represents the wind rose information. I interpreted the latter and I think this should be clarified forinstance in the figure text.

The former is correct. We changed the figure caption to make it clearer:
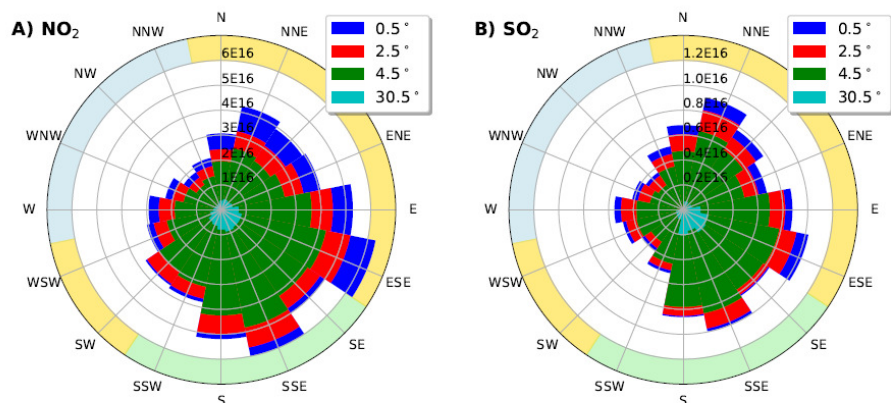
Figure 7: Overlayed wind roses for different elevation angles showing the wind direction distribution of the UV NO_2 (A) and SO_2 (B) differential slant column densities measured in the main viewing direction in 0.5°, 2.5°, 4.5° and 30.5° elevation in the years 2013 and 2014. The wind roses are plotted on top of each other, i.e. the highest values were measured in the lowest elevation angle (blue bars). The colored sectors show directions with wind from land (green), open North Sea (blue) and mixed origin (yellow).

Row 500 p 17: You here discuss the results in Fig 8. The differences in the UV and visible are explained from the penetration length, but should the Visible not in general be higher since it gives the chance of penetrating plumes further away, rather than the opposite which appears to be the case for all plumes here? You explain that the UV should be stronger for close by plumes since a higher fraction of the photons are then affected by absorption. Is is not so that the O4 can only simulate slow variations? Please elaborate..

The relevant point here is the position of the ships relative to the measurement site. On average, the measured NO2 slant column densities are higher in the visible than in the UV due to the longer horizontal light path. However, the data shown in Figure 8 are path-averaged mean volume mixing ratios. Typical path lengths are 10 km in the UV and 15 km in the visible. If the measured ship exhaust plume is closer to the instrument than 10 km, which is usually the case for all northerly wind directions since the ships pass the instrument in a distance of 6 to 7 km, the path averaged volume mixing ratio on the visible path will be lower due to the longer averaging distance. We have included two sketches below to make things clearer:

Vis
UV
- Higher peak in UV than in visible due to averaging over longer path length

Vis
UV
- No NO_2 peak in UV
- Peak in visible

Vis
UV
- NO_2 peaks in UV & vis
- Relative heights depend on geometry

NO_2 VMR — time

NO_2 VMR — time

NO_2 VMR — time (one possible example)

UV: 10 km
Vis: 15 km
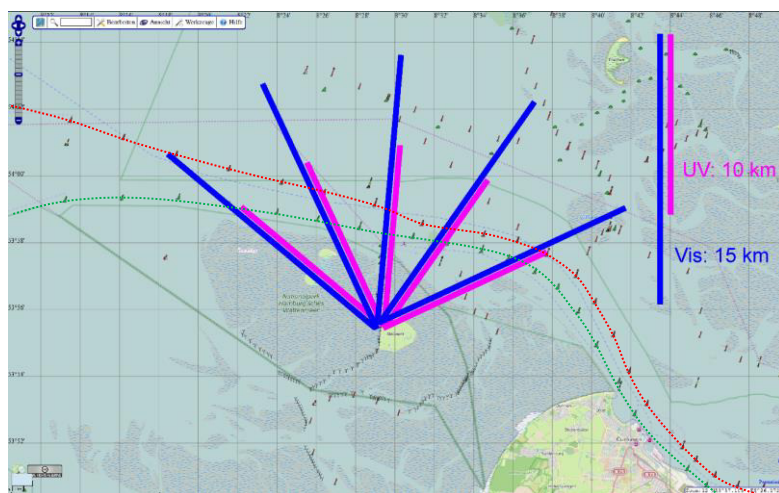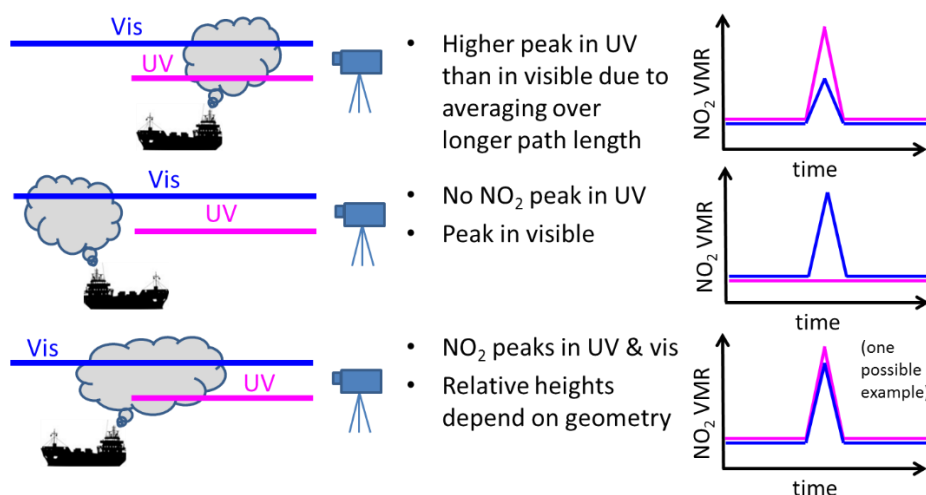
Map showing the azimuthal viewing directions and the typical averaging path lengths. The green and red dotted lines highlight the boundaries (line of buoys) of the main shipping lane.

Row 614 p 25: You claim that fig 12/fig 13 shows good agreement between MAX DOAS and in situ, but in my mind this is the case for Fig 13 but not for fig 12, where there appears to be rather big difference in he averages of the two sensors with factor 2-3?

In this Section we do not claim a good agreement in absolute values (which due to the characteristics of both measurement techniques and different measurement geometries is also not expected), but a good agreement in the shape (or course) of the curves. This means that apart from a scaling factor, the day-to-day trends in both time series of daily means are well reproduced.

Row 665 p 27: You suddenly refer to fig 20, without having mentioned fig 17-19 yet in the text. You should consider reordering.

This reference has been deleted.

Row 891 p 35: As concluded here and discussed in section 4.9, the ratio of SO2/NO2 gives an indication of sulfur fuel content in ship plumes. Are you aware that SO2/NO2 ratio measurements from airborne DOAS is used operationally since 2015 by Beecken and Mellqvist (Chalmers University) in the CompMon project and surveillance around Denmark and that this has been presented on several official workshops last year?

Thank you very much for that hint. The methodology presented in the CompMon Report "Best Practices Airborne MARPOL Annex VI Monitoring" (Van Roy, 2016)[4] is very interesting. We added the following paragraph to the chapter on SO_2/NO_2 ratios:

"By comparing SO_2 to NO2 ratios from different ships it is possible to roughly distinguish whether a ship is using fuel with high or low sulfur content (giving a high or low SO_2 to NO_2 ratio). *Beecken and Mellqvist from Chalmers University (Sweden) use this relationship for airborne DOAS measurements of ship exhaust plumes on an operational basis in the CompMon project (Compliance monitoring pilot for MARPOL Annex VI) (Van Roy, 2016). Following the ships and measuring across the stack gas plume they can discriminate between low (0.1 %) and high (1 %) fuel sulfur content ships with a probability of 80-90% (Van Roy, 2016).*"
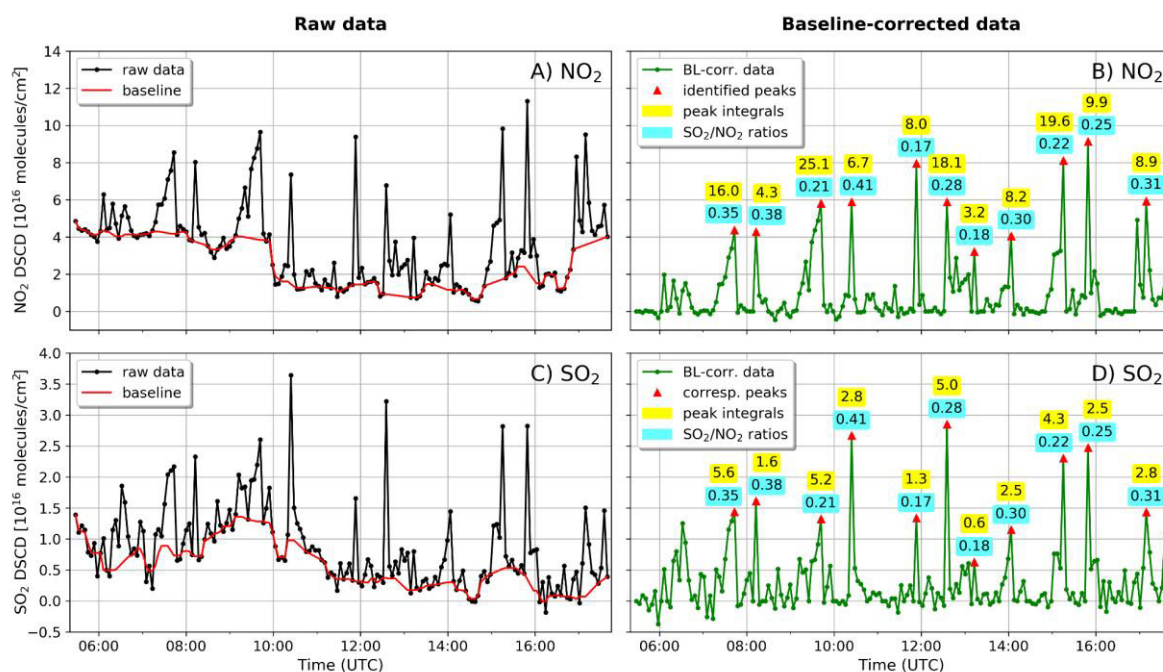
You mention that the +2015 measurements are biased by noise since you don't really observe any SO2 then. I don't think it then makes sense to show the green data (+2015) in figure 5 since these histograms then only represent noise? Secondly you don't mention when comparing to other measurements that the amount of NO to NO2 titration is very important for the ratio, and this will depend on the distance to the plume, whether you are over land or sea etc. Please add some discussion on this.

To address this shortcoming in our study we have completely redone the SO_2 to NO_2 ratio peak analysis. The baseline determination has improved substantially (using a second running median filterapplied to the lower 50% quartile when necessary) and the positive bias in the measurements since 2015 is now gone. In addition to that, the section has been rewritten taking into account your comments. Also, the importance of NO to NO_2 titration especially for the comparison to other studies is now mentioned in this section.
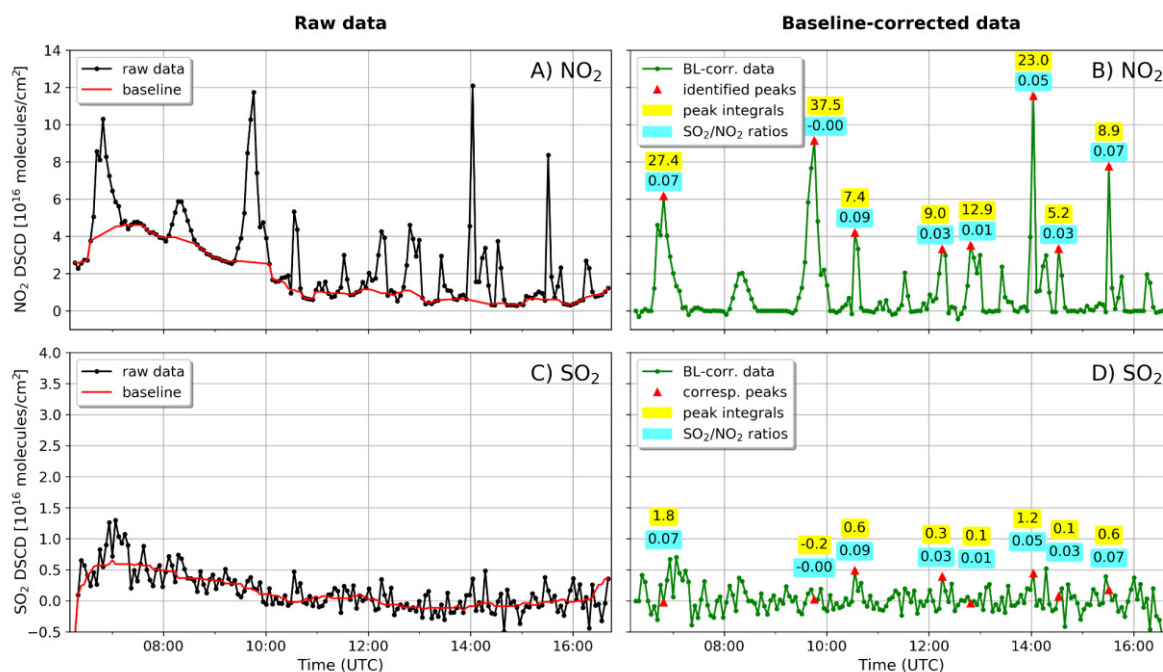
Updated plots:

---

[4] Van Roy, W. (2016). Best Practices Airborne MARPOL Annex VI Monitoring. Retrieved from http://ec.europa.eu/transparency/regexpert/index.cfm?do=groupDetail.groupDetailDoc&id=29311&no=7
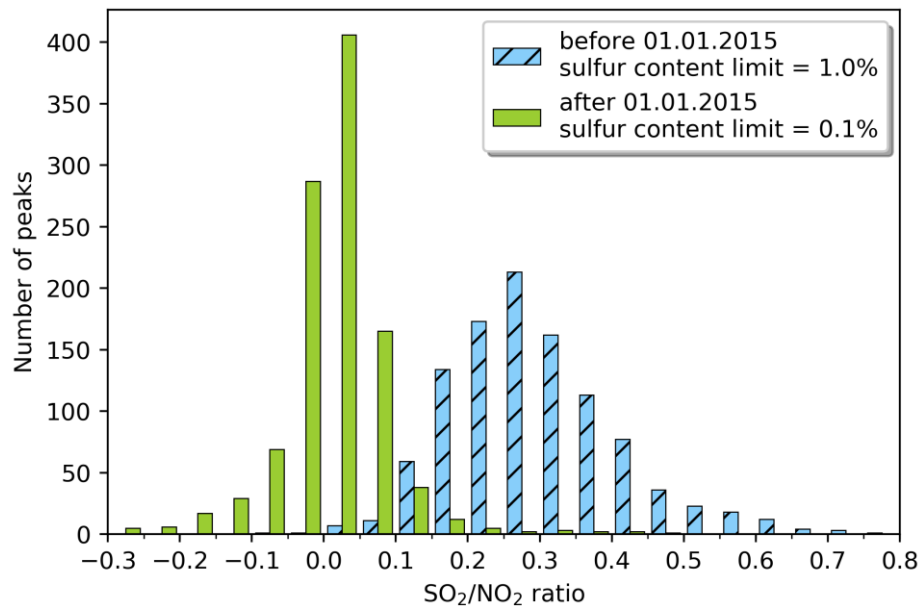
For an example day (23.07.2014) before the change in regulations:

For an example day (03.07.2015) after the change in regulations:

And the updated histogram:

Row 903 p 35: It is mentioned that there are still SO2 coming from land. This is surprising since there are very few SO2 emission sources anymore and power plants generally have abatement equipment. It would be interesting to understand this better ?

SO_2 concentrations in Germany decreased significantly in the last decade (-93% since 1990) due to advanced filter techniques and are now stable on a low level [5]. Still, the most important source is energy production, followed by industry. In Bremen, typical annual mean values are 1 to 2 $\mu g/m^3$, with short-time peaks (maximum 1-hour-means) of 20 to 80 $\mu g/m^3$, with the highest values close to industrial sites [6]. The German Federal Environmental Agency (Umweltbundesamt) operates a network of several in-situ air quality measurement stations throughout Germany [7]. The following two plots show SO_2 daily mean concentrations for the last 18 months for five rural stations and five urban stations in Northern Germany. The overall mean value for each station is given in the legend.

[5] https://www.umweltbundesamt.de/daten/luftbelastung/luftschadstoff-emissionen-in-deutschland/schwefeldioxid-emissionen (16.05.2017)
[6] Der Senator für Umwelt, Bau und Verkehr
Contrescarpe 72, *Das Bremer Luftüberwachungssystem - Jahresbericht 2015*
http://www.bauumwelt.bremen.de/sixcms/media.php/13/BdV_L_2016-08_Jahresbericht_Luftmessnetz_2015_Anhang.pdf (16.05.2017)
[7] https://www.umweltbundesamt.de/daten/luftbelastung/aktuelle-luftdaten (16.05.2017)
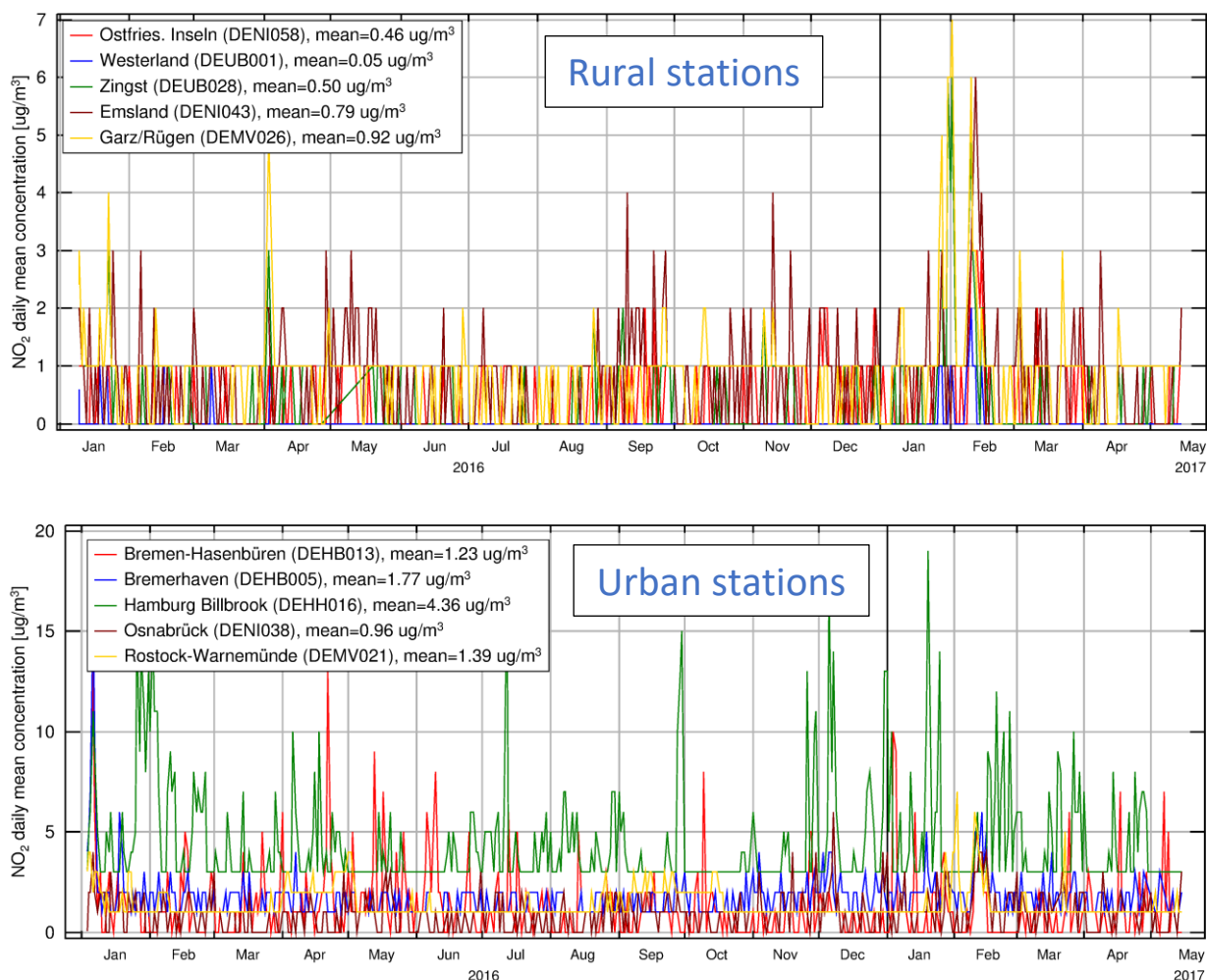
Rural stations

Urban stations

The typical average SO₂ concentrations measured by the German Federal Environmental Agency ("Umweltbundesamt") for rural stations are around 0.5 to1 $\mu g/m^3$, corresponding to 0.2 – 0.4 ppbv (Conversion factor: 1 ppb = 2.62 $\mu g/m^3$ for SO_2). Measurements in cities and especially close to industrial areas show higher values. Bremerhaven, which is the station closest to our instrument, has a mean concentration of 1.77 $\mu g/m^3$, corresponding to 0.67 ppbv.

We measured mean SO₂ mixing ratios from land between 0.3 and 0.4 ppbv since January 2015 (see Figure 17), which in our opinion fits very well to those measurements.

Technical Corrections: Well written in most places.

Row 812 p 31: Change limis to limits

Done.

Row 873 p 33: Change This to These

Done.

Interactive comment on Atmos. Chem. Phys. Discuss., doi:10.5194/acp-2016-1153, 2017.

Monitoring shipping emissions in the German Bight using MAX-DOAS measurements

André Seyler[1], Folkard Wittrock[1], Lisa Kattner[1,2], Barbara Mathieu-Üffing[1,2], Enno Peters[1], Andreas Richter[1], Stefan Schmolke[2], and John P. Burrows[1]

[1]Institute of Environmental Physics, University of Bremen, Germany
[2]Federal Maritime and Hydrographic Agency (BSH), Hamburg, Germany

Correspondence to: A. Seyler (aseyler@iup.physik.uni-bremen.de)

Abstract

A three-year time series of ground-based MAX-DOAS measurements of NO_2 and SO_2 on the island Neuwerk has been analyzed for contributions from shipping emissions. The island is located in the German Bight, close to the main shipping lane (in a distance of 6–7 km) into the river Elbe towards the harbor of Hamburg. Measurements of individual ship plumes as well as of background pollution are possible from this location. A simple approach using the column amounts of the oxygen molecule dimer or collision complex, O_4, for the determination of the horizontal light path length has been applied to retrieve path-averaged volume mixing ratios. An excellent agreement between mixing ratios determined from NO_2 retrievals in the UV and visible parts of the spectrum has been found, showing the validity of the approach. Obtained mixing ratios of NO_2 and SO_2 are compared to co-located in-situ measurements showing good correlation on average but also a systematic underestimation by the MAX-DOAS O_4-scaling approach. Comparing data before and after the introduction of stricter fuel sulfur content limits (from 1 % to 0.1 %) on 1 January 2015 in the North Sea emission control area (ECA), a significant reduction in SO_2 levels has been observed. For situations with wind from the open North Sea, where ships are the only local source of air pollution, the average mixing ratio of SO_2 decreased by a factor of eight, while for NO_2 in the whole time series from 2013 till 2016 no significant change in emissions has been observed. More than 2000 individual ship emission plumes have been identified in the data and analyzed for the emission ratio of SO_2 to NO_2, yielding an average ratio of 0.3 for the years 2013/2014, decreasing significantly presumably due to lower fuel sulfur content in 2015/2016. By sorting measurements according to the prevailing wind direction and selecting two angular reference sectors representative for wind from open North Sea and coast excluding data with mixed air mass origin, relative contributions of ships and land-based sources to air pollution levels in the German Bight have been estimated to be around 40 % : 60 % for NO_2 as well as SO_2 in 2013/2014, dropping to 14 % : 86 % for SO_2 in 2015/2016.

1 Introduction

1.1 Shipping – a fast growing sector

Shipping has always been an important mode of transportation throughout the course of history. In contrast to the past, nowadays ships are almost exclusively carrying freight with the exception of a

small number of cruise ships and ferries. Globalization of markets has lead to an enormous increase in world trade and shipping traffic in the last decades, with growth rates being typically about twice that of the world gross domestic product (GDP) (Bollmann et al., 2010).

Shipping is generally the most energy efficient transportation mode, having the lowest greenhouse gas emissions per tonne per kilometer (3–$60\,gCO_2/t/km$), followed by rail (10–$120\,gCO_2/t/km$), road (80–$180\,gCO_2/t/km$) and air transport (435–$1800\,gCO_2/t/km$), which is by far the least efficient (Bollmann et al., 2010; IEA/OECD, 2009). At the same time, with a volume of 9.84 billion tons in 2014 it accounts for four fifths of the worldwide total merchandise trade volume (UNCTAD, 2015), as compared to for example the total air cargo transport volume of 51.3 million tons in 2014 (International Air Transport Association (IATA), 2015). As a result, shipping accounts for a significant part of the emissions from the transportation sector (Eyring et al., 2005a).

Despite growth rates now being lower compared to those prior to the 2008 economic crisis, seaborne trade is growing faster than the rest of the transportation sector, with an annual growth rate of 3–4 % in the years 2010 to 2014, compared to 2.0–2.6 % for the global merchandise volume (UNCTAD, 2014, 2015). The number of ships > 100 gross tonnage increased from around $31\,000$ in 1950 over $52\,000$ in 1970 to $89\,000$ in 2001 (Eyring et al., 2005b) and is estimated to increase to about $150\,000$ in 2050 (Eyring et al., 2005a). At the same time, total fuel consumption and emissions increased as well (Corbett and Koehler, 2003; Eyring et al., 2005a,b; Eyring et al., 2010b). Eyring et al. (2005a) predicted that future development of shipping emissions will depend more on the usage of new technologies and imposed regulations than on the economic growth rates.

1.2 Ship emission chemistry

The most important pollutants emitted by ships are carbon dioxide (CO_2), carbon monoxide (CO), nitrogen oxides ($NO_x = NO + NO_2$), sulfur dioxide (SO_2), black carbon (BC), volatile organic compounds (VOC) and particulate matter (PM) (Eyring et al., 2010a). This study focuses on NO_2 and SO_2, because both are emitted in considerable amounts and both absorb light in the uv-visible spectral range and therefore can readily be measured by Differential Optical Absorption Spectroscopy (DOAS), which is explained in Sect. 3.1. In 2001, shipping emissions accounted for 15 % of all anthropogenic NO_x and provided 8 % of all anthropogenic SO_2 emissions (Eyring et al., 2010a).

NO_x is predominantly formed thermally from atmospheric molecular nitrogen (N_2) and oxygen (O_2) during high temperature combustion processes in ship engines in an endothermic chain reaction called the Zeldovich mechanism. The emitted NO_x comprises mainly NO, with less than 25 % of NO_x being emitted as NO_2 (Alföldy et al., 2013). Zhang et al. (2016) measured emission factors for gaseous and particulate pollutants on-board three Chinese vessels and found that more than 80 % of the NO_x was emitted as NO and that emission factors were significantly different during different operation modes.

In the ambient atmosphere, NO is rapidly converted to NO_2 by reaction with ozone (O_3) leading to a life time of only a few minutes. During daytime NO_2 is photolyzed by UV radiation ($\lambda < 420\,nm$) releasing NO and ground state oxygen radicals ($O(^3P)$). In a three-body-collision reaction involving N_2 or O_2 the oxygen radical reacts with an oxygen molecule to reform ozone (Singh, 1987). When daylight is available, these reactions form a "null-cycle" and transformation between NO and NO_2 is very fast, leading to a dynamic equilibrium. This is also known as the Leighton photostationary state. Owing to the lack of photolysis, NO reacts rapidly with O_3 to form NO_2 during the night. In addition, the nitrate radical (NO_3) is formed by reaction of NO_2 with O_3. An equilibrium of NO_2 with NO_3 forming N_2O_5, the acid anhydride of nitric acid HNO_3, results (Seinfeld and Pandis, 2006; Wayne, 2006).

During the day OH reacts with NO_2 in a three body reaction to form HNO_3. An important sink for NO_2 in the troposphere is wet deposition of the resulting HNO_3. The mean tropospheric lifetime of NO_x varies between a few hours in summer and a few days in winter (Singh, 1987), depending on altitude. Inside ship plumes, Chen et al. (2005) found a substantially reduced lifetime of NO_x of about 1.8 h compared to approximately 6.5 h in the background marine boundary layer (around noon). This is attributed to enhanced levels of OH radicals in the plume.

Unlike for NO_x, ship emissions of SO_2 are directly linked to the fuel sulfur content. Around 86 % of the fuel sulfur content is emitted as SO_2 (Balzani Lööv et al., 2014). Alföldy et al. (2013) found a linear relationship between SO_2 and sulfate particle emission and that only around 4.8 % of the total sulfur content is either directly emitted as or immediately transformed into particles after the emission. An important sink for SO_2 is wet deposition after oxidation by OH radicals to the extremely hygroscopic sulfur trioxide (SO_3) reacting rapidly with liquid water to form sulfuric acid (H_2SO_4) (Brasseur, 1999). Another important sink is dry deposition, leading to a lifetime of approximately one day in the boundary layer, which can be even shorter in the presence of clouds (Seinfeld and Pandis, 2006).

1.3 Influence on air quality and climate

Sulfate aerosols influence climate directly by scattering and absorption of solar radiation and indirectly by increasing cloud condensation, changing cloud reflectivity and lifetime (Eyring et al., 2010b; Lauer et al., 2007; Lawrence and Crutzen, 1999). In the presence of volatile organic compounds (VOC), nitrogen oxides are important precursors for the formation of tropospheric ozone and therefore photochemical smog. The release of both NO_2 and SO_2 leads to an increase in acidification of 3–10 % in coastal regions, contributing significantly to acid rain formation damaging eco-systems (Endresen et al., 2003; Jonson et al., 2000). The deposition of reactive nitrogen compounds causes eutrophication of ecosystems and decreases biodiversity (Galloway et al., 2003).

Around 70 % of shipping emissions occur within 400 km of land (Corbett et al., 1999), contributing substantially to air pollution in coastal areas (Eyring et al., 2010b). Ship emissions were found to provide a dominant source of air pollution in harbor cities (Eyring et al., 2010a). In addition to that, transport of tropospheric ozone and aerosol precursors over several hundreds of kilometers also affect air quality, human health and vegetation further inland, far away from their emission point (Corbett et al., 2007; Eyring et al., 2010a; Eyring et al., 2010b).

NO_2 and SO_2 can cause a variety of respiratory problems. Tropospheric ozone is harmful to animals and plants, causing various health problems. The EU legislation for O_3 exposure to humans has set a target limit of $120\,\mu g/m^3$ (~ 60 ppbv) for an maximum daily 8 hour mean but allows exceedences on 25 days averaged over 3 years (EU, 2008, 2016). As mentioned above, both NO_2 and SO_2 play a role in the formation of particles. Fine particles are associated with various health impacts like lung cancer, heart attacks, asthma and allergies (Corbett et al., 2007; Pandya et al., 2002; WHO, 2006).

1.4 Attempts to decrease shipping emissions by stricter regulations

International ship traffic is subject to regulations of the International Maritime Organization (IMO). Shipping emissions are regulated by the International Convention for the Prevention of Pollution from Ships (MARPOL 73/78) Annex VI (DNV, 2008). This Annex was added in 1997 and entered into force in 2005. A revision with more stringent emission limits was adopted in 2008 and went into force 2010. With this, limits on sulfur content in heavy fuel oils globally are set and local Sulfur Emission Control Areas (SECA), later revised to general Emission Control Areas (ECA), along the North American coast and in the Baltic and North Sea (including the English Channel) are established with more stringent restrictions and controls. MARPOL introduced a global fuel sulfur limit of 4.5 %, which was reduced to 3.5 % in 2012 and will be further reduced in 2020 (or 2025 depending on a review

in 2018) to 0.5 %. In the established ECAs, from 2010 on the limit was set to 1.5 % and was further
reduced in 2010 to 1.0 %. Carrying out airborne in-situ measurements in several flight campaigns in
the English Channel, North and Baltic Sea, Beecken et al. (2014) measured a 85 % compliance in 2011
and 2012 with the 1 % fuel sulfur limit. In the Gulf of Finland and Neva Bay area, Beecken et al.
(2015) found a 90 % compliance in 2011 and 97 % compliance in 2012 with the 1 % fuel sulfur limit
from ground-based, ship-based and helicopter-based in-situ measurements.

Recently, from 1 January 2015 on, the allowed fuel sulfur content in SECAs was further reduced
to 0.1 %. Using in-situ measurements in Wedel at the bank of the river Elbe, a few kilometers
downstream from Hamburg, Germany, Kattner et al. (2015) showed that in late 2014 more than 99 %
of the measured ships complied with the 1 % sulfur limit and in early 2015 95.4 % of the measured ships
complied with the new 0.1 % sulfur limit. By analyzing one and a half years of SO_2 measurements
at the English Channel, Yang et al. (2016) found a three-fold reduction in SO_2 from 2014 to 2015.
They estimated the lifetime of SO_2 in the marine boundary layer to be around half a day. Lack et al.
(2011) measured a substantial drop of SO_2 emissions by 91 % when the investigated container ships
entered the Californian ECA and switched from heavy fuel oil (HFO) with 3.15 % fuel sulfur content
to marine gas oil (MGO) with 0.07 % fuel sulfur content. These estimates were obtained performing
airborne in-situ measurements.

MARPOL Annex VI also establishes limits dependent on engine power for the emission of NO_x from
engines built after 2000 (Tier I), 2011 (Tier II) and 2016 (Tier III), but due to the slow penetration
to the full shipping fleet, the impact on NO_x emissions is not yet clear. Since 2010, a NO_x emission
control area exists around the North American coast and in the Caribbean, while for North and
Baltic Sea the establishment of such a NECA is planned and was recently agreed on, but the future
enforcement date is still unclear. The European Union also established a sulfur content limit of 0.1 %
for inland waterway vessels and ships at berth in Community ports, which is in force since 1 January
2010 (EU, 2005).

The impact of shipping emissions on the North Sea for different regulation scenarios was investigated
in a model study by the Helmholtz-Zentrum Geesthacht (HZG) within the scope of the Clean North Sea
Shipping project. For current emissions, a relative contribution of shipping emissions to air pollution
in coastal regions of up to 25 % in summer and 15 % in winter for NO_2 and 30 % in summer and
12 % in winter for SO_2 was found (Aulinger et al., 2016). For the year 2030, the contribution of the
continuously growing shipping sector to the NO_2 concentrations is predicted to decrease. The extent
of reduction depends on the date on which the stricter Tier III regulations enter into force and on the
fraction of the fleet complying to these regulations (i. e. the age of the fleet), with up to 80 % reduction
if all ships comply (in the improbable case of a new ships only fleet). For SO_2, the established fuel
sulfur content limit of 0.1 % (ECA) and 0.5 % (globally) will lead to significant reductions, a further
decrease is expected if the fraction of LNG powered ships grows (Matthias et al., 2016).

1.5 DOAS measurements of shipping emissions – previous studies

Optical remote sensing using the Differential Optical Absorption Spectroscopy (DOAS) technique to
measure shipping emissions has been conducted before. For example, Berg et al. (2012) performed
airborne (from airplane and helicopter) DOAS measurements of NO_2 and SO_2 in ship plumes by
measuring sea scattered light. Masieri et al. (2009) and Premuda et al. (2011) measured flow rate
emissions (mass per second) of NO_2 and SO_2 for single ships with ground based MAX-DOAS measure-
ments across the Giudecca Channel in the Venice lagoon. McLaren et al. (2012) measured nocturnal
NO_2/SO_2 ratios in ship plumes in the Strait of Georgia with the active long path DOAS technique.
Balzani Lööv et al. (2014) tested and compared optical remote sensing methods (DOAS, LIDAR, UV
camera) and in-situ (sniffer) methods for the measurement of shipping emissions in the framework
of the SIRENAS-R campaign in the harbour of Rotterdam in 2009. Prata (2014) showed that a UV

(SO$_2$) imaging camera can be used to measure SO$_2$ in ship plumes at the Kongsfjord at Ny Ålesund, Svalbard and the harbor of Rotterdam.

The global pathways of the ships can be seen in long time averaged NO$_2$ measurements from various satellite instruments: from GOME over the Indian Ocean (Beirle et al., 2004), from SCIAMACHY on board ENVISAT over the Indian Ocean and the Red Sea (Richter et al., 2004), in even more detail with a lot more visible ship tracks from GOME-2 on board MetOp-A (Richter et al., 2011). The higher resolution of OMI yielded ship tracks in the Baltic Sea (Ialongo et al., 2014) and in all European seas (Vinken et al., 2014).

1.6 The MeSMarT project

The current study is part of the project MeSMarT (Measurements of Shipping emissions in the Marine Troposphere), which is a cooperation between the University of Bremen (Institute of Environmental Physics, IUP) and the Federal Maritime and Hydrographic Agency (Bundesamt für Seeschifffahrt und Hydrographie, BSH), supported by the Helmholtz Zentrum Geesthacht (HZG). It aims to monitor background concentration as well as elevated signals of gases and particles related to ship emissions with various methods to cover a wide range of relevant pollutants and their spatial and seasonal distribution to estimate the influence of ship emissions on the chemistry of the atmospheric boundary layer (for further information visit: `http://www.mesmart.de/`).

1.7 Aims of this study

The objectives of this study are to assess whether measurements of individual ship plumes are feasible with a ground-based MAX-DOAS instrument, to compare MAX-DOAS with co-located in-situ measurements, to estimate the contribution of ships and land-based sources to air pollution in a North Sea coastal region, to survey the effect of fuel sulfur content regulations on SO$_2$ concentrations in the marine boundary layer and to analyze the SO$_2$ to NO$_2$ ratio in plumes to gain information about plume chemistry and the sulfur content in shipping fuels.

In the following, first the measurement site is described, followed by a presentation of the wind statistics and data availability. After this, the Differential Optical Absorption Spectroscopy (DOAS), the MAX-DOAS instrumentation and measurement geometry as well as the DOAS data analysis approach used are briefly described. In the next section, selected results from this study are presented: the measured differential slant column densities (DSCD), the retrieved path-averaged volume mixing ratios, the comparison to in-situ measurements, the diurnal and weekly variability, the contribution estimates for ships as well as land-based pollution sources and the analysis of SO$_2$ to NO$_2$ ratios in ship plumes. Finally, a summary is given and conclusions are drawn.

2 Measurement site

The measurements presented within this study were taken on Neuwerk, a small island in the North Sea (German Bight) with the size of about $3\,\mathrm{km}^2$ and 33 inhabitants. It is located in the Wadden Sea northwest of Cuxhaven at the mouth of the river Elbe, roughly 8–9 km off the Coast, as can be seen from the map in Fig. 1 A).

The North Sea has one of the highest ship densities in the world (Matthias et al., 2016). The majority of ships that arrive in the port of Hamburg sail through the German Bight and the river Elbe and therefore pass Neuwerk. Hamburg is among the largest ports worldwide, together with Rotterdam and Antwerp one of the three largest ports in Europe, having a 4–5 % increase in container

volume in the last years (UNCTAD, 2014, 2015). Hamburg also experiences a large increase in the number of cruise ships, having 176 ship calls in 2014 compared to 25 in the year 2005 (Statistische Ämter des Bundes und der Länder (Statistikamt Nord), 2015).

220   Neuwerk is relatively close to the main shipping lane from the North Sea into the river Elbe. On this highly frequented waterway, nearly all ships to and from the port of Hamburg and the Kiel canal (connection to the Baltic Sea) pass the island at a distance of 6–7 km, as shown in Fig. 1 B). Still close, but further away to the west are the shipping lanes to the Weser river to the ports of Bremerhaven and Bremen and to Wilhelmshaven (JadeWeserPort).

225   Neuwerk is surrounded by the Hamburg Wadden Sea National Park and there are no significant sources of air pollution on the island itself, making it a very suitable station for measurements of shipping emissions.
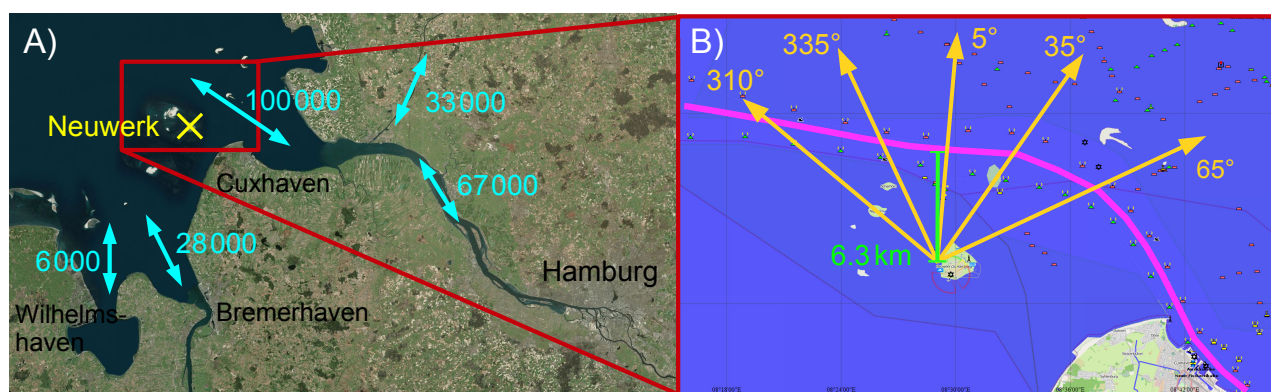

Figure 1: **A)** Location of the measurement site Neuwerk in the German Bight, close to the mouth of the river Elbe. Number of ship movements (data from 2011/2012) is given by the white numbers. Data source: German Federal Waterways and Shipping Administration (WSV, 2013, 2014) Map source: `http://www.bing.com/maps/` (01.04.2014)
B) Azimuthal viewing directions of the MAX-DOAS instrument towards the main shipping lane (highlighted by the magenta line), passing the island in the north in a distance of 6–7 km. Map source: `http://www.freie-tonne.de` (16.07.2013)

The ship emission measurements presented in this study were carried out with a MAX-DOAS instrument (see Sect. 3.2) which measures in multiple azimuthal viewing directions, as shown in Fig.
230 1 B), pointing directly towards the shipping lane while the different viewing azimuth angles cover a large part of the region.

     Several measurement devices, including the two-channel MAX-DOAS instrument (for UV and visible spectral range), an Airpointer in-situ measurement device (measuring CO_2, NOx, SO_2 and O_3), a high volume filter sampler and passive samplers as well as a weather station and an AIS (Automatic
235 Identification System) signal receiver, are positioned on the main platform of a radar tower at a height of about 30 m (see Fig. 2).

     Additional wind data is available from measurements by the Hamburg Port Authority (HPA) on Neuwerk and the neighboring island Scharhörn. The seasonal distribution of wind directions on Neuwerk is shown in Fig. 3.

240   In spring and summer, on a high percentage of days the wind blows from the open North Sea, where shipping emissions are the only significant source of local air pollution. Consequently, the site provides an optimal opportunity for measurements of ship emission plumes. In winter, southerly directions prevail, bringing potentially polluted air masses from the land and blowing the ship emission plumes away from the measurement site. In addition, as the MAX-DOAS technique requires daylight and
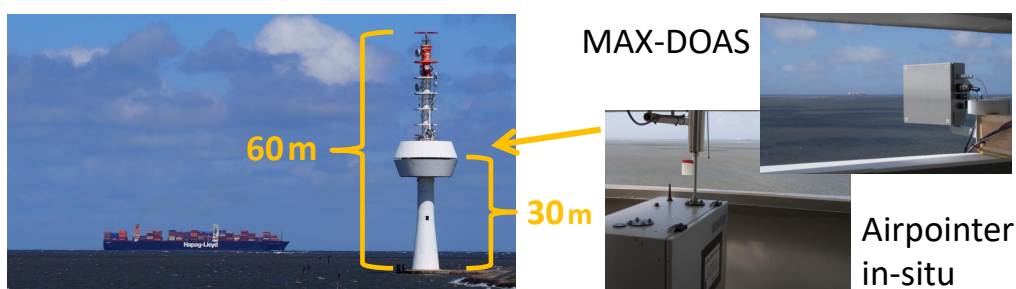
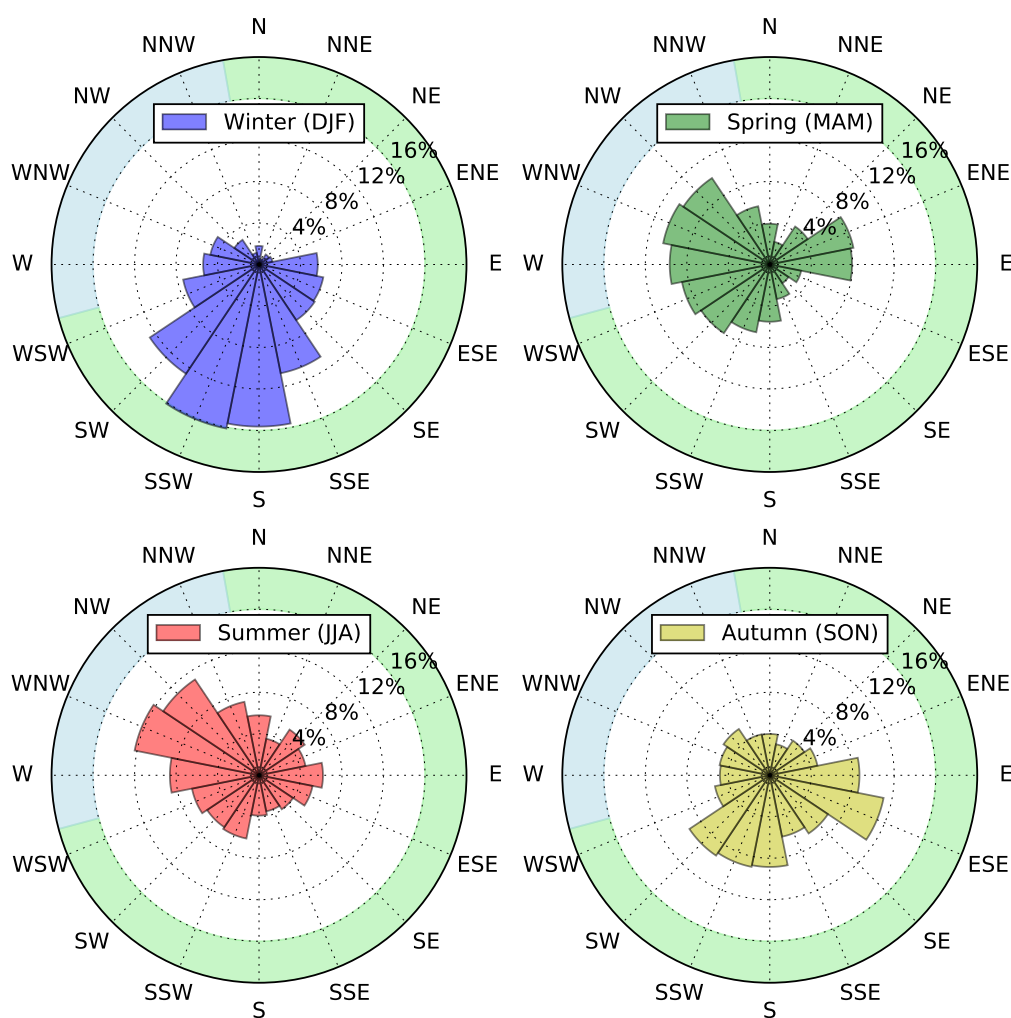Figure 2: Radar tower Neuwerk with MAX-DOAS and in-situ measurement device

Figure 3: Seasonal wind direction distribution for Neuwerk (Data from 04.07.2013 to 26.10.2015). The colored sectors show directions with wind from the coast (green) and from the open North Sea (blue).

245 because of the short days and the low sun resulting in less UV light reaching the surface, measurements are in general sparse in winter months, especially for SO_2, which has its strong absorption features in the UVB. This effect can be seen in winter gaps in Fig. 4, which presents the data availability for more than two years of measurements on Neuwerk.
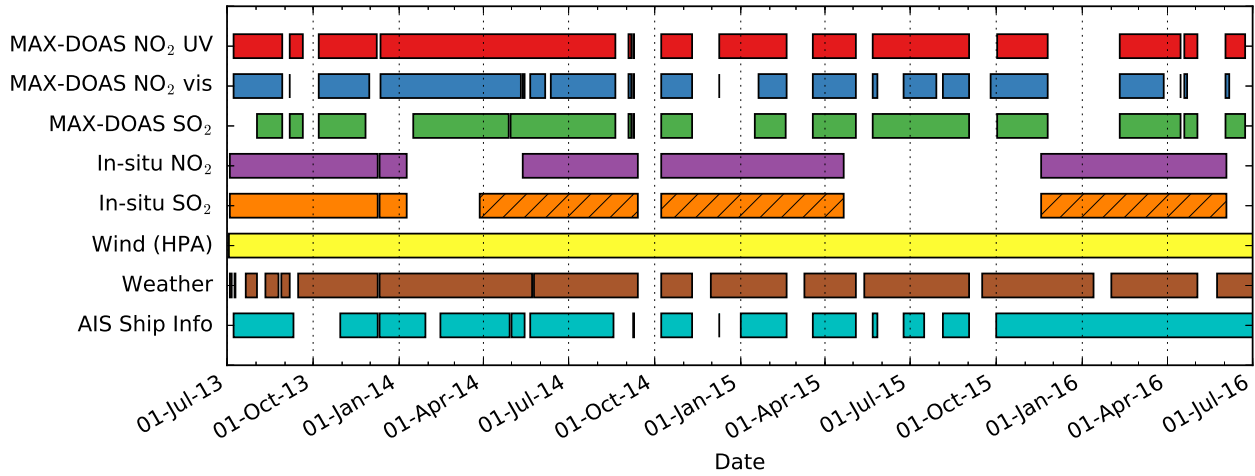

Figure 4: Data availability in the analyzed measurement period between July 2013 and July 2016. From March 2014 on (hatched), there were instrumental problems with the in-situ SO_2 instrument resulting in a strong oscillation of ± 0.5 ppb superimposing the data. However, this data can still be used for the comparison of long-term averages.

3 Measurement techniques, instruments and data analysis

3.1 Differential Optical Absorption Spectroscopy (DOAS)

The principle of optical absorption spectroscopy is the attenuation of light intensity while passing through an absorbing medium, described by the well-known Lambert-Beer-law (also known as Beer–Lambert–Bouguer law). For the general case of electromagnetic radiation passing through an anisotropic medium having a number density n and a temperature and pressure dependent absorption cross section σ of an absorbing species along the light path s, the measured intensity at wavelength λ is given by

$$I(s, \lambda) = I_0(\lambda) \cdot \exp\left\{-\int_0^s n(s') \cdot \sigma(\lambda, T(s'), p(s')) \cdot \mathrm{d}s'\right\} \tag{1}$$

where the intensity of radiation entering the medium is I_0. For measurements in the atmosphere, this simple model has to be extended by considering multiple trace gases having different absorption cross sections and light scattering on air molecules (Rayleigh scattering), aerosol particles or water droplets (Mie scattering) as well as inelastic scattering by air and trace gas molecules (Raman scattering). The latter is responsible for the Ring effect (Grainger and Ring, 1962), another important extinction process, which can be described by a pseudo cross-section.

The key and original idea of the Differential Optical Absorption Spectroscopy (DOAS) is to separate the optical depth and the absorption cross-sections $\sigma_i(\lambda)$ into a slowly varying function $\sigma_{i,0}(\lambda)$ accounting for elastic scattering and broadband absorption structures and described by a low-order polynomial and a rapidly varying part $\sigma_i'(\lambda)$, the *differential* cross-section, considering the narrow-band absorption structures (Platt and Perner, 1980; Platt and Stutz, 2008). The absorption cross-sections

are measured in the laboratory. Neglecting the temperature and pressure dependence of the absorption cross section, polynomial and differential cross sections are fitted to the measured optical thickness $\ln(I/I_0)$ in the linearized so-called DOAS equation:

$$\ln\left(\frac{I(\lambda)}{I_0(\lambda)}\right) = -\sum_{i=1}^{N} \text{SCD}_i \cdot \sigma_i'(\lambda) - \sum_p c_p \cdot \lambda^p + \text{Residual}(\lambda) \tag{2}$$

The retrieved quantities are the coefficients of the polynomial c_p and the slant column density of the trace gas which is the integrated number density along the light path: $\text{SCD}_i = \int n_i(s)\mathrm{d}s$.

3.2 MAX-DOAS instrument and viewing geometry

The Multi-AXis DOAS (MAX-DOAS) technique (Hönninger et al., 2004; Wittrock et al., 2004) is a passive remote sensing method measuring scattered sunlight. The MAX-DOAS instrument used in this study, comprises of a telescope mounted on a pan-tilt head, an optical fiber bundle, two spectrometers for UV and visible spectral range respectively, equipped with two CCD (charge coupled device) 2D array detectors operated by a computer. The telescope which is attached to the outer sheathing of the circular platform of the Neuwerk radar tower is used to collect the light from a specific viewing direction and to focus the light onto the entrance of the optical fiber. The combination of converging lens and light fiber leads to an field-of-view of about 1°. The pan-tilt head allows the instrument to point in different azimuth angles (panning) as well as different elevation angles (tilting). Dark measurements, which are needed for the determination of the CCD's dark signal are undertaken on a daily basis. Also on a daily basis line lamp measurements are taken using an internally mounted HgCd lamp for the wavelength calibration of the spectra and the determination of the slit function of the instrument. The spectral resolution, represented by the FWHM of the slit function of the instrument, is about 0.4 nm for the UV and 0.7 nm for the visible channel.

The Y-shaped optical light fiber cable is a bundle of 2×38 cylindrical, thin and flexible quartz fibers, guiding the light from the telescope to the two temperature-stabilized spectrometers with attached CCD detectors inside the weatherproof platform building. Each single fiber has a diameter of 150 μm and is 20 m long.

The UV and visible instrument consist of identical Andor Shamrock SR-303i imaging spectrographs, a grating spectrometer in "Czerny-Turner" design with a focal length of 303 mm. The gratings in use are different, the UV instrument is equipped with a 1200 grooves/mm, 300 nm blaze angle grating and the visible instrument with a 600 grooves/mm, 500 nm blaze angle grating. The UV instrument covers the wavelength range 304.6–371.7 nm, the visible spectrometer covers 398.8–536.7 nm. For the UV, a Princeton NTE/CCD 1340/400-EMB detector with a resolution of 1340×400 pixels and a pixel size of 20×20 microns, cooled to $-35\,°C$, is used. For the visible spectral range, an Andor iDus DV420-BU back-illuminated CCD detector with a resolution of 1024×255 pixels and a pixel size of 26×26 microns, cooled as well to $-35\,°C$, is used.

The measurement geometry for the ground-based MAX-DOAS measurements on Neuwerk is sketched in Fig. 5. To measure ship emissions, the telescope is pointed towards the horizon, collecting light that passed directly through the emitted ship plumes. A close-in-time zenith sky measurement is used as a reference so that the retrieved tropospheric differential slant column density (DSCD) is the difference of the slant column densities (SCD) along the two paths 1 and 2 in Fig. 5: $\text{DSCD} = \text{SCD}_1 - \text{SCD}_2 = \text{SCD}_{\text{off-axis}} - \text{SCD}_{\text{reference}}$. The stratospheric light path and trace gas absorption is approximately the same for both measurements and therefore cancels out which is important for NO_2 which is also present in the stratosphere. This approach also minimizes possible instrumental artifacts.

The assumption that the vertical part of the light path cancels out when taking the difference between off-axis and zenith sky (reference) measurement off course is only valid if the NO_2 in the air
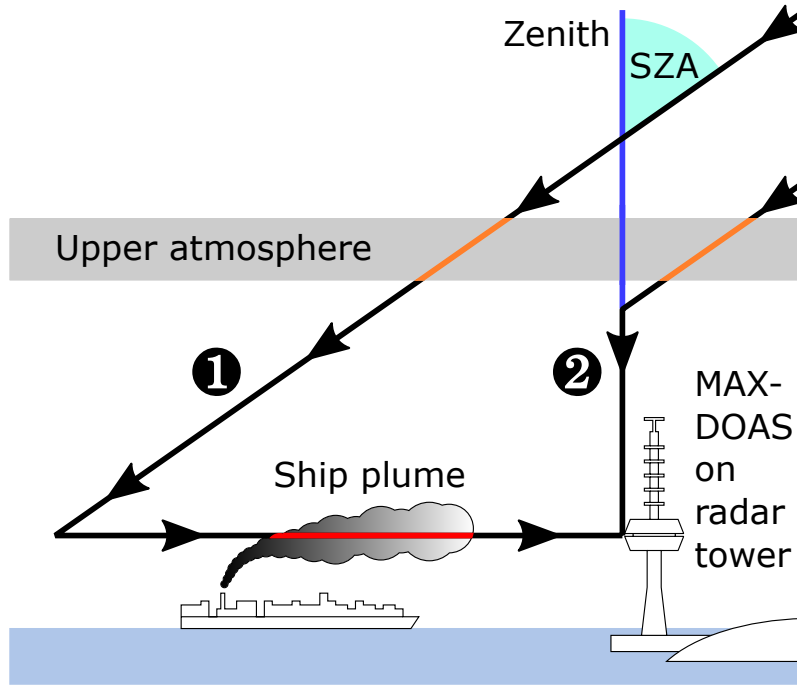
Figure 5: Measurement geometry for MAX-DOAS measurements on Neuwerk with schematic light paths for off-axis (1) and zenith sky reference measurements (2) for an exemplary solar zenith angle (SZA) of 55°

above the instrument, which is of no interest to us here, is spatially homogeneously distributed. This is usually the case for stratospheric NO_2. If a spatially limited pollution plume from point sources like ships or power plants is blown above the radar tower and no plume is in the horizontal light path, the mentioned assumption is violated, leading to an underestimation of the derived DSCD. Also clouds or fog can make the interpretation of the measured DSCD more challenging due to multiple scattering.

3.3 DOAS data analysis and fit settings

The recorded spectra are spectrally calibrated using a daily acquired HgCd line lamp spectrum and the dark signal of the CCD detector is corrected using daily nighttime dark measurements. The logarithm of the ratio of measured off-axis (viewing towards the horizon) spectrum and reference (zenith sky) spectrum gives the optical thickness (also called optical depth) for the DOAS equation (2). Multiple (differential) trace gas absorption cross sections obtained from laboratory measurements, as well as a low-order polynomial, are then fitted simultaneously to the optical depth. The retrieved fit parameters are the slant column densities of the various absorbers and the coefficients of the polynomial. The fits were performed with the software NLIN_D (Richter, 1997).

The settings and fitted absorbers vary according to the spectral range used. For the retrieval of NO_2 in the UV, a fitting window of 338–370 nm was used and for NO_2 in the visible a fitting window of 425–497 nm, both adapted from experiences during the CINDI (Roscoe et al., 2010) and MAD-CAT (http://joseba.mpch-mainz.mpg.de/mad_cat.htm) inter-comparison campaigns. The oxygen-collision complex O_2–O_2, often denoted as O_4, is simultaneously retrieved from both NO_2 fits. The fit parameters for the DOAS fit of NO_2 and SO_2 are summarized in detail in Table 1.

For the retrieval of SO_2, several different fitting windows between 303 and 325 nm have been used in previous ground-based studies (Bobrowski and Platt, 2007; Galle et al., 2010; Irie et al., 2011; Lee et al., 2008; Wang et al., 2014a). This results from the need to find a compromise between the

low light intensity caused by the strong ozone absorption around 300 nm on the one hand and the rapid decrease of the differential absorption of SO_2 at higher wavelengths on the other hand, limiting the choice of the fitting window. In this study, a fitting window of 307.5–317.5 nm was found as the optimal range for our instrument, which is similar to recommendations in Wang et al. (2014a). The fit parameters for the DOAS fit of SO_2 are summarized in detail in Table 2.

Only SO_2 measurements with a RMS lower than 2.5×10^{-3} have been taken into account for the statistics, filtering out bad fits with ozone interferences in low light and bad weather conditions.

Under optimal conditions, the typical fit RMS is around 1×10^{-4} for NO_2 in the visible, 2×10^{-4} for NO_2 in the UV and 5×10^{-4} for SO_2. By assuming that an optical density of twice the RMS can be detected (Peters, 2013), it is possible to estimate the detection limit of our instrument regarding the different trace gases. The differential absorption cross section of NO_2 is in the oder of $1 \times 10^{-19}\,\mathrm{cm^2/molec}$, for SO_2 in the order of $2 \times 10^{-19}\,\mathrm{cm^2/molec}$. Combining this yields a NO_2 detection limit of around $1 \times 10^{15}\,\mathrm{molec/cm^2}$ corresponding to 0.05 pbb in the visible and $2 \times 10^{15}\,\mathrm{molec/cm^2}$ corresponding to 0.1 pbb in the UV. The SO_2 detection limit lies around $2.5 \times 10^{16}\,\mathrm{molec/cm^2}$ corresponding to 0.2 pbb. The typical absolute fit errors are $2 - 3 \times 10^{14}\,\mathrm{molec/cm^2}$ for NO_2 in the visible, $5 - 6 \times 10^{14}\,\mathrm{molec/cm^2}$ for NO_2 in the UV and $2 \times 10^{15}\,\mathrm{molec/cm^2}$ for SO_2, a factor of 5 to 10 smaller than the detection limit.

Table 1: DOAS fit settings for the retrieval of NO_2 and O_4 in UV and visible spectral range

Parameter	NO_2 (UV)	NO_2 (visible)
Fitting window	338–370 nm	425–497 nm
Polynomial degree	4	3
Intensity offset	Constant	Constant
Zenith reference	Coinciding zenith measurement[1]	Coinciding zenith measurement[1]
SZA range	Up to 85° SZA	Up to 85° SZA
O_3	223 K & 243 K (Serdyuchenko et al., 2014)	223 K (Serdyuchenko et al., 2014)
NO_2	298 K (Vandaele et al., 1996)	298 K (Vandaele et al., 1996)
O_4	293 K (Thalman and Volkamer, 2013)	293 K (Thalman and Volkamer, 2013)
H_2O	–	293 K (Lampel et al., 2015)
HCHO	297 K (Meller and Moortgat, 2000)	–
Ring	SCIATRAN (Rozanov et al., 2014)	SCIATRAN (Rozanov et al., 2014)

[1] Interpolation in time between the zenith measurements directly before and after the off-axis scan.

Table 2: DOAS fit settings for the retrieval of SO$_2$

Parameter	SO$_2$ (UV)
Fitting window	307.5–317.5 nm
Polynomial degree	3
Intensity offset	Constant & slope
Zenith reference	Coinciding zenith measurement[1]
SZA range	Up to 75° SZA
O$_3$	223 K & 243 K (Serdyuchenko et al., 2014)
NO$_2$	298 K (Vandaele et al., 1996)
SO$_2$	293 K (Bogumil et al., 2003)
Ring	SCIATRAN (Rozanov et al., 2014)

[1] Interpolation in time between the zenith measurements directly before and after the off-axis scan.

3.4 Retrieval of path-averaged near-surface VMRs from MAX-DOAS SCDs

To measure shipping emissions at our measurement site, our MAX-DOAS telescope is pointed towards the horizon, where the ships pass our site in a distance of 6–7 km. Since our instrument has a field-of-view of approximately 1°, the lowest usable elevation angle avoiding looking onto the ground is 0.5°, providing us with the highest sensitivity to near-surface pollutants. This is the elevation in which at our site usually the highest slant columns are measured. To convert a MAX-DOAS trace gas column which is the concentration of the absorber integrated along the effective light path into concentrations or volume mixing ratios, the length of this light path has to be known. This effective light path length depends on the atmospheric visibility, which is limited by scattering on air molecules as well as aerosols. As described in Section 3.2, trace gas absorptions in the higher atmosphere like stratospheric NO$_2$ nearly cancel out using a close-in-time zenith-sky reference spectrum. Following this, we can assume that the signal for our horizontal line-of-sight is dominated by the horizontal part of the light path after the last scattering event. As introduced by Sinreich et al. (2013), the length L of this horizontal part of the light path can then be estimated using the slant column density of the O$_4$-molecule which has a well-known number density in the atmosphere:

$$L_{O_4} = \frac{\text{SCD}_{O_4,\text{horiz}} - \text{SCD}_{O_4,\text{zenith}}}{n_{O_4}} = \frac{\text{DSCD}_{O_4}}{n_{O_4}} \qquad (3)$$

The surface number density of O$_4$ is proportional to the square of the molecular oxygen concentration (Greenblatt et al., 1990; Wagner et al., 2004) and can be easily calculated from the temperature and pressure measured on the radar tower:

$$n_{O_4} = (n_{O_2})^2 = (0.20942 \cdot n_{\text{air}})^2 \qquad \text{with} \qquad n_{\text{air}} = \frac{N_{\text{air}}}{V_{\text{air}}} = \frac{p_{\text{air}} \cdot k_B}{T_{\text{air}}} = \frac{p_{\text{air}} \cdot N_A}{T_{\text{air}} \cdot R} \qquad (4)$$

with the Boltzmann constant k_B, Avogadro constant N_A and universal gas constant R.

Knowing the path length, it is then possible to calculate the average number density of our trace gas x along this horizontal path and the path-averaged volume mixing ratio:

$$n_x = \frac{\text{SCD}_{x,\text{horiz}} - \text{SCD}_{x,\text{zenith}}}{L_{\text{O}_4}} = \frac{\text{DSCD}_x}{L_{\text{O}_4}} \qquad \text{and} \qquad \text{VMR}_x = \frac{n_x}{n_{\text{air}}} \tag{5}$$

This O_4-scaling in principle takes into account the actual light path and its variation with aerosol loading and also needs no assumption on the typical mixing layer height, therefore overcoming the disadvantages of a simple geometric approximation.

However, when the atmospheric profile of the investigated trace gas x has a shape that differs from that of the proxy O_4, systematic errors are introduced as has been shown by Sinreich et al. (2013) and Wang et al. (2014b) in extensive and comprehensive radiative transfer model (RTM) simulations. Pollutants like NO_2 and SO_2 have a profile shape very different from O_4. They are emitted close to the ground (e.g. from ships), have high concentrations in low altitude layers and tend to decrease very rapidly with height above the boundary layer. They are often approximated as box profiles, while the O_4 concentration simply decreases exponentially with altitude. This difference in profile shapes violates the basic assumption that the O_4 DSCD is a good proxy for the light path through the NO_2 and SO_2 layers. The resulting near-surface volume mixing ratios will not be representative for the amount of trace gases directly at the surface, but for some kind of average over a certain height range in the boundary layer.

The studies like Sinreich et al. (2013) and Wang et al. (2014b) use correction factors from radiative transfer calculations to account for this. These correction factors depend on the amount of aerosols present in the atmosphere, often described by the aerosol optical density (AOD), the solar zenith angle (SZA) as well as the relative solar azimuth angle (RSAA), the height of the pollutant box profile and the extend and vertical position of the aerosol layer in relation to this box profile (Sinreich et al., 2013). The strong dependence of the correction factors on the height of the box profile for trace gas layer heights of less than 1 km makes it necessary for the application of the suggested parameterization method to have additional knowledge about the trace gas layer height, ideally from measurements (e.g. LIDAR) or otherwise from estimations. The use of this method for low boundary layer heights below 500 m without knowing the actual height is not recommended by the authors (Sinreich et al., 2013).

At our measurement site, no additional knowledge (measurements) about the height of the NO_2 and SO_2 layers is available and the trace gay layer heights are typically around 200–300 m. A comparison of the uncorrected MAX-DOAS VMRs retrieved with the upper equations to our simultaneous in-situ measurements (see Section 4.5) confirms the need for a correction factor but also shows that the scaling factor needed changes from day to day as well as during the course of the day. This indicates, that the NO_2 and SO_2 layer height is very variable, depending on wind speed, wind direction, atmospheric conditions and chemistry. The lack of comparability between both measurement techniques and geometries, which is further discussed in Section 4.5, prevents us from estimating diurnally varying correction factors from this.

The non-consideration of these scaling factors will lead to a systematic overestimation of the effective horizontal path length and therefore to a systematic underestimation of MAX-DOAS VMRs, up to a factor of three (Sinreich et al., 2013; Wang et al., 2014b).

In summary, a detailed radiative transfer study for the determination of the right correction factors is out of scope of this study which focuses on the statistic evaluation of a three year dataset of shipping emission measurements in the German Bight. Therefore, when in the following MAX-DOAS VMRs are shown, it has to be kept in mind that these are uncorrected VMRs obtained by above formulas.

This approach has been applied successfully by Sinreich et al. (2013) and Wang et al. (2014b) for measurements in urban polluted air masses over Mexico City and the city of Hefei (China) using MAX-DOAS measurements in $1°$ and $3°$ (Sinreich et al., 2013) and only in $1°$ elevation (Wang et al., 2014b), respectively. Gomez et al. (2014) applied this approach to measurements on a high mountain site at

415 the Izaña Atmospheric observatory on Tenerife (Canary Islands), Schreier et al. (2016) at Zugspitze (Germany) and Pico Espejo (Venezuela). Due to the low aerosol amounts in such heights the latter two studies applied the approach without using correction factors. The fact that our instrument is located on a radar tower in a height of about 30 m above totally flat surroundings (the German Wadden Sea) allows an unblocked view to the horizon in all feasible azimuthal viewing directions. This led to the
420 idea of trying to apply this approach to our shipping emission measurements on Neuwerk.

Since the O_4-DSCD is retrieved simultaneously to NO_2 in both the UV and visible DOAS fit for NO_2, this approach can be applied to NO_2 retrieved in both fitting ranges. The approach can also be applied to SO_2, although the difference of light paths due to the different fitting windows in the UV for O_4 (NO_2) and SO_2 introduces an uncertainty which has to be accounted for. Wang et al. (2014b)
425 derived an empirical formula from RTM calculations for a variety of aerosol scenarios to convert the path length at 310 nm from the path length at the O_4 absorption at 360 nm:

$$L_{310} = 0.136 + 0.897 \times L_{360} - 0.023 \times L_{360}^2 \qquad (6)$$

where L_{310} and L_{360} are given in km. This formula was also applied to our measurements to correct the light path length for the SO_2 fitting window. Although this formula has been calculated for polluted sites, the authors state that the deviations for other sites with different conditions are
430 expected to be small (Wang et al., 2014b).

Using equations 3 to 5, several problems can arise from the division by the differential slant column density of O_4. For example if the O_4 DSCD is negative, which can happen at low signal-to-noise-ratio DOAS fits (e.g. under bad weather conditions), the resulting path length will be negative. If at the same time the trace gas DSCD is positive, then the trace gas volume mixing ratio will be negative as
435 well, a non-physical result. However, even when there is no NO_2 or SO_2, there is still some noise and therefore the retrieved VMR are not exactly zero, but scatter around zero, so slightly negative values have to be included when averaging over time to avoid creating a systematic bias. If, on the other hand, the O_4 DSCD is close to zero, the path length will be very small leading to extremely high (positive or negative) mixing ratios which are also unrealistic. To adress both problems, measurements with
440 negative or small retrieved horizontal path lengths are discarded. For the measurements on Neuwerk, with respect to the characteristics of the measurement site, a minimum path length of 5 km seems to be a reasonable limit. This value provides the best compromise between the number of rejected bad measurements and the total number of remaining measurements for NO_2 in UV and visible as well as for SO_2. For statistics on differential slant column densities on the other hand, no such filtering is
445 applied since negative values are not unphysical in this case and just mean that there is more trace gas absorption in the reference measurement than in the off-axis measurement.

3.5 In-situ instrumentation

In addition to the MAX-DOAS instrument, also in-situ observations are taken, using the Airpointer, a commercially available system which combines four different instruments in a compact, air-conditioned
450 housing. The manufacturer is recordum (Austria), distributed by MLU (`http://mlu.eu/recordum-airpointer/`). The Airpointer device measures carbon dioxide (CO_2), nitrogen oxides ($NO_x = NO + NO_2$), sulfur dioxide (SO_2) and ozone (O_3) using standard procedures. Table 3 shows more detailed information about the different included instruments, their measurement methods, precision, and time resolution.

455 In this study the in-situ 1-minute-means of all compounds were used. NO_2 itself is not directly measured but calculated internally by subtracting the measured NO from the measured NO_x concentration.

Table 3: Airpointer in-situ device: measured trace gases, corresponding measuring techniques, measuring ranges and detection limits [Source: recordum/MLU (manufacturer), `http://mlu.eu/recordum-airpointer/`]

Trace gas	CO_2	O_3	NO, NO_2	SO_2
Measuring technique	Non-dispersive IR spectroscopy LI-COR LI820	UV absorption (EN 14625)	NO Chemi-luminescence (EN 14211)	UV fluorescence (EN 14212)
Detection limit	1 ppm	0.5 ppb	0.4 ppb	0.25 ppb
Measuring range	up to 20 000 ppm	up to 200 ppm	up to 20 ppm	up to 10 ppm
Time resolution	1 s	<30 s	<60 s	<90 s

4 Results

4.1 Measured slant column densities of NO_2 and SO_2

460   In this study, three years of continuous MAX-DOAS measurements on Neuwerk have been evaluated. Figure 6 shows for one example day in summer 2014 the measured differential slant column densities of NO_2 in UV and visible spectral range as well as of SO_2 for the 0.5° elevation angle (viewing to the horizon) and the $-25°$ azimuth angle (approximately NNW direction, see Fig. 1). Sharp peaks in the curves originate from ship emission plumes passing the line of sight of the instrument. On this
465   day, elevated levels of NO_2 have been measured in the morning, corresponding to a polluted air mass coming from land, which appears as an enhanced, slowly varying NO_2 background signal below the peaks. The systematic difference between the NO_2 in the UV (red curve) and the NO_2 in the visible (blue curve) emerges from the longer light-path in the visible due to stronger Rayleigh scattering in the UV (wavelength dependence $\propto \lambda^{-4}$). This is further investigated in Sect. 4.3 below.

470   By comparing SO_2 (green curve) with NO_2 (red and blue curves) it can be seen that for many of the NO_2 peaks there is a corresponding and simultaneous SO_2 peak, but not for all of them. This indicates a varying sulfur content in the fuel of the measured ships. Fuel with higher sulfur content leads to higher SO_2 emissions (see also Sect. 1).

By comparing measurements in different azimuthal viewing directions, the movement direction of
475   the ship (and its plume) can be easily distinguished. The zoom in on the right of Fig. 6 shows the visible NO_2 measurements in different azimuth directions for one example peak from the time series shown on the left. The color-coded viewing directions (see also Fig. 1) are sketched schematically below. From the measurements it can be seen that the emitted plume was consecutively measured in all directions at different times. It was first measured in the easternmost viewing directions and at
480   last in the westernmost direction, indicating that the ship and its plume moved from east to west.

For the identification of sources for air pollution on Neuwerk, the wind direction distribution for the differential slant column densities of NO_2 and SO_2 measured in 2013 and 2014 is plotted for four different elevation angles (0.5°, 2.5°, 4.5° and 30.5°) in Fig. 7. When the wind is coming from the open North Sea (blue shaded sector) the measured NO_2 and SO_2 DSCD are clearly lower than for
485   other directions, for which the wind is coming from the coast (green and yellow shaded sectors) and blows land-based air pollution to the island. The wind direction dependence is more or less similar for both trace gases but with a higher fraction of ship related signals in the overall SO_2 columns. The values are especially high when the wind is coming from the cities of Cuxhaven (ESE direction) and Bremerhaven (SSE) for both NO_2 and SO_2.
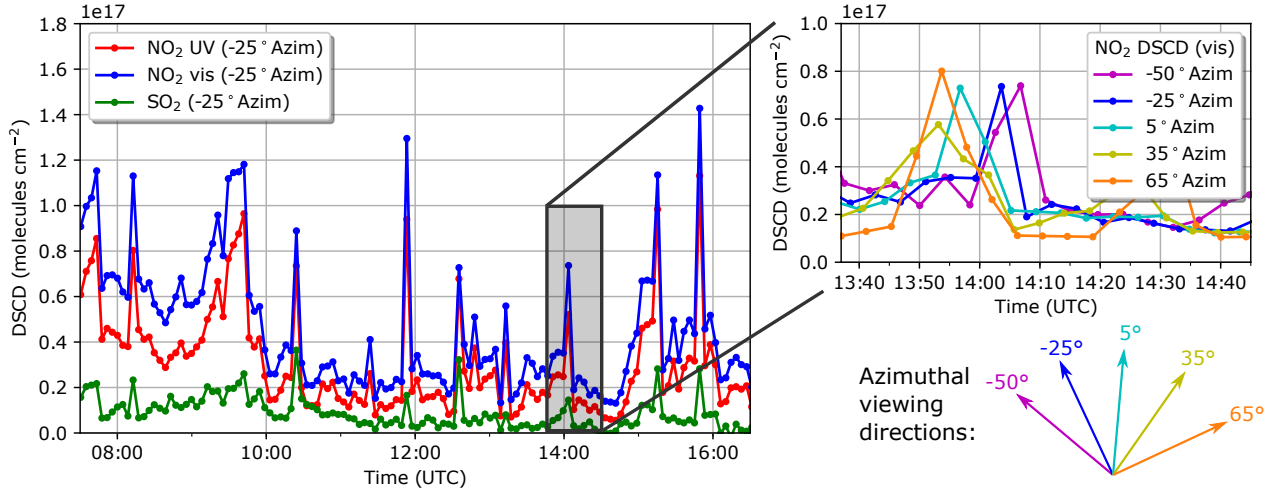
Figure 6: NO$_2$ (UV and visible) and SO$_2$ differential slant column densities measured in 0.5° elevation and the $-25°$ viewing azimuth angle (approximately NNW direction) on Neuwerk on Wednesday, 23 July 2014. The excerpt on the right shows for one example peak the NO$_2$ (vis) measurements in different azimuth viewing directions.

490 Elevation angle sequences of slant columns (i.e. vertical scanning) contain information on the vertical distribution of trace gases. For lower elevation angles, the measured trace gas slant columns for tropospheric absorbers are usually higher because of the longer light path in the boundary layer.

As expected, higher elevations show on average lower DSCDs due to the shorter light path in the boundary layer. The highest NO$_2$ and SO$_2$ DSCD in the lowest elevation angle (0.5°, blue bars) in

495 relation to DSCDs in higher elevations are measured especially for wind from all northern directions, in a sector ranging from WSW to ESE. These directions coincide with the course of the main shipping lane coming from the WSW direction (the English Channel, the Netherlands, East Frisian Islands), passing the island in the north and running close to the city of Cuxhaven (ESE direction) into the river Elbe. This indicates that the enhanced columns in the 0.5° elevation angle is pollution emitted

500 from ships in a surface-near layer.

For southerly wind directions no major shipping lane is in the direct surrounding and land-based pollution sources dominate. The average DSCDs in 0.5° and 2.5° elevation are nearly the same for both NO$_2$ and SO$_2$ indicating that the pollution is located higher up in the troposphere.
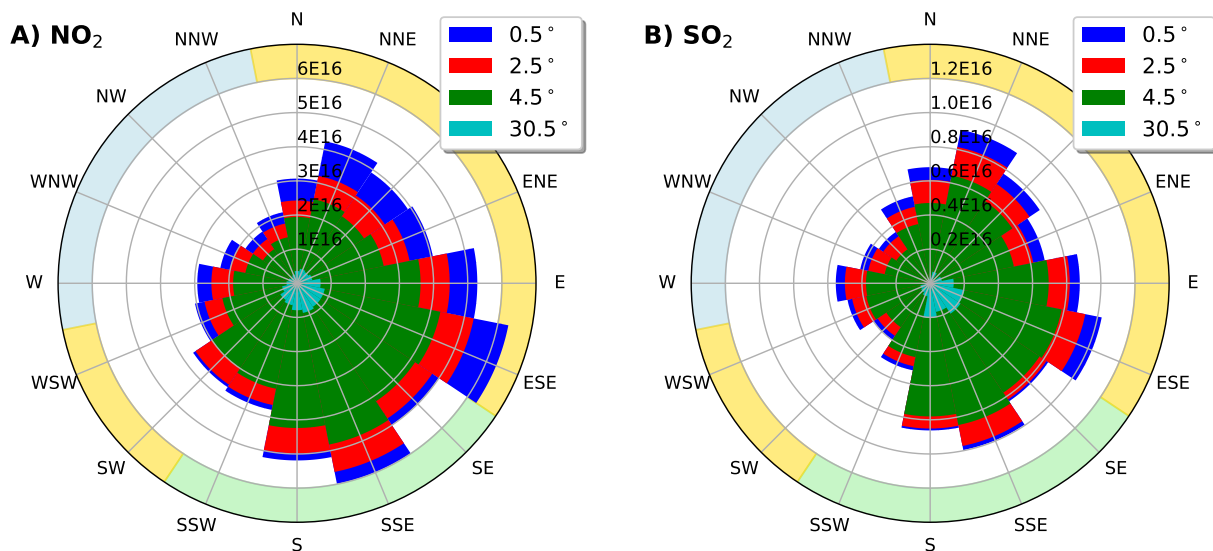
Figure 7: Overlayed wind roses for different elevation angles showing the wind direction distribution of the UV NO_2 (A) and SO_2 (B) differential slant column densities measured in the main viewing direction in 0.5°, 2.5°, 4.5° and 30.5° elevation in the years 2013 and 2014. The wind roses are plotted on top of each other, i.e. the highest values were measured in the lowest elevation angle (blue bars). The colored sectors show directions with wind from land (green), open North Sea (blue) and mixed origin (yellow).

4.2 Volume mixing ratios of NO_2 and SO_2

505 For the example day presented in Fig. 6 the path-averaged volume mixing ratios retrieved with the approach presented in Sect. 3.4 are shown in Fig. 8.

From the mathematics of the approach one would expect a good agreement between the NO_2 volume mixing ratios retrieved in UV and visible if NO_2 is well mixed in the boundary layer, since averaging constant values over different paths should give equal mean values. In the figure, in fact one can see a 510 very good agreement between both NO_2 volume mixing ratios, in particular for situations characterized by background pollution.

Although the light path in the visible spectral range is clearly longer than in the UV, for all the peaks shown here the UV instrument measured a higher path-averaged VMR. The reason for that are spatial inhomogeneities along the line-of-sight.

515 If NO_2 is not distributed homogeneously along the light path, which is the case in the presence of individual ship exhaust plumes, one can expect different values for the means over the two light paths as they probe different parts of the NO_2 field. Such differences can be identified in the figure by looking at the peaks.

The light path in the visible spectral range is longer than in the UV because of more intensive 520 Rayleigh scattering in the UV. The difference between UV and visible peak values depends on the exact location of the plume within the light paths.

A short distance of the plume to the instrument and its complete coverage by the shorter UV path leads to higher values in the UV since the part of the light path probing the higher NO_2 values has a larger relative contribution to the signal than for the longer visible path.

525 If the plume is further away from the instrument and only in the visible path or close to the UV scattering point, one will retrieve a higher volume mixing ratio in the visible. This relationship contains
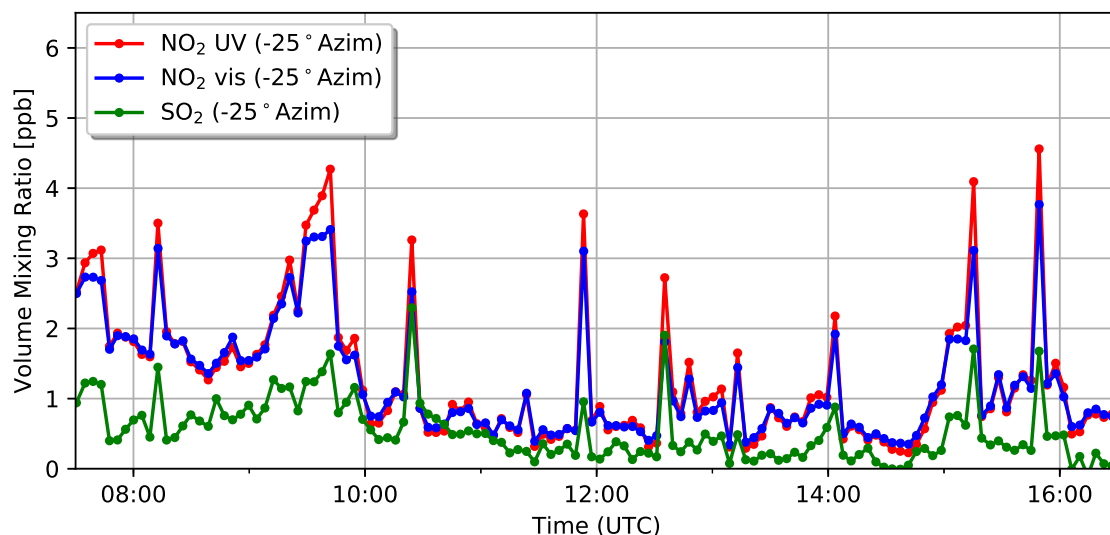
Figure 8: NO_2 (UV and visible) and SO_2 path-averaged volume mixing ratios measured in 0.5° elevation angle and $-25°$ viewing azimuth angle (approximately NNW direction) on Neuwerk on Wednesday, 23 July 2014.

information on the horizontal distribution of the absorber and will be further investigated in a second manuscript.

4.3 Statistical evaluation of UV and visible NO_2 data

530 To investigate quantitatively the relationship between the NO_2 slant column densities measured simultaneously in the UV and visible spectral range, all single pairs of DSCD measurements with an RMS better than 1×10^{-3} are plotted into a scatter plot, shown in Panel A of Fig. 9.

As can be seen from the figure, NO_2 DSCDs in UV and visible are strongly positively correlated with a Pearson correlation coefficient of 0.983. Because of the difference in the horizontal light path
535 lengths in both spectral regions (due to more intense Rayleigh scattering in the UV), the slope of the regression line is 1.30 corresponding to a 30 % longer light path in the visible. The intercept of the regression line is small. Panel B of Fig. 9 shows a histogram of the ratios between both slant column densities. The distribution peaks for ratios of 1.3, in good agreement with the retrieved slope from the scatter plot.

540 When converting the slant column densities to mixing ratios using the O_4-scaling, the dependence on light path should be removed and quantitative agreement is expected between the UV and visible VMRs. A scatter plot for the horizontal path averaged volume mixing ratios is shown in Panel C of Fig. 9. It is clearly visible that the points scatter symmetrically along the 1:1 identity line. Comparing this plot with the plot in Panel A shows that the difference in light path lengths is in fact corrected
545 for by the O_4-scaling approach. The slope of the regression line is close to unity and the intercept is very small. The Pearson correlation coefficient has further increased to 0.984. The histogram (Panel D of Fig. 9) peaks at 1.0.

As discussed above, differences are still expected not only as a result of measurement uncertainties but also due to different averaging volumes in case of inhomogeneous NO_2 distributions (which is
550 especially the case for ship plumes under certain wind directions). For the horizontal light path lengths, a mean value of 9.3 km with a standard deviation of 2.3 km was retrieved in the UV, and a mean value of 12.9 km with a standard deviation of 4.5 km was retrieved in the visible. On days with
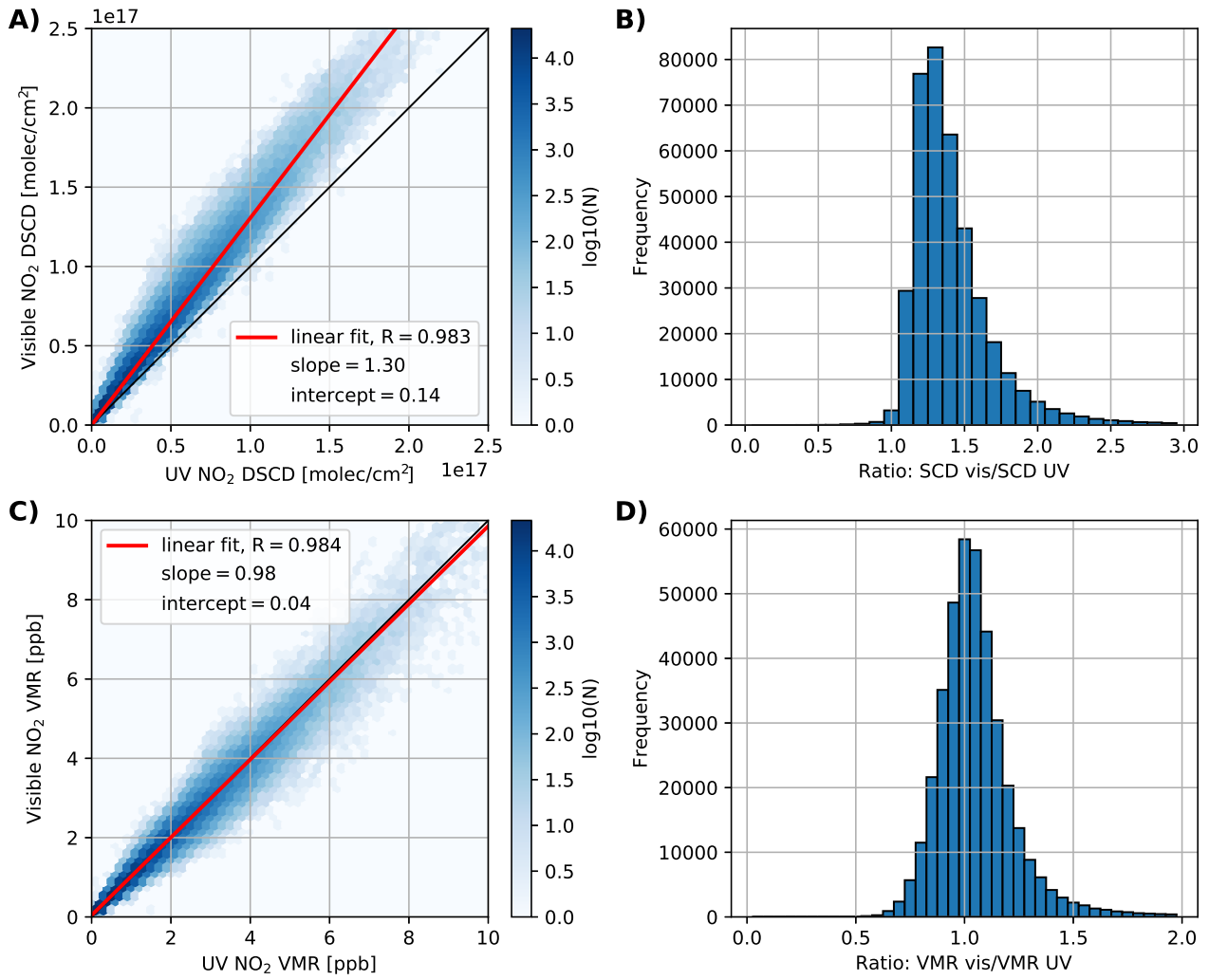
Figure 9: **A**) Scatter plot: NO_2 slant column density retrieved in the visible vs. UV measured in all azimuth angles at 0.5° elevation for solar zenith angles smaller than 75°. The parameters derived from the linear fit by orthogonal distance regression (Deming regression) are also shown. **B**) Histogram of the ratio of the two NO_2 slant column densities (visible/UV). **C**) As A, but for volume mixing ratios. **D**) Histogram of the ratio of the two NO_2 volume mixing ratios (visible/UV).

optimal measurement conditions (clear sky days), typical horizontal light paths are around 10 km in the UV and 15 km in the visible spectral range.

4.4 Allocation of ship emission peaks to ships using wind and AIS data

The detailed information on passing ships transmitted via the *Automatic Identification System* (AIS) and the acquired weather and wind data can be used to allocate the measured pollutant peaks to individual ships.

Measurements from Wednesday, 9 July 2014 are shown in Figure 10. Panel A shows the MAX-DOAS differential slant column density of NO_2. Panel B includes various information about passing ships: The vertical bars indicate when a ship was in the line-of-sight of the MAX-DOAS instrument. Solid bars represent ships coming from the left and going to the right (from west to east, i.e. sailing into the river Elbe), dashed bars vice versa. The colors of the bars indicate the ship length, with small ships shown in blue and very large ships (>350 m) in red. Panel C displays the wind speed and direction.
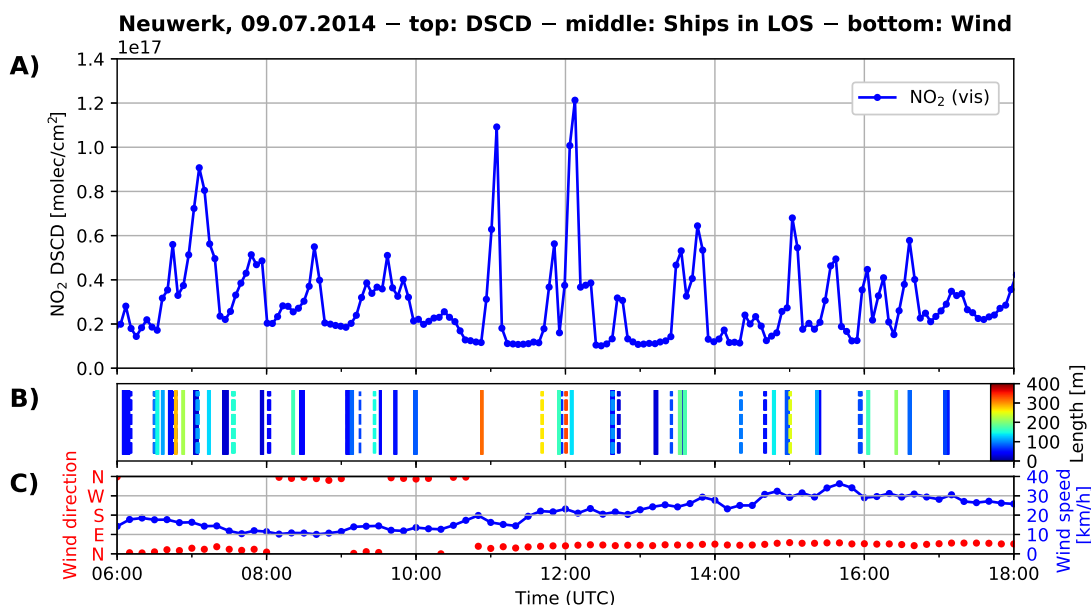

Figure 10: NO_2 differential slant column densities, AIS and wind data for Neuwerk on Wednesday, 9 July 2014.
A) NO_2 DSCD in 0.5° elevation for the 35° azimuth viewing direction
B) Vertical bars indicating that a ship is in the line-of-sight of the instrument, solid bars: ship moves from left to right (west to east), dashed vice versa, colors representing ship length
C) Wind speed and direction measured on Scharhörn (HPA)

On this day, the wind was coming from northern directions, directly from the shipping lane, with moderate wind speeds of 10–35 km/h, resulting in low background pollution values (1–2×10^{16} molecules/cm^2) as well as sharp and distinct ship emission peaks (up to 1.2×10^{17} molecules/cm^2) of NO_2. By comparing the ship emission peak positions to the vertical bars (representing times when ships crossed the MAX-DOAS line-of-sight) in the schematic representation below it can be seen that most of the peaks can be allocated to individual ships. In some cases, when two or more ships simultaneously cross the line-of-sight, the single contributions can not be separated. Large ships (orange and red bars) tend to

exhaust more NO_2 while the contribution of small ships (length $< 30\,\mathrm{m}$) represented by the dark blue bars is usually not measurable.

4.5 Comparison of MAX-DOAS VMR to in-situ measurements

The fact that our measurement site is also equipped with an in-situ device (see Section 3.5 for a description), makes it possible to compare the MAX-DOAS VMRs of NO_2 and SO_2 to our simultaneous in-situ measurements. The differences of both measurement techniques need to be considered for such a comparison: The MAX-DOAS averages over a long horizontal light path, while the in-situ device measures at a single location inside the plume. Since ship plumes usually never cover the whole light path but rather a small fraction of it, very high concentration peaks are usually underestimated in the MAX-DOAS VMR.

Figure 11 shows the horizontal path averaged NO_2 volume mixing ratio retrieved from the differential slant column densities shown in Fig. 10 as well as the in-situ NO_2 volume mixing ratio (Panel A) in combination with ship data (Panel B) and wind data (Panel C).
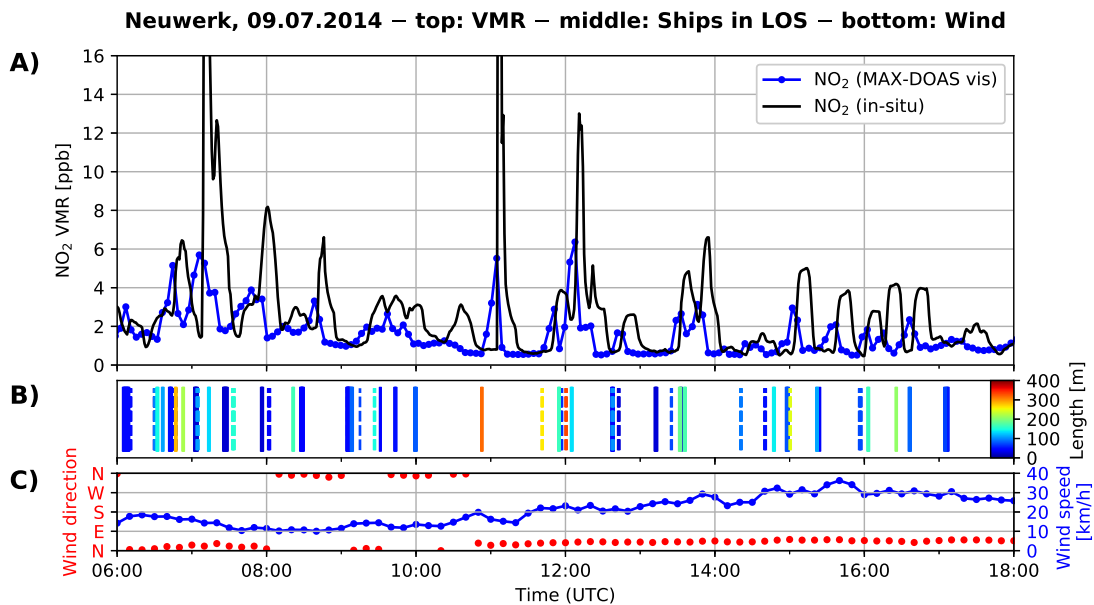

Figure 11: MAX-DOAS and in-situ NO_2 volume mixing ratio, AIS and wind data on Wednesday, 9 July 2014:
A) MAX-DOAS (visible) and in-situ NO_2 VMR
B) Vertical bars indicating that a ship is in the line-of-sight of the instrument, solid bars: ship moves from left to right (west to east), dashed vice versa, colors representing ship length
C) Wind speed and direction measured on Scharhörn (HPA)

Ship emission peaks measured by the in-situ instrument are both higher and broader than the corresponding MAX-DOAS peaks, leading to a considerably larger integrated peak area, showing the systematic underestimation of the NO_2 concentrations inside ship plumes by the MAX-DOAS instrument due to the averaging along the horizontal light path.

Normally, a time-shift between MAX-DOAS and in-situ peaks exists, which is due to the long distance of about 6–$7\,\mathrm{km}$ to the shipping lane, that the plumes have to travel until they reach the radar tower. This time-shift depends on the wind velocity and gets smaller for higher wind speeds. In the figure, this dependency can be seen when comparing the magnitude of the time delay for

measurements in the morning (low wind speeds) and evening (higher wind speeds) This travel time also explains the broader peaks in the in-situ measurements, since the emitted plume spreads and dilutes on its way to the radar tower.

However, if the pollution is horizontally well-mixed in the measured air mass, which is approximately the case for background pollution coming from the coast but not for ship plumes, MAX-DOAS and in-situ instrument should in principle measure the same values. However, as discussed in Section 3.4, correction factors need to be applied to the MAX-DOAS VMRs to account for the different profile shapes of O_4 and the investigated pollutants NO_2 and SO_2, but in our case cannot be determined because no measurements of the height of the NO_2 and SO_2 layer exist. The uncorrected VMRs shown here can be strongly underestimated (up to a factor of 3), because they have been calculated with an overestimated path length. This is the case for background pollution as well as shipping emission measurements.

Since the lack of comparability between both instruments for individual measurements, for a meaningful comparison and the computation of a correlation coefficient at this measurement site an averaging over longer time spans was applied to reduce the impact of the differences between both measurement methods. The fact that MAX-DOAS averages over a large horizontal distance should therefore cancel out on temporal average when comparing to in-situ measurements.

Figure 12 shows in Panel A three months of daily mean NO_2 VMRs from the in-situ and MAX-DOAS UV instrument in summer 2014 and in Panel B due to instrumental problems with the in-situ SO_2 device (see Fig. 4) six weeks of SO_2 daily mean VMRs from summer 2013. To have comparable conditions, for the in-situ instrument all measurements between the start of the MAX-DOAS measurements in the morning (with sunrise) and the end of measurements in the evening (with sunset) have been averaged. The shaded areas show the corresponding standard deviation and indicate the variability during the single days.

The long gap in the SO_2 time series was caused by a power outage.

It is clearly visible that the in-situ NO_2 VMRs are systematically higher than the uncorrected MAX-DOAS VMRs. The scaling factors which would be needed to bring both time series into agreement differ from day to day. A closer look into the individual days shows that these scaling factors also vary over the course of the day, even when wind direction and speed do not change. The scatter plot for this time-series of NO_2 measurements in Fig. 13 Panel A shows a good correlation between MAX-DOAS and in-situ daily means, but a slope strongly deviating from one and also some scatter.

The most important reason for the systematic differences is certainly the non-consideration of the correction factors arising from the different profile shapes of O_4 and NO_2, leading to a systematic underestimation of the VMRs from the MAX-DOAS instrument (see Section 3.4 for a more detailed discussion). But also "light dilution", i.e. light scattered into the line-of-sight between the instrument and the trace gas plume (Kern et al., 2010) might play a role reducing the measured off-axis SCDs .

For SO_2, the daily mean VMRs from MAX-DOAS and in-situ instrument in Fig. 12 Panel B show a much better agreement. The scatter plot in 13 Panel B confirms this with a slope much closer to unity, but more scatter around the fitted line.

The difference in scaling factors for NO_2 and SO_2 can be attributed to plume chemistry. During combustion, mainly nitric oxide (NO) is produced. This has to be converted to NO_2 (through reaction with tropospheric ozone) before it can be measured by the MAX-DOAS instrument. Since the MAX-DOAS instrument sees the ship plumes in an earlier state, the fraction of NO_2 should be lower than in the in-situ measurements, explaining at least a part of the difference.

Although MAX-DOAS and in-situ VMRs show systematic deviations in the absolute values, a very good agreement of the shape (the course) of the curves is found for NO_2 as well as SO_2. This illustrates
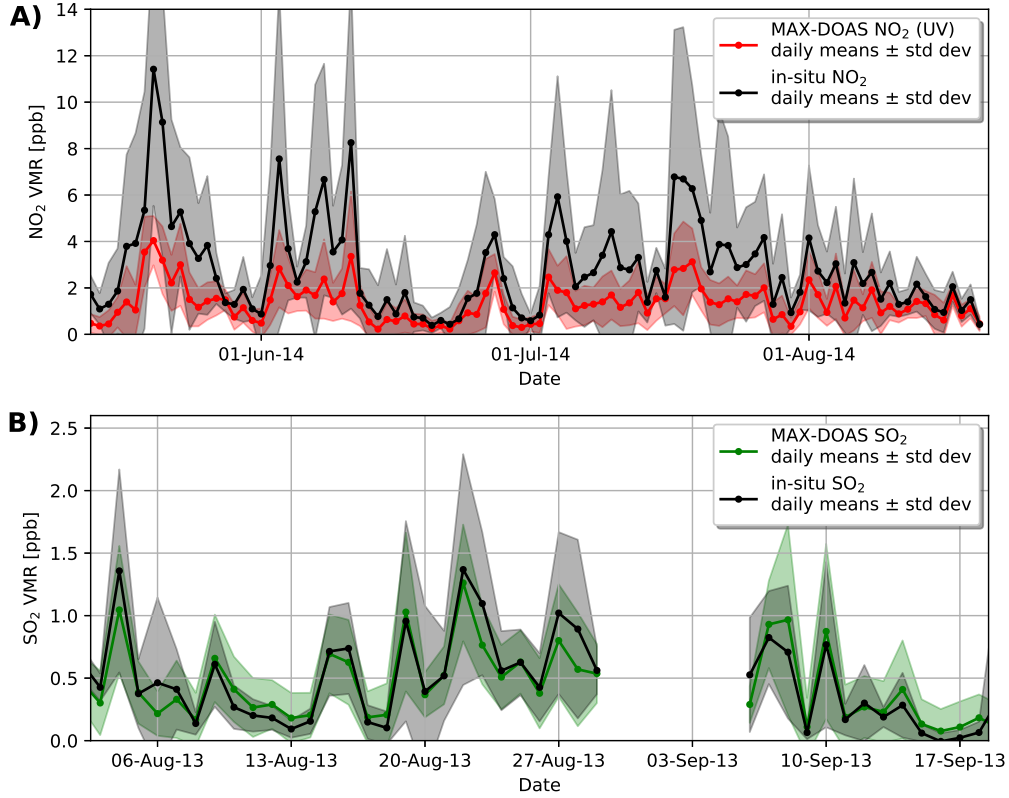
Figure 12: Comparison of MAX-DOAS (UV) and in-situ daily mean VMRs of NO_2 during summer 2014 (A) and SO_2 during summer 2013 (B). Shaded areas show the standard deviation for each daily mean value.

Figure 13: Scatter plot of A) NO_2 VMR and B) SO_2 VMR from MAX-DOAS vs. in-situ. For NO_2 daily means from summer 2014, for SO_2 daily means from summer 2013 are shown. For the MAX-DOAS instrument, to get a better statistic, all measurements in all azimuth viewing directions have been averaged. For the in-situ instrument, the mean of all measurements during the daily MAX-DOAS measurement periods (sunrise till sunset) has been taken. The linear fits were calculated with orthogonal distance regression (Deming regression), parameters are shown in the figures.

640   that MAX-DOAS can determine day-to-day trends as in-situ measurements, even though no correction factors have been applied.

4.6 Diurnal and weekly variability of NO_2

Although our measurement station is located on a small island in the German Bight close to the mouths of the Elbe and Weser river, our measurements are strongly influenced by air pollution from
645   traffic and industry on land, depending on the prevailing wind direction. As can be seen from Fig. 1 A) and 3, wind coming from northeasterly, easterly, southerly and southwesterly directions will blow polluted air masses from the German North Sea Coast and hinterland to our site. In Figure 14 the average diurnal variation of the measured NO_2 volume mixing ratios is shown as hourly mean values. Solid curves show the respective curve for all measurements (with all wind directions), dashed lines
650   show the subset of measurements with wind coming only from the open North Sea with no coastal background pollution. Looking at the diurnal variation in all measurements, the typical daily cycle for road-traffic-influenced air masses with enhanced values in the morning and in the late afternoon during rush hour can be seen. If we restrain the data to periods with wind from the open North Sea (dashed curves), this diurnal cycle vanishes and values are more or less constant over day and also
655   considerably lower. This result is in accordance with the expectations that the amount of ship traffic should be almost independent from the time of day.
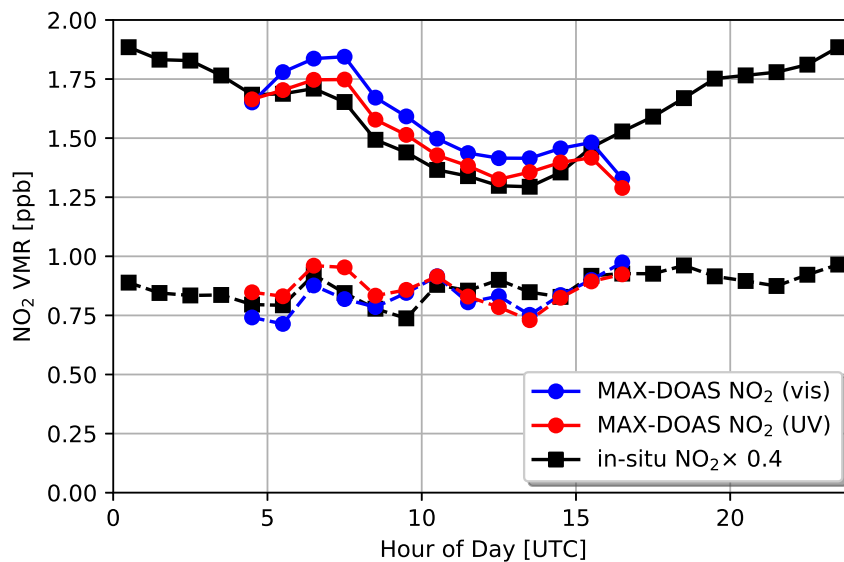

Figure 14: Average diurnal cycle of MAX-DOAS (UV and visible) and in-situ NO_2 volume mixing ratios for all measurements (solid lines) and for a subset of measurements with wind from the open North Sea (dashed lines). For a better visual comparability the in-situ values are scaled by a factor of 0.4.

The mean NO_2 volume mixing ratios for each weekday shown in Fig. 15 illustrate again the influence of land-based road traffic. If we consider the whole time series (solid lines), lowest values are measured on Sundays, when road traffic is less intense. There is only little weekly cycle for air masses coming from
660   the open North Sea (dashed lines). Measurements are more or less constant and again considerably lower. Such a weekly cycle for NO_2 in polluted regions has been observed and discussed several times before, for example in Beirle et al. (2003), Kaynak et al. (2009), Bell et al. (2009) and Ialongo et al. (2016).

It is also remarkable that except for a scaling factor of approximately 0.4, the shape of the diurnal
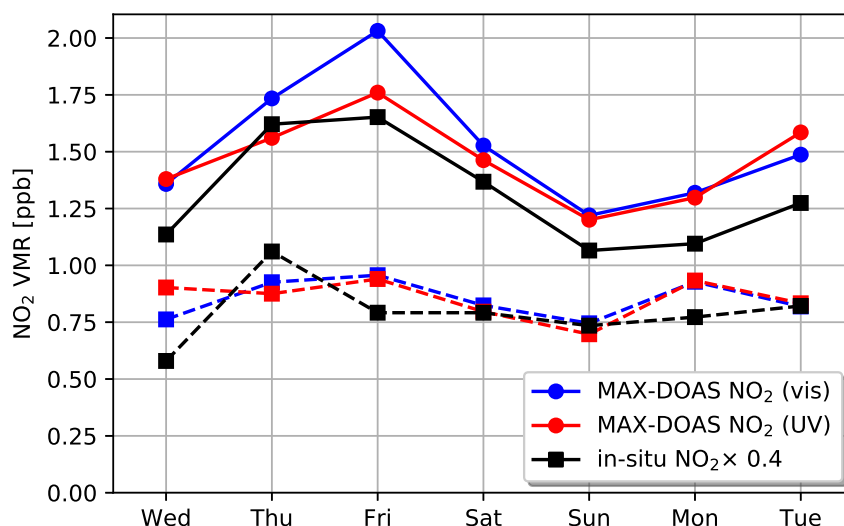
24

Figure 15: Average weekly cycle of MAX-DOAS (UV and visible) and in-situ NO_2 volume mixing ratios for all measurements (solid lines) and for a subset of measurements with wind from the open North Sea (dashed lines). For a better visual comparability the in-situ values are scaled by a factor of 0.4.

665 and weekly cycle retrieved from MAX-DOAS and in-situ measurements agrees very well for both instruments.

4.7 Dependence of NO_2 and SO_2 pollution levels on wind direction

As already mentioned in Sect. 1, on the 1st of January 2015, the sulfur content of marine fuels allowed inside the North and Baltic Sea Emission Control Areas (ECA) has been substantially decreased from 670 1.0 % to 0.1 %. Therefore, one would expect lower sulfur dioxide (SO_2) values in 2015 compared to the years before, especially when the wind is blowing from the open North Sea, where shipping emissions are the only source of SO_2. This expectation is confirmed by the measurements. In the data since 2015, no distinct ship emission peaks are visible anymore (for an example day see Section 4.9 below). For a more detailed analysis, mean values over the whole time series before and after 1 January 2015 675 have been investigated, separated according to the prevailing wind direction.

Two days of SO_2 measurements (20 and 30 October 2014) showing very high values over several hours have been excluded from the time-series. Comparisons with our simultaneous in-situ measurements and measurements from the German Umweltbundesamt at the coast of the North Sea in Westerland/Sylt and at the coast of the Baltic Sea on the island Zingst showing a similar behavior 680 as well as HYSPLIT backward trajectories suggest that on both days SO_2 plumes of the Icelandic volcano Bárdarbunga have influenced the measurements in northern Germany.

Figure 16 shows the wind direction distribution of the mean NO_2 and SO_2 path averaged volume mixing ratios for all measurements before and after the change in fuel sulfur limit regulations.

For SO_2, a significant decrease is found, particularly for wind directions from West to North with 685 wind from the open North Sea. For this sector, values in 2015 are close to zero. This shows that the new and more restrictive fuel sulfur content limits lead to a clear improvement in coastal air quality. For wind directions with mainly land-based sources, no or only a small decrease is observed.

The typical average SO_2 concentrations measured by the German Federal Environmental Agency (Umweltbundesamt, 2017) in 2016 for rural stations in Northern Germany are around 0.5–1 µg/m^3,
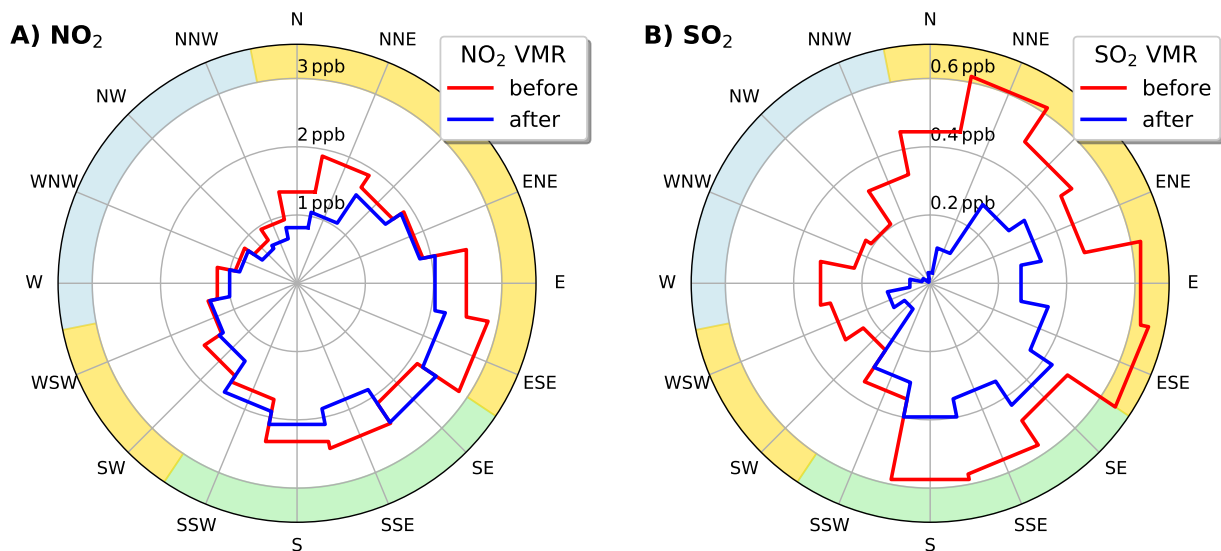
Figure 16: Wind direction distribution of the measured NO$_2$ (A) and SO$_2$ (B) volume mixing ratio in 0.5° elevation before and after the change in fuel sulfur limit regulations on 1 January 2015. The colored sectors show directions with wind mainly from land (green), open North Sea (blue) and mixed origin (yellow).

corresponding to 0.2–0.4 ppb (Conversion factor: 1 ppb $\widehat{=}$ 2.62 µg/m^3 for SO$_2$). Measurements in cities and especially close to industrial areas show higher values. Bremerhaven, which is the station closest to our instrument, has a mean concentration of 1.77 µg/m^3, corresponding to 0.67 ppb. The reported values for rural stations are in good agreement with our measurements of 0.3–0.4 ppb for wind directions with mainly land-based pollution sources (green sector in Fig. 16 Panel B) since January 2015.

For NO$_2$ on the other hand, both the directional distribution and the absolute values are nearly identical for both time periods, implying no considerable changes in NO$_x$ emissions. This result meets the expectations, since no NO$_x$ emission limits have been set into force up to now for the North and Baltic Sea emission control area.

4.8 Contributions of ships vs. land-based pollution sources on coastal air quality on Neuwerk

The distribution of measured NO$_2$ and SO$_2$ volume mixing ratios depending on the wind direction shown in Fig. 16 can be used to estimate the contributions of ships and land-based sources to coastal air pollution levels. To trade ship emissions off against land-based emissions (e.g. industry, road transport), two representative sectors of wind directions have been chosen, both 90 degrees wide: A north-westerly sector (258.75° to 348.75°) with wind from the open North Sea and ships as the only local source of air pollution and a south-easterly sector (123.75° to 213.75°) with wind mainly coming from land and almost no ship traffic. Air masses brought by wind from the other directions, for example from the mouth of the river Elbe in the East of Neuwerk, can contain emissions from land-based pollution sources as well as ship emissions. These remaining directions will be called "mixed" in the following. It is now assumed, that trace gas concentrations measured during periods with wind from one of these sectors have their source in the according sector. For getting a good statistic, measurements in all azimuth angles have been included. Figure 17 shows the results in several pie charts.

Figure 17: Contributions of ships and land-based pollution sources to measured NO_2 (top row) and SO_2 (middle and bottom row) levels on Neuwerk. For NO_2 the complete time series of measurements from 2013 to 2016 has been taken into account, for SO_2 the data have been divided into the time before and after the change in fuel sulfur content limits. The leftmost column of pie plots show the percentage of measurements with wind coming mainly from land (green), only from sea (blue) and from directions with mixed contributions (yellow). The middle column shows the contributions to the integrated, total volume mixing ratios from these source regions in percent. The rightmost column of pie plots shows analogous the percentage and mean VMR contribution by considering only the land and sea sector. It can clearly be seen that the lower fuel sulfur limit lead to a strong decrease in the SO_2 contribution from shipping since 2015.

715   For both NO_2 and SO_2, more than half (around 50–60 %) of all measurements have been taken while wind was coming from either the assigned sea or land sector. This implies that not only a small sample, but the majority of measurements can be used for the estimation of source contributions, making the assumption of using these sectors as representative samples for ships and land-based source regions a reasonable approximation. There are differences in the time series of NO_2 and SO_2 coming from the

720   fact that the SO_2 fit delivers realistic values only up to 75° solar zenith angle and the NO_2 was fitted until 85° SZA, leading to less measurements for SO_2 than for NO_2, especially pronounced in winter times. Despite this, the general distribution pattern of wind direction frequency for NO_2 and SO_2 is quite similar, with wind coming from the sea 32–42 % of the time and from the land sector 18–24 % of the time.

725   For NO_2 (upper row in Fig. 17), more than half of the total NO_2 measured on Neuwerk can be attributed to wind from either of both sectors, with 21 % coming from ships and 31 % coming from land.

    If we consider only the two sectors, for which we can identify the primary sources and take theses as representative, we can say that 40 % of the NO_2 on Neuwerk is coming from shipping emissions,

730   but with 60 %, the majority, is coming from land. One reason for that is that the island Neuwerk is relatively close to the coastline (around 10 km) and is obviously still impacted by polluted air masses from land, which has also been observed in the diurnal and weekly cycle analysis shown in Figures 14 and 15. This might also give us a hint that in coastal regions in Germany land-based sources like road traffic and industry are, despite the heavy ship traffic, the strongest source of air pollution and

735   ship emissions come in second.

    For SO_2 the whole time series of measurements from 2013 to 2016 was divided into two periods of nearly the same length: The first period is 2013 and 2014, which was before the introduction of stricter sulfur limits for maritime fuels in the North Sea on 1 January 2015. The according statistics to this period are shown in the middle row in Fig. 17. The second time period, after the change in

740   fuel sulfur limits, includes all measurements from 2015 and 2016, with the corresponding pie plots in the bottom row of Fig. 17.

    Before the change, 32 % of the measurements were taken when the wind was coming from the sea sector and about 24 % when it was blowing from the dedicated land sector. After the change, the wind was coming a bit more often from sea (42 %) and less often from land (18 %), but in general the

745   situation was quite similar. The contributions of the three sectors (land, sea and mixed) to the total integrated SO_2 with 21 % coming from ships, 30 % from land and 49 % from the mixed sector for the time before the change in sulfur limits are very similar to those of NO_2, too. After the change, the contribution from the sea sector shrinks significantly from 21 to 7 %, while the relative contribution from the land sector increased from 29 to 44 %, the contribution from the mixed sector staying the

750   same as around 49 %. This increase for the land source sector is only a relative increase while the absolute contributions slightly decreased, as can be seen from Fig. 16. The relative contribution from the sea sector (shipping only source) decreased by a factor of 3 while the absolute contribution from this sector decreased by a factor of 8, even though the wind was coincidentally blowing more often from the open sea in this time period.

755   The overall mean SO_2 volume mixing ratio before 2015 is (0.39 ± 0.45) ppb (mean $\pm$ standard deviation). For 2015 and 2016, the total mean value declined by two-thirds to (0.15 ± 0.34) ppb (mean $\pm$ standard deviation).

    These results show clearly that the stricter limitations on the fuel sulfur content are working and significantly improved air quality in the North Sea coastal regions with respect to SO_2. This is in good

760   agreement with other studies such as Kattner et al. (2015), who found that around 95 % of the ships are sticking to the new limits. This implies that the cheaper high sulfur heavy oil fuel is no longer in use in the region of measurement.

If again the two selected sectors are considered as representative for both land and sea sources, the shares of the contributions from sea/land changed from $42\%/58\%$ (which is very similar to those of NO$_2$) to $14\%/86\%$. This again shows that since 2015, the vast majority of SO$_2$ emissions can be attributed to land sources and ships play only a negligible role. Prior to 2015, shipping emissions have been a significant source for SO$_2$ in coastal regions.

One aspect which is neglected in the source allocation to wind sectors is that in situations with good visibility and low wind speeds even for wind coming from southern directions, the MAX-DOAS instrument can measure ship emissions peaks in the north of the island, but being typically very small. Compared to the often strongly enhanced background pollution in cases with southerly winds, the contribution from these peaks is negligible (in the order of a 1–3%), but certainly leads to a small overestimation of land sources.

4.9 Determination of SO$_2$ to NO$_2$ ratios in ship plumes

A monitoring of emissions from single ships requires the analysis of individual plume peaks in the NO$_2$ and SO$_2$ data sets. It is difficult to derive the absolute amounts (e.g. in mass units) of the emitted gaseous pollutants by our MAX-DOAS remote sensing technique. The height and width of the measured peaks does not only depend on the amount of emitted pollutants), but also strongly on the geometry, while getting the highest values when measuring alongside the plumes, and much smaller values when the plume moves orthogonal to the line-of-sight of our instrument. In addition to that, also the time span between emission and measurement plays a role for the height of the NO$_2$ peaks because of NO to NO$_2$ titration.

To determine the mixing ratio inside the plumes, additional information on the length of the light path inside the plume would be needed, which cannot be retrieved from our measurements. This means that without further assumptions, we cannot determine emission factors for the emitted gases (e.g for emission inventories, which are used as input for model simulations).

Although emission factors cannot be measured by MAX-DOAS directly, the NO$_2$ and SO$_2$ signals yield the ratio of both. These ratios can then be compared to ratios of emission factors reported in other studies as well as measurements on other sites or with different instruments, bearing in mind possible deviations due to NO to NO$_2$ titration.

By comparing SO$_2$ to NO$_2$ ratios from different ships it is possible to roughly distinguish whether a ship is using fuel with high or low sulfur content (giving a high or low SO$_2$ to NO$_2$ ratio). Beecken and Mellqvist from Chalmers University (Sweden) use this relationship for airborne DOAS measurements of ship exhaust plumes on an operational basis in the CompMon project (Compliance monitoring pilot for MARPOL Annex VI) (Van Roy, 2016). Following the ships and measuring across the stack gas plume they can discriminate between low (0.1%) and high (1%) fuel sulfur content ships with a probability of 80–90% (Van Roy, 2016).

From the spectra measured by our MAX-DOAS UV instrument both SO$_2$ and NO$_2$ columns can be retrieved at once. The two columns are measured at the exact same time along nearly the same light path. To calculate SO$_2$ to NO$_2$ ratios for the measured pollutant peaks simply the ratio of the measured differential slant column densities has to be computed.

In order to separate ship related signals from smooth background pollution, first a running median filter was applied to the time series of NO$_2$ and SO$_2$ measurements with a large kernel size (e.g. over 21 points). If too many broad peaks are contained in the time series this is not sufficient and the resulting median might be systematically higher than the actual baseline. In this case, on the values in the lower 50% quantile again a running median with a smaller kernel size (e.g. 5) was applied, giving a good approximation of the real baseline.

In the next step, this baseline is subtracted from the raw signal. A simple peak detection algorithm was used to identify the peaks in the baseline-corrected NO_2 signal. Then the corresponding peaks in the SO_2 were assigned, thus accounting for cases when no SO_2 enhancement is measured. In a final manual checkup, all the identified peaks were looked through, filtering out for example all the cases when peaks are too close together to be separated and fine-tuning the baseline detection algorithm parameters if necessary.

To achieve a better signal-to-noise ratio, the integrals over both the NO_2 and SO_2 peak are calculated and the ratio of both values is computed in the last step.

Figure 18 shows the approach as well as the results for an example day in summer 2014, before the stricter fuel sulfur content limits were introduced. Both the NO_2 and SO_2 signal show high and sharp peaks, originating from ship plumes. Most of the peaks are of similar shape in NO_2 as well as SO_2 signal. The measured SO_2 to NO_2 ratios lie in the range from 0.17 to 0.41. The SO_2 to NO_2 ratio can vary strongly for different ships. For example, the plume of the ship passing the line-of-sight around 12:00 UTC has a high NO_2 content, but is low in SO_2, whereas the opposite is true for the ship passing at 12:30 UTC, indicating that the second ship was using fuel with a considerably higher sulfur content than the first one.

Figure 19 shows one example day in summer 2015, after the establishment of stricter sulfur limits. For better comparison to Fig. 18, the y-axis limits are the same. High NO2 peaks also occur on this day. However, the SO_2 signal shows no clearly distinguishable peaks anymore, a result of much less sulfur in the fuel. Consequentially, the measured SO_2 to NO_2 ratios are much smaller on this day and range from 0 to 0.09. There might be some small peaks in the SO_2 signal, but for most of them it cannot be determined if these are real enhancements or just noise fluctuations. The two peaks at 10:40 and 14:00 UTC, slightly above noise level but still very small, might be real SO_2 signals from ships with a higher than average fuel sulfur content.

For a statistically meaningful comparison of both time periods two representative samples of ship emission peaks have been selected by hand for days with good measurement conditions, which were identified by using the solar radiation measurement data of our weather station. One sample of more than 1000 peaks, measured in 2013 and 2014 representing the state before introduction of stricter fuel sulfur content limits, and another equally-sized sample of more than 1000 peaks measured in 2015 and 2016, representing the situation afterwards, were analyzed in a semi-automatic way. It has to be noted that it cannot be ruled out that a certain fraction of ships were measured repeatedly on different days. It is also highly probable that the plume from some individual ships was measured multiple times at different locations in the different azimuth directions while the ship was passing the island.

The distributions of the SO_2 to NO_2 ratios derived from the peak integrals for the two samples are shown in a histogram in Fig. 20. It can be seen that SO_2 to NO_2 ratios were considerably higher before 2015, with a mean of 0.30, a standard deviation of 0.13 and a median value of 0.28. After the change in fuel sulfur content limits, the SO_2 to NO_2 ratios became much lower with a mean of 0.007, a standard deviation of 0.089 and a median value of 0.013, a drastic reduction. A Welch's t-test (unequal variances t-test) shows that the reduction is statistically highly significant. These results can be compared to the overall average SO_2 to NO_2 ratios on all days with good measurement conditions from which the peaks have been selected: For the time before 2015, this gives a mean value of 0.10 and a median of 0.17 and for 2015 and 2016, one gets a mean value of 0.024 and a median of 0.058. As expected, these values are significantly lower than the SO_2 to NO_2 ratios obtained from the ship plumes which do not include background pollution.

It is also interesting to compare our results with those from other studies, bearing in mind possible systematic differences due to different measurement geometries, techniques and sites and therefore different NO to NO_2 titration in the plumes.

Figure 18: Calculation of SO_2 to NO_2 ratios for ship emission peaks for one example day (23.07.2014) before the change in sulfur emission limits. Panel A) shows the UV NO_2-DSCD raw data for $0.5°$ elevation and $-25°$ azimuth and the determined baseline. Panel B) shows the baseline-corrected NO_2 data for which the automatically identified peaks are highlighted with red triangles. Numbers close to the peaks denote the peak integrals in 1×10^{16} molecules/cm^2 (marked in yellow) and the SO_2 to NO_2 ratios (marked in blue). C) and D) show the corresponding plots for SO_2.

Figure 19: As Figure 18 but for an example day (03.07.2015) after the introduction of stricter fuel sulfur content limits. Measurements in 0.5° elevation and 65° azimuth are shown. Peak integrals are given in 10^{16} molecules/cm^2
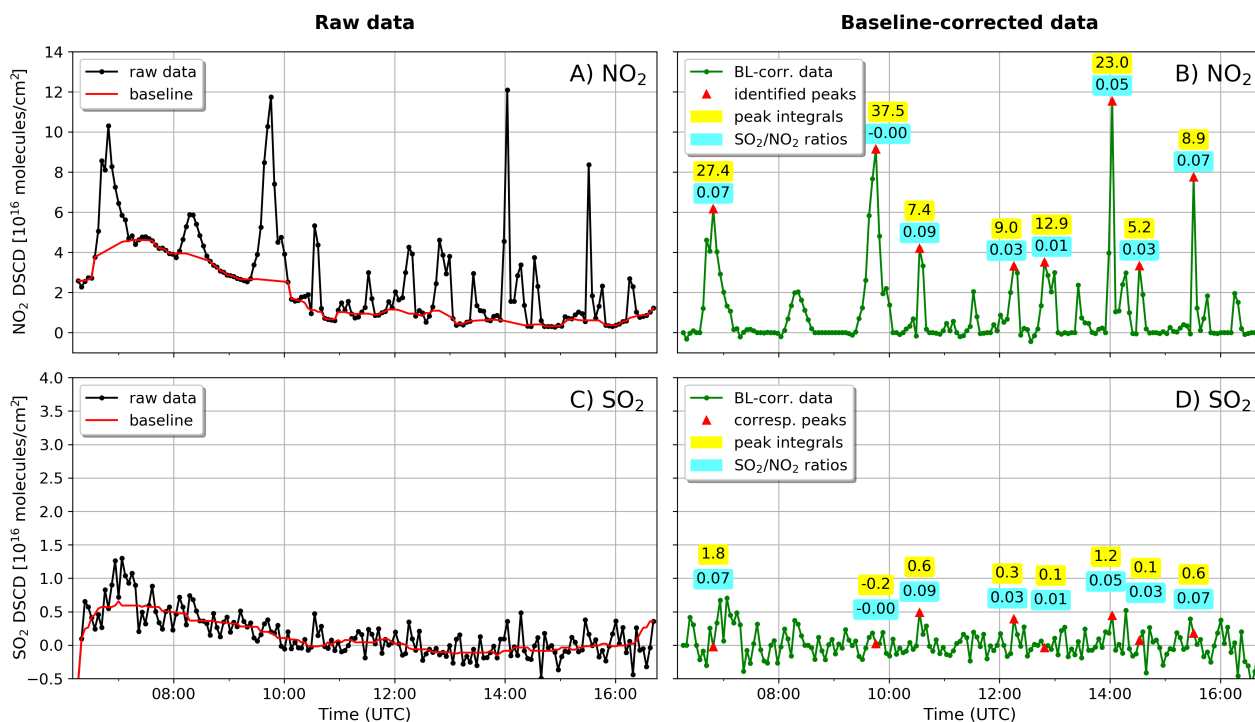
McLaren et al. (2012) measured NO_2 to SO_2 emission ratios in marine vessel plumes in the Strait of Georgia in summer 2005. In a sample of 17 analyzed plumes, a median molar NO_2/SO_2 ratio of 2.86 was found. Translated into a SO_2/NO_2 ratio this yields a value of 0.35 which is, considering the small sample size, in good agreement with our findings for the time before 2015.

Another study was carried out by Diesch et al. (2013) measuring gaseous and particulate emissions from various marine vessel types and a total of 139 ships on the banks of the river Elbe in 2011. SO_2 to NO_2 emission ratios can also be derived from from their reported SO_2 and NO_2 emission factors: For small ships (<5000 tons) a ratio 0.13 and an average fuel sulfur content (FSC) of $(0.22 \pm 0.21)\%$ was found, for medium size ships (5000–30 000 tons) a ratio of 0.24 and a FSC of $(0.46 \pm 0.40)\%$ and for large ships ($>30\,000$ tons) a ratio of 0.28 and a FSC of $(0.55 \pm 0.20)\%$. Especially the values for medium size and large ships fit quite well to our results while plumes from very small vessels (if measurable at all) have often not been taken into account for the statistic because of the low signal-to-noise ratio.

When assuming that the dependency of SO_2 to NO_2 ratio to fuel sulfur content is also applicable to our dataset, we can roughly estimate that the ships measured by us before 2015 used an average sulfur content of 0.5–0.7 %, in good agreement with the results of Kattner et al. (2015), which since 2015 decreased drastically with 0.1 % as an upper limit.
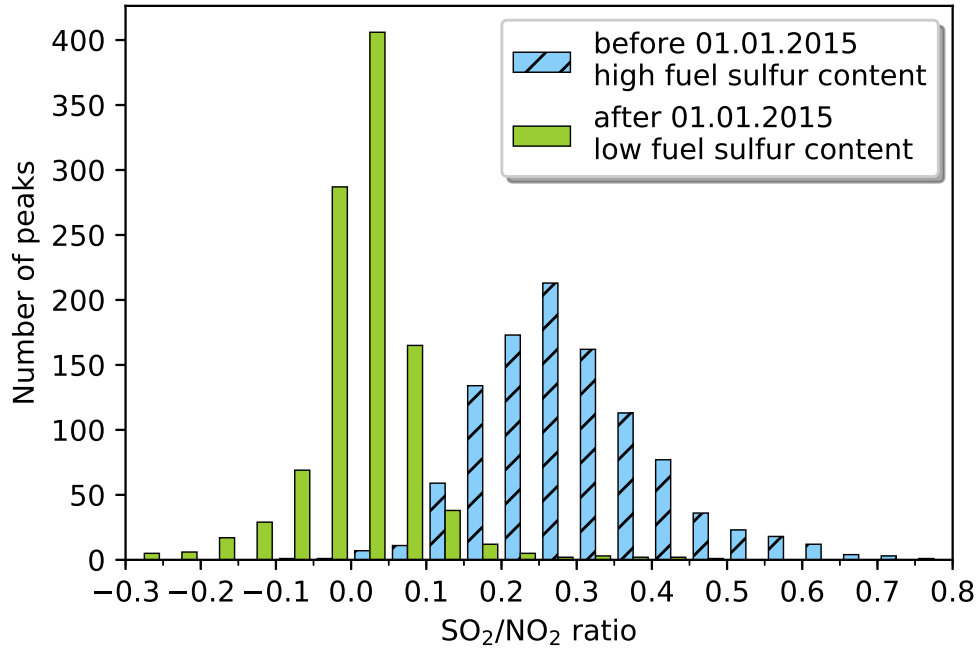
Figure 20: Histogram showing the distribution SO_2 to NO_2 ratios in two samples ($N = 1060$ for each) of ship emission peaks measured in 0.5° elevation and all azimuth angles for the time before (blue) and after (green) the change in fuel sulfur content regulation on the 1st of January 2015.

5 Summary and conclusions

In this study, three years of MAX-DOAS observations of NO_2 and SO_2 taken on the island of Neuwerk close to the shipping lane towards the harbor of Hamburg, Germany were analyzed for pollution emitted from ships. Using measurements taken at 0.5° elevation and different azimuthal directions, both background pollution and plumes from individual ships could be identified. Using simultaneously retrieved O_4 columns, path averaged volume mixing ratios for NO_2 and SO_2 could be determined. Comparison of NO_2 measurements in the UV and visible parts of the spectrum showed excellent agreement between mixing ratios determined from the two retrievals, demonstrating consistency in the results.

MAX-DOAS measurements were also compared to co-located in-situ observations. High correlation was found between mixing ratios derived with the two methods on average, in-situ measurements showing systematically larger values, in particular during ship emission peaks. These deviations can be understood by the difference in measurement volume, the MAX-DOAS measurements averaging over light paths of several kilometers and a systematic underestimation of MAX-DOAS VMRs due to different profile shapes of O_4 and the pollutants NO_2 and SO_2. For NO_2, the difference is larger than for SO_2, probably because of conversion of NO to NO_2 during the transport from the ship where the signal is detected by MAX-DOAS to the measurement site where the in-situ instrument was located.

Although the measurement site is within a few kilometers from one of the main shipping lanes, it is influenced by land based pollution depending on wind direction. Comparing measurements taken under wind direction from the shipping lane and from land, systematic differences in the diurnal and weekly cycles of NO_2 are found. While NO_2 from land shows high values in the morning and evening and lower values around noon and on weekends, NO_2 levels from sea are more or less constant over time as expected from continuous shipping operations. These results are found in both MAX-DOAS

and in-situ observations. Both NO_2 and SO_2 levels are often higher when wind is coming from land, indicating that land based sources contribute significantly to pollution levels on the island in spite of its vicinity to the shipping lanes. Analyzing the wind dependence of the signals in more detail, and excluding data with mixed air mass origin, the contribution of shipping sources to pollution on Neuwerk could be estimated to be 40 % for NO_2 and 41 % for SO_2 in the years 2013 and 2014. As nearly half of the measurements were taken under wind coming from mixed directions, this is only a rough estimate but is still a surprisingly small fraction.

Although the MAX-DOAS measurements cannot be used to directly determine NO_x or SO_2 emissions from individual ships due to the measurement geometry, the ratio of SO_2 to NO_2 column averaged mixing ratios gives a good estimate of the SO_2 to NO_x emission ratio. Using the data from Neuwerk, more than 2000 individual ship emission plumes were identified and the ratio of SO_2 to NO_2 computed after subtraction of the background values. The results varied between ships but on average yielded values of about 0.3 for the years 2013/2014, in good agreement with results from other studies.

Since January 2015, much lower fuel sulfur content limits of 0.1 % apply in the North and Baltic Sea. This resulted in large changes in SO_2 levels in the MAX-DOAS measurements when the wind is coming from the shipping lanes. In fact, ship related SO_2 peaks are rarely observed anymore since 2015. Applying the same analysis as for the period before the change in legislation, no significant changes were found for NO_2 in terms of ratio between ship and land contribution or absolute levels. For SO_2 in contrast overall levels were reduced by two-thirds, and the relative contribution of shipping sources was reduced from 41 % to 14 %. It is interesting to note that a reduction in SO_2 levels was also observed in most wind directions coming from land, presumably because shipping emissions also contributed to SO_2 levels in coastal areas.

In summary, long-term measurements of NO_2 and SO_2 using a MAX-DOAS instrument demonstrated the feasibility of monitoring pollution originating from ships remotely. Pollution signals from individual ships can be identified and path averaged mixing ratios can be determined, which on average correlate well with in-situ observations, reproducing day-to-day trends. MAX-DOAS measurements do not provide emission estimates for individual ships but allow statistical analysis of signals from thousands of ships at a distance and even under unfavorable wind conditions. Implementation of stricter sulfur limits in shipping fuel lead to a large reduction in SO_2/NO_x ratios in shipping emissions and a significant reduction in SO_2 levels at the German coast. The amounts of NO_2 are as expected not significantly impacted by the change of sulfur content in the fuel. This implies that combustion temperatures were probably not significantly changed. The overall contribution of ship emissions to pollution levels at the measurement site is large but land based sources still dominate, even in the immediate vicinity of shipping lanes.

Acknowledgements

References

Alföldy, B., Lööv, J. B., Lagler, F., Mellqvist, J., Berg, N., Beecken, J., Weststrate, H., Duyzer, J., Bencs, L., Horemans, B., Cavalli, F., Putaud, J. P., Janssens-Maenhout, G., Csordás, A. P., Van Grieken, R., Borowiak, A., and Hjorth, J. (2013). "Measurements of air pollution emission factors for marine transportation in SECA". In: *Atmospheric Measurement Techniques* 6.7, pp. 1777–1791. ISSN: 18671381. DOI: 10.5194/amt-6-1777-2013.

Aulinger, A., Matthias, V., Zeretzke, M., Bieser, J., Quante, M., and Backes, A. (2016). "The impact of shipping emissions on air pollution in the greater North Sea region – Part 1: Current emissions and concentrations". In: *Atmospheric Chemistry and Physics* 16.2, pp. 739–758. DOI: 10.5194/acp-16-739-2016. URL: http://www.atmos-chem-phys.net/16/739/2016/.

Balzani Lööv, J. M., Alfoldy, B., Gast, L. F. L., Hjorth, J., Lagler, F., Mellqvist, J., Beecken, J., Berg, N., Duyzer, J., Westrate, H., Swart, D. P. J., Berkhout, A. J. C., Jalkanen, J. P., Prata, A. J., Van Der Hoff, G. R., and Borowiak, A. (2014). "Field test of available methods to measure remotely SOx and NOx emissions from ships". In: *Atmospheric Measurement Techniques* 7.8, pp. 2597–2613. ISSN: 18678548. DOI: 10.5194/amt-7-2597-2014.

Beecken, J., Mellqvist, J., Salo, K., Ekholm, J., and Jalkanen, J. P. (2014). "Airborne emission measurements of SO2, NOx and particles from individual ships using a sniffer technique". In: *Atmospheric Measurement Techniques* 7.7, pp. 1957–1968. ISSN: 18678548. DOI: 10.5194/amt-7-1957-2014.

Beecken, J., Mellqvist, J., Salo, K., Ekholm, J., Jalkanen, J. P., Johansson, L., Litvinenko, V., Volodin, K., and Frank-Kamenetsky, D. A. (2015). "Emission factors of SO2, NOx and particles from ships in Neva Bay from ground-based and helicopter-borne measurements and AIS-based modeling". In: *Atmospheric Chemistry and Physics* 15.9, pp. 5229–5241. ISSN: 16807324. DOI: 10.5194/acp-15-5229-2015.

Beirle, S., Platt, U., Glasow, R. von, Wenig, M., and Wagner, T. (2004). "Estimate of nitrogen oxide emissions from shipping by satellite remote sensing". In: *Geophysical Research Letters* 31.18, pp. 4–7. ISSN: 00948276. DOI: 10.1029/2004GL020312.

Beirle, S., Platt, U., Wenig, M., and Wagner, T. (2003). "Weekly cycle of NO2 by GOME measurements: a signature of anthropogenic sources". In: *Atmospheric Chemistry and Physics* 3.2, pp. 2225–2232. ISSN: 16807324. DOI: 10.5194/acpd-3-3451-2003.

Bell, T. L., Rosenfeld, D., and Kim, K. M. (2009). "Weekly cycle of lightning: Evidence of storm invigoration by pollution". In: *Geophysical Research Letters* 36.23, pp. 1–5. ISSN: 00948276. DOI: 10.1029/2009GL040915.

Berg, N., Mellqvist, J., Jalkanen, J. P., and Balzani, J. (2012). "Ship emissions of SO 2 and NO 2: DOAS measurements from airborne platforms". In: *Atmospheric Measurement Techniques* 5.5, pp. 1085–1098. ISSN: 18671381. DOI: 10.5194/amt-5-1085-2012.

Bobrowski, N. and Platt, U. (2007). "SO2/BrO ratios studied in five volcanic plumes". In: *Journal of Volcanology and Geothermal Research* 166.3-4, pp. 147–160. ISSN: 03770273. DOI: 10.1016/j.jvolgeores.2007.07.003.

Bogumil, K., Orphal, J., Homann, T., Voigt, S., Spietz, P., Fleischmann, O. C., Vogel, A., Hartmann, M., Kromminga, H., Bovensmann, H., Frerick, J., and Burrows, J. P. (2003). "Measurements of molecular absorption spectra with the SCIAMACHY pre-flight model: instrument characterization and reference data for atmospheric remote-sensing in the 230-2380 nm region". In: *Journal of Photochemistry and Photobiology A: Chemistry* 157.2-3, pp. 167–184. ISSN: 10106030. DOI: 10.1016/S1010-6030(03)00062-5. URL: http://linkinghub.elsevier.com/retrieve/pii/S1010603003000625.

Bollmann, M., Bosch, T., Colijn, F., Ebinghaus, R., Körtzinger, A., Latif, M., Matthiessen, B., Melzner, F., Oschlies, A., Petersen, S., Proelß, A., Quaas, M., Requate, T., Reusch, T., Rosenstiel, P., Schrottke, K., Sichelschmidt, H., Siebert, U., Soltwedel, R., Sommer, U., Stattegger, K., Sterr, H., Sturm, R., Treude, T., Vafeidis, A., Bernem, C. van, Beusekom, J. van, Visbeck, M., Wahl, M.,

985   Wallmann, K., and Weinberger, F. (2010). "Living With the Oceans". In: *World Ocean Review: Living with the oceans* 1, p. 236.

Brasseur, G. P. (1999). *Atmospheric chemistry and global change: [a textbook prepared by scientists at the National Center for Atmospheric Research, Boulder].* Topics in environmental chemistry. New York, NY [u.a.]: Oxford Univ. Press. ISBN: 0195105214.

990 Chen, G., Huey, L. G., Trainer, M., Nicks, D., Corbett, J., Ryerson, T., Parrish, D., Neuman, J. A., Nowak, J., Tanner, D., Holloway, J., Brock, C., Crawford, J., Olson, J. R., Sullivan, A., Weber, R., Schauffler, S., Donnelly, S., Atlas, E., Roberts, J., Flocke, F., Hübler, G., and Fehsenfeld, F. (2005). "An investigation of the chemistry of ship emission plumes during ITCT 2002". In: *Journal of Geophysical Research D: Atmospheres* 110.10, pp. 1–15. ISSN: 01480227. DOI: 10.1029/
995   2004JD005236.

Corbett, J. J. and Koehler, H. W. (2003). "Updated emissions from ocean shipping". In: *Journal of Geophysical Research* 108.D20, p. 4650. ISSN: 0148-0227. DOI: 10.1029/2003JD003751. URL: http://doi.wiley.com/10.1029/2003JD003751.

Corbett, J. J., Fischbeck, P. S., and Pandis, S. N. (1999). "Global nitrogen and sulfur inventories for
1000   oceangoing ships". In: *Journal of Geophysical Research* 104.D3, pp. 3457–3470. ISSN: 0148-0227. DOI: 10.1029/1998JD100040.

Corbett, J. J., Winebrake, J. J., Green, E. H., Kasibhatla, P., Eyring, V., and Lauer, A. (2007). "Mortality from ship emissions: A global assessment". In: *Environmental Science and Technology* 41.24, pp. 8512–8518. ISSN: 0013936X. DOI: 10.1021/es071686z.

1005 Diesch, J. M., Drewnick, F., Klimach, T., and Borrmann, S. (2013). "Investigation of gaseous and particulate emissions from various marine vessel types measured on the banks of the Elbe in Northern Germany". In: *Atmospheric Chemistry and Physics* 13.7, pp. 3603–3618. ISSN: 16807316. DOI: 10.5194/acp-13-3603-2013.

DNV (2008). "Marpol 73/78 Annex VI - Regulations of Air Polution from Ships - Technical and
1010   Operational implications". In: *Fuel*, pp. 1–32.

Endresen, Ø., Sørgard, E., Sundet, J., Dalsøren, S., Isaksen, I., and Berglen, T. (2003). "Emission from international sea transportation and environmental impact". In: *Journal of Geophysical Research* 108.D17, pp. 1–22. ISSN: 0148-0227. DOI: 10.1029/2002JD002898.

EU (2005). "Directive 2005/33/EC of the European Parliament and of the Council". In: *Official
1015   Journal of the European Union* 1882, pp. 59–69. DOI: 10.3000/17252555.L_2009.140.eng. URL: http://eur-lex.europa.eu/LexUriServ/LexUriServ.do?uri=OJ:L:2005:191:0059:0069:EN:PDF.

— (2008). "Directive 2008/50/EC of the European Parliament and of the Council of 21 May 2008 on ambient air quality and cleaner air for Europe". In: *Official Journal of the European Communities*
1020   152, pp. 1–43. URL: http://eur-lex.europa.eu/LexUriServ/LexUriServ.do?uri=OJ:L:2008:152:0001:0044:EN:PDF.

— (2016). *Air Quality Standards*. URL: http://ec.europa.eu/environment/air/quality/standards.htm (visited on 12/15/2016).

Eyring, V., Bovensmann, H., Cionni, I., Dall'Amico, M., Franke, K., Khlystova, I., Klinger, C., Lauer,
1025   A., Paxian, A., Righi, M., and Schreier, M. (2010a). *Impact of Ship Emissions on Atmosphere and Climate, SeaKLIM Final Report*. Tech. rep. DLR, p. 23. URL: http://www.pa.op.dlr.de/SeaKLIM/SeaKLIM%7B%5C_%7DNachwuchsgruppe%7B%5C_%7DSchlussbericht%7B%5C_%7DFINAL.pdf.

Eyring, V., Köhler, H. W., Aardenne, J. van, and Lauer, A. (2005a). "Emissions from international
1030   shipping: 1. The last 50 years". In: *Journal of Geophysical Research* 110.D17, p. D17305. ISSN: 0148-0227. DOI: 10.1029/2004JD005619. URL: http://doi.wiley.com/10.1029/2004JD005619.

Eyring, V., Köhler, H. W., Lauer, A., and Lemper, B. (2005b). "Emissions from international shipping: 2. Impact of future technologies on scenarios until 2050". In: *Journal of Geophysical Research* 110.D17, p. D17306. ISSN: 0148-0227. DOI: 10.1029/2004JD005620. URL: http://doi.wiley.
1035   com/10.1029/2004JD005620.

Eyring, V., Isaksen, I. S., Berntsen, T., Collins, W. J., Corbett, J. J., Endresen, O., Grainger, R. G., Moldanova, J., Schlager, H., and Stevenson, D. S. (2010b). "Transport impacts on atmosphere and climate: Shipping". In: *Atmospheric Environment* 44.37, pp. 4735–4771. ISSN: 13522310. DOI: 10.1016/j.atmosenv.2009.04.059. URL: http://linkinghub.elsevier.com/retrieve/pii/S1352231009003379.

Galle, B., Johansson, M., Rivera, C., Zhang, Y., Kihlman, M., Kern, C., Lehmann, T., Platt, U., Arellano, S., and Hidalgo, S. (2010). "Network for Observation of Volcanic and Atmospheric Change (NOVAC) - A global network for volcanic gas monitoring: Network layout and instrument description". In: *Journal of Geophysical Research Atmospheres* 115.D5, pp. 1–19. ISSN: 21698996. DOI: 10.1029/2009JD011823.

Galloway, J. N., Aber, J. D., Erisman, J. W., Seitzinger, S. P., Howarth, R. W., Cowling, E. B., and Cosby, B. J. (2003). "The Nitrogen Cascade". In: *American Institute of Biological Sciences* 53.4, p. 341. ISSN: 0006-3568. DOI: 10.1641/0006-3568(2003)053[0341:TNC]2.0.CO;2. arXiv: arXiv:1011.1669v3. URL: http://www.jstor.org/stable/1314367.

Gomez, L., Navarro-Comas, M., Puentedura, O., Gonzalez, Y., Cuevas, E., and Gil-Ojeda, M. (2014). "Long-path averaged mixing ratios of O3 and NO2 in the free troposphere from mountain MAX-DOAS". In: *Atmospheric Measurement Techniques* 7.10, pp. 3373–3386. ISSN: 18678548. DOI: 10.5194/amt-7-3373-2014.

Grainger, J. F. and Ring, J. (1962). "Anomalous Fraunhofer Line Profiles". In: *Nature* 193, p. 762.

Greenblatt, G. D., Orlando, J. J., Burkholder, J. B., and Ravishankara, A. R. (1990). "Absorption measurements of oxygen between 330 and 1140 nm". In: *Journal of Geophysical Research* 95.D11, p. 18577. ISSN: 0148-0227. DOI: 10.1029/JD095iD11p18577. URL: http://doi.wiley.com/10.1029/JD095iD11p18577.

Hönninger, G., Friedeburg, C. von, and Platt, U. (2004). "Multi axis differential optical absorption spectroscopy (MAX-DOAS)". In: *Atmos. Chem. Phys.* 4, pp. 231–254.

Ialongo, I., Hakkarainen, J., Hyttinen, N., Jalkanen, J. P., Johansson, L., Boersma, K. F., Krotkov, N., and Tamminen, J. (2014). "Characterization of OMI tropospheric NO2 over the Baltic Sea region". In: *Atmospheric Chemistry and Physics* 14.15, pp. 7795–7805. ISSN: 16807324. DOI: 10.5194/acp-14-7795-2014.

Ialongo, I., Herman, J., Krotkov, N., Lamsal, L., Boersma, F., Hovila, J., and Tamminen, J. (2016). "Comparison of OMI NO2 observations and their seasonal and weekly cycles with ground-based measurements in Helsinki". In: *Atmospheric Measurement Techniques Discussions* 2, pp. 1–13. ISSN: 1867-8610. DOI: 10.5194/amt-2016-212. URL: http://www.atmos-meas-tech-discuss.net/amt-2016-212/.

IEA/OECD (2009). *Transport, Energy and CO2 – moving towards sustainability.* Paris: International Energy Agency. ISBN: 9789264073166.

International Air Transport Association (IATA) (2015). "IATA Annual Review 2015". In: p. 62. URL: http://www.iata.org/about/Documents/iata-annual-review-2015.pdf.

Irie, H., Takashima, H., Kanaya, Y., Boersma, K. F., Gast, L., Wittrock, F., Brunner, D., Zhou, Y., and Van Roozendael, M. (2011). "Eight-component retrievals from ground-based MAX-DOAS observations". In: *Atmospheric Measurement Techniques* 4.6, pp. 1027–1044. ISSN: 18671381. DOI: 10.5194/amt-4-1027-2011.

Jonson, J. E., Tarrason, L., and Bartnicki, J. (2000). *Effects of international shipping on European pollution levels. 2000.* Tech. rep. Oslo, Norway: The Norwegian Metrorological Institute.

Kattner, L., Mathieu-Üffing, B., Burrows, J. P., Richter, A., Schmolke, S., Seyler, A., and Wittrock, F. (2015). "Monitoring compliance with sulfur content regulations of shipping fuel by in situ measurements of ship emissions". In: *Atmospheric Chemistry and Physics* 15.17, pp. 10087–10092. ISSN: 1680-7324. DOI: 10.5194/acp-15-10087-2015. URL: http://www.atmos-chem-phys.net/15/10087/2015/.

Kaynak, B., Hu, Y., Martin, R. V., Sioris, C. E., and Russell, a. G. (2009). "Comparison of weekly cycle of NO2 satellite retrievals and NOx emission inventories for the continental United States".

In: *Journal of Geophysical Research: Atmospheres* 114.5, pp. 1–10. ISSN: 01480227. DOI: 10.1029/2008JD010714.

Kern, C., Deutschmann, T., Vogel, L., Wöhrbach, M., Wagner, T., and Platt, U. (2010). "Radiative transfer corrections for accurate spectroscopic measurements of volcanic gas emissions". In: *Bulletin of Volcanology* 72.2, pp. 233–247. ISSN: 02588900. DOI: 10.1007/s00445-009-0313-7.

Lack, D. A., Cappa, C. D., Langridge, J., Bahreini, R., Buffaloe, G., Brock, C., Cerully, K., Coffman, D., Hayden, K., Holloway, J., Lerner, B., Massoli, P., Li, S. M., McLaren, R., Middlebrook, A. M., Moore, R., Nenes, A., Nuaaman, I., Onasch, T. B., Peischl, J., Perring, A., Quinn, P. K., Ryerson, T., Schwartz, J. P., Spackman, R., Wofsy, S. C., Worsnop, D., Xiang, B., and Williams, E. (2011). "Impact of fuel quality regulation and speed reductions on shipping emissions: Implications for climate and air quality". In: *Environmental Science and Technology* 45.20, pp. 9052–9060. ISSN: 0013936X. DOI: 10.1021/es2013424.

Lampel, J., Pohler, D., Tschritter, J., Frieß, U., and Platt, U. (2015). "On the relative absorption strengths of water vapour in the blue wavelength range". In: *Atmospheric Measurement Techniques* 8.10, pp. 4329–4346. ISSN: 18678548. DOI: 10.5194/amt-8-4329-2015.

Lauer, a., Eyring, V., Hendricks, J., Jöckel, P., and Lohmann, U. (2007). "Global model simulations of the impact of ocean-going ships on aerosols, clouds, and the radiation budget". In: *Atmospheric Chemistry and Physics Discussions* 7.4, pp. 9419–9464. ISSN: 1680-7375. DOI: 10.5194/acpd-7-9419-2007.

Lawrence, M. G. and Crutzen, P. J. (1999). "Influence of NOx emissions from ships on tropospheric photochemistry and climate". In: *Nature* 402.6758, pp. 167–170. ISSN: 0028-0836. DOI: 10.1038/46013.

Lee, C., Richter, A., Lee, H., Kim, Y. J., Burrows, J. P., Lee, Y. G., and Choi, B. C. (2008). "Impact of transport of sulfur dioxide from the Asian continent on the air quality over Korea during May 2005". In: *Atmospheric Environment* 42.7, pp. 1461–1475. ISSN: 13522310. DOI: 10.1016/j.atmosenv.2007.11.006.

Masieri, S., Premuda, M., Bortoli, D., Kostadinov, I., Petritoli, A., Ravegnani, F., and Giovanelli, G. (2009). "Cruise ships flow rate emission evaluated by means of a passive DOAS instrument". In: *SPIE Europe Remote Sensing* 7478, 74781S—-74781S—10. DOI: 10.1117/12.830309. URL: http://dx.doi.org/10.1117/12.830309.

Matthias, V., Aulinger, A., Backes, A., Bieser, J., Geyer, B., Quante, M., and Zeretzke, M. (2016). "The impact of shipping emissions on air pollution in the greater North Sea region-Part 2: Scenarios for 2030". In: *Atmospheric Chemistry and Physics* 16.2, pp. 759–776. ISSN: 16807324. DOI: 10.5194/acp-16-759-2016.

McLaren, R., Wojtal, P., Halla, J. D., Mihele, C., and Brook, J. R. (2012). "A survey of NO2:SO2 emission ratios measured in marine vessel plumes in the Strait of Georgia". In: *Atmospheric Environment* 46.2, pp. 655–658. ISSN: 13522310. DOI: 10.1016/j.atmosenv.2011.10.044. URL: http://linkinghub.elsevier.com/retrieve/pii/S135223101101123X.

Meller, R. and Moortgat, G. K. (2000). "Temperature dependence of the absorption cross sections of formaldehyde between 223 and 323 K in the wavelength range 225-375 nm". In: *Journal of Geophysical Research: Atmospheres* 105.D6, pp. 7089–7101. ISSN: 2156-2202. DOI: 10.1029/1999JD901074. URL: http://dx.doi.org/10.1029/1999JD901074.

Pandya, R. J., Solomon, G., Kinner, A., and Balmes, J. R. (2002). "Diesel exhaust and asthma: Hypotheses and molecular mechanisms of action". In: *Environmental Health Perspectives* 110.SUPPL. 1, pp. 103–112. ISSN: 00916765. DOI: 10.1289/ehp.02110s1103.

Peters, E. (2013). "Improved MAX-DOAS measurements and retrievals focused on the marine boundary layer". In: *Ph.D. thesis, University of Bremen*.

Platt, U. and Perner, D. (1980). "Direct measurements of atmospheric CH2O, HNO2, O3, NO2, and SO2 by differential optical absorption in the near UV". In: *Journal of Geophysical Research: Oceans* 85.C12, pp. 7453–7458. ISSN: 2156-2202. DOI: 10.1029/JC085iC12p07453. URL: http://dx.doi.org/10.1029/JC085iC12p07453.

Platt, U. and Stutz, J. (2008). *Differential optical absorption spectroscopy*. Physics of Earth and Space Environments. Berlin ; Heidelberg: Springer, XV, 597 S. ISBN: 3-540-21193-4 ; 978-3-540-21193-8 ; 978-3-540-75776-4.

Prata, A. J. (2014). "Measuring SO2 ship emissions with an ultraviolet imaging camera". In: *Atmospheric Measurement Techniques* 7.5, pp. 1213–1229. ISSN: 18678548. DOI: 10.5194/amt-7-1213-2014.

Premuda, M., Masieri, S., Bortoli, D., Kostadinov, I., Petritoli, A., and Giovanelli, G. (2011). "Evaluation of vessel emissions in a lagoon area with ground based Multi axis DOAS measurements". In: *Atmospheric Environment* 45.29, pp. 5212–5219. ISSN: 13522310. DOI: 10.1016/j.atmosenv.2011.05.067. URL: http://dx.doi.org/10.1016/j.atmosenv.2011.05.067.

Richter, A., Begoin, M., Hilboll, A., and Burrows, J. P. (2011). "An improved NO2 retrieval for the GOME-2 satellite instrument". In: *Atmospheric Measurement Techniques* 4.6, pp. 1147–1159. ISSN: 18671381. DOI: 10.5194/amt-4-1147-2011.

Richter, A. (1997). "Absorptionsspektroskopische Messungen stratosphärischer Spurengase über Bremen, 53° N". PhD Thesis. Göttingen: Universität Bremen. ISBN: 3897120585.

Richter, A., Eyring, V., Burrows, J. P., Bovensmann, H., Lauer, A., Sierk, B., and Crutzen, P. J. (2004). "Satellite measurements of NO2 from international shipping emissions". In: *Geophys. Res. Lett.* 31, p. L23110. ISSN: 0094-8276. DOI: 10.1029/2004GL020822.

Roscoe, H. K., Van Roozendael, M., Fayt, C., Du Piesanie, A., Abuhassan, N., Adams, C., Akrami, M., Cede, A., Chong, J., Clémer, K., Friess, U., Gil Ojeda, M., Goutail, F., Graves, R., Griesfeller, A., Grossmann, K., Hemerijckx, G., Hendrick, F., Herman, J., Hermans, C., Irie, H., Johnston, P. V., Kanaya, Y., Kreher, K., Leigh, R., Merlaud, A., Mount, G. H., Navarro, M., Oetjen, H., Pazmino, A., Perez-Camacho, M., Peters, E., Pinardi, G., Puentedura, O., Richter, A., Schönhardt, A., Shaiganfar, R., Spinei, E., Strong, K., Takashima, H., Vlemmix, T., Vrekoussis, M., Wagner, T., Wittrock, F., Yela, M., Yilmaz, S., Boersma, F., Hains, J., Kroon, M., Piters, A., and Kim, Y. J. (2010). "Intercomparison of slant column measurements of NO2 and O4 by MAX-DOAS and zenith-sky UV and visible spectrometers". In: *Atmospheric Measurement Techniques* 3.6, pp. 1629–1646. ISSN: 18671381. DOI: 10.5194/amt-3-1629-2010.

Rozanov, V. V., Rozanov, A. V., Kokhanovsky, A. A., and Burrows, J. P. (2014). "Radiative transfer through terrestrial atmosphere and ocean: Software package SCIATRAN". In: *Journal of Quantitative Spectroscopy and Radiative Transfer* 133, pp. 13–71. ISSN: 00224073. DOI: 10.1016/j.jqsrt.2013.07.004. URL: http://dx.doi.org/10.1016/j.jqsrt.2013.07.004.

Schreier, S. F., Richter, A., Wittrock, F., and Burrows, J. P. (2016). "Estimates of free-tropospheric NO2 and HCHO mixing ratios derived from high-altitude mountain MAX-DOAS observations in the mid-latitudes and tropics". In: *Atmospheric Chemistry and Physics* 16.5, pp. 2803–2817. ISSN: 16807324. DOI: 10.5194/acp-16-2803-2016.

Seinfeld, J. H. and Pandis, S. N. (2006). *Atmospheric chemistry and physics: from air pollution to climate change*. 2. ed. Hoboken, NJ: Wiley. ISBN: 0471720186 and 9780471720188 and 0471720178 and 9780471720171.

Serdyuchenko, A., Gorshelev, V., Weber, M., Chehade, W., and Burrows, J. P. (2014). "High spectral resolution ozone absorption cross-sections – Part 2: Temperature dependence". In: *Atmospheric Measurement Techniques* 7.2, pp. 625–636. ISSN: 1867-8548. DOI: 10.5194/amt-7-625-2014.

Singh, H. B. (1987). "Reactive nitrogen in the troposphere". In: *Environmental Science & Technology* 21.4, pp. 320–327. ISSN: 0013-936X. DOI: 10.1021/es00158a001.

Sinreich, R., Merten, A., Molina, L., and Volkamer, R. (2013). "Parameterizing radiative transfer to convert MAX-DOAS dSCDs into near-surface box-averaged mixing ratios". In: *Atmospheric Measurement Techniques* 6.6, pp. 1521–1532. ISSN: 18671381. DOI: 10.5194/amt-6-1521-2013.

Statistische Ämter des Bundes und der Länder (Statistikamt Nord) (2015). *Anzahl der Ankünfte von Kreuzfahrtschiffen im Hamburger Hafen in den Jahren 2005 bis 2014*. URL: http://de.statista.com/statistik/daten/studie/29729/umfrage/ankuenfte-von-kreuzfahrtschiffen-in-hamburg/.

Thalman, R. and Volkamer, R. (2013). "Temperature dependent absorption cross-sections of O2-O2 collision pairs between 340 and 630 nm and at atmospherically relevant pressure." In: *Physical chemistry chemical physics* 15, pp. 15371–15381. ISSN: 1463-9084. DOI: 10.1039/c3cp50968k. URL: http://www.ncbi.nlm.nih.gov/pubmed/23928555.

Umweltbundesamt (2017). *Aktuelle Luftdaten.* URL: https://www.umweltbundesamt.de/daten/luftbelastung/aktuelle-luftdaten (visited on 05/16/2017).

UNCTAD (2014). *Review of Maritime Transport 2014*, p. 34. ISBN: 9789211128789. URL: http://unctad.org/en/PublicationsLibrary/rmt2014%7B%5C_%7Den.pdf.

— (2015). *Review of Maritime Transport 2015*. October. ISBN: 978-92-1-112892-5. URL: http://unctad.org/en/PublicationsLibrary/rmt2015%7B%5C_%7Den.pdf.

Van Roy, W. (2016). "Best Practices Airborne MARPOL Annex VI Monitoring". In: URL: https://www.trafi.fi/filebank/a/1482762219/d80cdd7de80e58885ce5a4dd0af86c02/23541-Best%7B%5C_%7DPractices%7B%5C_%7DAirborne%7B%5C_%7DMARPOL%7B%5C_%7DAnnex%7B%5C_%7DVI%7B%5C_%7DMonitoring.pdf.

Vandaele, A. C., Hermans, C., Simon, P. C., Roozendael, M. V., Guilmot, J. M., Carleer, M., and Colin, R. (1996). "Fourier Transform Measurement of NO2 Absorption Cross-Section in the Visible Range at Room Temperature". In: *J. Atmos. Chem.* 25, pp. 289–305.

Vinken, G. C. M., Boersma, K. F., Donkelaar, A. van, and Zhang, L. (2014). "Constraints on ship NOx emissions in Europe using GEOS-Chem and OMI satellite NO2 observations". In: *Atmospheric Chemistry and Physics* 14.3, pp. 1353–1369. ISSN: 1680-7324. DOI: 10.5194/acp-14-1353-2014. URL: http://www.atmos-chem-phys.net/14/1353/2014/acp-14-1353-2014.html.

Wagner, T., Dix, B., Friedeburg, C. V., Frieß, U., Sanghavi, S., Sinreich, R., and Platt, U. (2004). "MAX-DOAS O4 measurements: A new technique to derive information on atmospheric aerosols - Principles and information content". In: *Journal of Geophysical Research D: Atmospheres* 109.22, pp. 1–19. ISSN: 01480227. DOI: 10.1029/2004JD004904.

Wang, T., Hendrick, F., Wang, P., Tang, G., Clémer, K., Yu, H., Fayt, C., Hermans, C., Gielen, C., Müller, J. F., Pinardi, G., Theys, N., Brenot, H., and Van Roozendael, M. (2014a). "Evaluation of tropospheric SO2 retrieved from MAX-DOAS measurements in Xianghe, China". In: *Atmospheric Chemistry and Physics* 14.20, pp. 11149–11164. ISSN: 16807324. DOI: 10.5194/acp-14-11149-2014.

Wang, Y., Li, A., Xie, P. H., Wagner, T., Chen, H., Liu, W. Q., and Liu, J. G. (2014b). "A rapid method to derive horizontal distributions of trace gases and aerosols near the surface using multi-axis differential optical absorption spectroscopy". In: *Atmospheric Measurement Techniques* 7.6, pp. 1663–1680. ISSN: 18678548. DOI: 10.5194/amt-7-1663-2014.

Wayne, R. P. (2006). *Chemistry of atmospheres: an introduction to the chemistry of the atmospheres of earth, the planets, and their satellites.* 3. ed., re. Oxford [u.a.]: Oxford Univ. Press. ISBN: 019850375X and 9780198503750.

WHO (2006). *Air Quality Guidelines: Global Update 2005 : Particulate Matter, Ozone, Nitrogen Dioxide, and Sulfur Dioxide.* A EURO Publication. World Health Organization. ISBN: 9789289021920.

Wittrock, F., Oetjen, H., Richter, A., Fietkau, S., Medeke, T., Rozanov, A., and Burrows, J. P. (2004). "MAX-DOAS measurements of atmospheric trace gases in Ny-Ålesund - Radiative transfer studies and their application". In: *Atmos. Chem. Phys.* 4, pp. 955–966.

WSV (2013). *Verkehr und Güterumschlag.* URL: http://www.ast-nordwest.gdws.wsv.de/schifffahrt/verkehr%7B%5C_%7Dgueterumschlag/index.html (visited on 11/01/2016).

— (2014). *Schiffsverkehr und Güterumschlag.* URL: http://www.wsd-nord.wsv.de/Schiff-WaStr/Schifffahrt/Schiffsverkehr%7B%5C_%7Dund%7B%5C_%7DGueterumschlag/index.html (visited on 11/01/2016).

Yang, M., Bell, T. G., Hopkins, F. E., and Smyth, T. J. (2016). "Attribution of atmospheric sulfur dioxide over the English Channel to dimethyl sulfide and changing ship emissions". In: *Atmospheric Chemistry and Physics* 16.8, pp. 4771–4783. ISSN: 16807324. DOI: 10.5194/acp-16-4771-2016.

1240   Zhang, F., Chen, Y., Tian, C., Lou, D., Li, J., Zhang, G., and Matthias, V. (2016). "Emission factors for gaseous and particulate pollutants from offshore diesel engine vessels in China". In: *Atmospheric Chemistry and Physics* 16.10, pp. 6319–6334. ISSN: 16807324. DOI: 10.5194/acp-16-6319-2016.

Monitoring shipping emissions in the German Bight using MAX-DOAS measurements

André Seyler[1], Folkard Wittrock[1], Lisa Kattner[1,2], Barbara Mathieu-Üffing[1,2], Enno Peters[1], Andreas Richter[1], Stefan Schmolke[2], and John P. Burrows[1]

[1]Institute of Environmental Physics, University of Bremen, Germany
[2]Federal Maritime and Hydrographic Agency (BSH), Hamburg, Germany

Correspondence to: A. Seyler (aseyler@iup.physik.uni-bremen.de)

Abstract

A three-year time series of ground-based MAX-DOAS measurements of NO_2 and SO_2 on the island Neuwerk has been analyzed for contributions from shipping emissions. The island is located in the German Bight, close to the main shipping lane (in a distance of 6–7 km) into the river Elbe towards the harbor of Hamburg. Measurements of individual ship plumes as well as of background pollution are possible from this location, which is a few kilometers from the shipping lane. A simple approach using the column amounts of the oxygen molecule dimer or collision complex, O_4, for the determination of the horizontal light path length has been applied to retrieve path-averaged volume mixing ratios. An excellent agreement between mixing ratios retrieved determined from NO_2 retrievals in the UV and visible parts of the spectrum has been found, showing the validity of the approach. Obtained mixing ratios of NO_2 and SO_2 are compared to co-located in-situ measurements showing good correlation on average with good agreement for well-mixed background pollution but systematic underestimation of plume concentrations but also a systematic underestimation by the MAX-DOAS O_4-scaling approach. Comparing data before and after the introduction of stricter fuel sulfur content limits (from 1 % to 0.1 %) on 1 January 2015 in the North Sea emission control area (ECA), a significant reduction in SO_2 levels has been observed. For situations with wind from the open North Sea, where ships are the only local source of air pollution, the average mixing ratio of SO_2 decreased by a factor of eight, while for NO_2 in the whole time series from 2013 till 2016 no significant change in emissions has been observed. More than 2000 individual ship emission plumes have been identified in the data and analyzed for the emission ratio of SO_2 to NO_2, yielding an average ratio of 0.3 for the years 2013/2014, decreasing significantly presumably due to lower fuel sulfur content in 2015/2016. By sorting measurements according to the prevailing wind direction and selecting two angular reference sectors representative for wind from open North Sea and coast excluding data with mixed air mass origin, relative contributions of ships and land-based sources to air pollution levels in the German Bight have been estimated to be around 40 % : 60 % for NO_2 as well as SO_2 in 2013/2014, dropping to 14 % : 86 % for SO_2 in 2015/2016.

1 Introduction

1.1 Shipping – a fast growing sector

Shipping has always been an important mode of transportation throughout the course of history. In contrast to the past, nowadays ships are almost exclusively carrying freight with the exception of a small number of cruise ships and ferries. Globalization of markets has lead to an enormous increase in world trade and ~~consequently~~ shipping traffic in the last decades, with growth rates being typically about twice that of the world gross domestic product (GDP) (Bollmann et al., 2010).

Shipping is generally the most energy efficient transportation mode, having the lowest greenhouse gas emissions per tonne per kilometer (3–$60\,\mathrm{gCO_2/t/km}$), followed by rail (10–$120\,\mathrm{gCO_2/t/km}$), road (80–$180\,\mathrm{gCO_2/t/km}$) and air transport (435–$1800\,\mathrm{gCO_2/t/km}$), which is by far the least efficient (Bollmann et al., 2010; IEA/OECD, 2009). At the same time, with a volume of 9.84 billion tons in 2014 it accounts for four fifths of the worldwide total merchandise trade volume (UNCTAD, 2015), as compared to for example the total air cargo transport volume of 51.3 million tons in 2014 (International Air Transport Association (IATA), 2015). As a result, shipping accounts for a significant part of the emissions from the transportation sector (Eyring et al., 2005a).

Despite growth rates now being lower compared to those prior to the 2008 economic crisis, seaborne trade is growing faster than the rest of the transportation sector, with an annual growth rate of 3–$4\,\%$ in the years 2010 to 2014, compared to 2.0–$2.6\,\%$ for the global merchandise volume (UNCTAD, 2014, 2015). The number of ships > 100 gross tonnage increased from around $31\,000$ in 1950 ~~to~~ over $52\,000$ in 1970 to $89\,000$ in 2001 (Eyring et al., 2005b) and is estimated to increase to about $150\,000$ in 2050 (Eyring et al., 2005a). At the same time, total fuel consumption and emissions increased as well (Corbett and Koehler, 2003; Eyring et al., 2005a,b; Eyring et al., 2010b). Eyring et al. (2005a) predicted that future development of shipping emissions will depend more on the usage of new technologies and imposed regulations than on the economic growth rates.

1.2 Ship emission chemistry

The most important pollutants emitted by ships are carbon dioxide (CO_2), carbon monoxide (CO), nitrogen oxides ($NO_x = NO + NO_2$), sulfur dioxide (SO_2), black carbon (BC), volatile organic compounds (VOC) and particulate matter (PM) (Eyring et al., 2010a). This study focuses on NO_2 and SO_2, because both are emitted in considerable amounts and both absorb light in the uv-visible spectral range and therefore can readily be measured by Differential Optical Absorption Spectroscopy (DOAS), which is explained in Sect. 3.1. In 2001, shipping emissions accounted for $15\,\%$ of all anthropogenic NO_x and provided $8\,\%$ of all anthropogenic SO_2 emissions (Eyring et al., 2010a).

NO_x is predominantly formed thermally from atmospheric ~~nitrogen and oxygen~~ molecular nitrogen (N_2) and oxygen (O_2) during high temperature combustion processes in ship engines in an endothermic chain reaction called the Zeldovich mechanism. The emitted NO_x comprises mainly NO, with less than $25\,\%$ of NO_x being emitted as NO_2 (Alföldy et al., 2013). Zhang et al. (2016) measured emission factors for gaseous and ~~particualte~~ particulate pollutants on-board three Chinese vessels and found that more than $80\,\%$ of the NO_x was emitted as NO and that emission factors were significantly different during different operation modes.

In the ambient atmosphere, NO is rapidly converted to NO_2 by reaction with ozone (O_3) leading to a life time of only a few minutes. During daytime NO_2 is photolyzed by UV radiation ($\lambda < 420\,\mathrm{nm}$) releasing NO and ground state oxygen radicals ($O(^3P)$). In a three-body-collision reaction involving N_2 or O_2 the oxygen radical reacts with an oxygen molecule to reform ozone (Singh, 1987). When daylight is available, these reactions form a "null-cycle" and transformation between NO and NO_2 is

very fast, leading to a dynamic equilibrium. This is also known as the Leighton photostationary state. ~~Deviations from the Leighton photostationary state occur in air masses, if the rates of the reactions of free radicals such as hydroperoxyl, HO$_2$, or organic peroxy radicals, RO$_2$, or Halogen oxides XO, where X=Cl, Br or I, compete with the reaction of NO with O$_3$. The NO$_2$ formed in the reactions of HO$_2$ or RO$_2$ with NO is photolyzed and the O atoms reacts in the termolecular reaction with oxygen molecules O$_2$ to form O$_3$. In tropospheric air-masses, typically, the X atoms released by the reaction of NO with XO typically reacts rapidly with O$_3$ to reform XO. This changes the reaction of NO$_2$ to NO but does not produce O$_3$. During night due to~~ Owing to the lack of photolysis, NO reacts rapidly with O$_3$ to form NO$_2$ during the night. In addition~~NO$_3$~~, the nitrate radical ~~,~~ (NO$_3$) is formed by reaction of NO$_2$ with O$_3$. An equilibrium of NO$_2$ with NO$_3$ forming N$_2$O$_5$, the acid anhydride of nitric acid HNO$_3$, results (Seinfeld and Pandis, 2006; Wayne, 2006).

During the day OH reacts with NO$_2$ in a three body reaction to form HNO$_3$. An important sink for NO$_2$ in the troposphere is wet deposition of the resulting HNO$_3$. The mean tropospheric lifetime of NO$_x$ varies between a few hours in summer and a few days in winter (Singh, 1987), depending on altitude. Inside ship plumes, Chen et al. (2005) found a substantially reduced lifetime of NO$_x$ of about 1.8 h compared to approximately 6.5 h in the background marine boundary layer (around noon). This is attributed to enhanced levels of OH radicals in the plume.

Unlike for NO$_x$, ship emissions of SO$_2$ are directly linked to the fuel sulfur content. Around 86 % of the fuel sulfur content is emitted as SO$_2$ (Balzani Lööv et al., 2014). Alföldy et al. (2013) found a linear relationship between SO$_2$ and sulfate particle emission and that only around 4.8 % of the total sulfur content is either directly emitted as or immediately transformed into particles after the emission. An important sink for SO$_2$ is wet deposition after oxidation by OH radicals to the extremely hygroscopic sulfur trioxide (SO$_3$) reacting rapidly with liquid water to form sulfuric acid (H$_2$SO$_4$) (Brasseur, 1999). Another important sink is dry deposition, leading to a lifetime of approximately one day in the boundary layer, which can be even shorter in the presence of clouds (Seinfeld and Pandis, 2006).

1.3 Influence on air quality and climate

Sulfate aerosols influence climate directly by scattering and absorption of solar radiation and indirectly by increasing cloud condensation, changing cloud reflectivity and lifetime (Eyring et al., 2010b; Lauer et al., 2007; Lawrence and Crutzen, 1999). In the presence of volatile organic compounds (VOC), nitrogen oxides are important precursors for the formation of tropospheric ozone and therefore photochemical smog. The release of both NO$_2$ and SO$_2$ leads to an increase in acidification of 3–10 % in coastal regions, contributing significantly to acid rain formation damaging eco-systems (Endresen et al., 2003; Jonson et al., 2000). The deposition of reactive nitrogen compounds causes eutrophication of ~~ecosystem~~ ecosystems and decreases biodiversity (Galloway et al., 2003).

Around 70 % of shipping emissions occur within 400 km of land (Corbett et al., 1999), contributing substantially to air pollution in coastal areas (Eyring et al., 2010b). Ship emissions were found to provide a dominant source of air pollution in harbor cities (Eyring et al., 2010a). In addition to that, transport of tropospheric ozone and aerosol precursors over several hundreds of kilometers also affect air quality, human health and vegetation further inland, far away from their emission point (Corbett et al., 2007; Eyring et al., 2010a; Eyring et al., 2010b).

NO$_2$ and SO$_2$ can cause a variety of respiratory problems. Tropospheric ozone is harmful to animals and plants, causing various health problems. The EU legislation for O$_3$ exposure to humans has set a target limit of ~~120 μg/m3~~ 120 μg/m^3 ($\sim$ 60 ppbv) for an maximum daily 8 hour mean but allows exceedences on 25 days averaged over 3 years (EU, 2008, 2016). As mentioned above, both NO$_2$ and SO$_2$ play a role in the formation of particles. Fine particles are associated with various health impacts like lung cancer, heart attacks, asthma and allergies (Corbett et al., 2007; Pandya et al., 2002; WHO, 2006).

1.4 Attempts to decrease shipping emissions by stricter regulations

International ship traffic is subject to regulations of the International Maritime Organization (IMO).
Shipping emissions are regulated by the International Convention for the Prevention of Pollution from
Ships (MARPOL 73/78) Annex VI (DNV, 2008). This Annex was added in 1997 and entered into
force in 2005. A revision with more stringent emission limits was adopted in 2008 and went into
force 2010. With this, limits on sulfur content in heavy fuel oils globally are set and local Sulfur
Emission Control Areas (SECA), later revised to general Emission Control Areas (ECA), along the
North American coast and in the Baltic and North Sea (including the English Channel) are established
with more stringent restrictions and controls. MARPOL introduced a global fuel sulfur limit of 4.5 %,
which was reduced to 3.5 % in 2012 and will be further reduced in 2020 (or 2025 depending on a review
in 2018) to 0.5 %. In the established ECAs, from 2010 on the limit was set to 1.5 % and was further
reduced in 2010 to 1.0 %. Carrying out airborne in-situ measurements in several flight campaigns in
the English Channel, North and Baltic Sea, Beecken et al. (2014) measured a 85 % compliance in 2011
and 2012 with the 1 % fuel sulfur limit. In the Gulf of Finland and Neva Bay area, Beecken et al.
(2015) found a 90 % compliance in 2011 and 97 % compliance in 2012 with the 1 % fuel sulfur limit
from ground-based, ship-based and helicopter-based in-situ measurements.

Recently, from 1 January 2015 on, the allowed fuel sulfur content in SECAs was further reduced
to 0.1 %. Using in-situ measurements in Wedel at the bank of the river Elbe, a few kilometers
downstream from Hamburg, Germany, Kattner et al. (2015) showed that in late 2014 more than 99 %
of the measured ships complied with the 1 % sulfur limit and in early 2015 95.4 % of the measured ships
complied with the new 0.1 % sulfur limit. By analyzing one and a half years of SO_2 measurements
at the English Channel, Yang et al. (2016) found a three-fold reduction in SO_2 from 2014 to 2015.
They estimated the lifetime of SO_2 in the marine boundary layer to be around half a day. Lack et al.
(2011) measured a substantial drop of SO_2 emissions by 91 % when the investigated container ships
entered the Californian ECA and switched from heavy fuel oil (HFO) with 3.15 % fuel sulfur content
to marine gas oil (MGO) with 0.07 % fuel sulfur content. These estimates were obtained performing
airborne in-situ measurements.

MARPOL Annex VI also establishes limits dependent on engine power for the emission of NO_x from
engines built after 2000 (Tier I), 2011 (Tier II) and 2016 (Tier III), but due to the slow penetration
to the full shipping fleet, the impact on NO_x emissions is not yet clear. Since 2010, a NO_x emission
control area exists around the North American coast and in the Caribbean, while for North and
Baltic Sea the establishment of such a NECA is planned and was recently agreed on, but the future
enforcement date is still unclear. The European Union also established a sulfur content limit of 0.1 %
for inland waterway vessels and ships at berth in Community ports, which is in force since 1 January
2010 (EU, 2005).

The impact of shipping emissions on the North Sea for different regulation scenarios was investigated
in a model study by the Helmholtz-Zentrum Geesthacht (HZG) within the scope of the Clean North Sea
Shipping project. For current emissions, a relative contribution of shipping emissions to air pollution
in coastal regions of up to 25 % in summer and 15 % in winter for NO_2 and 30 % in summer and
12 % in winter for SO_2 was found (Aulinger et al., 2016). For the year 2030, the contribution of the
continuously growing shipping sector to the NO_2 concentrations is predicted to decrease. The extent
of reduction depends on the date on which the stricter Tier III regulations enter into force and on the
fraction of the fleet complying to these regulations (i. e. the age of the fleet), with up to 80 % reduction
if all ships comply (in the improbable case of a new ships only fleet). For SO_2, the established fuel
sulfur content limit of 0.1 % (ECA) and 0.5 % (globally) will lead to significant reductions, a further
decrease is expected if the fraction of LNG powered ships grows (Matthias et al., 2016).

1.5 DOAS measurements of shipping emissions – previous studies

175 Optical remote sensing using the Differential Optical Absorption Spectroscopy (DOAS) technique to measure shipping emissions has been conducted before. For example, Berg et al. (2012) performed airborne (from airplane and helicopter) DOAS measurements of NO_2 and SO_2 in ship plumes by measuring sea scattered light. Masieri et al. (2009) and Premuda et al. (2011) measured flow rate emissions (mass per second) of NO_2 and SO_2 for single ships with ground based MAX-DOAS measure-
180 ments across the Giudecca Channel in the Venice lagoon. McLaren et al. (2012) measured nocturnal NO_2/SO_2 ratios in ship plumes in the Strait of Georgia with the active long path DOAS technique. Balzani Lööv et al. (2014) tested and compared optical remote sensing methods (DOAS, LIDAR, UV camera) and in-situ (sniffer) methods for the measurement of shipping emissions in the framework of the SIRENAS-R campaign in the harbour of Rotterdam in 2009. Prata (2014) showed that a UV
185 (SO_2) imaging camera can be used to measure SO_2 in ship plumes at the Kongsfjord at Ny Ålesund, Svalbard and the harbor of Rotterdam.

The global pathways of the ships can be seen in long time averaged NO_2 measurements from various satellite instruments: from GOME over the Indian Ocean (Beirle et al., 2004), from SCIAMACHY on board ENVISAT over the Indian Ocean and the Red Sea (Richter et al., 2004), in even more detail
190 with a lot more visible ship tracks from GOME-2 on board MetOp-A (Richter et al., 2011). The higher resolution of OMI yielded ship tracks in the Baltic Sea (Ialongo et al., 2014) and in all European seas (Vinken et al., 2014).

1.6 The MeSMarT project

The current study is part of the project MeSMarT (Measurements of Shipping emissions in the Marine
195 Troposphere), which is a cooperation between the University of Bremen (Institute of Environmental Physics, IUP) and the Federal Maritime and Hydrographic Agency (Bundesamt für Seeschifffahrt und Hydrographie, BSH), supported by the Helmholtz Zentrum Geesthacht (HZG). It aims to monitor background concentration as well as elevated signals of gases and particles related to ship emissions with various methods to cover a wide range of relevant pollutants and their spatial and seasonal
200 distribution to estimate the influence of ship emissions on the chemistry of the atmospheric boundary layer (for further information visit: http://www.mesmart.de/).

1.7 Aims of this study

The objectives of this study are to assess whether measurements of individual ship plumes are feasible with a ground-based MAX-DOAS instrument, to compare MAX-DOAS with co-located in-situ mea-
205 surements, to estimate the contribution of ships and land-based sources to air pollution in a North Sea coastal region, to survey the effect of fuel sulfur content regulations on SO_2 concentrations in the marine boundary layer and to analyze the SO_2 to NO_2 ratio in plumes to gain information about plume chemistry and the sulfur content in shipping fuels.

In the following, first the measurement site is described, followed by a presentation of the wind
210 statistics and data availability is shown. After this, the Differential Optical Absorption Spectroscopy (DOAS), the MAX-DOAS instrumentation and measurement geometry as well as the DOAS data analysis approach used are briefly described. In the next section, selected results from this study are presented: for example the measured differential slant column densities (DSCD), the retrieved path-averaged volume mixing ratios, the comparison to in-situ measurements, the diurnal and weekly
215 variability, the contribution estimates for ships as well as land-based pollution sources and the analysis of SO_2 to NO_2 ratios in ship plumes. Finally, a summary is given and conclusions are drawn.

2 Measurement site

The measurements presented within this study were taken on ~~the North Sea island Neuwerk. This is~~ Neuwerk, a small island in the North Sea (German Bight) with the size of about $3\,km^2$ and 33 inhabitants ~~in the German Wadden Sea in the German Bight~~. It is located in the Wadden Sea northwest of Cuxhaven at the mouth of the river Elbe, roughly 8–9 km off the Coast, as can be seen from the map in Fig. 1 A).

The North Sea has one of the highest ship densities in the world (Matthias et al., 2016). The majority of ships that arrive in the port of Hamburg sail through the German Bight and the river Elbe and therefore pass ~~the island Neuwerk, where our measurement site is located~~ Neuwerk. Hamburg is among the largest ports worldwide, together with Rotterdam and Antwerp one of the three largest ports in Europe, having a 4–5 % increase in container volume in the last years (UNCTAD, 2014, 2015). Hamburg also experiences a large increase in the number of cruise ships, having 176 ship calls in 2014 compared to 25 in the year 2005 (Statistische Ämter des Bundes und der Länder (Statistikamt Nord), 2015).

Neuwerk is relatively close to the main shipping lane from the North Sea into the river Elbe. On this highly frequented waterway, nearly all ships to and from the port of Hamburg and the Kiel canal (connection to the Baltic Sea) pass the island at a distance of 6–7 km, as shown in Fig. 1 B). Still close, but further away to the west are the shipping lanes to the Weser river to the ports of Bremerhaven and Bremen and to Wilhelmshaven (JadeWeserPort).

Neuwerk is surrounded by the Hamburg Wadden Sea National Park and there are no significant sources of air pollution on the island itself, making it a very suitable station for measurements of shipping emissions.
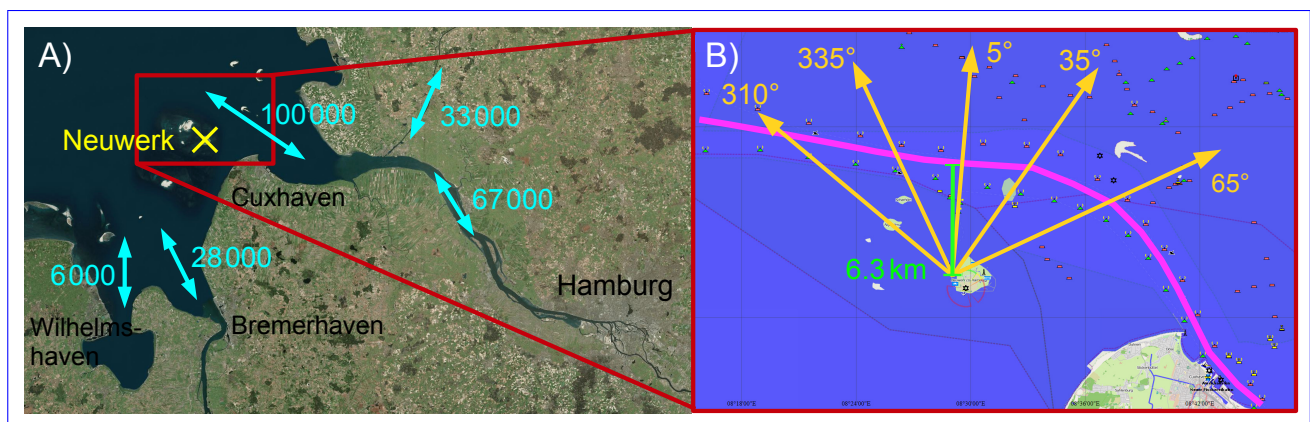

Figure 1: **A)** Location of the measurement site Neuwerk in the German Bight, close to the mouth of the river Elbe. Number of ship movements (data from 2011/2012) is given by the white numbers. Data source: German Federal Waterways and Shipping Administration (WSV, 2013, 2014) Map source: `http://www.bing.com/maps/` (01.04.2014)
B) Azimuthal viewing directions of the MAX-DOAS instrument towards the main shipping lane (highlighted by the magenta line), passing the island in the north in a distance of 6–7 km. Map source: `http://www.freie-tonne.de` (16.07.2013)

The ship emission measurements presented in this study were carried out with a MAX-DOAS instrument (see Sect. 3.2) which measures in multiple azimuthal viewing directions, as shown in Fig. 1 B), pointing directly towards the shipping lane while the different viewing azimuth angles cover a large part of the region.

Several measurement devices, including the two-channel MAX-DOAS instrument (for UV and visible spectral range), an Airpointer in-situ measurement device (measuring CO_2, NOx, SO_2 and O_3), a high volume filter sampler and passive samplers as well as a weather station and an AIS (Automatic Identification System) signal receiver, are positioned on the main platform of a radar tower at a height of about 30 m (see Fig. 2).
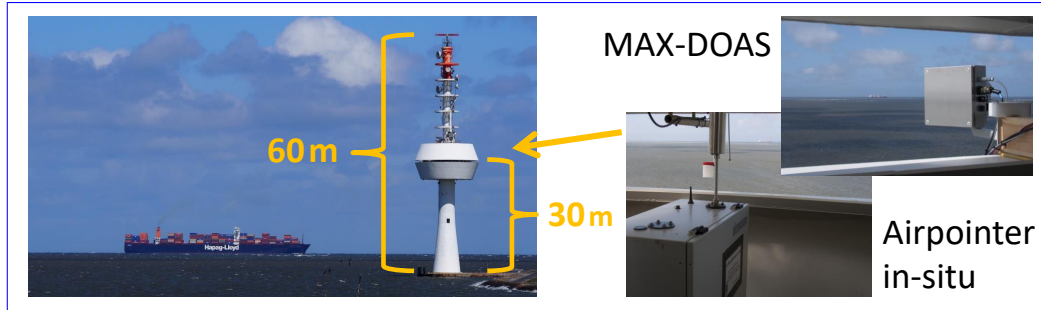

Figure 2: Radar tower Neuwerk with MAX-DOAS and in-situ measurement device

Additional wind data is available from measurements by the Hamburg Port Authority (HPA) on Neuwerk and the neighboring island Scharhörn. The seasonal distribution of wind directions on Neuwerk is shown in Fig. 3.

In spring and summer, on a high percentage of days the wind blows from the open North Sea, where shipping emissions are the only significant source of local air pollution. Consequently, the site ~~for the measurements~~ provides an optimal opportunity for measurements of ship emission plumes. In winter, southerly directions prevail, bringing potentially polluted air masses from the land and blowing the ship emission plumes away from the measurement site. In addition, as the MAX-DOAS technique requires daylight and because of the short days and the low sun resulting in less UV light reaching the surface, measurements are in general sparse in winter months, especially for SO_2, which has its strong absorption features in the UVB. This effect can be seen in winter gaps in Fig. 4, which presents the data availability for more than two years of measurements on Neuwerk.
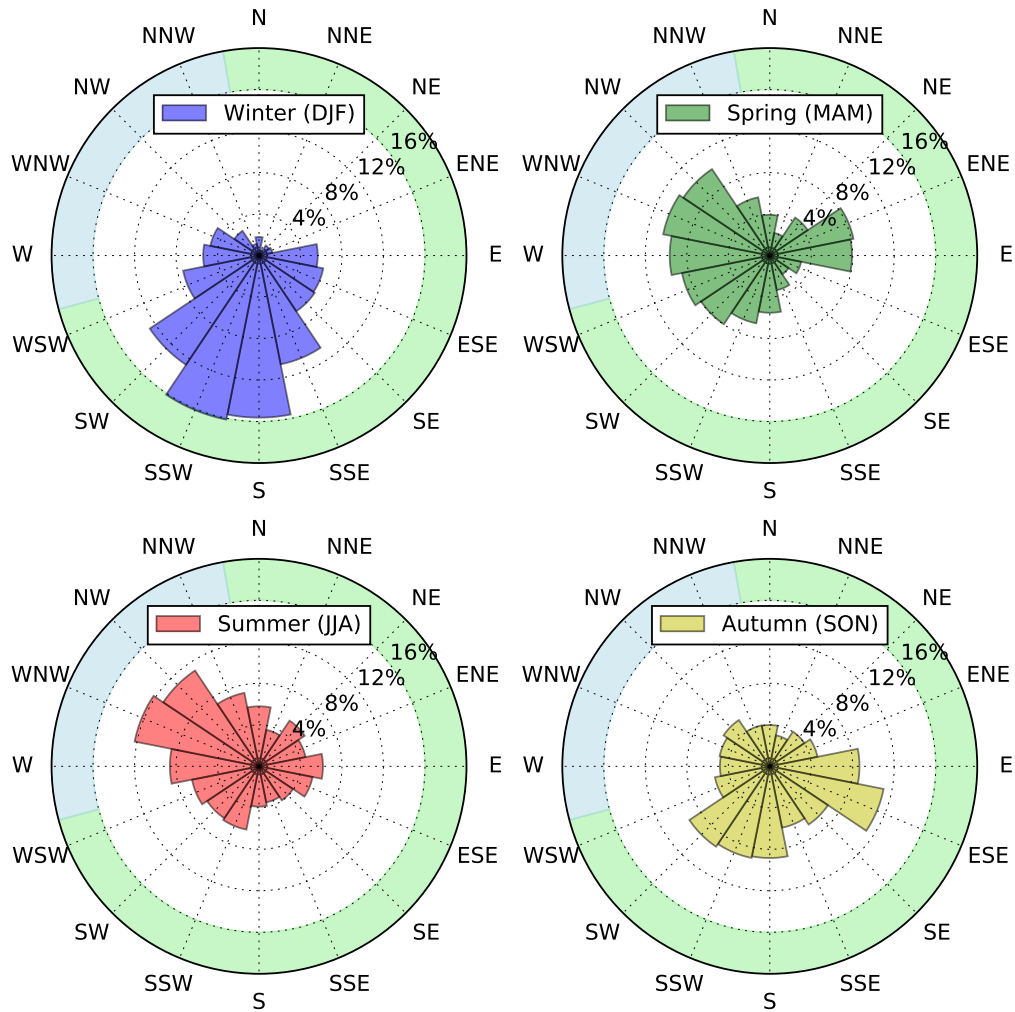
Figure 3: Seasonal wind direction distribution for Neuwerk (Data from 04.07.2013 to 26.10.2015). The colored sectors show directions with wind from the coast (green) and from the open North Sea (blue).
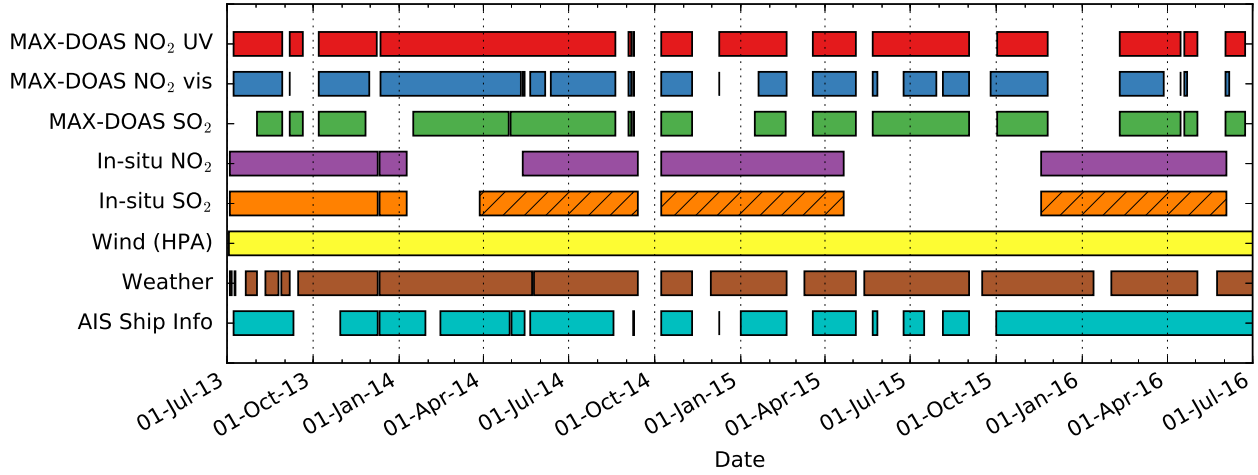
Figure 4: Data availability in the analyzed measurement period between July 2013 and July 2016. From March 2014 on (hatched), there were instrumental problems with the in-situ SO$_2$ instrument resulting in a strong oscillation of ± 0.5 ppb superimposing the data. However, this data can still be used for the comparison of long-term averages.

3 Measurement techniques, instruments and data analysis

3.1 Differential Optical Absorption Spectroscopy (DOAS)

The principle of optical absorption spectroscopy is the attenuation of light intensity while passing through an absorbing medium, described by the well-known Lambert-Beer-law (also known as Beer–Lambert–Bouguer law). For the general case of electromagnetic radiation passing through an anisotropic medium having a number density n and a temperature and pressure dependent absorption cross section σ of an absorbing species along the light path s, the measured intensity at wavelength λ is given by

$$I(s, \lambda) = I_0(\lambda) \cdot \exp\left\{ -\int_0^s n(s') \cdot \sigma(\lambda, T(s'), p(s')) \cdot \mathrm{d}s' \right\} \tag{1}$$

where the intensity of radiation entering the medium is I_0. For measurements in the atmosphere, this simple model has to be extended by considering multiple trace gases having different absorption cross sections and light scattering on air molecules (Rayleigh scattering), aerosol particles or water droplets (Mie scattering) as well as inelastic scattering by air and trace gas molecules (Raman scattering). The latter is responsible for the Ring effect (Grainger and Ring, 1962), another important extinction process, which can be described by a pseudo cross-section.

The key and original idea of the Differential Optical Absorption Spectroscopy (DOAS) is to separate the optical depth and the absorption cross-sections $\sigma_i(\lambda)$ into a slowly varying function $\sigma_{i,0}(\lambda)$ accounting for elastic scattering and broadband absorption structures and described by a low-order polynomial and a rapidly varying part $\sigma_i'(\lambda)$, the *differential* cross-section, considering the narrow-band absorption structures (Platt and Perner, 1980; Platt and Stutz, 2008). The absorption cross-sections are measured in the laboratory. ~~Polynomial and~~ Neglecting the temperature and pressure dependence of the absorption cross section, polynomial and differential cross sections are fitted to the measured optical thickness $\ln(I/I_0)$ in the linearized so-called DOAS equation~~to retrieve the~~:

$$\ln\left(\frac{I(\lambda)}{I_0(\lambda)} \right) = -\sum_{i=1}^{N} \mathrm{SCD}_i \cdot \sigma_i'(\lambda) - \sum_p c_p \cdot \lambda^p + \mathrm{Residual}(\lambda) \tag{2}$$

9

The retrieved quantities are the coefficients of the polynomial c_p and the slant column density of ~~a trace gas as~~ the trace gas which is the integrated number density along the light path~~$SCD_i = \int n_i(s)ds$~~:

$$\ln\left(\frac{I(\lambda)}{I_0(\lambda)}\right) = -\sum_{i=1}^{N} \mathrm{SCD}_i \cdot \sigma_i'(\lambda) - \sum_p c_p \cdot \lambda^p + \mathrm{RESIDUAL}(\lambda)$$

: $\mathrm{SCD}_i = \int n_i(s)\mathrm{d}s$.

3.2 MAX-DOAS instrument and viewing geometry

The Multi-AXis DOAS (MAX-DOAS) technique (Hönninger et al., 2004; Wittrock et al., 2004) is a passive remote sensing method measuring scattered sunlight. The MAX-DOAS instrument used in this study, comprises of a telescope mounted on a pan-tilt head, an optical fiber bundle, two spectrometers for UV and visible spectral range respectively, equipped with two CCD (charge coupled device) 2D array detectors operated by a computer. The telescope which is attached to the outer sheathing of the circular platform of the Neuwerk radar tower is used to collect the light from a specific viewing direction and to ~~inject the light into the~~ focus the light onto the entrance of the optical fiber. The combination of converging lens and light fiber leads to an ~~opening angle of about 1.1°~~field-of-view of about 1°. The pan-tilt head allows the instrument to point in different azimuth angles (panning) as well as different elevation angles (tilting). Dark measurements, which are needed for the determination of the CCD's dark signal are undertaken on a daily basis. Also on a daily basis line lamp measurements are taken using an internally mounted HgCd lamp for the wavelength calibration of the spectra and the determination of the slit function of the instrument. The spectral resolution, represented by the FWHM of the slit function of the instrument, is about 0.4 nm for the UV and 0.7 nm for the visible channel.

The Y-shaped optical light fiber cable is a bundle of 2×38 cylindrical, thin and flexible quartz fibers, guiding the light from the telescope to the two temperature-stabilized spectrometers with attached CCD detectors inside the weatherproof platform building. Each single fiber has a diameter of 150 μm and is 20 m long.

The UV and visible instrument consist of identical Andor Shamrock SR-303i imaging spectrographs, a grating spectrometer in "Czerny-Turner" design with a focal length of 303 mm. The gratings in use are different, the UV instrument is equipped with a 1200 grooves/mm, 300 nm blaze angle grating and the visible instrument with a 600 grooves/mm, 500 nm blaze angle grating. The UV instrument covers the wavelength range 304.6–371.7 nm, the visible spectrometer covers 398.8–536.7 nm. For the UV, a Princeton NTE/CCD 1340/400-EMB detector with a resolution of 1340×400 pixels and a pixel size of 20×20 microns, cooled to $-35\,°C$, is used. For the visible spectral range, an Andor iDus DV420-BU back-illuminated CCD detector with a resolution of 1024×255 pixels and a pixel size of 26×26 microns, cooled as well to $-35\,°C$, is used.

The measurement geometry for the ground-based MAX-DOAS measurements on Neuwerk is sketched in Fig. 5. To measure ship emissions, the telescope is pointed towards the horizon, ~~measuring right~~ collecting light that passed directly through the emitted ship plumes. A close-in-time zenith sky measurement is used as a reference so that the retrieved tropospheric differential slant column density (DSCD) is the difference of the slant column densities (SCD) along the two paths ~~: DSCD = SCD$_1$ − SCD$_2$~~1 and 2 in Fig. 5: $\mathrm{DSCD} = \mathrm{SCD}_1 - \mathrm{SCD}_2 = \mathrm{SCD}_{\text{off-axis}} - \mathrm{SCD}_{\text{reference}}$. The stratospheric light path and trace gas absorption is approximately the same for both measurements and therefore cancels out which is important for NO$_2$ which is also present in the stratosphere. This approach also minimizes possible instrumental artifacts.
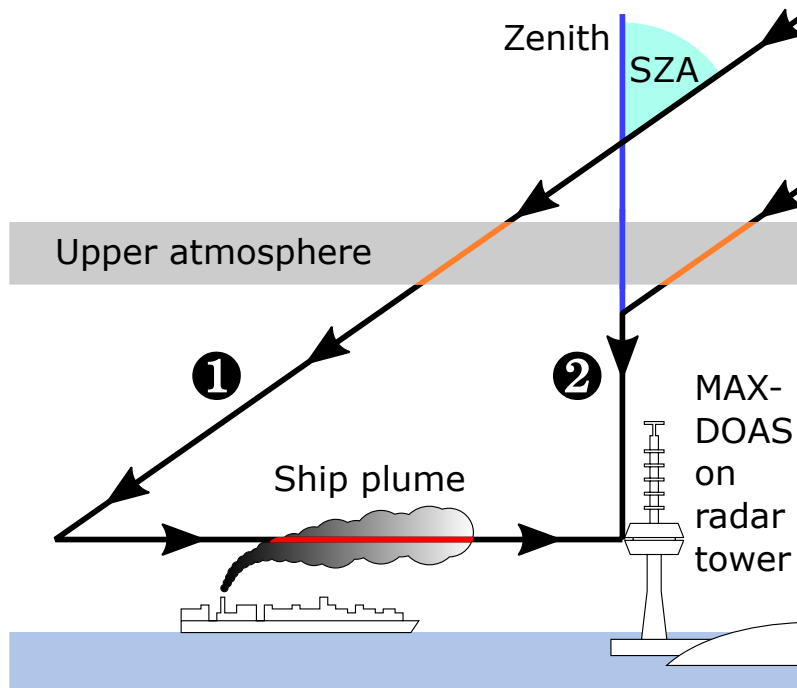
Figure 5: Measurement geometry for MAX-DOAS measurements on Neuwerk with schematic light paths for off-axis (1) and zenith sky reference measurements (2) for an exemplary solar zenith angle (SZA) of 55°

The assumption that the vertical part of the light path cancels out when taking the difference between off-axis and zenith sky (reference) measurement off course is only valid if the NO_2 in the air above the instrument, which is of no interest to us here, is spatially homogeneously distributed. This is usually the case for stratospheric NO_2. If a spatially limited pollution plume from ~~ships, power plants etc.~~ point sources like ships or power plants is blown above the radar tower ~~, the mentioned assumption is violated, leading to errors in the derived qualities.~~

~~If there is no plume~~ and no plume is in the horizontal light path, ~~but in the air above the radar tower,~~ the ~~retrieved DSCDwould be negative. This happens if urban pollution plumes from land pass over the site. Should significant amounts of the radiation reaching the instrument pass through clouds then as a result of the multiple scattering in the cloud the~~ mentioned assumption is violated, leading to an underestimation of the derived DSCD. Also clouds or fog can make the interpretation of the measured DSCD ~~is more challenging .~~ more challenging due to multiple scattering.

~~Remark concerning the elevation angles of our instrument:~~ ~~The value in the following text is referred to as 0° elevation angle is in reality an elevation angle of 0.6°. The acceptance angle of our telescope is about 1.1° and it has a circular field of view. This means that the field of view extends vertically from 0.05° to 1.05° (nearly 0° to 1°). Thus the 0° line-of-sight represents an average over this field of view. This has the advantage that the surface, which may have spectral structures, is not explicitly probed. The same averaging over the relevant solid angle occurs for the higher elevation angles like 2, 4, 30 and 90°.~~

3.3 DOAS data analysis and fit settings

The recorded spectra are spectrally calibrated using a daily acquired HgCd line lamp spectrum and the dark signal of the CCD detector is corrected using daily nighttime dark measurements. The logarithm of the ratio of measured off-axis (viewing towards the horizon) spectrum and reference (zenith sky)

spectrum gives the optical thickness (also called optical depth) for the DOAS equation (2). Multiple
(differential) trace gas absorption cross sections obtained from laboratory measurements, as well as a
low-order polynomial, are then fitted simultaneously to the optical depth. The retrieved fit parameters
are the slant column densities of the various absorbers and the coefficients of the polynomial. The fits
were performed with the software NLIN_D (Richter, 1997).

The settings and fitted absorbers vary according to the spectral range used. For the retrieval of
NO_2 in the UV, a fitting window of 338–370 nm was used and for NO_2 in the visible a fitting window
of 425–497 nm, both adapted from experiences during the CINDI (Roscoe et al., 2010) and MAD-
CAT (`http://joseba.mpch-mainz.mpg.de/mad_cat.htm`) inter-comparison campaigns. The oxygen-
collision complex O_2-O_2, often denoted as O_4, is simultaneously retrieved from both NO_2 fits. The
fit parameters for the DOAS fit of NO_2 and SO_2 are summarized in detail in Table 1.

For the retrieval of SO_2, several different fitting windows between 303 and 325 nm have been used
in previous ground-based studies (Bobrowski and Platt, 2007; Galle et al., 2010; Irie et al., 2011;
Lee et al., 2008; Wang et al., 2014a). This results from the need to find a compromise between the
low light intensity caused by the strong ozone absorption around 300 nm on the one hand and the
rapid decrease of the differential absorption of SO_2 at higher wavelengths on the other hand, limiting
the choice of the fitting window. In this study, a fitting window of 307.5–317.5 nm was found as the
optimal range for our instrument, which is similar to recommendations in Wang et al. (2014a). The
fit parameters for the DOAS fit of SO_2 are summarized in detail in Table 2.

Only SO_2 measurements with a RMS lower than 2.5×10^{-3} have been taken into account for the
statistics, filtering out bad fits with ozone interferences in low light and bad weather conditions.

Under optimal conditions, the typical fit RMS is around 1×10^{-4} for NO_2 in the visible, 2×10^{-4}
for NO_2 in the UV and 5×10^{-4} for SO_2. By assuming that an optical density of twice the RMS can
be detected (Peters, 2013), it is possible to estimate the detection limit of our instrument regarding the
different trace gases. The differential absorption cross section of NO_2 is in the oder of 1×10^{-19} cm²/molec,
for SO_2 in the order of 2×10^{-19} cm²/molec. Combining this yields a NO_2 detection limit of around
1×10^{15} molec/cm² corresponding to 0.05 pbb in the visible and 2×10^{15} molec/cm² corresponding to
0.1 pbb in the UV. The SO_2 detection limit lies around 2.5×10^{16} molec/cm² corresponding to 0.2 pbb.
The typical absolute fit errors are $2 - 3 \times 10^{14}$ molec/cm² for NO_2 in the visible, $5 - 6 \times 10^{14}$ molec/cm²
for NO_2 in the UV and 2×10^{15} molec/cm² for SO_2, a factor of 5 to 10 smaller than the detection limit.

Table 1: DOAS fit settings for the retrieval of NO_2 and O_4 in UV and visible spectral range

Parameter	NO_2 (UV)	NO_2 (visible)
Fitting window	338–370 nm	425–497 nm
Polynomial degree	4	3
Intensity offset	Constant	Constant
Zenith reference	Coinciding zenith measurement[1]	Coinciding zenith measurement[1]
SZA range	Up to 85° SZA	Up to 85° SZA
O_3	223 K & 243 K (Serdyuchenko et al., 2014)	223 K (Serdyuchenko et al., 2014)
NO_2	298 K (Vandaele et al., 1996)	298 K (Vandaele et al., 1996)
O_4	293 K (Thalman and Volkamer, 2013)	293 K (Thalman and Volkamer, 2013)
H_2O	–	293 K (Lampel et al., 2015)
HCHO	297 K (Meller and Moortgat, 2000)	–
Ring	SCIATRAN (Rozanov et al., 2014)	SCIATRAN (Rozanov et al., 2014)

[1] Interpolation in time between the zenith measurements directly before and after the off-axis scan.

Table 2: DOAS fit settings for the retrieval of SO_2

Parameter	SO_2 (UV)
Fitting window	307.5–317.5 nm
Polynomial degree	3
Intensity offset	Constant & slope
Zenith reference	Coinciding zenith measurement[1]
SZA range	Up to 75° SZA
O_3	223 K & 243 K (Serdyuchenko et al., 2014)
NO_2	298 K (Vandaele et al., 1996)
SO_2	293 K (Bogumil et al., 2003)
Ring	SCIATRAN (Rozanov et al., 2014)

[1] Interpolation in time between the zenith measurements directly before and after the off-axis scan.

3.4 ~~Conversion~~ Retrieval of ~~slant column densities (SCD) to volume mixing ratios (VMR)~~ path-averaged near-surface VMRs from MAX-DOAS SCDs

To ~~compare DOAS measurements (trace gas columns) with, for example, in-situ measurements (concentrations), the retrieved slant column densities need to be converted to volume mixing ratios. The volume mixing ratio VMR = n_x/n_{air} of a gas x is defined as the ratio of the number densities of the gas and air and describes its atmospheric number fraction. The number density of air can be estimated using the ideal gas law:~~

$$n_{air} = \frac{N_{air}}{V_{air}} = \frac{p_{air} \cdot k_B}{T_{air}} = \frac{p_{air} \cdot N_A}{T_{air} \cdot R}$$

~~with the Boltzmann constant k_B, Avogadro constant N_A and universal gas constant R. The retrieval of the number density of the trace gas from the DOAS measurements can be done in different ways:~~

~~One possibility is to use a geometric approximation with a simple geometric air mass factor $AMF_{geom} = \frac{1}{\sin(\alpha)}$ for the elevation angle α to first convert the slant columns to vertical columns. The tropospheric vertical column density (VCD) divided by a typical mixing layer height (MLH) in which the trace gas is assumed to be well-mixed then gives the number density of the trace gas:~~

$$n_{x,geom} = \frac{VCD_{trop}}{MLH} \qquad \text{with} \qquad VCD_{trop} = \frac{SCD_\alpha - SCD_{90°}}{\sin(\alpha)^{-1} - \sin(90°)^{-1}} = \frac{DSCD_\alpha}{\sin(\alpha)^{-1} - 1}$$

~~A disadvantage of this method is the assumption of a typical mixing layer height, if no independent measurements of the MLH (e. g. using LIDAR) is available. Another disadvantage is that this approach does not account for changes in the light path due to changing weather (clouds, fog) and aerosol conditions. In addition, the profile will not be box-shaped in reality and the geometric AMF does only hold for large elevation angles.~~

~~A second possibility, which was applied for the measurements presented in this study, is to use the mountain MAX-DOAS-approach developed by Gomez et al. (2014). The basic principle of this method is the assumption~~ measure shipping emissions at our measurement site, our MAX-DOAS telescope is pointed towards the horizon, where the ships pass our site in a distance of 6–7 km. Since our instrument has a field-of-view of approximately 1°, the lowest usable elevation angle avoiding looking onto the ground is 0.5°, providing us with the highest sensitivity to near-surface pollutants. This is the elevation in which at our site usually the highest slant columns are measured. To convert a MAX-DOAS trace gas column which is the concentration of the absorber integrated along the effective light path into concentrations or volume mixing ratios, the length of this light path has to be known. This effective light path length depends on the atmospheric visibility, which is limited by scattering on air molecules as well as aerosols. As described in Section 3.2, trace gas absorptions in the higher atmosphere like stratospheric NO_2 nearly cancel out using a close-in-time zenith-sky reference spectrum. Following this, we can assume that the signal for ~~horizontal measurements (i. e. for an elevation angle of 0°)~~ our horizontal line-of-sight is dominated by the horizontal part of the light path after the last scattering event. ~~The~~ As introduced by Sinreich et al. (2013), the length L of this horizontal part of the light path can then be estimated using the slant column density of the O_4-molecule which has a well-known number density in the atmosphere:

$$L_{O_4} = \frac{\text{SCD}_{O_4,\text{horiz}} - \text{SCD}_{O_4,\text{zenith}}}{n_{O_4}} = \frac{\text{DSCD}_{O_4}}{n_{O_4}} \tag{3}$$

~~Here, $n_{O_4} = (n_{O_2})^2 = (0.20942 \cdot n_{\text{air}})^2$~~ The surface number density of O_4 is proportional to the square of the molecular oxygen concentration (Greenblatt et al., 1990; Wagner et al., 2004) and can be easily calculated ~~via Eq. (??) from the measured~~ from the temperature and pressure measured on the radar tower:

$$n_{O_4} = (n_{O_2})^2 = (0.20942 \cdot n_{\text{air}})^2 \qquad \text{with} \qquad n_{\text{air}} = \frac{N_{\text{air}}}{V_{\text{air}}} = \frac{p_{\text{air}} \cdot k_B}{T_{\text{air}}} = \frac{p_{\text{air}} \cdot N_A}{T_{\text{air}} \cdot R} \tag{4}$$

415 with the Boltzmann constant k_B, Avogadro constant N_A and universal gas constant R.

Knowing the path length, it is then possible to calculate the average number density of our trace gas x along this horizontal path and the path-averaged volume mixing ratio:

$$n_{x,O_4 \underline{x}} = \frac{\text{SCD}_{x,\text{horiz}} - \text{SCD}_{x,\text{zenith}}}{L_{O_4}} = \frac{\text{DSCD}_x}{L_{O_4}} \qquad \text{and} \qquad \text{VMR}_{\underline{x}} = \frac{n_x}{n_{\text{air}}} \tag{5}$$

~~As using the O_4 slant column density, this approach~~ This O_4-scaling in principle takes into account the actual light path and its variation with aerosol loading and also needs no assumption on the

420 typical mixing layer height, therefore overcoming the disadvantages of ~~the~~ a simple geometric approximation.

However, when the atmospheric profile of the investigated trace gas x has a shape that differs from that of the proxy O_4, systematic errors are introduced as has been shown by Sinreich et al. (2013) and Wang et al. (2014b) in extensive and comprehensive radiative transfer model (RTM) simulations.

425 Pollutants like NO_2 and SO_2 have a profile shape very different from O_4. They are emitted close to the ground (e.g. from ships), have high concentrations in low altitude layers and tend to decrease very rapidly with height above the boundary layer. They are often approximated as box profiles, while the O_4 concentration simply decreases exponentially with altitude. This difference in profile shapes violates the basic assumption that the O_4 DSCD is a good proxy for the light path through the NO_2

430 and SO_2 layers. The resulting near-surface volume mixing ratios will not be representative for the amount of trace gases directly at the surface, but for some kind of average over a certain height range in the boundary layer.

The studies like Sinreich et al. (2013) and Wang et al. (2014b) use correction factors from radiative transfer calculations to account for this. These correction factors depend on the amount of aerosols

435 present in the atmosphere, often described by the aerosol optical density (AOD), the solar zenith angle (SZA) as well as the relative solar azimuth angle (RSAA), the height of the pollutant box profile and the extend and vertical position of the aerosol layer in relation to this box profile (Sinreich et al., 2013). The strong dependence of the correction factors on the height of the box profile for trace gas layer heights of less than 1 km makes it necessary for the application of the suggested parameterization

440 method to have additional knowledge about the trace gas layer height, ideally from measurements (e.g. LIDAR) or otherwise from estimations. The use of this method for low boundary layer heights below 500 m without knowing the actual height is not recommended by the authors (Sinreich et al., 2013).

At our measurement site, no additional knowledge (measurements) about the height of the NO_2 and SO_2 layers is available and the trace gay layer heights are typically around 200–300 m. A comparison of the uncorrected MAX-DOAS VMRs retrieved with the upper equations to our simultaneous in-situ measurements (see Section 4.5) confirms the need for a correction factor but also shows that the scaling factor needed changes from day to day as well as during the course of the day. This indicates, that the NO_2 and SO_2 layer height is very variable, depending on wind speed, wind direction, atmospheric conditions and chemistry. The lack of comparability between both measurement techniques and geometries, which is further discussed in Section 4.5, prevents us from estimating diurnally varying correction factors from this.

The non-consideration of these scaling factors will lead to a systematic overestimation of the effective horizontal path length and therefore to a systematic underestimation of MAX-DOAS VMRs, up to a factor of three (Sinreich et al., 2013; Wang et al., 2014b).

In summary, a detailed radiative transfer study for the determination of the right correction factors is out of scope of this study which focuses on the statistic evaluation of a three year dataset of shipping emission measurements in the German Bight. Therefore, when in the following MAX-DOAS VMRs are shown, it has to be kept in mind that these are uncorrected VMRs obtained by above formulas.

This approach has been applied successfully by Sinreich et al. (2013) and Wang et al. (2014b) for measurements in urban polluted air masses over Mexico City and the city of Hefei (China) using MAX-DOAS measurements in 1° and 3° (Sinreich et al., 2013) and only in 1° elevation (Wang et al., 2014b), respectively. Gomez et al. (2014) applyed this approach to measurements on a high mountain site at the Izaña Atmospheric observatory on Tenerife (Canary Islands), Schreier et al. (2016) at Zugspitze (Germany) and Pico Espejo (Venezuela). Due to the low aerosol amounts in such heights the latter two studies applied the approach without using correction factors. The fact that our instrument is located on a radar tower in a height of about 30 m above totally flat surroundings (the German Wadden Sea) allows an unblocked view to the horizon in all feasible azimuthal viewing directions. This led to the idea of trying to apply this approach to our shipping emission measurements on Neuwerk.

Since the O_4-DSCD is retrieved simultaneously to NO_2 in both the UV and visible DOAS fit for NO_2, this approach can be applied to NO_2 retrieved in both fitting ranges. The approach can also be applied to SO_2, although the difference of light paths due to the ~~slightly~~ different fitting windows in the UV for O_4 (NO_2) and SO_2 introduces an uncertainty which has to be accounted for. ~~In this study, a scaling factor of 0.8 was used, retrieved from extrapolation of the ratio of the O_4 columns in the longer wavelength UV and visible measurements .~~ Wang et al. (2014b) derived an empirical formula from RTM calculations for a variety of aerosol scenarios to convert the path length at 310 nm from the path length at the O_4 absorption at 360 nm:

$$L_{310} = 0.136 + 0.897 \times L_{360} - 0.023 \times L_{360}^2 \tag{6}$$

where L_{310} and L_{360} are given in km. This formula was also applied to our measurements to correct the light path length for the SO_2 fitting window. Although this formula has been calculated for polluted sites, the authors state that the deviations for other sites with different conditions are expected to be small (Wang et al., 2014b).

Using ~~this approach~~equations 3 to 5, several problems can arise from the division by the differential slant column density of O_4. For example if the O_4 DSCD is negative, which can happen at low signal-to-noise-ratio ~~(SNR)~~ DOAS fits (e. g. under bad weather conditions), the resulting path length will be negative. If at the same time the trace gas DSCD is positive, then the trace gas volume mixing ratio will be negative as well, a non-physical result. However, even when there is no NO_2 or SO_2,

there is still some noise and therefore the retrieved VMR are not exactly zero, but scatter around zero, so slightly negative values have to be included when averaging over time to avoid ~~a high~~ creating a systematic bias. If, on the other hand, the O_4 DSCD is close to zero, the path length will be very small leading to extremely high (positive or negative) mixing ratios which are ~~unrealistic.~~

also unrealistic. To adress both problems, measurements with negative or small retrieved horizontal path lengths are ~~filtered~~discarded. For the measurements on Neuwerk, with respect to the characteristics of the measurement site, a minimum path length of 5 km seems to be a reasonable limit. This value provides the best compromise between the number of rejected bad measurements and the total number of remaining measurements for NO_2 in UV and visible as well as for SO_2. For statistics on differential slant column densities on the other hand, no such filtering is applied since negative values are not unphysical in this case and just mean that there is more trace gas absorption in the reference measurement than in the off-axis measurement.

~~The O_4 scaling approach was previously applied to measurements from high mountain sites only, for example by Gomez et al. (2014) at the Izaña Atmospheric observatory on Tenerife (Canary Islands) or by Schreier et al. (2016) at Zugspitze (Germany) and Pico Espejo (Venezuela). The fact that our instrument is located on a radar tower in a height of about 30 m above totally flat surroundings (the German Wadden Sea) means that it is appropriate to apply this approach to our measurements on Neuwerk.~~

~~**Remark concerning the elevation angles of our instrument:** Since the opening angle or field of view of our instrument is about 1.1°, looking at 0° elevation towards the horizon would result in partially (with the lower half of our circular field of view) looking onto the ground (or sea surface, depending on tide). To avoid possible problems arising from this like spectral interferences, our instrument is looking slightly upward. What in this study is referred to as 0° elevation angle is in reality an elevation angle of around 0.6°. With our opening angle of about 1.1° and a circular field of view this means the field of view extends vertically from 0.05° to 1.05°, so 0° elevation means actually a field of view from nearly 0° to 1°. The same is true for the higher elevation angles like 2, 4, 30 and 90°. Since deviations arising from this are small, this is neglected in the following.~~

3.5 In-situ instrumentation

In addition to the MAX-DOAS instrument, also in-situ observations are taken, using the Airpointer, a commercially available system which combines four different instruments in a compact, air-conditioned housing. The manufacturer is recordum (Austria), distributed by MLU (`http://mlu.eu/recordum-airpointer/`). The Airpointer device measures carbon dioxide (CO_2), nitrogen oxides ($NO_x = NO + NO_2$), sulfur dioxide (SO_2) and ozone (O_3) using standard procedures. Table 3 shows more detailed information about the different included instruments, their measurement methods, precision, and time resolution.

In this study the in-situ 1-minute-means of all compounds were used. NO_2 itself is not directly measured but calculated internally by subtracting the measured NO from the measured NO_x concentration.

Table 3: Airpointer in-situ device: measured trace gases, corresponding measuring techniques, measuring ranges and detection limits [Source: recordum/MLU (manufacturer), `http://mlu.eu/recordum-airpointer/`]

Trace gas	CO_2	O_3	NO, NO_2	SO_2
Measuring technique	Non-dispersive IR spectroscopy LI-COR LI820	UV absorption (EN 14625)	NO Chemi-luminescence (EN 14211)	UV fluorescence (EN 14212)
Detection limit	1 ppm	0.5 ppb	0.4 ppb	0.25 ppb
Measuring range	up to 20 000 ppm	up to 200 ppm	up to 20 ppm	up to 10 ppm
Time resolution	1 s	<30 s	<60 s	<90 s

4 Results

4.1 Measured slant column densities of NO_2 and SO_2

In this study, three years of continuous MAX-DOAS measurements on Neuwerk have been evaluated. Figure 6 shows for one example day in summer 2014 the measured differential slant column densities of NO_2 in UV and visible spectral range as well as of SO_2 for the ~~0°~~ 0.5° elevation angle (viewing to the horizon) and the $-25°$ azimuth angle (approximately NNW direction, see Fig. 1). Sharp peaks in the curves originate from ship emission plumes passing the line of sight of the instrument. On this day, elevated levels of ~~the pollutant~~ NO_2 have been measured in the morning, corresponding to a polluted air mass coming from land, which appears as an enhanced, slowly varying NO_2 background signal below the peaks. The systematic difference between the ~~red curve (~~NO_2 in the UV (red curve) and the ~~blue curve (~~NO_2 in the visible (blue curve) emerges from the longer light-path in the visible due to ~~more intense~~ stronger Rayleigh scattering in the UV (wavelength dependence $\propto \lambda^{-4}$). This is further investigated in Sect. 4.3 below.

By comparing ~~the black SO_2 curve with the~~ SO_2 (green curve) with NO_2 (red and blue ~~NO_2 curves~~ curves) it can be seen that for many of the NO_2 peaks there is a corresponding and simultaneous SO_2 peak, but not for all of them. This ~~illustrates that the~~ indicates a varying sulfur content in the fuel of the measured ships ~~varies. A more dirty fuel~~. Fuel with higher sulfur content leads to higher SO_2 emissions (see also Sect. 1).

By comparing measurements in different azimuthal viewing directions, the movement direction of the ship (and its plume) can be easily distinguished. The zoom in on the right of Fig. 6 shows the visible NO_2 measurements in different azimuth directions for one example peak from the time series shown on the left. The color-coded viewing directions (see also Fig. 1) are sketched schematically below. From the measurements it can be seen that the emitted plume was consecutively measured in all directions at different ~~points in time~~ times. It was first measured in the easternmost viewing directions and at last in the westernmost direction, indicating that the ship and its plume moved from east to west.

For the identification of sources for air pollution on Neuwerk, the wind direction distribution for the differential slant column densities of NO_2 and SO_2 measured in 2013 and 2014 is plotted for four different elevation angles (~~0°, 2°, 4° and 30°~~ 0.5°, 2.5°, 4.5° and 30.5°) in Fig. 7. When the wind is coming from the open North Sea (blue shaded sector) the measured NO_2 and SO_2 DSCD are clearly lower than for other directions, for which the wind is coming from the coast (green ~~shaded sector~~ and yellow shaded sectors) and blows land-based air pollution to the island. The wind direction dependence is more or less similar for both trace gases but with a higher fraction of ship related signals
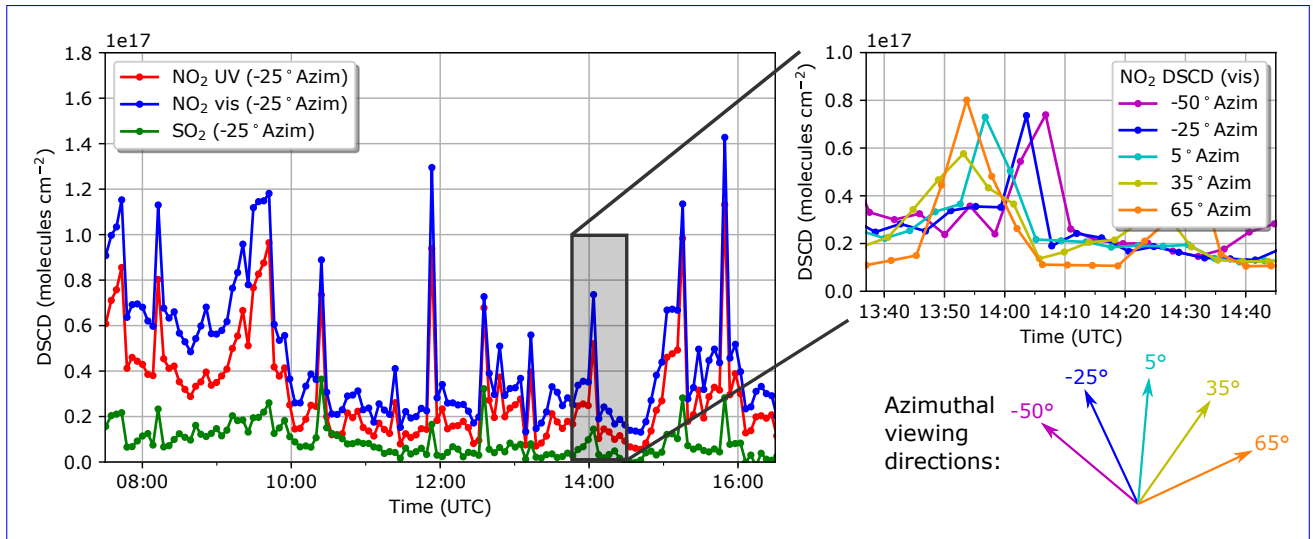
Figure 6: NO$_2$ (UV and visible) and SO$_2$ differential slant column densities measured in ~~0°~~ 0.5° elevation and the $-25°$ viewing azimuth angle (approximately NNW direction) on Neuwerk on Wednesday, 23 July 2014. The excerpt on the right shows for one example peak the NO$_2$ (vis) measurements in different azimuth viewing directions~~, which are schematically sketched below~~.

in the overall SO$_2$ columns. The values are especially high when the wind is coming from the cities of
560 Cuxhaven (ESE direction) and Bremerhaven (SSE) for both NO$_2$ and SO$_2$.

Elevation angle sequences of slant columns (i.e. vertical scanning) contain information on the vertical distribution of trace gases. For lower elevation angles, the measured trace gas slant columns for tropospheric absorbers are usually higher ~~,~~ because of the longer light path in the boundary layer. ~~This can be seen in Fig. 7, showing~~

565 As expected, higher elevations show on average lower DSCDs due to the shorter light path in the boundary layer. The highest NO$_2$ and SO$_2$ DSCD in the lowest elevation angle (~~0°~~0.5°, blue bars) ~~, and decreasing values while scanning upwards. The relative proportions of the NO$_2$ measurements (Figure 7 A) in 0° elevation compared to the measurements in 2° and 4° elevation is clearly different for the various wind directions. For wind directions from WSW to N to ESE, the ratio between~~
570 ~~the differential slant column densities in the lowest elevation angle to the higher elevations is much larger than for the southerly wind directions, corresponding to more NO$_2$ in lower altitudes in the north of the island~~in relation to DSCDs in higher elevations are measured especially for wind from all northern directions, in a sector ranging from WSW to ESE. These directions ~~with enhanced values~~ coincide with the course of the main shipping lane ~~, which comes~~ coming from the WSW direction
575 (the English Channel, the Netherlands, East Frisian Islands), ~~passes~~ passing the island in the north and ~~runs~~ running close to the city of Cuxhaven (ESE direction) into the river Elbe. This indicates that ~~these enhanced columns measured in low altitudes are coming from ships . For SO$_2$ (Figure 7 B), the fraction of measurements from the shipping lane on the overall emissions is higher than for NO$_2$, showing that in the German Bight shipping is a very important source of SO$_2$ emissions, while for~~
580 ~~NO$_2$~~the enhanced columns in the 0.5° elevation angle is pollution emitted from ships in a surface-near layer.

For southerly wind directions no major shipping lane is in the direct surrounding and land-based pollution sources ~~(traffic, industry) are more important. This will be further discussed in Sect. 4.8~~ dominate. The average DSCDs in 0.5° and 2.5° elevation are nearly the same for both NO$_2$ and SO$_2$
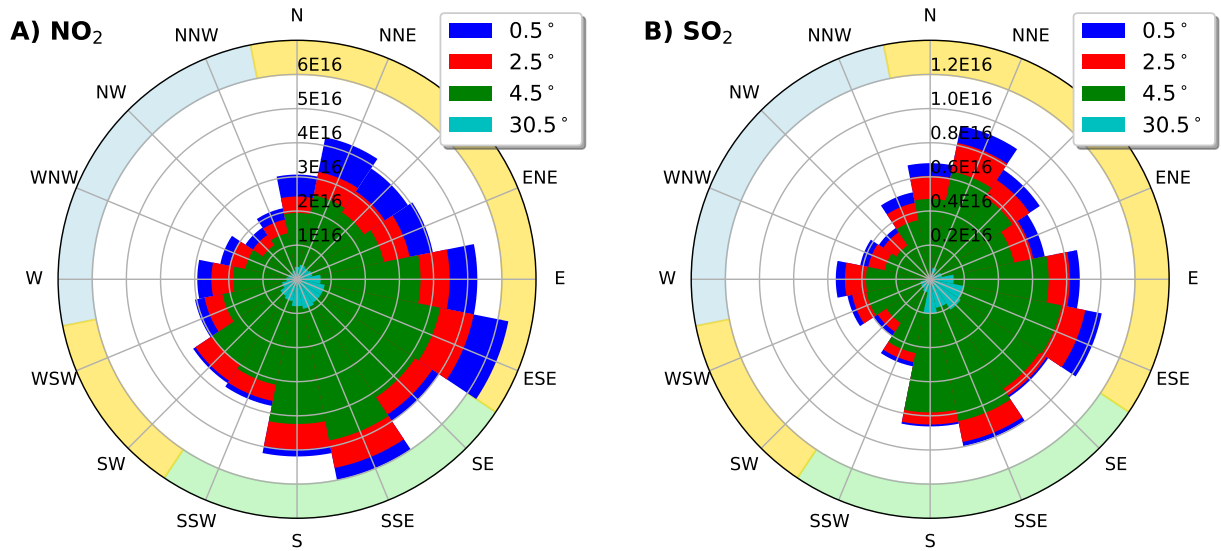585 indicating that the pollution is located higher up in the troposphere.

19

Figure 7: ~~Wind~~ Overlayed wind roses for different elevation angles showing the wind direction distribution of the UV NO_2 (A) and SO_2 (B) differential slant column densities measured in the main viewing direction in ~~0°~~0.5°, ~~2°~~2.5°, ~~4°~~4.5° and ~~30°~~30.5° elevation in the years 2013 and 2014. The ~~bars~~ wind roses are plotted on top of each other, i.e. the highest values were measured in the lowest elevation angle (blue bars). The colored sectors show directions with wind from ~~the coast~~ land (green)~~and~~, open North Sea (blue) and mixed origin (yellow).

4.2 ~~Retrieved volume~~ Volume mixing ratios of NO_2 and SO_2~~by using as a tracer for the horizontal light path length~~

For the example day presented in Fig. 6 the path-averaged volume mixing ratios retrieved with the approach presented in Sect. 3.4 ~~using O_4 as a tracer for the light path length~~ are shown in Fig. 8.

590   From the mathematics of the approach one would expect a good agreement between the NO_2 volume mixing ratios retrieved in UV and visible if NO_2 is well mixed in the boundary layer, since averaging constant values over different paths should give equal mean values. In the figure, in fact one can see a very good agreement between both NO_2 volume mixing ratios, in particular for situations characterized by background pollution.

595   Although the light path in the visible spectral range is clearly longer than in the UV, for all the peaks shown here the UV instrument measured a higher path-averaged VMR. The reason for that are spatial inhomogeneities along the line-of-sight.

If NO_2 is not distributed homogeneously along the light path, which is the case in the presence of individual ship exhaust plumes, one can expect different values for the means over the two light
600   paths as they probe different parts of the NO_2 field. Such differences can be identified in the figure by looking at the peaks.

The light path in the visible spectral range is longer than in the UV because of more intensive Rayleigh scattering in the UV. ~~How large the~~ The difference between UV and visible peak values ~~is then~~ depends on the exact location of the plume within the light paths. ~~If the plume is close~~

605   A short distance of the plume to the instrument and ~~completely covered~~ its complete coverage by the shorter UV path ~~, one will get~~ leads to higher values in the UV since the part of the light path probing the higher NO_2 values has a larger relative contribution to the signal than for the longer visible path.
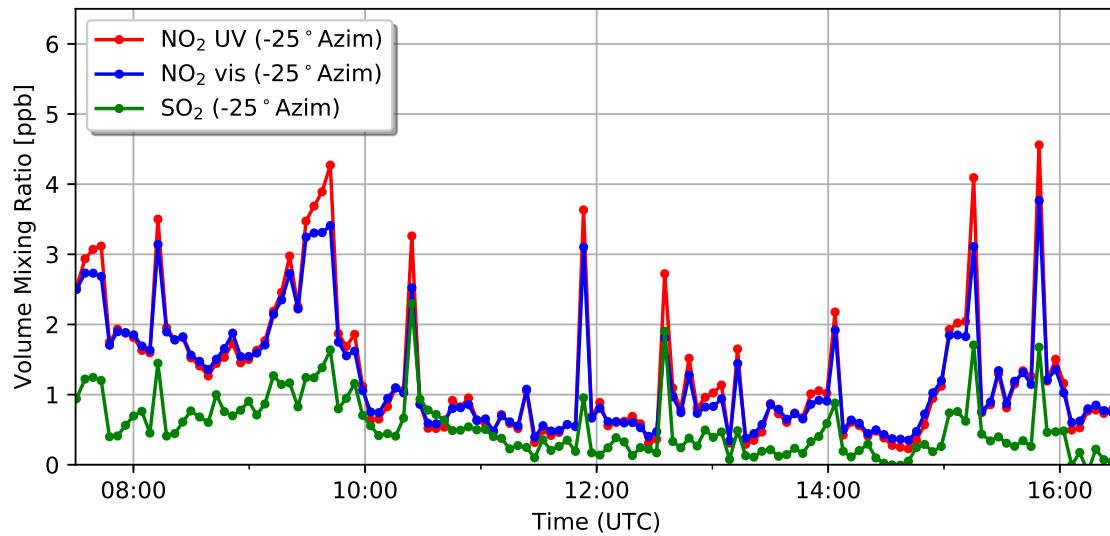
20

Figure 8: NO$_2$ (UV and visible) and SO$_2$ path-averaged volume mixing ratios measured in ~~0°~~ 0.5° elevation angle and $-25°$ viewing azimuth angle (approximately NNW direction) on Neuwerk on Wednesday, 23 July 2014.

If the plume is further away from the instrument and only in the visible path or close to the UV scattering point, one will retrieve a higher volume mixing ratio in the visible. This relationship contains information on the horizontal distribution of the absorber and will be further investigated in a second manuscript.

4.3 Statistical evaluation of ~~the approach~~UV and visible NO$_2$ data

To investigate quantitatively the relationship between the NO$_2$ slant column densities measured simultaneously in the UV and visible spectral range, all single pairs of ~~simultaneous measurements~~ DSCD measurements with an RMS better than 1×10^{-3} are plotted into a scatter plot, shown in ~~the left subplot in the upper row~~ Panel A of Fig. ~~(9)~~9.

As can be seen from the figure, ~~both measurements~~ NO$_2$ DSCDs in UV and visible are strongly positively correlated with a Pearson correlation coefficient of 0.983. Because of the difference in the horizontal light path lengths in both spectral regions (due to more intense Rayleigh scattering in the UV), the slope of the regression line is 1.30 corresponding to a 30 % longer light path in the visible. The intercept of the regression line is small. ~~The right subplot in the upper row~~ Panel B of Fig. ~~(9)~~9 shows a histogram of the ratios between both slant column densities. The distribution peaks for ratios of 1.3, in good agreement with the retrieved slope from the scatter plot.

When converting the slant column densities to mixing ratios using the O$_4$~~columns~~-scaling, the dependence on light path should be removed and quantitative agreement is expected between the UV and visible ~~retrievals~~VMRs. A scatter plot for the horizontal path averaged volume mixing ratios is shown in ~~the left subplot in the bottom row~~ Panel C of Fig. ~~(9)~~9. It is clearly visible that the points scatter symmetrically along the 1:1 identity line. Comparing this plot with the plot ~~directly above for the differential slant columns~~ in Panel A shows that the difference in light path lengths is in fact corrected for by the ~~approach (using the O$_4$DSCD as a tracer for the path length)~~O$_4$-scaling approach. The slope of the regression line is close to ~~1~~unity and the intercept is very small. The Pearson correlation coefficient has further increased to 0.984. The histogram (~~right plot) peaks close to one~~Panel D of Fig. 9) peaks at 1.0.
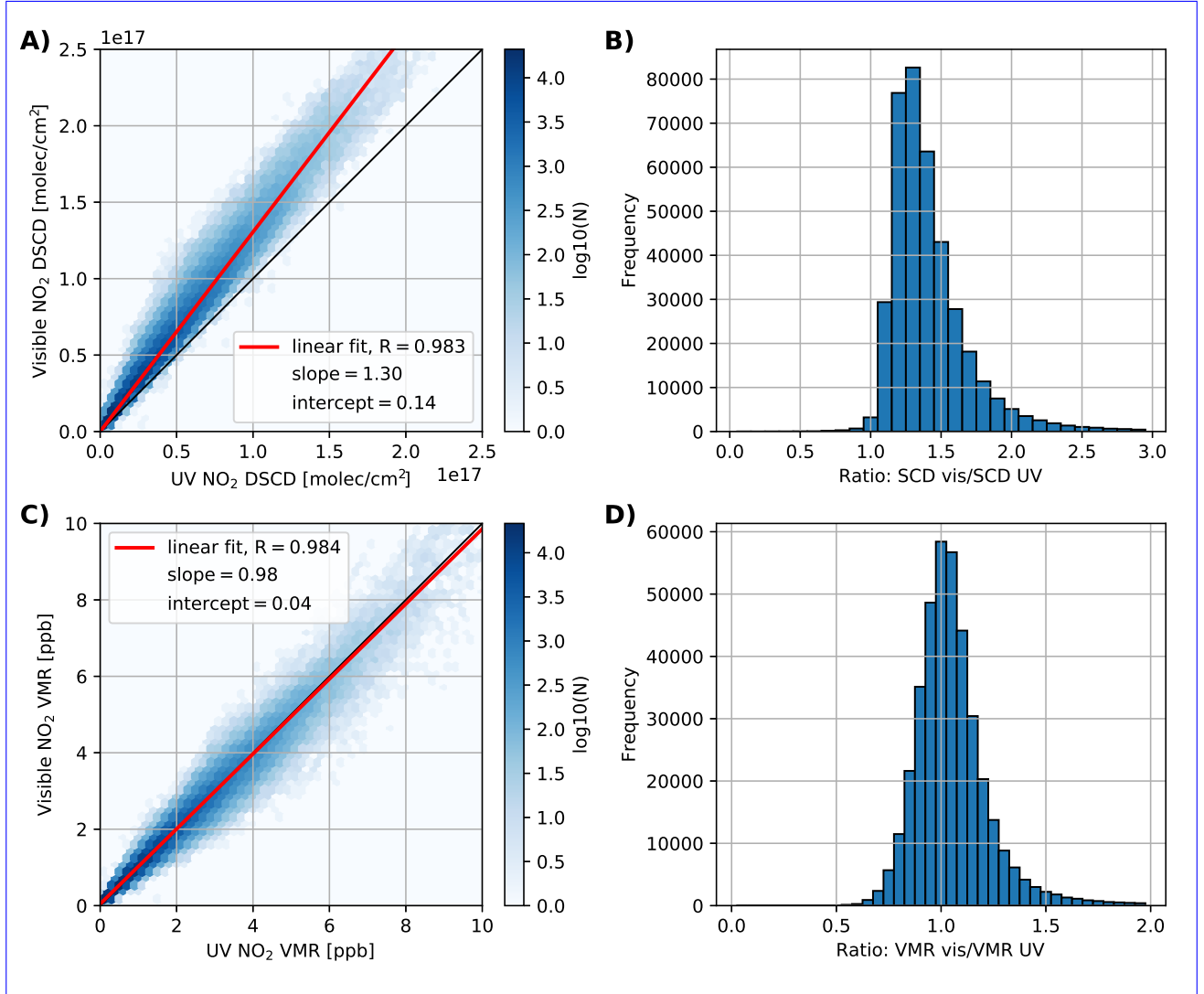
Figure 9: **A**) Scatter plot: NO$_2$ slant column density retrieved in the visible vs. UV measured in all azimuth angles at ~~0°~~ 0.5° elevation for solar zenith angles smaller than 75°. The ~~Pearson correlation coefficient is 0.982. The~~ parameters derived from the linear fit ~~was calculated via~~ by orthogonal distance regression (Deming regression) ~~and has a slope of 1.33 and an intercept of 0.09~~ are also shown. **B**) Histogram of the ratio of the two NO$_2$ slant column densities (visible/UV). **C**) As A, but for volume mixing ratios. ~~The pearson correlation coefficient increased to 0.984. The linear fit has a slope of 0.98 and an intercept of 0.05.~~ **D**) Histogram of the ratio of the two NO$_2$ volume mixing ratios (visible/UV).

As discussed above, differences are still expected not only as a result of measurement uncertainties but also due to different averaging volumes in case of inhomogeneous NO_2 distributions (which is especially the case for ship plumes under certain wind directions). For the horizontal light path lengths, a mean value of 9.3 km with a standard deviation of 2.3 km was retrieved in the UV, and a mean value of 12.9 km with a standard deviation of 4.5 km was retrieved in the visible. On days with optimal measurement conditions (clear sky days), typical horizontal light paths are around 10 km in the UV and 15 km in the visible spectral range.

~~The horizontal light path lengths retrieved in this study are lower than those retrieved in previous studies with the same approach applied on mountains. Schreier et al. (2016) retrieved a mean horizontal path length of 19 km in the UV for measurements on the German mountain Zugspitze (2650 m a.s.l., and 34 km on the Pico Espejo mountain (4765 m a.s.l.) in Venezuela. However, these sites at very high altitudes are located in a much cleaner surrounding atmosphere, with significantly lower aerosol concentrations and therefore much lower scattering probabilities. This should lead to much longer mean free path lengths between scattering events and longer horizontal light paths than on Neuwerk.~~

4.4 Allocation of ship emission peaks to ships using wind and AIS data

The ~~various~~ detailed information on passing ships transmitted via the *Automatic Identification System* (AIS) and the acquired weather and wind data can be used to allocate the measured pollutant peaks to individual ~~emitting~~ ships.

~~Figure 10, showing measurements~~ Measurements from Wednesday, 9 July 2014 ~~contains three sub-plots: The upper one~~ are shown in Figure 10. Panel A shows the MAX-DOAS differential slant column density of NO_2. ~~The middle one~~ Panel B includes various information about passing ships: The vertical bars indicate when a ship was in the line-of-sight of the MAX-DOAS instrument. Solid bars represent ships coming from the left and going to the right (from west to east, i.e. sailing into the river Elbe), dashed bars vice versa. The colors of the bars indicate the ship length, with small ships shown in blue and very large ships (>350 m) in red. ~~The lower sub-plot~~ Panel C displays the wind speed and direction.

On this day, the wind was coming from northern directions, directly from the shipping lane, with moderate wind speeds of 10–35 km/h, resulting in low background pollution values (1–2×10^{16} molecules/cm^2) as well as sharp and distinct ship emission peaks (up to 1.2×10^{17} molecules/cm^2) of NO_2. By comparing the ship emission peak positions to the vertical bars (representing ~~points in time~~ times when ships crossed the MAX-DOAS line-of-sight) in the schematic representation below it can be seen that most of the peaks can be allocated to individual ships. In some cases, when two or more ships simultaneously cross the line-of-sight, the single contributions can not be separated. Large ships (orange and red bars) tend to exhaust more NO_2 while the contribution of small ships (length < 30 m) represented by the dark blue bars is usually not measurable.
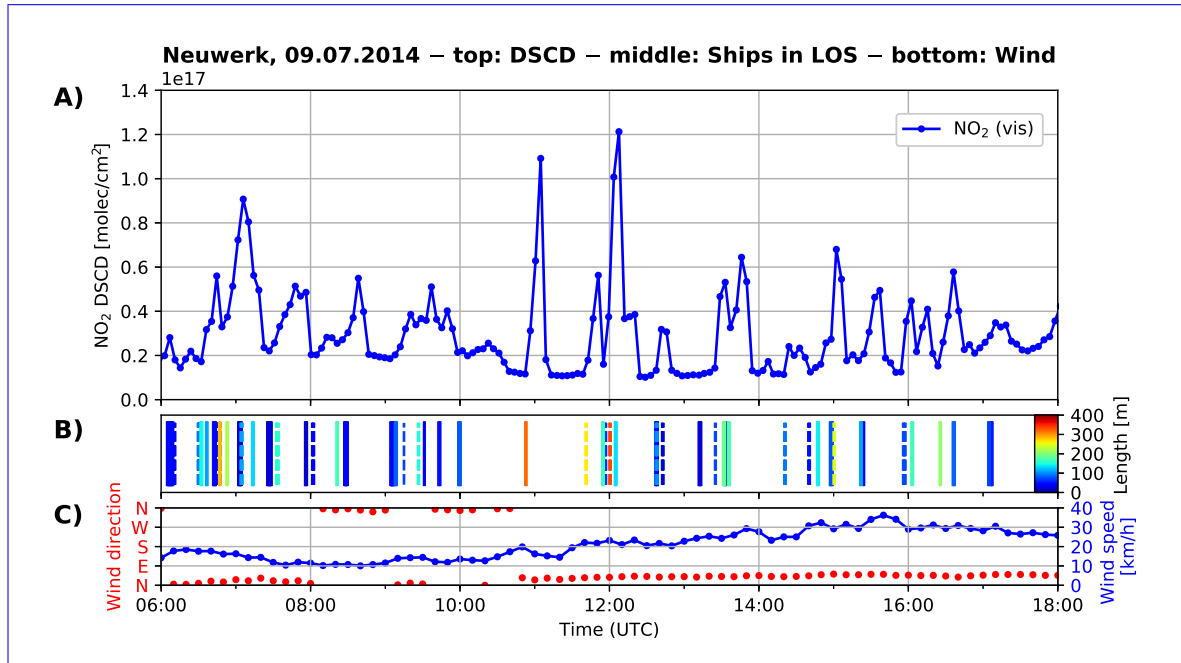
Figure 10: NO₂ ~~DSCD~~ differential slant column densities, AIS and wind data for Neuwerk on Wednesday, 9 July 2014.

Top: NO₂ differential slant column density (0° **A)** NO₂ DSCD in 0.5° elevation , for the 35° azimuth) viewing direction

Middle: **B)** Vertical bars indicating that a ship is in the line-of-sight of the instrument, solid bars: ship moves from left to right (west to east), dashed vice versa, colors representing ship length

Bottom: wind **C)** Wind speed and direction measured on Scharhörn (HPA)

24

4.5 Comparison of MAX-DOAS VMR to in-situ measurements

~~By converting the differential slant column densities to horizontal path averaged volume mixing ratios it is~~ The fact that our measurement site is also equipped with an in-situ device (see Section 3.5 for a description), makes it possible to compare the MAX-DOAS ~~measurements~~ VMRs of NO$_2$ and SO$_2$ to our simultaneous in-situ measurements. ~~For such a comparison, one has to consider the~~ The differences of both measurement techniques need to be considered for such a comparison: The MAX-DOAS averages over a long horizontal light path, while the in-situ device measures at ~~one point~~ a single location inside the plume. Since ship plumes usually never cover the whole light path but rather a small fraction of it, very high concentration peaks are usually underestimated in the MAX-DOAS VMR. ~~Besides, the peak height in the MAX-DOAS measurements strongly depends on the geometry of plume and line-of-sight of the instrument. If a ship's plume is blown along the line-of-sight, the measured value will be significantly higher than if it is orthogonally crossing the line-of-sight. However, this long light path is also a major advantage of the MAX-DOAS instrument over the in-situ instrument, since it provides measurements for ship plumes that never hit the radar tower and pass the island in a certain distance or are blown directly away from our instruments.~~

~~However, if the pollution is horizontally well-mixed in the measured air mass, which is often the case for background pollution coming from the coast but not for ship plumes, MAX-DOAS and in-situ instrument should in principle measure the same values.~~

Figure 11 shows the horizontal path averaged NO$_2$ volume mixing ratio retrieved from the differential slant column densities shown in Fig. 10 as well as the in-situ NO$_2$ volume mixing ratio ~~, again~~ (Panel A) in combination with ship data (~~middle~~Panel B) and wind data (~~bottom~~Panel C).
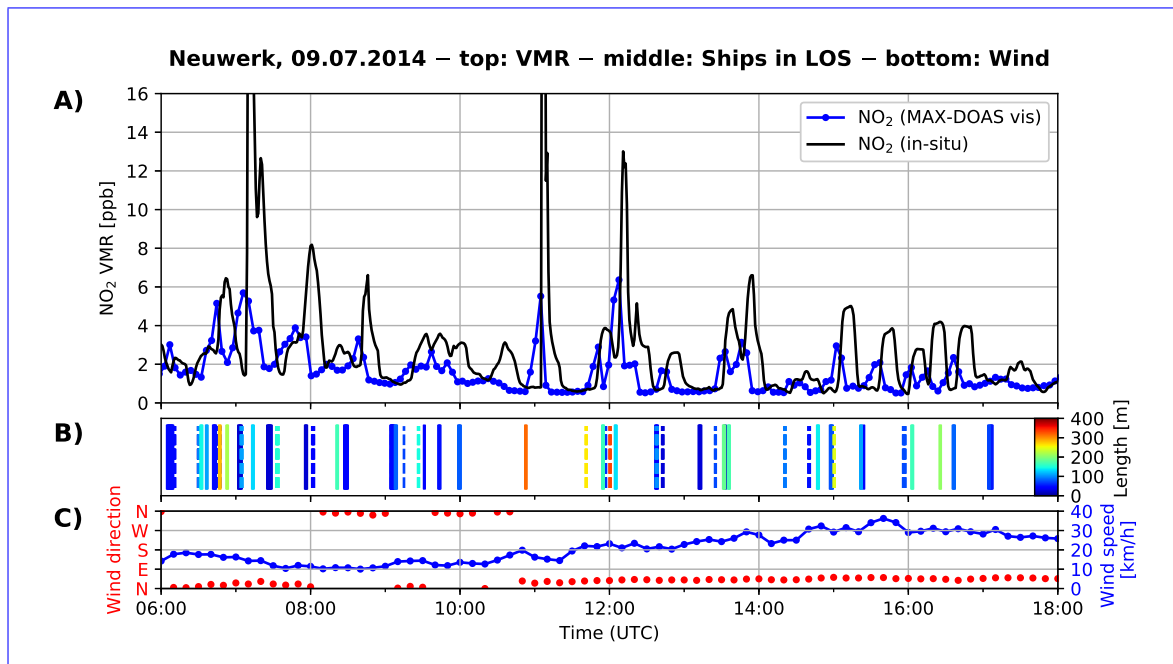

Figure 11: MAX-DOAS and in-situ ~~NO$_2$ VMR~~NO$_2$ volume mixing ratio, AIS and wind data on
Wednesday, 9 July ~~2014.~~2014:
~~Top:~~ **A)** MAX-DOAS (~~measured in the~~ visible~~spectral range~~) and in-situ ~~NO$_2$~~NO$_2$ VMR
~~Middle:~~ **B)** Vertical bars indicating that a ship is in the line-of-sight of the instrument,
solid bars: ship moves from left to right (west to east), dashed vice versa, colors representing ship length
~~Bottom:~~ ~~wind~~ **C)** Wind speed and direction measured on Scharhörn (HPA)

~~From the Figure, it can be easily identified that ship~~ Ship emission peaks measured by the in-situ instrument are both higher and broader than the corresponding MAX-DOAS peaks, leading to a considerably larger integrated peak area, showing ~~nicely~~ the systematic underestimation of the NO_2 concentrations inside ship plumes by the MAX-DOAS instrument due to the averaging along the horizontal light path.

~~It is also clearly visible, that often~~ Normally, a time-shift between MAX-DOAS and in-situ peaks exists, ~~and that the in-situ peaks are measured with a certain delay. This~~ which is due to the long distance of about 6–7 km to the shipping lane, that the plumes have to travel until they reach the radar tower. This time-shift depends on the wind velocity and gets smaller for higher wind speeds. In ~~Figure 11~~the figure, this dependency can be seen when comparing the magnitude of the time delay for measurements in the morning (low wind speeds) and evening (higher wind speeds) ~~.~~

This travel time also explains the broader peaks in the in-situ measurements, since the emitted plume spreads and dilutes on ~~it's~~its way to the radar tower.

~~This day of compared~~ However, if the pollution is horizontally well-mixed in the measured air mass, which is approximately the case for background pollution coming from the coast but not for ship plumes, MAX-DOAS ~~(visible) and in-situ NO₂ measurements is only a small cutout of three years of measurements on Neuwerk. Longer time-series comparisons for NO₂ (UV) and SO₂ volume mixing ratios are plotted in the upper subplots in Figures ?? and ??.~~

~~Figure ?? shows three months of continuous and simultaneous in-situ~~ and ~~MAX-DOAS (UV) NO₂ measurements in summer 2014. Because of problems with the~~ in-situ ~~SO₂ device from 2014 on mentioned above, for SO₂ a shorter time period with six weeks of measurements from the year before (summer 2013) is shown in Fig. ??.~~

~~What can be seen from all figures is a good agreement between both instruments for the low values (well-mixed background pollution), but large differences for individual high values (ship emission plumes). During night only the in-situ device can measure , explaining the small, periodically repeated gaps in~~ instrument should in principle measure the ~~MAX-DOAS time-series. Larger gaps are due to instrumental problems linked to power failures.~~

~~A) Long-term time-series comparison of NO₂ volume mixing ratios from in-situ and MAX-DOAS (UV) instruments during summer 2014. For the MAX-DOAS instrument, all measurements in all azimuth viewing directions are shown. B) Daily means of NO₂ VMR from MAX-DOAS (UV) and in-situ during summer 2014. For the MAX-DOAS instrument, all measurements in all azimuth viewing directions have been averaged. For the in-situ instrument, the mean of all measurements during the daily MAX-DOAS measurement periods (sunrise till sunset) have been taken.~~

~~A) Long-term time-series comparison of SO₂ volume mixing ratios from in-situ and MAX-DOAS instruments during summer 2013. For the MAX-DOAS instrument, all measurements in all azimuth viewing directions are shown. B) Daily means of SO₂ VMR from MAX-DOAS and in-situ during summer 2013. For the MAX-DOAS instrument, all measurements in all azimuth viewing directions have been averaged. For the in-situ instrument, the mean of all measurements during the daily MAX-DOAS measurement periods (sunrise till sunset) have been taken.~~

~~Because of~~ same values. However, as discussed in Section 3.4, correction factors need to be applied to the ~~differences between both measurement techniques and geometries, especially the different height and shape of the peaks~~ MAX-DOAS VMRs to account for the different profile shapes of O_4 and the investigated pollutants NO_2 and SO_2, but in our case cannot be determined because no measurements of the height of the NO_2 and SO_2 layer exist. The uncorrected VMRs shown here can be strongly underestimated (up to a factor of 3), because they have been calculated with an overestimated path length. This is the case for background pollution as well as ~~the wind speed dependent time-delay due to travel time of plumes, it makes no sense to correlate single measurements. To weaken the impact~~

~~of those differences, averaging of individual measurementsover certain time periods was applied .~~ shipping emission measurements.

~~Figures ?? and ?? show in the lower subplot daily means of the measurement periods presented above.~~ Since the lack of comparability between both instruments for individual measurements, for a meaningful comparison and the computation of a correlation coefficient at this measurement site an averaging over longer time spans was applied to reduce the impact of the differences between both measurement methods. The fact that MAX-DOAS averages over a large horizontal distance should therefore cancel out on temporal average when comparing to in-situ measurements.

Figure 12 shows in Panel A three months of daily mean NO_2 VMRs from the in-situ and MAX-DOAS UV instrument in summer 2014 and in Panel B due to instrumental problems with the in-situ SO_2 device (see Fig. 4) six weeks of SO_2 daily mean VMRs from summer 2013. To have comparable conditions, for the in-situ instrument all measurements between the start of the MAX-DOAS measurements in the morning (with sunrise) and the end of measurements in the evening (with sunset) ~~were~~ have been averaged. The shaded areas show the corresponding standard deviation and indicate the variability during the single days.

~~As can be seen in the figures, even though~~ The long gap in the SO_2 time series was caused by a power outage.
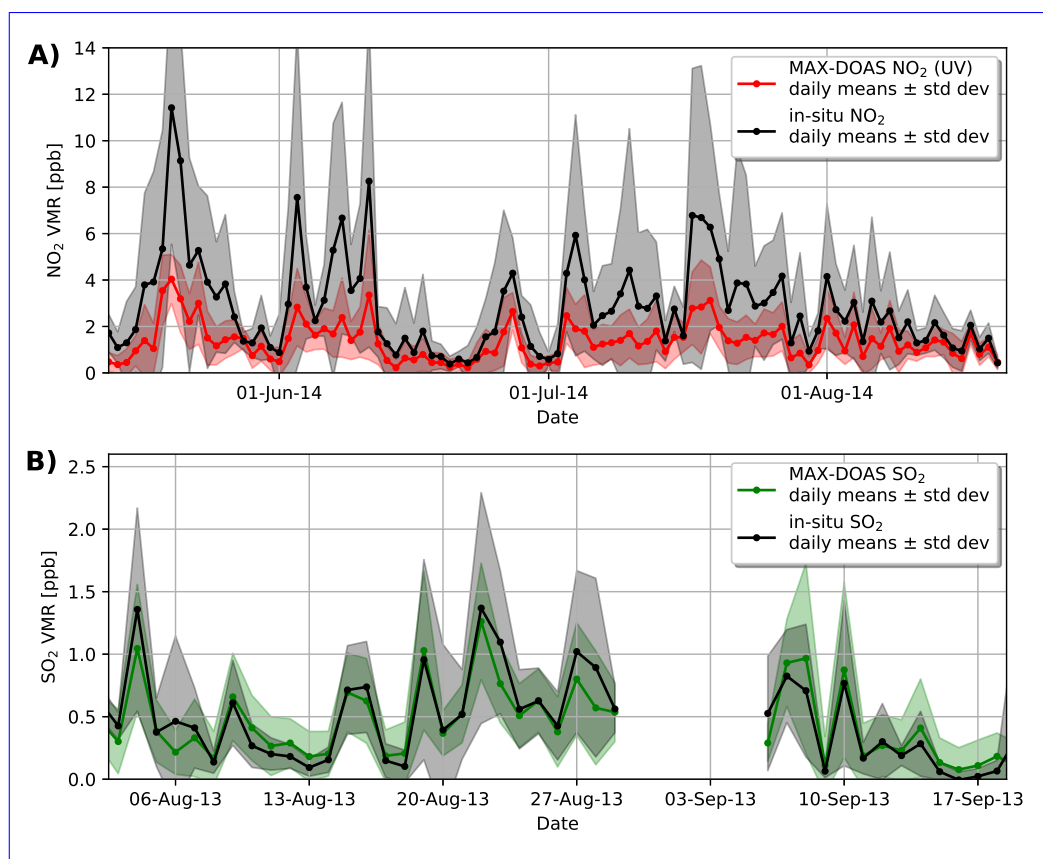

Figure 12: Comparison of MAX-DOAS (UV) and in-situ daily mean VMRs of NO_2 during summer 2014 (A) and SO_2 during summer 2013 (B). Shaded areas show the standard deviation for each daily mean value.

It is clearly visible that the in-situ ~~values are usually systematically higher , as expected, a very good agreement of the progression of both curves is found. This illustrates that~~ NO_2 VMRs are systematically higher than the uncorrected MAX-DOAS ~~can determine day-to-day trends as in-situ measurements.~~

760 ~~For the statistical evaluation of the correlation between both instruments, scatter plots for the presented~~ VMRs. The scaling factors which would be needed to bring both time series into agreement differ from day to day. A closer look into the individual days shows that these scaling factors also vary over the course of the day, even when wind direction and speed do not change. The scatter plot for this time-series of NO_2 ~~and SO_2 are shown~~ measurements in Fig. 13 ~~. A clear linear relationship~~

765 ~~exists between the daily mean measurements of both instruments with only small scatter. Pearson correlation coefficients of 0.87 0.93 prove that both are highly correlated. Using orthogonal distance regression (Deming regression), a linear regression line was fitted to the data. For NO_2 a slope of 2.71 ± 0.16 (visible)~~ Panel A shows a good correlation between MAX-DOAS and ~~2.72 ± 0.13 (UV) was found. For SO_2~~ in-situ daily means, but a slope strongly deviating from one and also some scatter.

770 The most important reason for the systematic differences is certainly the non-consideration of the ~~slope is smaller, 1.31 ± 0.09.~~ correction factors arising from the different profile shapes of O_4 and NO_2, leading to a systematic underestimation of the VMRs from the MAX-DOAS instrument (see Section 3.4 for a more detailed discussion). But also "light dilution", i.e. light scattered into the line-of-sight between the instrument and the trace gas plume (Kern et al., 2010) might play a role reducing the

775 measured off-axis SCDs .

For SO_2, the daily mean VMRs from MAX-DOAS and in-situ instrument in Fig. 12 Panel B show a much better agreement. The scatter plot in 13 Panel B confirms this with a slope much closer to unity, but more scatter around the fitted line.
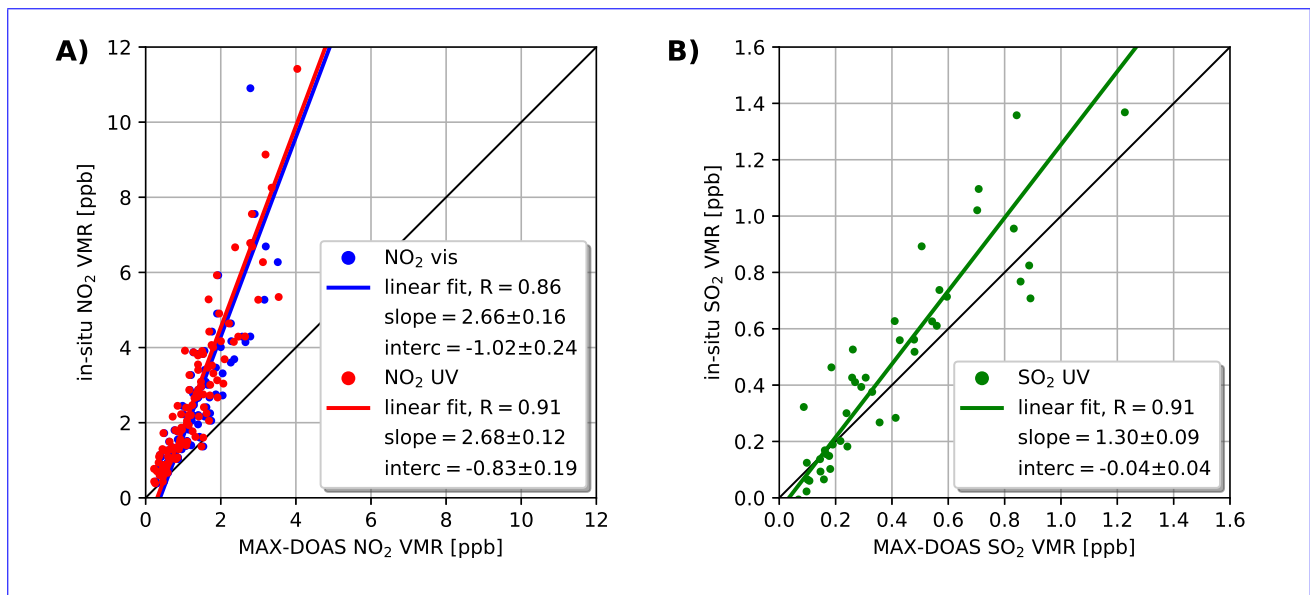

Figure 13: Scatter plot of A) NO_2 VMR and B) SO_2 VMR from MAX-DOAS vs. in-situ. For NO_2 daily means from summer 2014, for SO_2 daily means from summer 2013 are shown. For the MAX-DOAS instrument, to get a better statistic, all measurements in all azimuth viewing directions have been averaged. For the in-situ instrument, the mean of all measurements during the daily MAX-DOAS measurement periods (sunrise till sunset) has been taken. The linear fits were calculated with orthogonal distance regression (Deming regression), parameters are shown in the figures.

The difference in scaling factors for NO_2 and SO_2 ~~is due to a different fraction of shipping emissions~~

780 ~~on the measured overall emissions and also a different~~ can be attributed to plume chemistry. During combustion, mainly nitric oxide (NO) is produced. This has to be converted to NO_2 (through reaction with tropospheric ozone) before it can be measured by the MAX-DOAS instrument. Since the MAX-DOAS instrument sees the ship plumes in an earlier state, the fraction of NO_2 should be lower than in the in-situ measurements, explaining at least a part of the difference.

~~Scatter plot of A) NO₂ VMR and B) SO₂ VMR from MAX-DOAS vs. in-situ. For NO₂ measurements from 2014, for SO₂ measurements from 2013 are shown. For the MAX-DOAS instrument, to get a better statistic, all measurements in all azimuth viewing directions have been averaged. For the in-situ instrument, the mean of all measurements during the daily MAX-DOAS measurement periods (morning till evening) have been taken.~~ Although MAX-DOAS and in-situ VMRs show systematic
790 deviations in the absolute values, a very good agreement of the shape (the course) of the curves is found for NO₂ as well as SO₂. This illustrates that MAX-DOAS can determine day-to-day trends as in-situ measurements, even though no correction factors have been applied.

4.6 Diurnal and weekly variability of NO₂

Although our measurement station is located on a small island in the German Bight close to the
795 mouths of the Elbe and Weser river, our measurements are strongly influenced by air pollution from traffic and industry on land, depending on the prevailing wind direction. As can be seen from Fig. 1 A) and 3, wind coming from northeasterly, easterly, southerly and southwesterly directions will blow polluted air masses from the German North Sea Coast and hinterland to ~~Neuwerk~~our site. In Figure 14 the average diurnal variation of the measured NO₂ volume mixing ratios is shown as hourly mean
800 values. Solid curves show the respective curve for all measurements (~~for~~ with all wind directions), dashed lines show ~~only~~ the subset of measurements with wind coming only from the open North Sea with no coastal background pollution. Looking at the diurnal variation ~~for~~ in all measurements, ~~one can see quite nicely~~ the typical daily cycle for road-traffic-influenced air masses with ~~high~~ enhanced values in the morning and in the late afternoon during rush hour can be seen. If we restrain the data
805 to periods with wind from the open North Sea (dashed curves), this diurnal cycle ~~is gone~~ vanishes and values are more or less constant over day and also considerably lower. This result is in accordance with the expectations that the amount of ship traffic should be almost independent from the time of day.
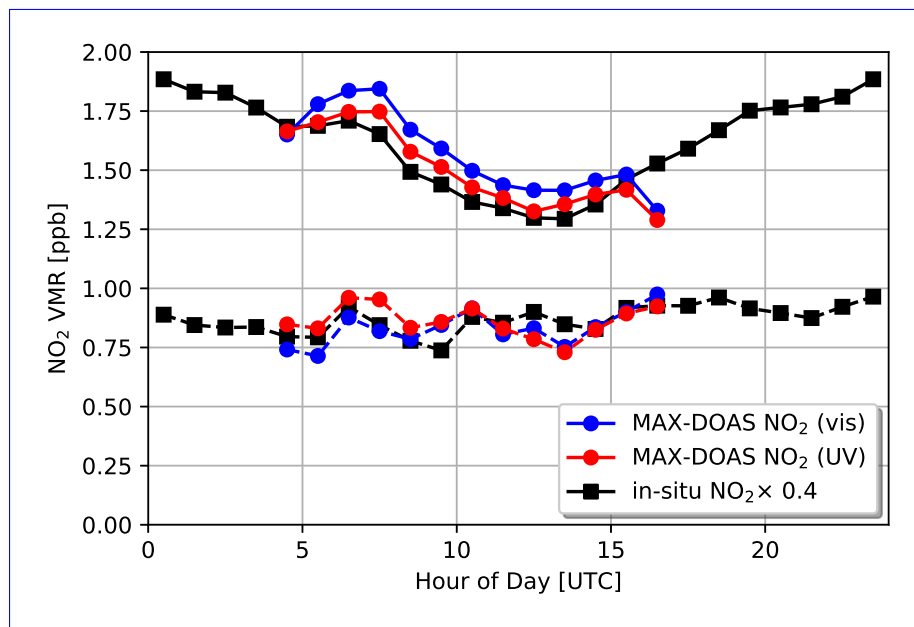

Figure 14: Average diurnal ~~cycles~~ cycle of ~~NO₂ volume mixing ratios measured with the~~ MAX-DOAS (UV and visible) and in-situ ~~instrument~~ NO₂ volume mixing ratios for all ~~wind directions~~ measurements (solid lines) and for ~~north-westerly winds~~ a subset of measurements with wind from the open North Sea (dashed lines). For a better visual comparability the in-situ values are scaled by a factor of 0.4.

810 ~~This influence of land-based road traffic is also visible if we take a look at the variability of NO_2 measurements during the week, as its~~ The mean NO_2 volume mixing ratios for each weekday shown in Fig. 15 ~~as means over the different weekdays. Again solid lines show mean values incorporating all measurements, dashed lines show the averaged subset of measurements with wind coming from northwesterly directions~~ illustrate again the influence of land-based road traffic. If we consider the whole time series (solid lines), lowest values are measured on Sundays, when road traffic is less intense.

815 ~~For wind~~ There is only little weekly cycle for air masses coming from the open North Sea ~~, the weekly signal is gone and measurements~~ (dashed lines). Measurements are more or less constant and again considerably lower. Such a weekly cycle for NO_2 in polluted regions has been observed and discussed several times before, for example in Beirle et al. (2003), Kaynak et al. (2009), Bell et al. (2009) and Ialongo et al. (2016).
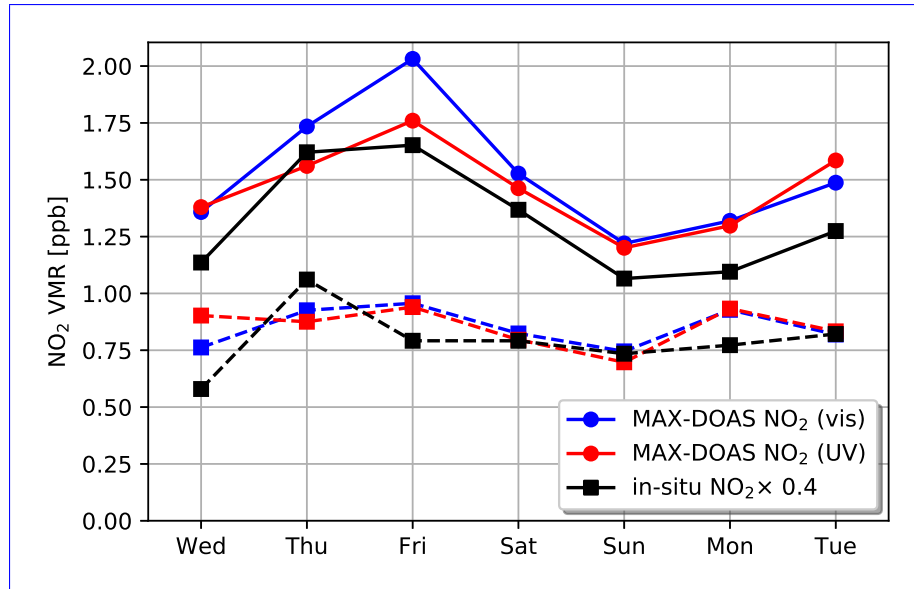

Figure 15: Average weekly cycle of ~~NO_2 volume mixing ratios measured with the~~ MAX-DOAS (UV and visible) and in-situ ~~instrument~~ NO_2 volume mixing ratios for all ~~wind directions~~ measurements (solid lines) and for ~~north-westerly winds~~ a subset of measurements with wind from the open North Sea (dashed lines). For a better visual comparability the in-situ values are scaled by a factor of 0.4.

820 It is also remarkable ~~in these two figures~~ that except for a scaling factor ~~(of approximately 0.4)~~, the ~~progression of the curves~~, the shape of the diurnal and weekly cycle retrieved from MAX-DOAS and in-situ measurements ~~show a very good agreement.~~

~~The observed difference in NO_2 mixing ratios between land-influenced and only ship-influenced air masses is in good agreement with a study from Aliabadi et al. (2015). They performed in-situ~~
825 ~~measurements of gases and particles in the Canadian Arctic in the 2013 shipping season and found 0.7–0.9 ppb (Cape Dorset) and 1.0–1.1 ppb (Resolute, Nunavut) higher NO_x concentrations for air masses influenced by local pollution compared to ship-influenced air masses~~ agrees very well for both instruments.

4.7 Dependence of NO_2 and SO_2 pollution levels on wind direction

830 As already mentioned in Sect. 1, on the 1st of January 2015, the sulfur content of marine fuels allowed inside the North and Baltic Sea Emission Control Areas (ECA) has been substantially decreased from 1.0 % to 0.1 %. Therefore, one would expect lower sulfur dioxide (SO_2) values in 2015 compared to the years before, especially when the wind is blowing from the open North Sea, where shipping emissions

are the only source of SO$_2$. This expectation is confirmed by the measurements. ~~Looking at single day measurements (see Fig. 19), no~~ <u>In the data since 2015, no distinct</u> ship emission peaks are visible ~~any more in the 2015 SO$_2$ data and most of the measured values are within the noise (SO$_2$ detection limit lies around 2.5 × 10^{16} corresponding to 0.2 pbb for good weather conditions~~<u>anymore (for an example day see Section 4.9 below</u>). For a more detailed analysis, mean values over the whole time series before and after 1 January 2015 have been investigated, separated according to the prevailing wind direction.

Two days of SO$_2$ measurements (20 and 30 October 2014) showing very high values over several hours have been excluded from the time-series. Comparisons with our simultaneous in-situ measurements and measurements from the German Umweltbundesamt at the coast of the North Sea in Westerland/Sylt and at the coast of the Baltic Sea on the island Zingst showing a similar behavior as well as HYSPLIT backward trajectories suggest that on both days SO$_2$ plumes of the Icelandic volcano Bárdarbunga have influenced the measurements in northern Germany.

Figure 16 shows the wind direction distribution of the mean NO$_2$ and SO$_2$ path averaged volume mixing ratios for all measurements before and after the change in fuel sulfur limit regulations.
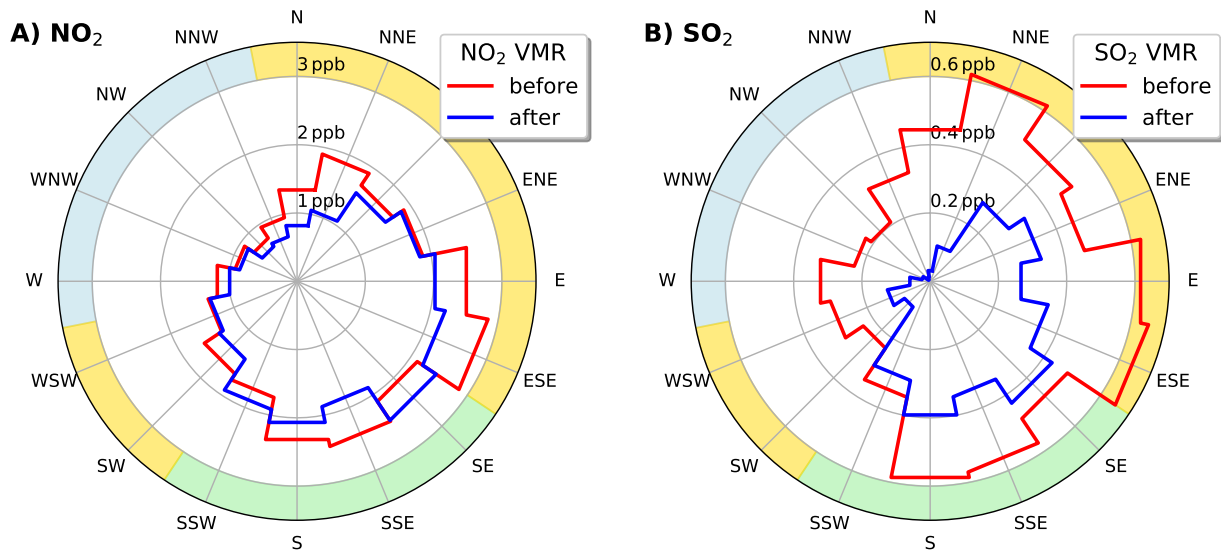

Figure 16: Wind direction distribution of the measured ~~SO$_2$~~ <u>NO$_2$</u> (A) and ~~NO$_2$~~ <u>SO$_2$</u> (B) volume mixing ratio in ~~0°~~ <u>0.5°</u> elevation before and after the change in fuel sulfur limit regulations on 1 January 2015. The colored sectors show directions with wind <u>mainly</u> from ~~the coast~~ <u>land</u> (green)~~and~~<u>,</u> open North Sea (blue) <u>and mixed origin (yellow)</u>.

For SO$_2$, a significant decrease is found, particularly for wind directions from West to North with wind from the open North Sea. For this sector, values in 2015 are close to zero. This shows that the new and more restrictive fuel sulfur content limits lead to a clear improvement in coastal air quality. ~~Only for wind from south-southwest there is no change in SO$_2$. This might be the influence of emissions from the coal-fired power plant Wilhelmshaven~~<u>For wind directions with mainly land-based sources, no or only a small decrease is observed.</u>

<u>The typical average SO$_2$ concentrations measured by the German Federal Environmental Agency (Umweltbundesamt, 2017) in 2016 for rural stations in Northern Germany are around 0.5–1 µg/m^3, corresponding to 0.2–0.4 ppb (Conversion factor: 1 ppb $\hat{=}$ 2.62 µg/m^3 for SO$_2$). Measurements in cities and especially close to industrial areas show higher values. Bremerhaven, which is ~~located exactly in this direction.~~ the station closest to our instrument, has a mean concentration of 1.77 µg/m^3, corresponding to 0.67 ppb. The reported values for rural stations are in good agreement with our</u>

measurements of 0.3–0.4 ppb for wind directions with mainly land-based pollution sources (green sector in Fig. 16 Panel B) since January 2015.

For NO_2 on the other hand, both the directional distribution and the absolute values are nearly identical for both time periods, implying no considerable changes in NO_x emissions. This result meets the expectations, since no NO_x emission limits have been set into force up to now for the North and Baltic Sea emission control area.

4.8 Contributions of ships vs. land-based pollution sources on coastal air quality on Neuwerk

The distribution of measured NO_2 and SO_2 volume mixing ratios depending on the wind direction shown in Fig. 16 can be used to estimate the contributions of ships and land-based sources to coastal air pollution levels. To trade ship emissions off against land-based emissions (e.g. industry, road transport), two representative sectors of wind directions have been chosen, both 90 degrees wide: A north-westerly sector (258.75° to 348.75°) with wind from the open North Sea and ships as the only local source of air pollution and a south-easterly sector (123.75° to 213.75°) with wind mainly coming from land and almost no ship traffic. Air masses brought by wind from the other directions, for example from the mouth of the river Elbe in the East of Neuwerk, can contain emissions from land-based pollution sources as well as ship emissions. These remaining directions will ~~therefore~~ be called "mixed" in the following. It is now assumed, that trace gas concentrations measured during periods with wind from one of these sectors have their source in the according sector. For getting a good statistic, measurements in all azimuth angles have been included. Figure 17 shows the results in several pie charts.

For both NO_2 and SO_2, more than half (around 50–60 %) of all measurements have been taken while wind was coming from either the assigned sea or land sector. This implies ~~,~~ that not only a small sample, but the majority of measurements can be used for the estimation of source contributions, making the assumption of using these sectors as representative samples for ships and land-based source regions a reasonable approximation. There are differences in the time series of NO_2 and SO_2 coming from the fact that the SO_2 fit delivers realistic values only up to 75° solar zenith angle and the NO_2 was fitted until 85° SZA, leading to less measurements for SO_2 than for NO_2, especially pronounced in winter times. Despite this, the general distribution pattern of wind direction frequency for NO_2 and SO_2 is quite similar, with wind coming from the sea 32–42 % of the time and from the land sector 18–24 % of the time.

For NO_2 (upper row in Fig. 17), more than half of the total NO_2 measured on Neuwerk can be attributed to wind from either of both sectors, with 21 % coming from ships and 31 % coming from land. ~~This means that from the mean NO_2 level of (1.49 ± 1.30) ppb (mean ± standard deviation) measured on Neuwerk (averaged over all measurements), at least 0.31 ppb is attributed to come from shipping emissions and 0.47 ppb from land-originated sources. The remaining 0.71 ppb is either from ships or coming from the land, or, which is most probable, a mixture of both. The precise shares for this contribution cannot be distinguished from the available data.~~

If we consider only the two sectors, for which we can identify the primary sources and take theses as representative, we can say that 40 % of the NO_2 on Neuwerk is coming from shipping emissions, but with 60 %, the majority, is coming from land. One reason for that is that the island Neuwerk is relatively close to the coastline (around 10 km) and is obviously still impacted by polluted air masses from land, which has also been observed in the diurnal and weekly cycle analysis shown in Figures 14 and 15. This might also give us a hint that in coastal regions in Germany land-based sources like road traffic and industry are, despite the heavy ship traffic, the strongest source of air pollution and ship emissions come in second.
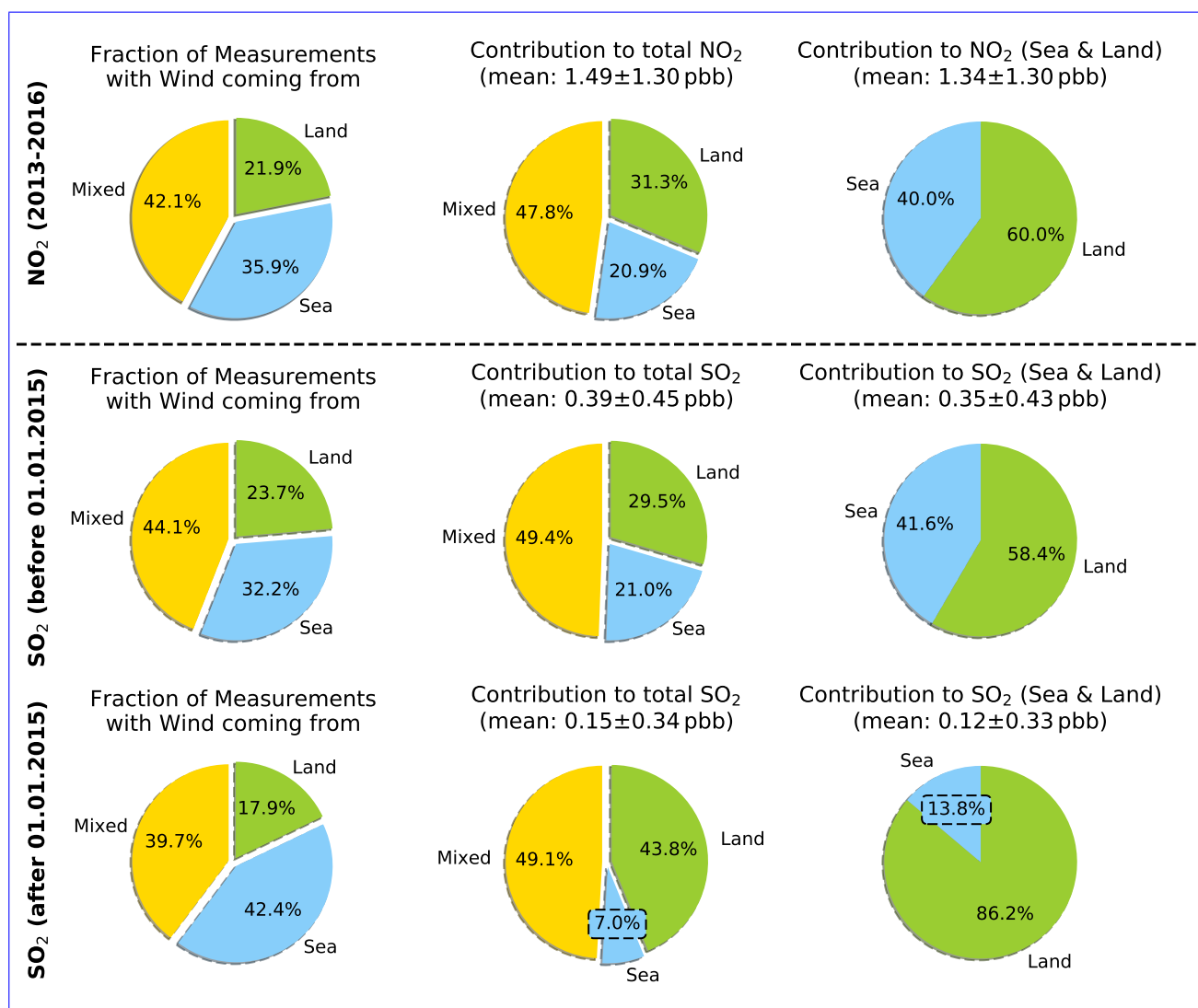
Figure 17: Contributions of ships and land-based pollution sources to measured NO_2 (top row) and SO_2 (middle and bottom row) levels on Neuwerk. For NO_2 the complete time series of measurements from 2013 to 2016 has been taken into account, for SO_2 the data have been divided into the time before and after the change in fuel sulfur content limits. The leftmost column of pie plots show the percentage of measurements with wind coming mainly from land (green), only from sea (blue) and from directions with mixed contributions (yellow). The middle column shows the contributions to the integrated, total volume mixing ratios from these source regions in percent. The rightmost column of pie plots shows analogous the percentage and mean VMR contribution by considering only the land and sea sector. It can clearly be seen that the lower fuel sulfur limit lead to a strong decrease in the SO_2 contribution from shipping since 2015.

For SO_2 the whole time series of measurements from 2013 to 2016 was divided into two periods of nearly the same length: The first period is 2013 and 2014, which was before the introduction of stricter sulfur limits for maritime fuels in the North Sea on 1 January 2015. The according statistics to this period are shown in the middle row in Fig. 17. The second time period, after the change in fuel sulfur limits, includes all measurements from 2015 and 2016, with the corresponding pie plots in the ~~lower~~ bottom row of Fig. 17.

Before the change, 32 % of the measurements were taken when the wind was coming from the sea sector and about 24 % when it was blowing from the dedicated land sector. After the change, the wind was coming a bit more often from sea (42 %) and less often from land (18 %), but in general the situation was quite similar. ~~Although there are certain differences and especially less measurements for SO_2 compared to NO_2, the wind direction distribution for the whole time series of NO_2 is more or less the average of both periods, like expected.~~

The contributions of the three sectors (land, sea and mixed) to the total integrated SO_2 with 21 % coming from ships, ~~29 %~~ 30 % from land and ~~50 %~~ 49 % from the mixed sector for the time before the change in sulfur limits are very similar to those of NO_2, too. After the change, the contribution from the sea sector shrinks significantly from 21 to 7 %, while the relative contribution from the land sector increased from 29 to 44 %, the contribution from the mixed sector staying the same as around 49 %. ~~That this~~ This increase for the land source sector is only a relative increase ~~can be better seen by comparing the absolute contributions:~~ while the absolute contributions slightly decreased, as can be seen from Fig. 16. The relative contribution from the sea sector (shipping only source) decreased by a factor of 3 while the absolute contribution from this sector decreased by a factor of 8, even though the wind was coincidentally blowing more often from the open sea in this time period.

The overall mean SO_2 volume mixing ratio before 2015 is ~~(0.35 ± 0.41) ppb~~ (0.39 ± 0.45) ppb (mean $\pm$ standard deviation)~~, to which the sea sector contributed 0.072 ppb and the land sector 0.102 ppb~~. For 2015 and 2016, the total mean value declined by two-thirds to ~~(0.13 ± 0.31) ppb~~ (0.15 ± 0.34) ppb (mean $\pm$ standard deviation). ~~While the contribution from the land sector decreased by 44 % to 0.058 ppb, the contribution from the sea sector (shipping only source) decreased by a factor of 8 to now 0.009 ppb, even though the wind was coincidentally blowing more often from the open sea in this time period. This result shows~~

These results show clearly that the stricter limitations on the fuel sulfur content are working and significantly improved air quality in the North Sea coastal regions with respect to SO_2. This is in good agreement with other studies such as Kattner et al. (2015), who found that around 95 % of the ships are sticking to the new limits. This implies that the cheaper high sulfur heavy oil fuel is no longer in use in the region of measurement.

If again the two selected sectors are considered as representative for both land and sea sources, the shares of the contributions from sea/land changed from ~~41 %~~ 42 %/~~59 %~~ 58 % (which is very similar to those of NO_2) to 14 %/86 %. This again shows that since 2015, the vast majority of SO_2 emissions can be attributed to land sources and ships play only a negligible role. Prior to 2015, shipping emissions have been a significant source for SO_2 in coastal regions.

One aspect which is neglected in ~~this approach~~ the source allocation to wind sectors is that in situations with good visibility and low wind speeds even for wind coming from southern directions, the MAX-DOAS instrument can measure ship emissions peaks in the north of the island, but being typically ~~much smaller and less distinct~~ very small. Compared to the often strongly enhanced background pollution in cases with southerly winds, ~~these peaks should not play a big roll. This issue will lead~~ the contribution from these peaks is negligible (in the order of a 1–3 %), but certainly leads to a small overestimation of land sources.

~~Contributions of ships and land-based pollution sources to measured NO_2 (top row) and SO_2 (middle and bottom row) levels on Neuwerk. For NO_2 the complete time series of measurements from 2013 to~~

955 2016 has been taken into account, for SO₂ the data have been divided into the time before and after the change in fuel sulfur content limits. The leftmost statistic shows the percentage of measurements with wind coming only from land (green), only from sea (blue) and from directions with mixed contributions (yellow). The next one to the right shows the contributions to the integrated, total volume mixing ratios from these source regions in percent. The adjacent pie plot shows the contributions to the total

960 mean in ppb. The rightmost pie plots show analogous the percentage and mean VMR contribution by considering only the land and sea sector. It can clearly be seen that the lower fuel sulfur limit lead to a strong decrease in the SO₂ contribution from shipping.

4.9 Determination of SO₂ to NO₂ ratios in ship plumes

For monitoring of pollutant A monitoring of emissions from single ships the individual plume measurement

965 peaks have to be analyzed requires the analysis of individual plume peaks in the NO₂ and SO₂ data sets. It is difficult to derive the absolute amounts (e.g. in mass units) of the emitted gaseous pollutants by our MAX-DOAS remote sensing technique. As explained before, the The height and width of the measured peaks does not only depend on the amount of emitted pollutants), but also strongly on the geometry, while getting the highest values when measuring alongside the plumes, and much

970 smaller values when the plume moves orthogonal to the line-of-sight of our instrument. The result of our measurements are integrated concentrations along a long and unknown light path. By using the measured O₄ columns as a tracer for the effective light path length as shown above, an approximation of the horizontal light path length is estimated. With this, long-path averaged volume mixing ratios can be calculated. But to get In addition to that, also the time span between emission and measurement

975 plays a role for the height of the NO₂ peaks because of NO to NO₂ titration.

To determine the mixing ratio inside the plume plumes, additional information on the length of the light path inside the plume would be needed, which cannot be retrieved from our measurements. This means that without further assumptions, we cannot determine emission factors for the emitted gases (e.g for emission inventories, which are used as input for model simulations).

980 Although measurements of emission factors cannot be measured by MAX-DOAS directly, both the NO₂ and SO₂ signals yield the ratio of both. These ratios can then be compared to ratios of emission factors reported in other studies as well as measurements on other sites or with different instruments, bearing in mind possible deviations due to NO to NO₂ titration.

By comparing SO₂ to NO₂ ratios from different ships it is possible to roughly distinguish whether

985 a ship is using fuel with high or low sulfur content (giving a high or low SO₂ to NO₂ ratio). The SO₂ to NO₂ ratio can also give insights into the chemistry inside the plumes, since the relative amounts of NO₂ and NO in the emitted NO_x depend on the time span from stack emission and the presence of tropospheric ozone for the conversion of the mainly produced NO to NO₂. Beecken and Mellqvist from Chalmers University (Sweden) use this relationship for airborne DOAS measurements of ship

990 exhaust plumes on an operational basis in the CompMon project (Compliance monitoring pilot for MARPOL Annex VI) (Van Roy, 2016). Following the ships and measuring across the stack gas plume they can discriminate between low (0.1 %) and high (1 %) fuel sulfur content ships with a probability of 80–90 % (Van Roy, 2016).

From the spectra measured by our MAX-DOAS UV instrument both SO₂ and NO₂ columns can

995 be retrieved at once. The two columns are measured at the exact same time along nearly the same light path. To calculate SO₂ to NO₂ ratios for the measured pollutant peaks simply the ratio of the measured differential slant column densities has to be computed.

In order to identify separate ship related signals from smooth background pollution, first a running median filter has been was applied to the time series of NO₂ and SO₂ measurements , to identify

1000 low values and to determine the baseline between the peaks, which originates from slowly varying

~~well-mixed background pollution levels. The median filter window (kernel size) was manually adapted for each day.~~ with a large kernel size (e.g. over 21 points). If too many broad peaks are contained in the time series this is not sufficient and the resulting median might be systematically higher than the actual baseline. In this case, on the values in the lower 50 % quantile again a running median with a smaller kernel size (e.g. 5) was applied, giving a good approximation of the real baseline.

In the next step, ~~by subtracting this baseline~~ this baseline is subtracted from the raw signal~~, one can get rid of the background pollution and only the pollutant peaks should remain~~. A simple peak detection algorithm was used to identify the peaks in the ~~NO$_2$ signal, and then~~ baseline-corrected NO$_2$ signal. Then the corresponding peaks in the SO$_2$ were assigned~~. This procedure using the NO$_2$, which peaks are always sharp and distinct, as a tracer for the identification makes it possible to detect the ship peaks even when the sulfur content in the fuel is very low and almost no SO$_2$~~, thus accounting for cases when no SO$_2$ enhancement is measured. In ~~the last step, to get~~ a final manual checkup, all the identified peaks were looked through, filtering out for example all the cases when peaks are too close together to be separated and fine-tuning the baseline detection algorithm parameters if necessary.

To achieve a better signal-to-noise ratio, the integrals over both the NO$_2$ and SO$_2$ peak are calculated and the ratio of both values is computed in the last step.

Figure 18 shows the approach as well as the results for ~~one~~ an example day in summer 2014, before the stricter fuel sulfur content limits were introduced. ~~In both~~ Both the NO$_2$ and SO$_2$ signal show high and sharp peaks~~are visible~~, originating from ~~measured~~ ship plumes. ~~The shape~~ Most of the peaks ~~is also often quite similar~~ are of similar shape in NO$_2$ as well as SO$_2$ signal. The measured SO$_2$ to NO$_2$ ratios lie in the range from ~~0.15 to 0.47 with most of the values around 0.3. How different these ratios sometimes are, can nicely be seen from the two ships close to~~ 0.17 to 0.41. The SO$_2$ to NO$_2$ ratio can vary strongly for different ships. For example, the plume of the ship passing the line-of-sight around 12:00 ~~and 12:30 UTC . The first one~~ UTC has a high NO$_2$ ~~value and a relatively small SO$_2$value, the second one a lower NO$_2$ peak and a very high SO$_2$ peak~~content, but is low in SO$_2$, whereas the opposite is true for the ship passing at 12:30 UTC, indicating that the second ship was using fuel with a considerably higher sulfur content than the first one.

~~In contrast to this,~~ Figure 19 shows one example day in summer 2015, after the establishment of stricter sulfur ~~limis~~limits. For better comparison to Fig. 18, the y-axis limits are the same. ~~Also~~ High NO2 peaks also occur on this day~~high NO$_2$ peaks are visible, however,~~. However, the SO$_2$ signal shows no clearly distinguishable peaks anymore, a result of much less sulfur in the fuel. Consequentially, the measured SO$_2$ to NO$_2$ ratios are much smaller on this day and range from ~~0.02 to 0.19, with most of them close to 0.1~~0 to 0.09. There might be some small peaks in the SO$_2$ signal, but for most of them it cannot be determined if these are real enhancements or just noise fluctuations. ~~Because of much less light in the SO$_2$ fitting window, SO$_2$ signals are noisier than NO$_2$, especially when the overall values are small. From this plot one can also see that this method slighty overestimate the SO$_2$ to NO$_2$ ratios when no SO$_2$ peaks can be measured, since the noise also consists of a lot of smallpeaks, which might be wrongly assigned to SO$_2$~~ The two peaks at 10:40 and 14:00 UTC, slightly above noise level but still very small, might be real SO$_2$ signals from ships with a higher than average fuel sulfur content.

For a statistically meaningful comparison of both time periods two representative samples of ship emission peaks have been selected by hand for days with good measurement conditions, which were identified by using the solar radiation measurement data of our weather station. One sample of ~~1060~~ more than 1000 peaks, measured in 2013 and 2014 representing the state before introduction of stricter fuel sulfur content limits, and another ~~sample of 1060~~ equally-sized sample of more than 1000 peaks measured in 2015 and 2016, representing the situation afterwards, were ~~retrieved~~analyzed in a semi-automatic way. It has to be noted that it cannot be ruled out that a certain fraction of ships were measured repeatedly on different days. It is also highly probable that the plume from some
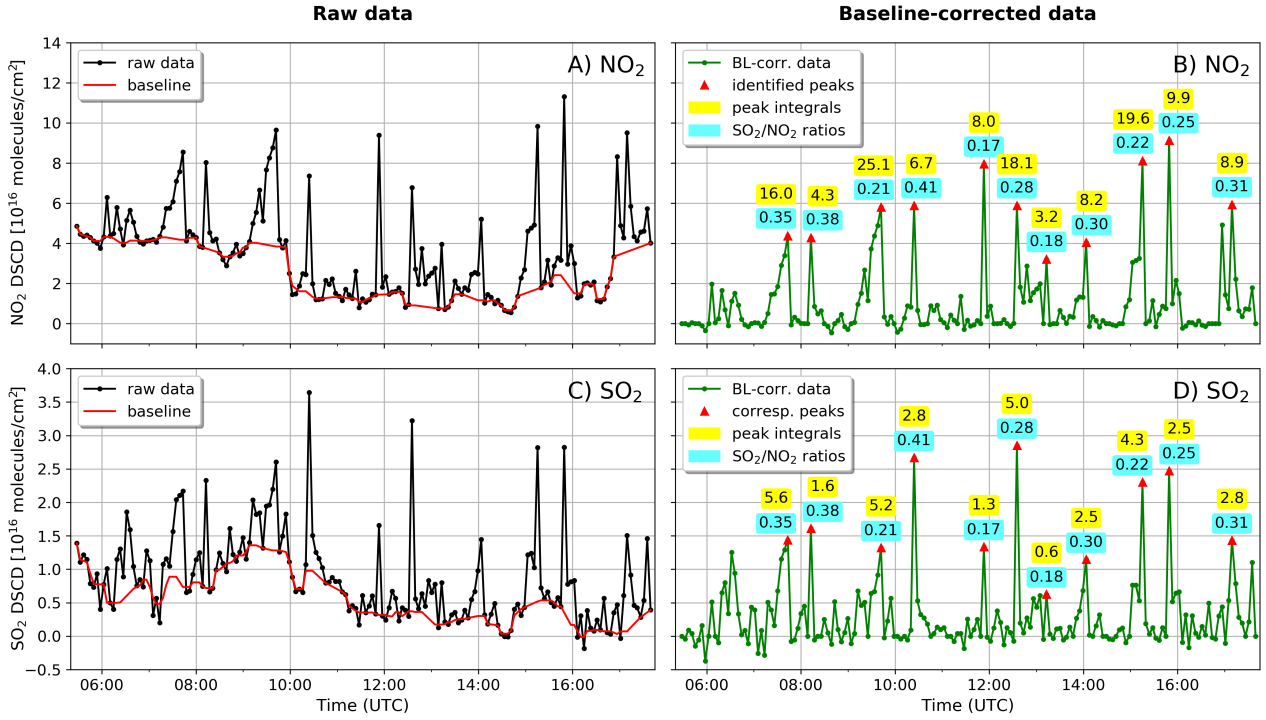
Figure 18: Calculation of SO_2 to NO_2 ratios for ship emission peaks for one example day (23.07.2014) before the change in sulfur emission limits. ~~Subplot~~ Panel A) shows the UV NO_2-DSCD raw data for ~~0°~~ 0.5° elevation and $-25°$ azimuth ~~. A running median filter (over 17 points) is used to determine low NO_2 values for~~ and the ~~subtraction of the background NO_2 signal~~ determined baseline. Panel B) shows the baseline-corrected NO_2 data for which the automatically identified peaks are highlighted with red triangles. Numbers close to the peaks denote the peak integrals in 1×10^{16} molecules/cm^2 (marked in yellow) and the SO_2 to NO_2 ratios (marked in blue). C) and D) show the corresponding plots for SO_2.~~For SO_2 a running median kernel size of 29 points has been used.~~
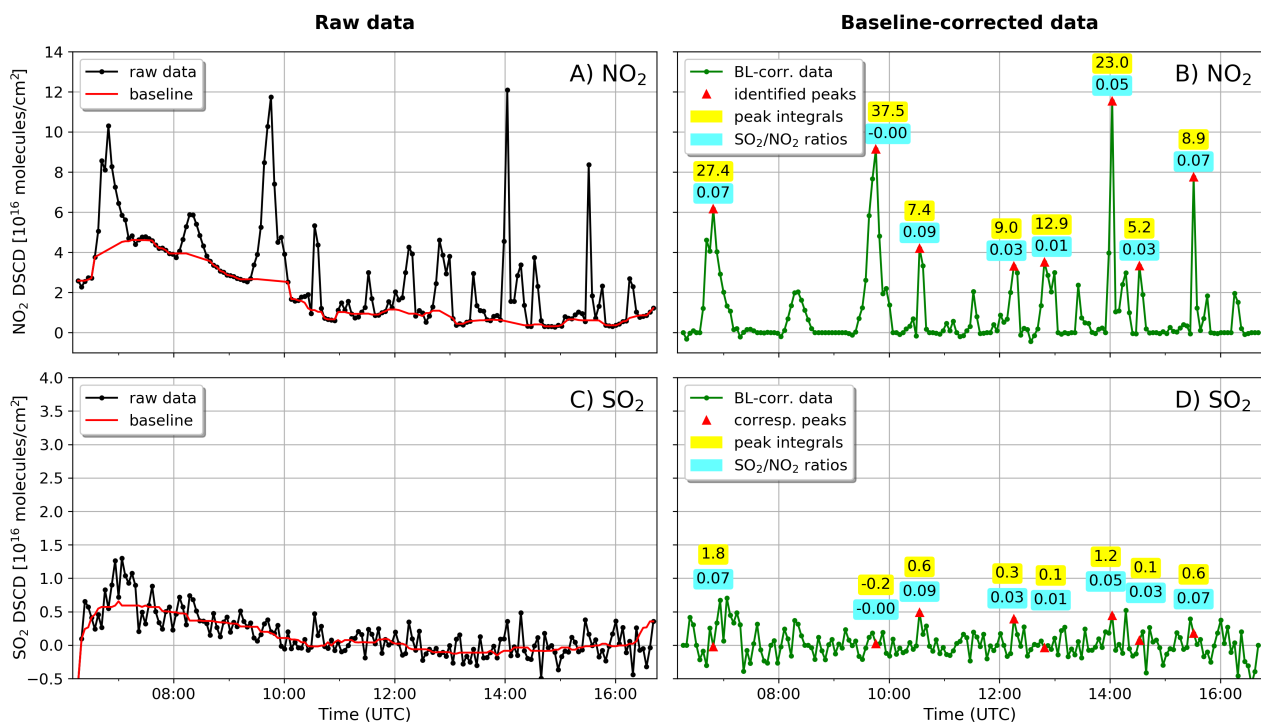
37

Figure 19: As Figure 18 but for an example day (03.07.2015) after the introduction of stricter fuel sulfur content limits. Measurements in ~~0°~~ 0.5° elevation and 65° azimuth are shown. ~~A running median filter over 21 (29) point for NO₂ (SO₂) has been used.~~ Peak integrals are given in ~~1×10^{16} molecules/cm²~~ 10^{16} molecules/cm²

individual ships was measured multiple times at different locations in the different azimuth directions while the ship was passing the island.

The distributions of the SO₂ to NO₂ ratios derived from the peak integrals for the two samples are shown in a histogram in Fig. 20. It can be seen that SO₂ to NO₂ ratios were considerably higher before 2015, with a mean of ~~0.31~~0.30, a standard deviation of 0.13 and a median value of ~~0.30~~0.28. After the change in fuel sulfur content limits, the SO₂ to NO₂ ratios became much lower with a mean of ~~0.087~~0.007, a standard deviation of ~~0.065~~0.089 and a median value of ~~0.074, a reduction by a factor of four~~0.013, a drastic reduction. A Welch's t-test (unequal variances t-test) ~~gives a p-value of zero (in double-precision floating-point format) indicating~~ shows that the reduction is statistically highly significant. These results can be compared to the overall average SO₂ to NO₂ ratios on all days with good measurement conditions from which the peaks have been selected: For the time before 2015, this gives a mean value of 0.10 and a median of 0.17 and for 2015 and 2016, one gets a mean value of 0.024 and a median of 0.058. As expected, these values are significantly lower than the SO₂ to NO₂ ratios obtained from the ship plumes which do not include background pollution.

~~Because the SO₂ noise interference mentioned above leading to overestimation of the ratios for low SO₂ levels, the results for the time period after the reduction in sulfur limits should be considered as upper limits. The reduction is expected to be even more pronounced in reality.~~

It is also interesting to compare our results with those from other studies~~.~~, bearing in mind possible systematic differences due to different measurement geometries, techniques and sites and therefore different NO to NO₂ titration in the plumes.

McLaren et al. (2012) measured NO₂ to SO₂ emission ratios in marine vessel plumes in the Strait of Georgia in summer 2005. In a sample of 17 analyzed plumes, a median molar NO₂/SO₂ ratio of

38

2.86 was found. Translated into a SO_2/NO_2 ratio this yields a value of 0.35 which is, considering the small sample size, in good agreement with our findings for the time before 2015.

Another study was carried out ~~from~~ by Diesch et al. (2013) measuring gaseous and particulate emissions from various marine vessel types and a total of 139 ships on the banks of the river Elbe in 2011. ~~From their reported SO_2 and NO_2 emission factors one can also derive SO_2~~ SO_2 to NO_2 emission ~~ratios~~ratios can also be derived from from their reported SO_2 and NO_2 emission factors: For small ships (<5000 tons) a ratio 0.13 and an average fuel sulfur content (FSC) of $(0.22 \pm 0.21)\,\%$ was found, for medium size ships (5000–30 000 tons) a ratio of 0.24 and a FSC of $(0.46 \pm 0.40)\,\%$ and for large ships (>30 000 tons) a ratio of 0.28 and a FSC of $(0.55 \pm 0.20)\,\%$. Especially the values for medium size and large ships fit quite well to our results while plumes from very small vessels (if measurable at all) have often not been taken into account for the statistic because of the low signal-to-noise ratio.

When assuming that ~~their dependence between~~ the dependency of SO_2 to NO_2 ratio ~~and~~ to fuel sulfur content is also applicable to our dataset, we can roughly estimate that the ships measured by us before 2015 used an average sulfur content of 0.5–0.7 %, in good agreement with the results of Kattner et al. (2015), which since 2015 decreased ~~to 0.1–0.2 %~~ drastically with 0.1 % as an upper limit.
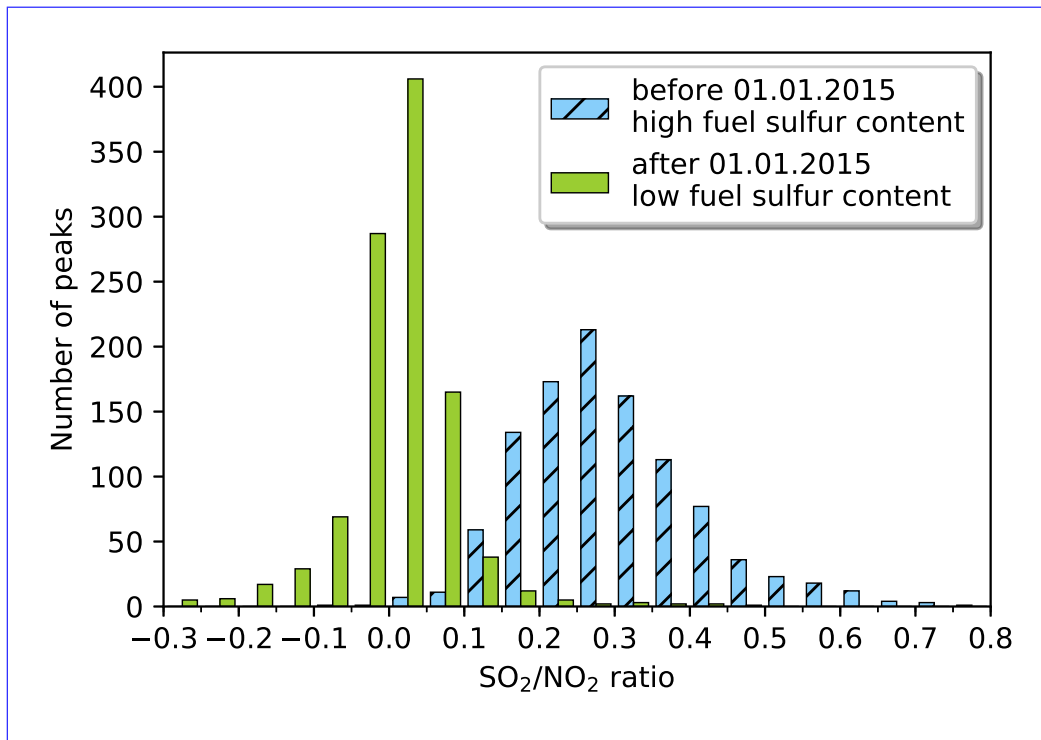

Figure 20: Histogram showing the distribution SO_2 to NO_2 ratios in two samples ($N = 1060$ for each) of ship emission peaks measured in ~~0°~~ 0.5° elevation and all azimuth angles for the time before (blue) and after (green) the change in fuel sulfur content regulation on the 1st of January 2015.

5 Summary and conclusions

In this study, three years of MAX-DOAS observations of NO_2 and SO_2 taken on the ~~Island~~ island of Neuwerk close to the shipping lane towards the harbor of Hamburg, Germany were analyzed for pollution emitted from ships. Using measurements taken at ~~0° elevation into~~ 0.5° elevation and different azimuthal directions, both background pollution and plumes from individual ships could be identified. Using simultaneously retrieved O_4 columns, path averaged volume mixing ratios for NO_2 and SO_2

could be determined. Comparison of NO_2 measurements in the UV and visible parts of the spectrum showed excellent agreement between mixing ratios determined from the two retrievals, demonstrating consistency in the results.

1095   MAX-DOAS measurements were also compared to co-located in-situ observations. High correlation was found between mixing ratios derived with the two methods on average, in-situ measurements showing systematically larger values, in particular during ship emission peaks. ~~This~~ These deviations can be understood by the difference in measurement volume, the MAX-DOAS measurements averaging over light paths of several kilometers and a systematic underestimation of MAX-DOAS VMRs due to

1100   different profile shapes of O_4 and the pollutants NO_2 and SO_2. For NO_2, the difference is larger than for SO_2, probably because of conversion of NO to NO_2 during the transport from the ship where the signal is detected by MAX-DOAS to the measurement site where the in-situ instrument was located.

Although the measurement site is within a few kilometers from one of the main shipping lanes, it is ~~also~~ influenced by land based pollution depending on wind direction. Comparing measurements taken

1105   under wind direction from the shipping lane and from land, systematic differences in the diurnal and weekly cycles of NO_2 are found. While NO_2 from land shows high values in the morning and evening and lower values around noon and on weekends, NO_2 levels from sea are more or less constant over time as expected from continuous shipping operations. These results are found in both MAX-DOAS and in-situ observations. Both NO_2 and SO_2 levels are often higher when wind is coming from land,

1110   indicating that land based sources contribute significantly to pollution levels on the island in spite of its vicinity to the shipping lanes. Analyzing the wind dependence of the signals in more detail, and excluding data with mixed air mass origin, the contribution of shipping sources to pollution on Neuwerk could be estimated to be 40 % for NO_2 and 41 % for SO_2 in the years 2013 and 2014. As nearly half of the measurements were taken under wind coming from mixed directions, this is only a

1115   rough estimate but is still a surprisingly small fraction.

Although the MAX-DOAS measurements cannot be used to directly determine NO_x or SO_2 emissions from individual ships due to the measurement geometry, the ratio of SO_2 to NO_2 column averaged mixing ratios gives a good estimate of the SO_2 to NO_x emission ratio. Using the data from Neuwerk, more than 2000 individual ship emission plumes were identified and the ratio of SO_2 to NO_2 computed

1120   after subtraction of the background values. The results varied between ships but on average yielded values of about 0.3 for the years 2013/2014, in good agreement with results from other studies.

Since January 2015, much lower fuel sulfur content limits of 0.1 % apply in the North and Baltic Sea. This resulted in large changes in SO_2 levels in the MAX-DOAS measurements when the wind is coming from the shipping lanes. In fact, ship related SO_2 peaks are rarely observed anymore since

1125   2015. Applying the same analysis as for the period before the change in legislation, no significant changes were found for NO_2 in terms of ratio between ship and land contribution or absolute levels. For SO_2 in contrast overall levels were reduced by two-thirds, and the relative contribution of shipping sources was reduced from 41 % to 14 %. It is interesting to note that a reduction in SO_2 levels was also observed in most wind directions coming from land, presumably because shipping emissions also

1130   contributed to SO_2 levels in coastal areas.

In summary, long-term measurements of NO_2 and SO_2 using a MAX-DOAS instrument demonstrated the feasibility of monitoring pollution originating from ships remotely. Pollution signals from individual ships can be identified and path averaged mixing ratios can be determined, which ~~under background pollution situations agree~~ on average correlate well with in-situ observations, reproducing

1135   day-to-day trends. MAX-DOAS measurements do not provide emission estimates for individual ships but allow statistical analysis of signals from thousands of ships at a distance and even under unfavorable wind conditions. Implementation of stricter sulfur limits in shipping fuel lead to a large reduction in SO_2/NO_x ratios in shipping emissions and a significant reduction in SO_2 levels at the German coast. The amounts of NO_2 are as expected not significantly impacted by the change of sulfur content

1140   in the fuel. This implies that combustion temperatures were probably not significantly changed. The

overall contribution of ship emissions to pollution levels at the measurement site is large but land based sources still dominate, even in the immediate vicinity of shipping lanes.

Acknowledgements

References

Alföldy, B., Lööv, J. B., Lagler, F., Mellqvist, J., Berg, N., Beecken, J., Weststrate, H., Duyzer, J., Bencs, L., Horemans, B., Cavalli, F., Putaud, J. P., Janssens-Maenhout, G., Csordás, A. P., Van Grieken, R., Borowiak, A., and Hjorth, J. (2013). "Measurements of air pollution emission factors for marine transportation in SECA". In: *Atmospheric Measurement Techniques* 6.7, pp. 1777–1791. ISSN: 18671381. DOI: 10.5194/amt-6-1777-2013.

Aliabadi, A. A., Staebler, R. M., and Sharma, S. (2015). "Air quality monitoring in communities of the Canadian Arctic during the high shipping season with a focus on local and marine pollution". In: *Atmospheric Chemistry and Physics* 15.5, pp. 2651–2673. ISSN: 16807324. DOI: 10.5194/acp-15-2651-2015.

Aulinger, A., Matthias, V., Zeretzke, M., Bieser, J., Quante, M., and Backes, A. (2016). "The impact of shipping emissions on air pollution in the greater North Sea region – Part 1: Current emissions and concentrations". In: *Atmospheric Chemistry and Physics* 16.2, pp. 739–758. DOI: 10.5194/acp-16-739-2016. URL: http://www.atmos-chem-phys.net/16/739/2016/.

Balzani Lööv, J. M., Alfoldy, B., Gast, L. F. L., Hjorth, J., Lagler, F., Mellqvist, J., Beecken, J., Berg, N., Duyzer, J., Westrate, H., Swart, D. P. J., Berkhout, A. J. C., Jalkanen, J. P., Prata, A. J., Van Der Hoff, G. R., and Borowiak, A. (2014). "Field test of available methods to measure remotely SOx and NOx emissions from ships". In: *Atmospheric Measurement Techniques* 7.8, pp. 2597–2613. ISSN: 18678548. DOI: 10.5194/amt-7-2597-2014.

Beecken, J., Mellqvist, J., Salo, K., Ekholm, J., and Jalkanen, J. P. (2014). "Airborne emission measurements of SO2, NOx and particles from individual ships using a sniffer technique". In: *Atmospheric Measurement Techniques* 7.7, pp. 1957–1968. ISSN: 18678548. DOI: 10.5194/amt-7-1957-2014.

Beecken, J., Mellqvist, J., Salo, K., Ekholm, J., Jalkanen, J. P., Johansson, L., Litvinenko, V., Volodin, K., and Frank-Kamenetsky, D. A. (2015). "Emission factors of SO2, NOx and particles from ships in Neva Bay from ground-based and helicopter-borne measurements and AIS-based modeling". In: *Atmospheric Chemistry and Physics* 15.9, pp. 5229–5241. ISSN: 16807324. DOI: 10.5194/acp-15-5229-2015.

Beirle, S., Platt, U., Glasow, R. von, Wenig, M., and Wagner, T. (2004). "Estimate of nitrogen oxide emissions from shipping by satellite remote sensing". In: *Geophysical Research Letters* 31.18, pp. 4–7. ISSN: 00948276. DOI: 10.1029/2004GL020312.

Beirle, S., Platt, U., Wenig, M., and Wagner, T. (2003). "Weekly cycle of NO2 by GOME measurements: a signature of anthropogenic sources". In: *Atmospheric Chemistry and Physics* 3.2, pp. 2225–2232. ISSN: 16807324. DOI: 10.5194/acpd-3-3451-2003.

Bell, T. L., Rosenfeld, D., and Kim, K. M. (2009). "Weekly cycle of lightning: Evidence of storm invigoration by pollution". In: *Geophysical Research Letters* 36.23, pp. 1–5. ISSN: 00948276. DOI: 10.1029/2009GL040915.

Berg, N., Mellqvist, J., Jalkanen, J. P., and Balzani, J. (2012). "Ship emissions of SO 2 and NO 2: DOAS measurements from airborne platforms". In: *Atmospheric Measurement Techniques* 5.5, pp. 1085–1098. ISSN: 18671381. DOI: 10.5194/amt-5-1085-2012.

Bobrowski, N. and Platt, U. (2007). "SO2/BrO ratios studied in five volcanic plumes". In: *Journal of Volcanology and Geothermal Research* 166.3-4, pp. 147–160. ISSN: 03770273. DOI: 10.1016/j.jvolgeores.2007.07.003.

Bogumil, K., Orphal, J., Homann, T., Voigt, S., Spietz, P., Fleischmann, O. C., Vogel, A., Hartmann, M., Kromminga, H., Bovensmann, H., Frerick, J., and Burrows, J. P. (2003). "Measurements of molecular absorption spectra with the SCIAMACHY pre-flight model: instrument characterization and reference data for atmospheric remote-sensing in the 230-2380 nm region". In: *Journal of Photochemistry and Photobiology A: Chemistry* 157.2-3, pp. 167–184. ISSN: 10106030. DOI: 10.1016/S1010-6030(03)00062-5. URL: http://linkinghub.elsevier.com/retrieve/pii/S1010603003000625.

Bollmann, M., Bosch, T., Colijn, F., Ebinghaus, R., Körtzinger, A., Latif, M., Matthiessen, B., Melzner, F., Oschlies, A., Petersen, S., Proelß, A., Quaas, M., Requate, T., Reusch, T., Rosenstiel, P., Schrottke, K., Sichelschmidt, H., Siebert, U., Soltwedel, R., Sommer, U., Stattegger, K., Sterr, H., Sturm, R., Treude, T., Vafeidis, A., Bernem, C. van, Beusekom, J. van, Visbeck, M., Wahl, M., Wallmann, K., and Weinberger, F. (2010). "Living With the Oceans". In: *World Ocean Review: Living with the oceans* 1, p. 236.

Brasseur, G. P. (1999). *Atmospheric chemistry and global change: [a textbook prepared by scientists at the National Center for Atmospheric Research, Boulder]*. Topics in environmental chemistry. New York, NY [u.a.]: Oxford Univ. Press. ISBN: 0195105214.

Chen, G., Huey, L. G., Trainer, M., Nicks, D., Corbett, J., Ryerson, T., Parrish, D., Neuman, J. A., Nowak, J., Tanner, D., Holloway, J., Brock, C., Crawford, J., Olson, J. R., Sullivan, A., Weber, R., Schauffler, S., Donnelly, S., Atlas, E., Roberts, J., Flocke, F., Hübler, G., and Fehsenfeld, F. (2005). "An investigation of the chemistry of ship emission plumes during ITCT 2002". In: *Journal of Geophysical Research D: Atmospheres* 110.10, pp. 1–15. ISSN: 01480227. DOI: 10.1029/2004JD005236.

Corbett, J. J. and Koehler, H. W. (2003). "Updated emissions from ocean shipping". In: *Journal of Geophysical Research* 108.D20, p. 4650. ISSN: 0148-0227. DOI: 10.1029/2003JD003751. URL: http://doi.wiley.com/10.1029/2003JD003751.

Corbett, J. J., Fischbeck, P. S., and Pandis, S. N. (1999). "Global nitrogen and sulfur inventories for oceangoing ships". In: *Journal of Geophysical Research* 104.D3, pp. 3457–3470. ISSN: 0148-0227. DOI: 10.1029/1998JD100040.

Corbett, J. J., Winebrake, J. J., Green, E. H., Kasibhatla, P., Eyring, V., and Lauer, A. (2007). "Mortality from ship emissions: A global assessment". In: *Environmental Science and Technology* 41.24, pp. 8512–8518. ISSN: 0013936X. DOI: 10.1021/es071686z.

Diesch, J. M., Drewnick, F., Klimach, T., and Borrmann, S. (2013). "Investigation of gaseous and particulate emissions from various marine vessel types measured on the banks of the Elbe in Northern Germany". In: *Atmospheric Chemistry and Physics* 13.7, pp. 3603–3618. ISSN: 16807316. DOI: 10.5194/acp-13-3603-2013.

DNV (2008). "Marpol 73/78 Annex VI - Regulations of Air Polution from Ships - Technical and Operational implications". In: *Fuel*, pp. 1–32.

Endresen, Ø., Sørgard, E., Sundet, J., Dalsøren, S., Isaksen, I., and Berglen, T. (2003). "Emission from international sea transportation and environmental impact". In: *Journal of Geophysical Research* 108.D17, pp. 1–22. ISSN: 0148-0227. DOI: 10.1029/2002JD002898.

EU (2005). "Directive 2005/33/EC of the European Parliament and of the Council". In: *Official Journal of the European Union* 1882, pp. 59–69. DOI: 10.3000/17252555.L_2009.140.eng. URL: http://eur-lex.europa.eu/LexUriServ/LexUriServ.do?uri=OJ:L:2005:191:0059:0069:EN:PDF.

EU (2008). "Directive 2008/50/EC of the European Parliament and of the Council of 21 May 2008 on ambient air quality and cleaner air for Europe". In: *Official Journal of the European Communities* 152, pp. 1–43. URL: http://eur-lex.europa.eu/LexUriServ/LexUriServ.do?uri=OJ:L:2008:152:0001:0044:EN:PDF.

1240 — (2016). *Air Quality Standards*. URL: http://ec.europa.eu/environment/air/quality/standards.htm (visited on 12/15/2016).

Eyring, V., Bovensmann, H., Cionni, I., Dall'Amico, M., Franke, K., Khlystova, I., Klinger, C., Lauer, A., Paxian, A., Righi, M., and Schreier, M. (2010a). *Impact of Ship Emissions on Atmosphere and Climate, SeaKLIM Final Report*. Tech. rep. DLR, p. 23. URL: http://www.pa.op.dlr.de/
1245 SeaKLIM/SeaKLIM%5C_Nachwuchsgruppe%5C_Schlussbericht%5C_FINAL.pdf.

Eyring, V., Köhler, H. W., Aardenne, J. van, and Lauer, A. (2005a). "Emissions from international shipping: 1. The last 50 years". In: *Journal of Geophysical Research* 110.D17, p. D17305. ISSN: 0148-0227. DOI: 10.1029/2004JD005619. URL: http://doi.wiley.com/10.1029/2004JD005619.

Eyring, V., Köhler, H. W., Lauer, A., and Lemper, B. (2005b). "Emissions from international shipping:
1250 2. Impact of future technologies on scenarios until 2050". In: *Journal of Geophysical Research* 110.D17, p. D17306. ISSN: 0148-0227. DOI: 10.1029/2004JD005620. URL: http://doi.wiley.com/10.1029/2004JD005620.

Eyring, V., Isaksen, I. S., Berntsen, T., Collins, W. J., Corbett, J. J., Endresen, O., Grainger, R. G., Moldanova, J., Schlager, H., and Stevenson, D. S. (2010b). "Transport impacts on atmosphere
1255 and climate: Shipping". In: *Atmospheric Environment* 44.37, pp. 4735–4771. ISSN: 13522310. DOI: 10.1016/j.atmosenv.2009.04.059. URL: http://linkinghub.elsevier.com/retrieve/pii/S1352231009003379.

Galle, B., Johansson, M., Rivera, C., Zhang, Y., Kihlman, M., Kern, C., Lehmann, T., Platt, U., Arellano, S., and Hidalgo, S. (2010). "Network for Observation of Volcanic and Atmospheric
1260 Change (NOVAC) - A global network for volcanic gas monitoring: Network layout and instrument description". In: *Journal of Geophysical Research Atmospheres* 115.D5, pp. 1–19. ISSN: 21698996. DOI: 10.1029/2009JD011823.

Galloway, J. N., Aber, J. D., Erisman, J. W., Seitzinger, S. P., Howarth, R. W., Cowling, E. B., and Cosby, B. J. (2003). "The Nitrogen Cascade". In: *American Institute of Biological Sciences* 53.4,
1265 p. 341. ISSN: 0006-3568. DOI: 10.1641/0006-3568(2003)053[0341:TNC]2.0.CO;2. arXiv: arXiv:1011.1669v3. URL: http://www.jstor.org/stable/1314367.

Gomez, L., Navarro-Comas, M., Puentedura, O., Gonzalez, Y., Cuevas, E., and Gil-Ojeda, M. (2014). "Long-path averaged mixing ratios of O3 and NO2 in the free troposphere from mountain MAX-DOAS". In: *Atmospheric Measurement Techniques* 7.10, pp. 3373–3386. ISSN: 18678548. DOI: 10.
1270 5194/amt-7-3373-2014.

Grainger, J. F. and Ring, J. (1962). "Anomalous Fraunhofer Line Profiles". In: *Nature* 193, p. 762.

Greenblatt, G. D., Orlando, J. J., Burkholder, J. B., and Ravishankara, A. R. (1990). "Absorption measurements of oxygen between 330 and 1140 nm". In: *Journal of Geophysical Research* 95.D11, p. 18577. ISSN: 0148-0227. DOI: 10.1029/JD095iD11p18577. URL: http://doi.wiley.com/10.
1275 1029/JD095iD11p18577.

Hönninger, G., Friedeburg, C. von, and Platt, U. (2004). "Multi axis differential optical absorption spectroscopy (MAX-DOAS)". In: *Atmos. Chem. Phys.* 4, pp. 231–254.

Ialongo, I., Hakkarainen, J., Hyttinen, N., Jalkanen, J. P., Johansson, L., Boersma, K. F., Krotkov, N., and Tamminen, J. (2014). "Characterization of OMI tropospheric NO2 over the Baltic Sea region".
1280 In: *Atmospheric Chemistry and Physics* 14.15, pp. 7795–7805. ISSN: 16807324. DOI: 10.5194/acp-14-7795-2014.

Ialongo, I., Herman, J., Krotkov, N., Lamsal, L., Boersma, F., Hovila, J., and Tamminen, J. (2016). "Comparison of OMI NO2 observations and their seasonal and weekly cycles with ground-based measurements in Helsinki". In: *Atmospheric Measurement Techniques Discussions* 2, pp. 1–13.
1285 ISSN: 1867-8610. DOI: 10.5194/amt-2016-212. URL: http://www.atmos-meas-tech-discuss.net/amt-2016-212/.

IEA/OECD (2009). *Transport, Energy and CO2 – moving towards sustainability.* Paris: International Energy Agency. ISBN: 9789264073166.

International Air Transport Association (IATA) (2015). "IATA Annual Review 2015". In: p. 62. URL: http://www.iata.org/about/Documents/iata-annual-review-2015.pdf.

Irie, H., Takashima, H., Kanaya, Y., Boersma, K. F., Gast, L., Wittrock, F., Brunner, D., Zhou, Y., and Van Roozendael, M. (2011). "Eight-component retrievals from ground-based MAX-DOAS observations". In: *Atmospheric Measurement Techniques* 4.6, pp. 1027–1044. ISSN: 18671381. DOI: 10.5194/amt-4-1027-2011.

Jonson, J. E., Tarrason, L., and Bartnicki, J. (2000). *Effects of international shipping on European pollution levels. 2000.* Tech. rep. Oslo, Norway: The Norwegian Metrorological Institute.

Kattner, L., Mathieu-Üffing, B., Burrows, J. P., Richter, A., Schmolke, S., Seyler, A., and Wittrock, F. (2015). "Monitoring compliance with sulfur content regulations of shipping fuel by in situ measurements of ship emissions". In: *Atmospheric Chemistry and Physics* 15.17, pp. 10087–10092. ISSN: 1680-7324. DOI: 10.5194/acp-15-10087-2015. URL: http://www.atmos-chem-phys.net/15/10087/2015/.

Kaynak, B., Hu, Y., Martin, R. V., Sioris, C. E., and Russell, a. G. (2009). "Comparison of weekly cycle of NO2 satellite retrievals and NOx emission inventories for the continental United States". In: *Journal of Geophysical Research: Atmospheres* 114.5, pp. 1–10. ISSN: 01480227. DOI: 10.1029/2008JD010714.

Kern, C., Deutschmann, T., Vogel, L., Wöhrbach, M., Wagner, T., and Platt, U. (2010). "Radiative transfer corrections for accurate spectroscopic measurements of volcanic gas emissions". In: *Bulletin of Volcanology* 72.2, pp. 233–247. ISSN: 02588900. DOI: 10.1007/s00445-009-0313-7.

Lack, D. A., Cappa, C. D., Langridge, J., Bahreini, R., Buffaloe, G., Brock, C., Cerully, K., Coffman, D., Hayden, K., Holloway, J., Lerner, B., Massoli, P., Li, S. M., McLaren, R., Middlebrook, A. M., Moore, R., Nenes, A., Nuaaman, I., Onasch, T. B., Peischl, J., Perring, A., Quinn, P. K., Ryerson, T., Schwartz, J. P., Spackman, R., Wofsy, S. C., Worsnop, D., Xiang, B., and Williams, E. (2011). "Impact of fuel quality regulation and speed reductions on shipping emissions: Implications for climate and air quality". In: *Environmental Science and Technology* 45.20, pp. 9052–9060. ISSN: 0013936X. DOI: 10.1021/es2013424.

Lampel, J., Pohler, D., Tschritter, J., Frieß, U., and Platt, U. (2015). "On the relative absorption strengths of water vapour in the blue wavelength range". In: *Atmospheric Measurement Techniques* 8.10, pp. 4329–4346. ISSN: 18678548. DOI: 10.5194/amt-8-4329-2015.

Lauer, a., Eyring, V., Hendricks, J., Jöckel, P., and Lohmann, U. (2007). "Global model simulations of the impact of ocean-going ships on aerosols, clouds, and the radiation budget". In: *Atmospheric Chemistry and Physics Discussions* 7.4, pp. 9419–9464. ISSN: 1680-7375. DOI: 10.5194/acpd-7-9419-2007.

Lawrence, M. G. and Crutzen, P. J. (1999). "Influence of NOx emissions from ships on tropospheric photochemistry and climate". In: *Nature* 402.6758, pp. 167–170. ISSN: 0028-0836. DOI: 10.1038/46013.

Lee, C., Richter, A., Lee, H., Kim, Y. J., Burrows, J. P., Lee, Y. G., and Choi, B. C. (2008). "Impact of transport of sulfur dioxide from the Asian continent on the air quality over Korea during May 2005". In: *Atmospheric Environment* 42.7, pp. 1461–1475. ISSN: 13522310. DOI: 10.1016/j.atmosenv.2007.11.006.

Masieri, S., Premuda, M., Bortoli, D., Kostadinov, I., Petritoli, A., Ravegnani, F., and Giovanelli, G. (2009). "Cruise ships flow rate emission evaluated by means of a passive DOAS instrument". In: *SPIE Europe Remote Sensing* 7478, 74781S—-74781S—10. DOI: 10.1117/12.830309. URL: http://dx.doi.org/10.1117/12.830309.

Matthias, V., Aulinger, A., Backes, A., Bieser, J., Geyer, B., Quante, M., and Zeretzke, M. (2016). "The impact of shipping emissions on air pollution in the greater North Sea region-Part 2: Scenarios for 2030". In: *Atmospheric Chemistry and Physics* 16.2, pp. 759–776. ISSN: 16807324. DOI: 10.5194/acp-16-759-2016.

McLaren, R., Wojtal, P., Halla, J. D., Mihele, C., and Brook, J. R. (2012). "A survey of NO2:SO2 emission ratios measured in marine vessel plumes in the Strait of Georgia". In: *Atmospheric Environment* 46.2, pp. 655–658. ISSN: 13522310. DOI: 10.1016/j.atmosenv.2011.10.044. URL: http://linkinghub.elsevier.com/retrieve/pii/S135223101101123X.

Meller, R. and Moortgat, G. K. (2000). "Temperature dependence of the absorption cross sections of formaldehyde between 223 and 323 K in the wavelength range 225-375 nm". In: *Journal of Geophysical Research: Atmospheres* 105.D6, pp. 7089–7101. ISSN: 2156-2202. DOI: 10.1029/1999JD901074. URL: http://dx.doi.org/10.1029/1999JD901074.

Pandya, R. J., Solomon, G., Kinner, A., and Balmes, J. R. (2002). "Diesel exhaust and asthma: Hypotheses and molecular mechanisms of action". In: *Environmental Health Perspectives* 110.SUPPL. 1, pp. 103–112. ISSN: 00916765. DOI: 10.1289/ehp.02110s1103.

Peters, E. (2013). "Improved MAX-DOAS measurements and retrievals focused on the marine boundary layer". In: *Ph.D. thesis, University of Bremen*.

Platt, U. and Perner, D. (1980). "Direct measurements of atmospheric CH2O, HNO2, O3, NO2, and SO2 by differential optical absorption in the near UV". In: *Journal of Geophysical Research: Oceans* 85.C12, pp. 7453–7458. ISSN: 2156-2202. DOI: 10.1029/JC085iC12p07453. URL: http://dx.doi.org/10.1029/JC085iC12p07453.

Platt, U. and Stutz, J. (2008). *Differential optical absorption spectroscopy*. Physics of Earth and Space Environments. Berlin ; Heidelberg: Springer, XV, 597 S. ISBN: 3-540-21193-4 ; 978-3-540-21193-8 ; 978-3-540-75776-4.

Prata, A. J. (2014). "Measuring SO2 ship emissions with an ultraviolet imaging camera". In: *Atmospheric Measurement Techniques* 7.5, pp. 1213–1229. ISSN: 18678548. DOI: 10.5194/amt-7-1213-2014.

Premuda, M., Masieri, S., Bortoli, D., Kostadinov, I., Petritoli, A., and Giovanelli, G. (2011). "Evaluation of vessel emissions in a lagoon area with ground based Multi axis DOAS measurements". In: *Atmospheric Environment* 45.29, pp. 5212–5219. ISSN: 13522310. DOI: 10.1016/j.atmosenv.2011.05.067. URL: http://dx.doi.org/10.1016/j.atmosenv.2011.05.067.

Richter, A., Begoin, M., Hilboll, A., and Burrows, J. P. (2011). "An improved NO2 retrieval for the GOME-2 satellite instrument". In: *Atmospheric Measurement Techniques* 4.6, pp. 1147–1159. ISSN: 18671381. DOI: 10.5194/amt-4-1147-2011.

Richter, A. (1997). "Absorptionsspektroskopische Messungen stratosphärischer Spurengase über Bremen, 53° N". PhD Thesis. Göttingen: Universität Bremen. ISBN: 3897120585.

Richter, A., Eyring, V., Burrows, J. P., Bovensmann, H., Lauer, A., Sierk, B., and Crutzen, P. J. (2004). "Satellite measurements of NO2 from international shipping emissions". In: *Geophys. Res. Lett.* 31, p. L23110. ISSN: 0094-8276. DOI: 10.1029/2004GL020822.

Roscoe, H. K., Van Roozendael, M., Fayt, C., Du Piesanie, A., Abuhassan, N., Adams, C., Akrami, M., Cede, A., Chong, J., Clémer, K., Friess, U., Gil Ojeda, M., Goutail, F., Graves, R., Griesfeller, A., Grossmann, K., Hemerijckx, G., Hendrick, F., Herman, J., Hermans, C., Irie, H., Johnston, P. V., Kanaya, Y., Kreher, K., Leigh, R., Merlaud, A., Mount, G. H., Navarro, M., Oetjen, H., Pazmino, A., Perez-Camacho, M., Peters, E., Pinardi, G., Puentedura, O., Richter, A., Schönhardt, A., Shaiganfar, R., Spinei, E., Strong, K., Takashima, H., Vlemmix, T., Vrekoussis, M., Wagner, T., Wittrock, F., Yela, M., Yilmaz, S., Boersma, F., Hains, J., Kroon, M., Piters, A., and Kim, Y. J. (2010). "Intercomparison of slant column measurements of NO2 and O4 by MAX-DOAS and zenith-sky UV and visible spectrometers". In: *Atmospheric Measurement Techniques* 3.6, pp. 1629–1646. ISSN: 18671381. DOI: 10.5194/amt-3-1629-2010.

Rozanov, V. V., Rozanov, A. V., Kokhanovsky, A. A., and Burrows, J. P. (2014). "Radiative transfer through terrestrial atmosphere and ocean: Software package SCIATRAN". In: *Journal of Quantitative Spectroscopy and Radiative Transfer* 133, pp. 13–71. ISSN: 00224073. DOI: 10.1016/j.jqsrt.2013.07.004. URL: http://dx.doi.org/10.1016/j.jqsrt.2013.07.004.

Schreier, S. F., Richter, A., Wittrock, F., and Burrows, J. P. (2016). "Estimates of free-tropospheric NO2 and HCHO mixing ratios derived from high-altitude mountain MAX-DOAS observations in

the mid-latitudes and tropics". In: *Atmospheric Chemistry and Physics* 16.5, pp. 2803–2817. ISSN: 16807324. DOI: 10.5194/acp-16-2803-2016.

Seinfeld, J. H. and Pandis, S. N. (2006). *Atmospheric chemistry and physics: from air pollution to climate change.* 2. ed. Hoboken, NJ: Wiley. ISBN: 0471720186 and 9780471720188 and 0471720178 and 9780471720171.

Serdyuchenko, A., Gorshelev, V., Weber, M., Chehade, W., and Burrows, J. P. (2014). "High spectral resolution ozone absorption cross-sections – Part 2: Temperature dependence". In: *Atmospheric Measurement Techniques* 7.2, pp. 625–636. ISSN: 1867-8548. DOI: 10.5194/amt-7-625-2014.

Singh, H. B. (1987). "Reactive nitrogen in the troposphere". In: *Environmental Science & Technology* 21.4, pp. 320–327. ISSN: 0013-936X. DOI: 10.1021/es00158a001.

Sinreich, R., Merten, A., Molina, L., and Volkamer, R. (2013). "Parameterizing radiative transfer to convert MAX-DOAS dSCDs into near-surface box-averaged mixing ratios". In: *Atmospheric Measurement Techniques* 6.6, pp. 1521–1532. ISSN: 18671381. DOI: 10.5194/amt-6-1521-2013.

Statistische Ämter des Bundes und der Länder (Statistikamt Nord) (2015). *Anzahl der Ankünfte von Kreuzfahrtschiffen im Hamburger Hafen in den Jahren 2005 bis 2014.* URL: http://de.statista.com/statistik/daten/studie/29729/umfrage/ankuenfte-von-kreuzfahrtschiffen-in-hamburg/.

Thalman, R. and Volkamer, R. (2013). "Temperature dependent absorption cross-sections of O2-O2 collision pairs between 340 and 630 nm and at atmospherically relevant pressure." In: *Physical chemistry chemical physics* 15, pp. 15371–15381. ISSN: 1463-9084. DOI: 10.1039/c3cp50968k. URL: http://www.ncbi.nlm.nih.gov/pubmed/23928555.

Umweltbundesamt (2017). *Aktuelle Luftdaten.* URL: https://www.umweltbundesamt.de/daten/luftbelastung/aktuelle-luftdaten (visited on 05/16/2017).

UNCTAD (2014). *Review of Maritime Transport 2014*, p. 34. ISBN: 9789211128789. URL: http://unctad.org/en/PublicationsLibrary/rmt2014%5C_en.pdf.

— (2015). *Review of Maritime Transport 2015*. October. ISBN: 978-92-1-112892-5. URL: http://unctad.org/en/PublicationsLibrary/rmt2015%5C_en.pdf.

Van Roy, W. (2016). "Best Practices Airborne MARPOL Annex VI Monitoring". In: URL: https://www.trafi.fi/filebank/a/1482762219/d80cdd7de80e58885ce5a4dd0af86c02/23541-Best%5C_Practices%5C_Airborne%5C_MARPOL%5C_Annex%5C_VI%5C_Monitoring.pdf.

Vandaele, A. C., Hermans, C., Simon, P. C., Roozendael, M. V., Guilmot, J. M., Carleer, M., and Colin, R. (1996). "Fourier Transform Measurement of NO2 Absorption Cross-Section in the Visible Range at Room Temperature". In: *J. Atmos. Chem.* 25, pp. 289–305.

Vinken, G. C. M., Boersma, K. F., Donkelaar, A. van, and Zhang, L. (2014). "Constraints on ship NOx emissions in Europe using GEOS-Chem and OMI satellite NO2 observations". In: *Atmospheric Chemistry and Physics* 14.3, pp. 1353–1369. ISSN: 1680-7324. DOI: 10.5194/acp-14-1353-2014. URL: http://www.atmos-chem-phys.net/14/1353/2014/acp-14-1353-2014.html.

Wagner, T., Dix, B., Friedeburg, C. V., Frieß, U., Sanghavi, S., Sinreich, R., and Platt, U. (2004). "MAX-DOAS O4 measurements: A new technique to derive information on atmospheric aerosols - Principles and information content". In: *Journal of Geophysical Research D: Atmospheres* 109.22, pp. 1–19. ISSN: 01480227. DOI: 10.1029/2004JD004904.

Wang, T., Hendrick, F., Wang, P., Tang, G., Clémer, K., Yu, H., Fayt, C., Hermans, C., Gielen, C., Müller, J. F., Pinardi, G., Theys, N., Brenot, H., and Van Roozendael, M. (2014a). "Evaluation of tropospheric SO2 retrieved from MAX-DOAS measurements in Xianghe, China". In: *Atmospheric Chemistry and Physics* 14.20, pp. 11149–11164. ISSN: 16807324. DOI: 10.5194/acp-14-11149-2014.

Wang, Y., Li, A., Xie, P. H., Wagner, T., Chen, H., Liu, W. Q., and Liu, J. G. (2014b). "A rapid method to derive horizontal distributions of trace gases and aerosols near the surface using multi-axis differential optical absorption spectroscopy". In: *Atmospheric Measurement Techniques* 7.6, pp. 1663–1680. ISSN: 18678548. DOI: 10.5194/amt-7-1663-2014.

Wayne, R. P. (2006). *Chemistry of atmospheres: an introduction to the chemistry of the atmospheres of earth, the planets, and their satellites*. 3. ed., re. Oxford [u.a.]: Oxford Univ. Press. ISBN: 019850375X and 9780198503750.

WHO (2006). *Air Quality Guidelines: Global Update 2005 : Particulate Matter, Ozone, Nitrogen Dioxide, and Sulfur Dioxide*. A EURO Publication. World Health Organization. ISBN: 9789289021920.

Wittrock, F., Oetjen, H., Richter, A., Fietkau, S., Medeke, T., Rozanov, A., and Burrows, J. P. (2004). "MAX-DOAS measurements of atmospheric trace gases in Ny-Ålesund - Radiative transfer studies and their application". In: *Atmos. Chem. Phys.* 4, pp. 955–966.

WSV (2013). *Verkehr und Güterumschlag*. URL: http://www.ast-nordwest.gdws.wsv.de/schifffahrt/verkehr%5C_gueterumschlag/index.html (visited on 11/01/2016).

— (2014). *Schiffsverkehr und Güterumschlag*. URL: http://www.wsd-nord.wsv.de/Schiff-WaStr/Schifffahrt/Schiffsverkehr%5C_und%5C_Gueterumschlag/index.html (visited on 11/01/2016).

Yang, M., Bell, T. G., Hopkins, F. E., and Smyth, T. J. (2016). "Attribution of atmospheric sulfur dioxide over the English Channel to dimethyl sulfide and changing ship emissions". In: *Atmospheric Chemistry and Physics* 16.8, pp. 4771–4783. ISSN: 16807324. DOI: 10.5194/acp-16-4771-2016.

Zhang, F., Chen, Y., Tian, C., Lou, D., Li, J., Zhang, G., and Matthias, V. (2016). "Emission factors for gaseous and particulate pollutants from offshore diesel engine vessels in China". In: *Atmospheric Chemistry and Physics* 16.10, pp. 6319–6334. ISSN: 16807324. DOI: 10.5194/acp-16-6319-2016.

Monitoring shipping emissions in the German Bight using MAX-DOAS measurements

André Seyler[1], Folkard Wittrock[1], Lisa Kattner[1,2], Barbara Mathieu-Üffing[1,2], Enno Peters[1], Andreas Richter[1], Stefan Schmolke[2], and John P. Burrows[1]

[1]Institute of Environmental Physics, University of Bremen, Germany
[2]Federal Maritime and Hydrographic Agency (BSH), Hamburg, Germany

Correspondence to: André Seyler (aseyler@iup.physik.uni-bremen.de)

Abstract. A three-year time series of ground-based MAX-DOAS measurements of NO_2 and SO_2 on the island Neuwerk has been analyzed for contributions from shipping emissions. The island is located in the German Bight, close to the main shipping lane (in a distance of 6–7 km) into the river Elbe towards the harbor of Hamburg. Measurements of individual ship plumes as well as of background pollution are possible from this location. A simple approach using the column amounts of the oxygen molecule dimer or collision complex, O_4, for the determination of the horizontal light path length has been applied to retrieve path-averaged volume mixing ratios. An excellent agreement between mixing ratios determined from NO_2 retrievals in the UV and visible parts of the spectrum has been found, showing the validity of the approach. Obtained mixing ratios of NO_2 and SO_2 are compared to co-located in-situ measurements showing good correlation on average but also a systematic underestimation by the MAX-DOAS O_4-scaling approach. Comparing data before and after the introduction of stricter fuel sulfur content limits (from 1 % to 0.1 %) on 1 January 2015 in the North Sea emission control area (ECA), a significant reduction in SO_2 levels has been observed. For situations with wind from the open North Sea, where ships are the only local source of air pollution, the average mixing ratio of SO_2 decreased by a factor of eight, while for NO_2 in the whole time series from 2013 till 2016 no significant change in emissions has been observed. More than 2000 individual ship emission plumes have been identified in the data and analyzed for the emission ratio of SO_2 to NO_2, yielding an average ratio of 0.3 for the years 2013/2014, decreasing significantly presumably due to lower fuel sulfur content in 2015/2016. By sorting measurements according to the prevailing wind direction and selecting two angular reference sectors representative for wind from open North Sea and coast excluding data with mixed air mass origin, relative contributions of ships and land-based sources to air pollution levels in the German Bight have been estimated to be around 40 % : 60 % for NO_2 as well as SO_2 in 2013/2014, dropping to 14 % : 86 % for SO_2 in 2015/2016.

---

1 Introduction

1.1 Shipping – a fast growing sector

Shipping has always been an important mode of transportation throughout the course of history. In contrast to the past, nowadays ships are almost exclusively carrying freight with the exception of a small number of cruise ships and ferries. Globalization of markets has lead to an enormous increase in world trade and shipping traffic in the last decades, with growth rates being typically about twice that of the world gross domestic product (GDP) (Bollmann et al., 2010).

Shipping is generally the most energy efficient transportation mode, having the lowest greenhouse gas emissions per tonne per kilometer (3–60 gCO$_2$/t/km), followed by rail (10–120 gCO$_2$/t/km), road (80–180 gCO$_2$/t/km) and air transport (435–1800 gCO$_2$/t/km), which is by far the least efficient (Bollmann et al., 2010; IEA/OECD, 2009). At the same time, with a volume of 9.84 billion tons in 2014 it accounts for four fifths of the worldwide total merchandise trade volume (UNCTAD, 2015), as compared to for example the total air cargo transport volume of 51.3 million tons

in 2014 (International Air Transport Association (IATA), 2015). As a result, shipping accounts for a significant part of the emissions from the transportation sector (Eyring et al., 2005b).

Despite growth rates now being lower compared to those prior to the 2008 economic crisis, seaborne trade is growing faster than the rest of the transportation sector, with an annual growth rate of 3–4 % in the years 2010 to 2014, compared to 2.0–2.6 % for the global merchandise volume (UNCTAD, 2014, 2015). The number of ships larger than 100 gross tonnage increased from around 31 000 in 1950 over 52 000 in 1970 to 89 000 in 2001 (Eyring et al., 2005a) and is estimated to increase to about 150 000 in 2050 (Eyring et al., 2005b). At the same time, total fuel consumption and emissions increased as well (Corbett and Koehler, 2003; Eyring et al., 2005a, b, 2010b). Eyring et al. (2005b) predicted that future development of shipping emissions will depend more on the usage of new technologies and imposed regulations than on the economic growth rates.

1.2 Ship emission chemistry

The most important pollutants emitted by ships are carbon dioxide (CO_2), carbon monoxide (CO), nitrogen oxides ($NO_x = NO + NO_2$), sulfur dioxide (SO_2), black carbon (BC), volatile organic compounds (VOC) and particulate matter (PM) (Eyring et al., 2010a). This study focuses on NO_2 and SO_2, because both are emitted in considerable amounts and both absorb light in the uv-visible spectral range and therefore can readily be measured by Differential Optical Absorption Spectroscopy (DOAS), which is explained in Sect. 3.1. In 2001, shipping emissions accounted for 15 % of all anthropogenic NO_x and provided 8 % of all anthropogenic SO_2 emissions (Eyring et al., 2010a).

NO_x is predominantly formed thermally from atmospheric molecular nitrogen (N2) and oxygen (O_2) during high temperature combustion processes in ship engines in an endothermic chain reaction called the Zeldovich mechanism. The emitted NO_x comprises mainly NO, with less than 25 % of NO_x being emitted as NO_2 (Alföldy et al., 2013). Zhang et al. (2016) measured emission factors for gaseous and particulate pollutants on-board three Chinese vessels and found that more than 80 % of the NO_x was emitted as NO and that emission factors were significantly different during different operation modes.

In the ambient atmosphere, NO is rapidly converted to NO_2 by reaction with ozone (O_3) leading to a life time of only a few minutes. During daytime NO_2 is photolyzed by UV radiation ($\lambda < 420$ nm) releasing NO and ground state oxygen radicals ($O(^3P)$). In a three-body-collision reaction involving N_2 or O_2 the oxygen radical reacts with an oxygen molecule to reform ozone (Singh, 1987). When daylight is available, these reactions form a "null-cycle" and transformation between NO and NO_2 is very fast, leading to a dynamic equilibrium. This is also known as the Leighton photostationary state. Owing to the lack of photolysis, NO reacts rapidly with O_3 to form NO_2 during the night. In addition, the nitrate radical (NO3) is formed by reaction of NO_2 with O_3. An equilibrium of NO_2 with NO3 forming N_2O_5, the acid anhydride of nitric acid HNO_3, results (Wayne, 2006; Seinfeld and Pandis, 2006).

During the day OH reacts with NO_2 in a three body reaction to form HNO_3. An important sink for NO_2 in the troposphere is wet deposition of the resulting HNO_3. The mean tropospheric lifetime of NO_x varies between a few hours in summer and a few days in winter (Singh, 1987), depending on altitude. Inside ship plumes, Chen et al. (2005) found a substantially reduced lifetime of NO_x of about 1.8 h compared to approximately 6.5 h in the background marine boundary layer (around noon). This is attributed to enhanced levels of OH radicals in the plume.

Unlike for NO_x, ship emissions of SO_2 are directly linked to the fuel sulfur content. Around 86 % of the fuel sulfur content is emitted as SO_2 (Balzani Lööv et al., 2014). Alföldy et al. (2013) found a linear relationship between SO_2 and sulfate particle emission and that only around 4.8 % of the total sulfur content is either directly emitted as or immediately transformed into particles after the emission. An important sink for SO_2 is wet deposition after oxidation by OH radicals to the extremely hygroscopic sulfur trioxide (SO_3) reacting rapidly with liquid water to form sulfuric acid (H_2SO_4) (Brasseur, 1999). Another important sink is dry deposition, leading to a lifetime of approximately one day in the boundary layer, which can be even shorter in the presence of clouds (Seinfeld and Pandis, 2006).

1.3 Influence on air quality and climate

Sulfate aerosols influence climate directly by scattering and absorption of solar radiation and indirectly by increasing cloud condensation, changing cloud reflectivity and lifetime (Lawrence and Crutzen, 1999; Lauer et al., 2007; Eyring et al., 2010b). In the presence of volatile organic compounds (VOC), nitrogen oxides are important precursors for the formation of tropospheric ozone and therefore photochemical smog. The release of both NO_2 and SO_2 leads to an increase in acidification of 3–10 % in coastal regions, contributing significantly to acid rain formation damaging eco-systems (Endresen et al., 2003; Jonson et al., 2000). The deposition of reactive nitrogen compounds causes eutrophication of ecosystems and decreases biodiversity (Galloway et al., 2003).

Around 70 % of shipping emissions occur within 400 km of land (Corbett et al., 1999), contributing substantially to air pollution in coastal areas (Eyring et al., 2010b). Ship emissions were found to provide a dominant source of air pollution in harbor cities (Eyring et al., 2010a). In addition to that, transport of tropospheric ozone and aerosol precursors over several hundreds of kilometers also affect air quality, human health and vegetation further inland, far away from their emission point (Corbett et al., 2007; Eyring et al., 2010a, b).

NO$_2$ and SO$_2$ can cause a variety of respiratory problems. Tropospheric ozone is harmful to animals and plants, causing various health problems. The EU legislation for O3 exposure to humans has set a target limit of 120 µg m^{-3} ($\sim$ 60 ppbv) for an maximum daily 8 hour mean but allows exceedences on 25 days averaged over 3 years (EU, 2008, 2016). As mentioned above, both NO$_2$ and SO$_2$ play a role in the formation of particles. Fine particles are associated with various health impacts like lung cancer, heart attacks, asthma and allergies (Corbett et al., 2007; Pandya et al., 2002; WHO, 2006).

1.4 Attempts to decrease shipping emissions by stricter regulations

International ship traffic is subject to regulations of the International Maritime Organization (IMO). Shipping emissions are regulated by the International Convention for the Prevention of Pollution from Ships (MARPOL 73/78) Annex VI (DNV, 2008). This Annex was added in 1997 and entered into force in 2005. A revision with more stringent emission limits was adopted in 2008 and went into force 2010. With this, limits on sulfur content in heavy fuel oils globally are set and local Sulfur Emission Control Areas (SECA), later revised to general Emission Control Areas (ECA), along the North American coast and in the Baltic and North Sea (including the English Channel) are established with more stringent restrictions and controls. MARPOL introduced a global fuel sulfur limit of 4.5 %, which was reduced to 3.5 % in 2012 and will be further reduced in 2020 (or 2025 depending on a review in 2018) to 0.5 %. In the established ECAs, from 2010 on the limit was set to 1.5 % and was further reduced in 2010 to 1.0 %. Carrying out airborne in-situ measurements in several flight campaigns in the English Channel, North and Baltic Sea, Beecken et al. (2014) measured a 85 % compliance in 2011 and 2012 with the 1 % fuel sulfur limit. In the Gulf of Finland and Neva Bay area, Beecken et al. (2015) found a 90 % compliance in 2011 and 97 % compliance in 2012 with the 1 % fuel sulfur limit from ground-based, ship-based and helicopter-based in-situ measurements.

Recently, from 1 January 2015 on, the allowed fuel sulfur content in SECAs was further reduced to 0.1 %. Using in-situ measurements in Wedel at the bank of the river Elbe, a few kilometers downstream from Hamburg, Germany, Kattner et al. (2015) showed that in late 2014 more than 99 % of the measured ships complied with the 1 % sulfur limit and in early 2015 95.4 % of the measured ships complied with the new 0.1 % sulfur limit. By analyzing one and a half years of SO$_2$ measurements at the English Channel, Yang et al. (2016) found a three-fold reduction in SO$_2$ from 2014 to 2015. They estimated the lifetime of SO$_2$ in the marine boundary layer to be around half a day. Lack et al. (2011) measured a substantial drop of SO$_2$ emissions by 91 % when the investigated container ships entered the Californian ECA and switched from heavy fuel oil (HFO) with 3.15 % fuel sulfur content to marine gas oil (MGO) with 0.07 % fuel sulfur

content. These estimates were obtained performing airborne in-situ measurements.

MARPOL Annex VI also establishes limits dependent on engine power for the emission of NO$_x$ from engines built after 2000 (Tier I), 2011 (Tier II) and 2016 (Tier III), but due to the slow penetration to the full shipping fleet, the impact on NO$_x$ emissions is not yet clear. Since 2010, a NO$_x$ emission control area exists around the North American coast and in the Caribbean, while for North and Baltic Sea the establishment of such a NECA is planned and was recently agreed on, but the future enforcement date is still unclear. The European Union also established a sulfur content limit of 0.1 % for inland waterway vessels and ships at berth in Community ports, which is in force since 1 January 2010 (EU, 2005).

The impact of shipping emissions on the North Sea for different regulation scenarios was investigated in a model study by the Helmholtz-Zentrum Geesthacht (HZG) within the scope of the Clean North Sea Shipping project. For current emissions, a relative contribution of shipping emissions to air pollution in coastal regions of up to 25 % in summer and 15 % in winter for NO$_2$ and 30 % in summer and 12 % in winter for SO$_2$ was found (Aulinger et al., 2016). For the year 2030, the contribution of the continuously growing shipping sector to the NO$_2$ concentrations is predicted to decrease. The extent of reduction depends on the date on which the stricter Tier III regulations enter into force and on the fraction of the fleet complying to these regulations (i. e. the age of the fleet), with up to 80 % reduction if all ships comply (in the improbable case of a new ships only fleet). For SO$_2$, the established fuel sulfur content limit of 0.1 % (ECA) and 0.5 % (globally) will lead to significant reductions, a further decrease is expected if the fraction of LNG powered ships grows (Matthias et al., 2016).

1.5 DOAS measurements of shipping emissions – previous studies

Optical remote sensing using the Differential Optical Absorption Spectroscopy (DOAS) technique to measure shipping emissions has been conducted before. For example, Berg et al. (2012) performed airborne (from airplane and helicopter) DOAS measurements of NO$_2$ and SO$_2$ in ship plumes by measuring sea scattered light. Masieri et al. (2009) and Premuda et al. (2011) measured flow rate emissions (mass per second) of NO$_2$ and SO$_2$ for single ships with ground based MAX-DOAS measurements across the Giudecca Channel in the Venice lagoon. McLaren et al. (2012) measured nocturnal NO$_2$ to SO$_2$ ratios in ship plumes in the Strait of Georgia with the active long path DOAS technique. Balzani Lööv et al. (2014) tested and compared optical remote sensing methods (DOAS, LIDAR, UV camera) and in-situ (sniffer) methods for the measurement of shipping emissions in the framework of the SIRENAS-R campaign in the harbour of Rotterdam in 2009. Prata (2014) showed that a UV (SO$_2$) imaging camera can be used to measure SO$_2$ in

ship plumes at the Kongsfjord at Ny Ålesund, Svalbard and the harbor of Rotterdam.

The global pathways of the ships can be seen in long time averaged NO_2 measurements from various satellite instruments: from GOME over the Indian Ocean (Beirle et al., 2004), from SCIAMACHY on board ENVISAT over the Indian Ocean and the Red Sea (Richter et al., 2004), in even more detail with a lot more visible ship tracks from GOME-2 on board MetOp-A (Richter et al., 2011). The higher resolution of OMI yielded ship tracks in the Baltic Sea (Ialongo et al., 2014) and in all European seas (Vinken et al., 2014).

1.6   The MeSMarT project

The current study is part of the project MeSMarT (Measurements of Shipping emissions in the Marine Troposphere), which is a cooperation between the University of Bremen (Institute of Environmental Physics, IUP) and the Federal Maritime and Hydrographic Agency (Bundesamt für Seeschifffahrt und Hydrographie, BSH), supported by the Helmholtz Zentrum Geesthacht (HZG). It aims to monitor background concentration as well as elevated signals of gases and particles related to ship emissions with various methods to cover a wide range of relevant pollutants and their spatial and seasonal distribution to estimate the influence of ship emissions on the chemistry of the atmospheric boundary layer (for further information visit: http://www.mesmart.de/).

1.7   Aims of this study

The objectives of this study are to assess whether measurements of individual ship plumes are feasible with a ground-based MAX-DOAS instrument, to compare MAX-DOAS with co-located in-situ measurements, to estimate the contribution of ships and land-based sources to air pollution in a North Sea coastal region, to survey the effect of fuel sulfur content regulations on SO_2 concentrations in the marine boundary layer and to analyze the SO_2 to NO_2 ratio in plumes to gain information about plume chemistry and the sulfur content in shipping fuels.

In the following, first the measurement site is described, followed by a presentation of the wind statistics and data availability. After this, the Differential Optical Absorption Spectroscopy (DOAS), the MAX-DOAS instrumentation and measurement geometry as well as the DOAS data analysis approach used are briefly described. In the next section, selected results from this study are presented: the measured differential slant column densities (DSCD), the retrieved path-averaged volume mixing ratios, the comparison to in-situ measurements, the diurnal and weekly variability, the contribution estimates for ships as well as land-based pollution sources and the analysis of SO_2 to NO_2 ratios in ship plumes. Finally, a summary is given and conclusions are drawn.

2   Measurement site

The measurements presented within this study were taken on Neuwerk, a small island in the North Sea (German Bight) with the size of about $3 \, km^2$ and 33 inhabitants. It is located in the Wadden Sea northwest of Cuxhaven at the mouth of the river Elbe, roughly 8–9km off the Coast, as can be seen from the map in Fig. 1 A).

The North Sea has one of the highest ship densities in the world (Matthias et al., 2016). The majority of ships that arrive in the port of Hamburg sail through the German Bight and the river Elbe and therefore pass Neuwerk. Hamburg is among the largest ports worldwide, together with Rotterdam and Antwerp one of the three largest ports in Europe, having a 4–5 % increase in container volume in the last years (UNCTAD, 2014, 2015). Hamburg also experiences a large increase in the number of cruise ships, having 176 ship calls in 2014 compared to 25 in the year 2005 (Statistische Ämter des Bundes und der Länder (Statistikamt Nord), 2015).

Neuwerk is relatively close to the main shipping lane from the North Sea into the river Elbe. On this highly frequented waterway, nearly all ships to and from the port of Hamburg and the Kiel canal (connection to the Baltic Sea) pass the island at a distance of 6–7 km, as shown in Fig. 1 B). Still close, but further away to the west are the shipping lanes to the Weser river to the ports of Bremerhaven and Bremen and to Wilhelmshaven (JadeWeserPort).

Neuwerk is surrounded by the Hamburg Wadden Sea National Park and there are no significant sources of air pollution on the island itself, making it a very suitable station for measurements of shipping emissions.

The ship emission measurements presented in this study were carried out with a MAX-DOAS instrument (see Sect. 3.2) which measures in multiple azimuthal viewing directions, as shown in Fig. 1 B), pointing directly towards the shipping lane while the different viewing azimuth angles cover a large part of the region.

Several measurement devices, including the two-channel MAX-DOAS instrument (for UV and visible spectral range), an Airpointer in-situ measurement device (measuring CO_2, NO_x, SO_2 and O_3), a high volume filter sampler and passive samplers as well as a weather station and an AIS (Automatic Identification System) signal receiver, are positioned on the main platform of a radar tower at a height of about 30m (see Fig. 2).

Additional wind data is available from measurements by the Hamburg Port Authority (HPA) on Neuwerk and the neighboring island Scharhörn. The seasonal distribution of wind directions on Neuwerk is shown in Fig. 3.

In spring and summer, on a high percentage of days the wind blows from the open North Sea, where shipping emissions are the only significant source of local air pollution. Consequently, the site provides an optimal opportunity for measurements of ship emission plumes. In winter, southerly directions prevail, bringing potentially polluted air masses
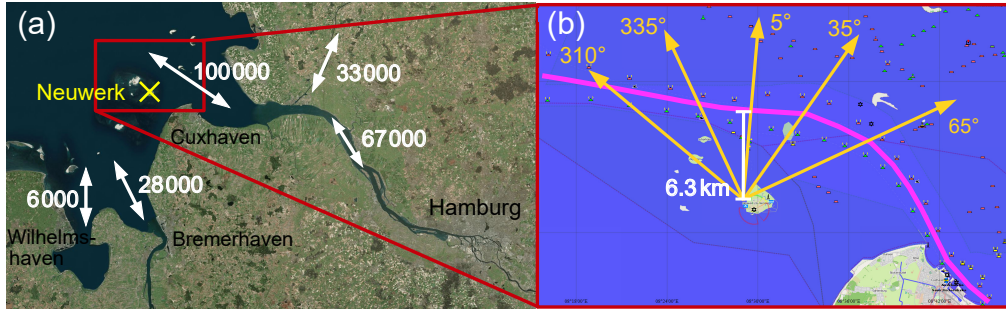
Figure 1. (a) Location of the measurement site Neuwerk in the German Bight, close to the mouth of the river Elbe. Number of ship movements (data from 2011/2012) is given by the white numbers. Data source: German Federal Waterways and Shipping Administration (WSV, 2013, 2014) Map source: http://www.bing.com/maps/ (01.04.2014)
(b) Azimuthal viewing directions of the MAX-DOAS instrument towards the main shipping lane (highlighted by the magenta line), passing the island in the north in a distance of 6–7 km. Map source: http://www.freie-tonne.de (16.07.2013)

Figure 2. Radar tower Neuwerk with MAX-DOAS and in-situ measurement device

from the land and blowing the ship emission plumes away from the measurement site. In addition, as the MAX-DOAS technique requires daylight and because of the short days and the low sun resulting in less UV light reaching the surface, measurements are in general sparse in winter months, especially for SO_2, which has its strong absorption features in the UVB. This effect can be seen in winter gaps in Fig. 4, which presents the data availability for more than two years of measurements on Neuwerk.

3 Measurement techniques, instruments and data analysis

3.1 Differential Optical Absorption Spectroscopy (DOAS)

The principle of optical absorption spectroscopy is the attenuation of light intensity while passing through an absorbing medium, described by the well-known Lambert-Beer-law (also known as Beer-Lamber-Bouguer law). For the general case of electromagnetic radiation passing through an anisotropic medium having a number density n and a temperature and pressure dependent absorption cross section σ of an absorbing species along the light path s, the measured intensity at wavelength λ is given by

$$I(s,\lambda) = I_0(\lambda) \cdot \exp\left\{ -\int_0^s n(s') \cdot \sigma(\lambda, T(s'), p(s')) \cdot ds' \right\}$$

where the intensity of radiation entering the medium is I_0. For measurements in the atmosphere, this simple model has to be extended by considering multiple trace gases having different absorption cross sections and light scattering on air molecules (Rayleigh scattering), aerosol particles or water droplets (Mie scattering) as well as inelastic scattering by air and trace gas molecules (Raman scattering). The latter is responsible for the Ring effect (Grainger and Ring, 1962), another important extinction process, which can be described by a pseudo cross-section.

The key and original idea of the Differential Optical Absorption Spectroscopy (DOAS) is to separate the optical depth and the absorption cross-sections $\sigma_i(\lambda)$ into a slowly varying function $\sigma_{i,0}(\lambda)$ accounting for elastic scattering and broadband absorption structures and described by a low-order polynomial and a rapidly varying part $\sigma_i'(\lambda)$, the *differential* cross-section, considering the narrow-band absorption structures (Platt and Perner, 1980; Platt and Stutz, 2008). The absorption cross-sections are measured in the laboratory. Neglecting the temperature and pressure dependence of the absorption cross section, polynomial and differential cross sections are fitted to the measured optical thickness $\ln\left(\frac{I}{I_0}\right)$ in the linearized so-called DOAS equation:

$$\ln\left(\frac{I(\lambda)}{I_0(\lambda)}\right) = -\sum_{i=1}^{N} SCD_i \cdot \sigma_i'(\lambda) - \sum_p c_p \cdot \lambda^p + \text{Residual}(\lambda)$$

The retrieved quantities are the coefficients of the polynomial c_p and the slant column density of the trace gas which is the integrated number density along the light path: $SCD_i = \int n_i(s) ds$.
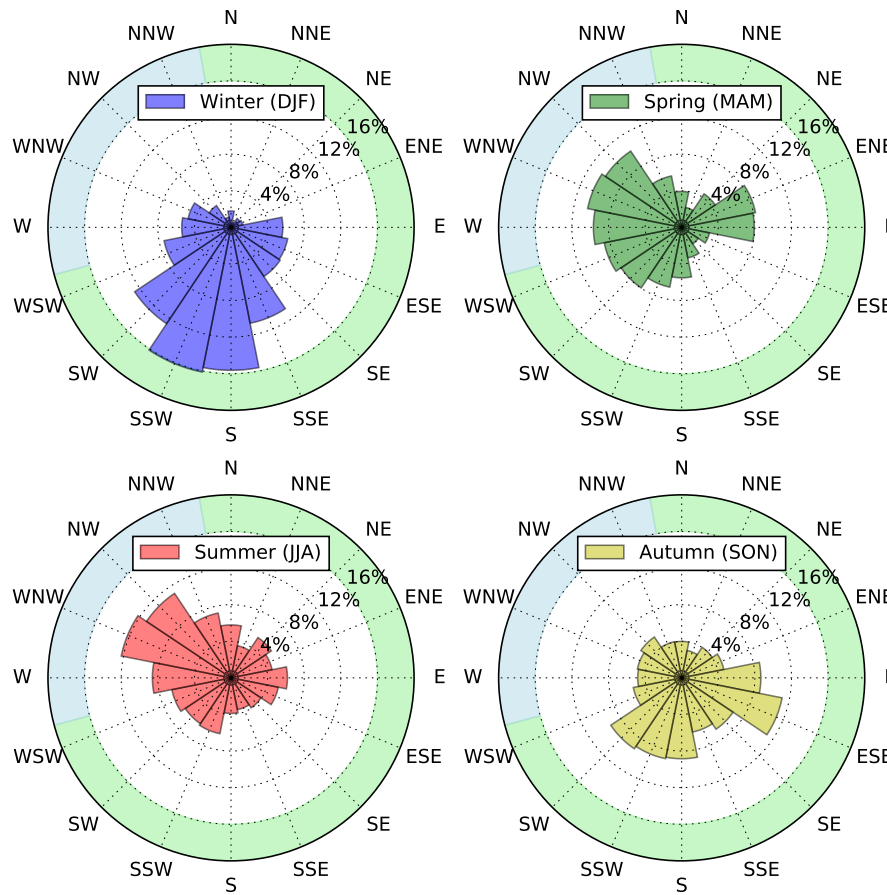
Figure 3. Seasonal wind direction distribution for Neuwerk (Data from 4 July 2013 to 27 June 2016). The colored sectors show directions with wind from the coast (green) and from the open North Sea (blue).
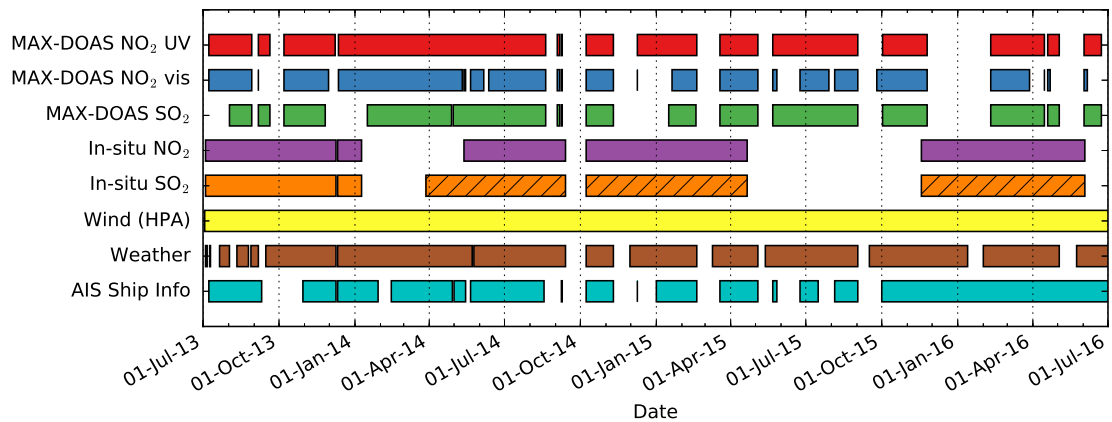

Figure 4. Data availability in the analyzed measurement period between July 2013 and July 2016. From March 2014 on (hatched), there were instrumental problems with the in-situ SO_2 instrument resulting in a strong oscillation of $\pm 0.5\,\mathrm{ppb}$ superimposing the data. However, this data can still be used for the comparison of long-term averages.

3.2 MAX-DOAS instrument and viewing geometry

The Multi-AXis DOAS (MAX-DOAS) technique (Hön-ninger et al., 2004; Wittrock et al., 2004) is a passive remote

sensing method measuring scattered sunlight. The MAX-DOAS instrument used in this study, comprises of a telescope mounted on a pan-tilt head, an optical fiber bundle, two spectrometers for UV and visible spectral range respectively, equipped with two CCD (charge coupled device) 2D array detectors operated by a computer. The telescope which is attached to the outer sheathing of the circular platform of the Neuwerk radar tower is used to collect the light from a specific viewing direction and to focus the light onto the entrance of the optical fiber. The combination of converging lens and light fiber leads to an field-of-view of approximately 1°. The pan-tilt head allows the instrument to point in different azimuth angles (panning) as well as different elevation angles (tilting). Dark measurements, which are needed for the determination of the CCD's dark signal are undertaken on a daily basis. Also on a daily basis line lamp measurements are taken using an internally mounted HgCd lamp for the wavelength calibration of the spectra and the determination of the slit function of the instrument. The spectral resolution, represented by the FWHM of the slit function of the instrument, is about 0.4 nm for the UV and 0.7 nm for the visible channel.

The Y-shaped optical light fiber cable is a bundle of 2×38 cylindrical, thin and flexible quartz fibers, guiding the light from the telescope to the two temperature-stabilized spectrometers with attached CCD detectors inside the weatherproof platform building. Each single fiber has a diameter of 150 μm and is 20 m long.

The UV and visible instrument consist of identical Andor Shamrock SR-303i imaging spectrographs, a grating spectrometer in "Czerny-Turner" design with a focal length of 303 mm. The gratings in use are different, the UV instrument is equipped with a 1200 grooves/mm, 300 nm blaze angle grating and the visible instrument with a 600 grooves/mm, 500 nm blaze angle grating. The UV instrument covers the wavelength range 304.6–371.7 nm, the visible spectrometer covers 398.8–536.7 nm. For the UV, a Princeton NTE/CCD 1340/400-EMB detector with a resolution of 1340×400 pixels and a pixel size of 20×20 microns, cooled to -35 °C, is used. For the visible spectral range, an Andor iDus DV420-BU back-illuminated CCD detector with a resolution of 1024×255 pixels and a pixel size of 26×26 microns, cooled as well to -35 °C, is used.

The measurement geometry for the ground-based MAX-DOAS measurements on Neuwerk is sketched in Fig. 5. To measure ship emissions, the telescope is pointed towards the horizon, collecting light that passed directly through the emitted ship plumes. A close-in-time zenith sky measurement is used as a reference so that the retrieved tropospheric differential slant column density (DSCD) is the difference of the slant column densities (SCD) along the two paths 1 and 2 in Fig. 5: $\text{DSCD} = \text{SCD}_1 - \text{SCD}_2 = \text{SCD}_{\text{off-axis}} - \text{SCD}_{\text{reference}}$. The stratospheric light path and trace gas absorption is approximately the same for both measurements and therefore cancels out which is important for NO_2 which
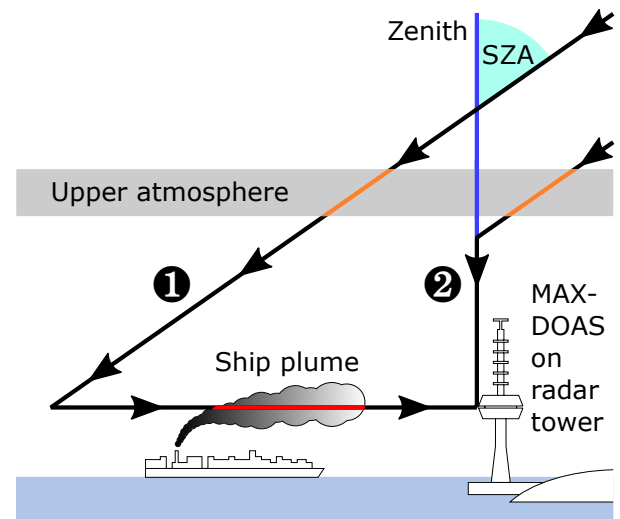

Figure 5. Measurement geometry for MAX-DOAS measurements on Neuwerk with schematic light paths for off-axis (1) and zenith sky reference measurements (2) for an exemplary solar zenith angle (SZA) of 55°

is also present in the stratosphere. This approach also minimizes possible instrumental artifacts.

The assumption that the vertical part of the light path cancels out when taking the difference between off-axis and zenith sky (reference) measurement off course is only valid if the NO_2 in the air above the instrument, which is of no interest to us here, is spatially homogeneously distributed. This is usually the case for stratospheric NO_2. If a spatially limited pollution plume from point sources like ships or power plants is blown above the radar tower and no plume is in the horizontal light path, the mentioned assumption is violated, leading to an underestimation of the derived DSCD. Also clouds or fog can make the interpretation of the measured DSCD more challenging due to multiple scattering.

3.3 DOAS data analysis and fit settings

The recorded spectra are spectrally calibrated using a daily acquired HgCd line lamp spectrum and the dark signal of the CCD detector is corrected using daily nighttime dark measurements. The logarithm of the ratio of measured off-axis (viewing towards the horizon) spectrum and reference (zenith sky) spectrum gives the optical thickness (also called optical depth). Multiple (differential) trace gas absorption cross sections obtained from laboratory measurements, as well as a low-order polynomial, are then fitted simultaneously to the optical depth. The retrieved fit parameters are the slant column densities of the various absorbers and the coefficients of the polynomial. The fits were performed with the software NLIN_D (Richter, 1997).

The settings and fitted absorbers vary according to the spectral range used. For the retrieval of NO_2 in the UV, a

fitting window of 338–370 nm was used and for NO_2 in the visible a fitting window of 425–497 nm, both adapted from experiences during the CINDI (Roscoe et al., 2010) and MAD-CAT (http://joseba.mpch-mainz.mpg.de/mad_cat.htm) inter-comparison campaigns. The oxygen-collision complex O_2-O_2, often denoted as O_4, is simultaneously retrieved from both NO_2 fits. The fit parameters for the DOAS fit of NO_2 and SO_2 are summarized in detail in Table 1.

For the retrieval of SO_2, several different fitting windows between 303 and 325 nm have been used in previous ground-based studies (Bobrowski and Platt, 2007; Lee et al., 2008; Galle et al., 2010; Irie et al., 2011; Wang et al., 2014a). This results from the need to find a compromise between the low light intensity caused by the strong ozone absorption around 300 nm on the one hand and the rapid decrease of the differential absorption of SO_2 at higher wavelengths on the other hand, limiting the choice of the fitting window. In this study, a fitting window of 307.5–317.5 nm was found as the optimal range for our instrument, which is similar to recommendations in Wang et al. (2014a). The fit parameters for the DOAS fit of SO_2 are summarized in detail in Table 2.

Only SO_2 measurements with a RMS lower than 2.5×10^{-3} have been taken into account for the statistics, filtering out bad fits with ozone interferences in low light and bad weather conditions.

Under optimal conditions, the typical fit RMS is around 1×10^{-4} for NO_2 in the visible, 2×10^{-4} for NO_2 in the UV and 5×10^{-4} for SO_2. By assuming that an optical density of twice the RMS can be detected (Peters, 2013), it is possible to estimate the detection limit of our instrument regarding the different trace gases. The differential absorption cross section of NO_2 is in the order of 1×10^{-19} cm² molec⁻¹, for SO_2 in the order of 2×10^{-19} cm² molec⁻¹. Combining this yields a NO_2 detection limit of around 1×10^{15} molec cm⁻² corresponding to 0.05 pbb in the visible and 2×10^{15} molec cm⁻² corresponding to 0.1 pbb in the UV. The SO_2 detection limit lies around 2.5×10^{16} molec cm⁻² corresponding to 0.2 ppb. The typical absolute fit errors are $2–3 \times 10^{14}$ molec cm⁻² for NO_2 in the visible, $5–6 \times 10^{14}$ molec cm⁻² for NO_2 in the UV and 2×10^{15} molec cm⁻² for SO_2, a factor of 5 to 10 smaller than the detection limit.

3.4 Retrieval of path-averaged near-surface VMRs from MAX-DOAS SCDs

To measure shipping emissions at our measurement site, our MAX-DOAS telescope is pointed towards the horizon, where the ships pass our site in a distance of 6–7 km. Since our instrument has a field-of-view of approximately 1°, the lowest usable elevation angle avoiding looking onto the ground is 0.5°, providing us with the highest sensitivity to near-surface pollutants. This is the elevation in which at our site usually the highest slant columns are measured. To convert a MAX-DOAS trace gas column which is the concentration of the absorber integrated along the effective light path into concen-

trations or volume mixing ratios, the length of this light path has to be known. This effective light path length depends on the atmospheric visibility, which is limited by scattering on air molecules as well as aerosols. As described in Section 3.2, trace gas absorptions in the higher atmosphere like stratospheric NO_2 nearly cancel out using a close-in-time zenith-sky reference spectrum. Following this, we can assume that the signal for our horizontal line-of-sight is dominated by the horizontal part of the light path after the last scattering event. As introduced by Sinreich et al. (2013), the length L of this horizontal part of the light path can then be estimated using the slant column density of the O_4-molecule which has a well-known number density in the atmosphere:

$$L_{O_4} = \frac{SCD_{O_4,horiz} - SCD_{O_4,zenith}}{n_{O_4}} = \frac{DSCD_{O_4}}{n_{O_4}} \quad (1)$$

The surface number density of O_4 is proportional to the square of the molecular oxygen concentration (Greenblatt et al., 1990; Wagner et al., 2004) and can be easily calculated from the temperature and pressure measured on the radar tower:

$$n_{O_4} = (n_{O_2})^2 = (0.20942 \cdot n_{air})^2 \quad (2)$$

$$\text{with} \qquad n_{air} = \frac{N_{air}}{V_{air}} = \frac{p_{air} \cdot k_B}{T_{air}} = \frac{p_{air} \cdot N_A}{T_{air} \cdot R} \quad (3)$$

with the Boltzmann constant k_B, Avogadro constant N_A and universal gas constant R.

Knowing the path length, it is then possible to calculate the average number density of our trace gas x along this horizontal path and the path-averaged volume mixing ratio:

$$n_x = \frac{SCD_{x,horiz} - SCD_{x,zenith}}{L_{O_4}} = \frac{DSCD_x}{L_{O_4}} \quad (4)$$

$$\text{and with that:} \qquad VMR_x = \frac{n_x}{n_{air}} \quad (5)$$

This O_4-scaling in principle takes into account the actual light path and its variation with aerosol loading and also needs no assumption on the typical mixing layer height, therefore overcoming the disadvantages of a simple geometric approximation.

However, when the atmospheric profile of the investigated trace gas x has a shape that differs from that of the proxy O_4, systematic errors are introduced as has been shown by Sinreich et al. (2013) and Wang et al. (2014b) in extensive and comprehensive radiative transfer model (RTM) simulations. Pollutants like NO_2 and SO_2 have a profile shape very different from O_4. They are emitted close to the ground (e.g. from ships), have high concentrations in low altitude layers and tend to decrease very rapidly with height above the boundary layer. They are often approximated as box profiles, while the

Table 1. DOAS fit settings for the retrieval of NO_2 and O_4 in UV and visible spectral range

Parameter	NO_2 (UV)	NO_2 (visible)
Fitting window	338–370 nm	425–497 nm
Polynomial degree	4	3
Intensity offset	Constant	Constant
Zenith reference	Coinciding zenith measurement[1]	Coinciding zenith measurement[1]
SZA range	Up to 85° SZA	Up to 85° SZA
O3	223 K & 243 K (Serdyuchenko et al., 2014)	223 K (Serdyuchenko et al., 2014)
NO_2	298 K (Vandaele et al., 1996)	298 K (Vandaele et al., 1996)
O_4	293 K (Thalman and Volkamer, 2013)	293 K (Thalman and Volkamer, 2013)
H2O	–	293 K (Lampel et al., 2015)
HCHO	297 K (Meller and Moortgat, 2000)	–
Ring	SCIATRAN (Rozanov et al., 2014)	SCIATRAN (Rozanov et al., 2014)

[1] Interpolation in time between the zenith measurements directly before and after the off-axis scan.

Table 2. DOAS fit settings for the retrieval of NO_2 and O_4 in UV and visible spectral range

Parameter	SO_2 (UV)
Fitting window	307.5–317.5 nm
Polynomial degree	3
Intensity offset	Constant & slope
Zenith reference	Coinciding zenith measurement[1]
SZA range	Up to 75° SZA
O3	223 K & 243 K (Serdyuchenko et al., 2014)
NO_2	298 K (Vandaele et al., 1996)
SO_2	293 K (Bogumil et al., 2003)
Ring	SCIATRAN (Rozanov et al., 2014)

[1] Interpolation in time between the zenith measurements directly before and after the off-axis scan.

O_4 concentration simply decreases exponentially with altitude. This difference in profile shapes violates the basic assumption that the O_4 DSCD is a good proxy for the light path through the NO_2 and SO_2 layers. The resulting near-surface volume mixing ratios will not be representative for the amount of trace gases directly at the surface, but for some kind of average over a certain height range in the boundary layer.

The studies like Sinreich et al. (2013) and Wang et al. (2014b) use correction factors from radiative transfer calculations to account for this. These correction factors depend on the amount of aerosols present in the atmosphere, often described by the aerosol optical density (AOD), the solar zenith angle (SZA) as well as the relative solar azimuth angle (RSAA), the height of the pollutant box profile and the extend and vertical position of the aerosol layer in relation to this box profile (Sinreich et al., 2013). The strong dependence of the correction factors on the height of the box profile for trace gas layer heights of less than 1 km makes it necessary for the application of the suggested parameterization method to have additional knowledge about the trace gas layer height, ideally from measurements (e.g. LIDAR) or otherwise from estimations. The use of this method for low boundary layer heights below 500 m without knowing the actual height is not recommended by the authors (Sinreich et al., 2013).

At our measurement site, no additional knowledge (measurements) about the height of the NO_2 and SO_2 layers is available and the trace gay layer heights are typically around 200–300 m. A comparison of the uncorrected MAX-DOAS VMRs retrieved with the upper equations to our simultaneous in-situ measurements (see Section 4.5) confirms the need for a correction factor but also shows that the scaling factor needed changes from day to day as well as during the course of the day. This indicates, that the NO_2 and SO_2 layer height is very variable, depending on wind speed, wind direction, atmospheric conditions and chemistry. The lack of comparability between both measurement techniques and geometries, which is further discussed in Section 4.5, prevents us from estimating diurnally varying correction factors from this.

The non-consideration of these scaling factors will lead to a systematic overestimation of the effective horizontal path length and therefore to a systematic underestimation of

MAX-DOAS VMRs, up to a factor of three (Sinreich et al., 2013; Wang et al., 2014b).

In summary, a detailed radiative transfer study for the determination of the right correction factors is out of scope of this study which focuses on the statistic evaluation of a three year dataset of shipping emission measurements in the German Bight. Therefore, when in the following MAX-DOAS VMRs are shown, it has to be kept in mind that these are uncorrected VMRs obtained by above formulas.

This approach has been applied successfully by Sinreich et al. (2013) and Wang et al. (2014b) for measurements in urban polluted air masses over Mexico City and the city of Hefei (China) using MAX-DOAS measurements in $1°$ and $3°$ (Sinreich et al., 2013) and only in $1°$ elevation (Wang et al., 2014b), respectively. Gomez et al. (2014) applied this approach to measurements on a high mountain site at the Izaña Atmospheric observatory on Tenerife (Canary Islands), Schreier et al. (2016) at Zugspitze (Germany) and Pico Espejo (Venezuela). Due to the low aerosol amounts in such heights the latter two studies applied the approach without using correction factors. The fact that our instrument is located on a radar tower in a height of about $30\,m$ above totally flat surroundings (the German Wadden Sea) allows an unblocked view to the horizon in all feasible azimuthal viewing directions. This led to the idea of trying to apply this approach to our shipping emission measurements on Neuwerk.

Since the O_4-DSCD is retrieved simultaneously to NO_2 in both the UV and visible DOAS fit for NO_2, this approach can be applied to NO_2 retrieved in both fitting ranges. The approach can also be applied to SO_2, although the difference of light paths due to the different fitting windows in the UV for O_4 (NO_2) and SO_2 introduces an uncertainty which has to be accounted for. Wang et al. (2014b) derived an empirical formula from RTM calculations for a variety of aerosol scenarios to convert the path length at $310\,nm$ from the path length at the O_4 absorption at 360nm:

$$L_{310} = 0.136 + 0.897 \times L_{360} - 0.023 \times L_{360}^2 \qquad (6)$$

where L_{310} and L_{360} are given in km. This formula was also applied to our measurements to correct the light path length for the SO_2 fitting window. Although this formula has been calculated for polluted sites, the authors state that the deviations for other sites with different conditions are expected to be small (Wang et al., 2014b).

Using equations 1 to 5, several problems can arise from the division by the differential slant column density of O_4. For example if the O_4 DSCD is negative, which can happen at low signal-to-noise-ratio DOAS fits (e. g. under bad weather conditions), the resulting path length will be negative. If at the same time the trace gas DSCD is positive, then the trace gas volume mixing ratio will be negative as well, a non-physical result. However, even when there is no NO_2 or SO_2, there is still some noise and therefore the retrieved VMR are

not exactly zero, but scatter around zero, so slightly negative values have to be included when averaging over time to avoid creating a systematic bias. If, on the other hand, the O_4 DSCD is close to zero, the path length will be very small leading to extremely high (positive or negative) mixing ratios which are also unrealistic. To address both problems, measurements with negative or small retrieved horizontal path lengths are discarded. For the measurements on Neuwerk, with respect to the characteristics of the measurement site, a minimum path length of $5\,km$ seems to be a reasonable limit. This value provides the best compromise between the number of rejected bad measurements and the total number of remaining measurements for NO_2 in UV and visible as well as for SO_2. For statistics on differential slant column densities on the other hand, no such filtering is applied since negative values are not unphysical in this case and just mean that there is more trace gas absorption in the reference measurement than in the off-axis measurement.

3.5 In-situ instrumentation

In addition to the MAX-DOAS instrument, also in-situ observations are taken, using the Airpointer, a commercially available system which combines four different instruments in a compact, air-conditioned housing. The manufacturer is recordum (Austria), distributed by MLU (http://mlu.eu/recordum-airpointer/). The Airpointer device measures carbon dioxide (CO_2), nitrogen oxides ($NO_x = NO + NO_2$), sulfur dioxide (SO_2) and ozone (O_3) using standard procedures. Table 3 shows more detailed information about the different included instruments, their measurement methods, precision, and time resolution.

In this study the in-situ 1-minute-means of all compounds were used. NO_2 itself is not directly measured but calculated internally by subtracting the measured NO from the measured NO_x concentration.

4 Results

4.1 Measured slant column densities of NO_2 and SO_2

In this study, three years of continuous MAX-DOAS measurements on Neuwerk have been evaluated. Figure 6 shows for one example day in summer 2014 the measured differential slant column densities of NO_2 in UV and visible spectral range as well as of SO_2 for the $0.5°$ elevation angle (viewing to the horizon) and the $-25°$ azimuth angle (approximately NNW direction, see Fig. 1). Sharp peaks in the curves originate from ship emission plumes passing the line of sight of the instrument. On this day, elevated levels of NO_2 have been measured in the morning, corresponding to a polluted air mass coming from land, which appears as an enhanced, slowly varying NO_2 background signal below the peaks. The systematic difference between the NO_2 in the UV (red curve) and the NO_2 in the visible (blue curve) emerges from the

Table 3. Specifications of the Airpointer in-situ device: measured trace gases, corresponding measuring techniques, measuring ranges and detection limits [Source: recordum/MLU (manufacturer), http://mlu.eu/recordum-airpointer/]

Trace gas	CO_2	O_3	NO, NO_2	SO_2
Measuring technique	Non-dispersive IR spectroscopy LI-COR LI820	UV absorption (EN 14625)	NO Chemi-luminescence (EN 14211)	UV fluorescence (EN 14212)
Detection limit	1 ppm	0.5 ppb	0.4 ppb	0.25 ppb
Measuring range	up to 20 000 ppm	up to 200 ppm	up to 20 ppm	up to 10 ppm
Time resolution	1 s	< 30 s	< 60 s	< 90 s

longer light-path in the visible due to stronger Rayleigh scattering in the UV (wavelength dependence $\propto \lambda^{-4}$). This is further investigated in Sect. 4.3 below.

By comparing SO_2 (green curve) with NO_2 (red and blue curves) it can be seen that for many of the NO_2 peaks there is a corresponding and simultaneous SO_2 peak, but not for all of them. This indicates a varying sulfur content in the fuel of the measured ships. Fuel with higher sulfur content leads to higher SO_2 emissions (see also Sect. 1).

By comparing measurements in different azimuthal viewing directions, the movement direction of the ship (and its plume) can be easily distinguished. The zoom in on the right of Fig. 6 shows the visible NO2 measurements in different azimuth directions for one example peak from the time series shown on the left. The color-coded viewing directions (see also Fig. 1) are sketched schematically below. From the measurements it can be seen that the emitted plume was consecutively measured in all directions at different times. It was first measured in the easternmost viewing directions and at last in the westernmost direction, indicating that the ship and its plume moved from east to west.

For the identification of sources for air pollution on Neuwerk, the wind direction distribution for the differential slant column densities of NO_2 and SO_2 measured in 2013 and 2014 is plotted for four different elevation angles ($0.5°$, $2.5°$, $4.5°$ and $30.5°$) in Fig. 7. When the wind is coming from the open North Sea (blue shaded sector) the measured NO_2 and SO_2 DSCD are clearly lower than for other directions, for which the wind is coming from the coast (green and yellow shaded sectors) and blows land-based air pollution to the island. The wind direction dependence is more or less similar for both trace gases but with a higher fraction of ship related signals in the overall SO_2 columns. The values are especially high when the wind is coming from the cities of Cuxhaven (ESE direction) and Bremerhaven (SSE) for both NO_2 and SO_2.

Elevation angle sequences of slant columns (i.e. vertical scanning) contain information on the vertical distribution of trace gases. For lower elevation angles, the measured trace gas slant columns for tropospheric absorbers are usually higher because of the longer light path in the boundary layer.

As expected, higher elevations show on average lower DSCDs due to the shorter light path in the boundary layer. The highest NO_2 and SO_2 DSCD in the lowest elevation angle ($0.5°$, blue bars) in relation to DSCDs in higher elevations are measured especially for wind from all northern directions, in a sector ranging from WSW to ESE. These directions coincide with the course of the main shipping lane coming from the WSW direction (the English Channel, the Netherlands, East Frisian Islands), passing the island in the north and running close to the city of Cuxhaven (ESE direction) into the river Elbe. This indicates that the enhanced columns in the $0.5°$ elevation angle is pollution emitted from ships in a surface-near layer.

For southerly wind directions no major shipping lane is in the direct surrounding and land-based pollution sources dominate. The average DSCDs in $0.5°$ and $2.5°$ elevation are nearly the same for both NO_2 and SO_2 indicating that the pollution is located higher up in the troposphere.

4.2 Volume mixing ratios of NO_2 and SO_2

For the example day presented in Fig. 6 the path-averaged volume mixing ratios retrieved with the approach presented in Sect. 3.4 are shown in Fig. 8.

From the mathematics of the approach one would expect a good agreement between the NO_2 volume mixing ratios retrieved in UV and visible if NO_2 is well mixed in the boundary layer, since averaging constant values over different paths should give equal mean values. In the figure, in fact one can see a very good agreement between both NO_2 volume mixing ratios, in particular for situations characterized by background pollution.

Although the light path in the visible spectral range is clearly longer than in the UV, for all the peaks shown here the UV instrument measured a higher path-averaged VMR. The reason for that are spatial inhomogeneities along the line-of-sight.

If NO_2 is not distributed homogeneously along the light path, which is the case in the presence of individual ship exhaust plumes, one can expect different values for the means
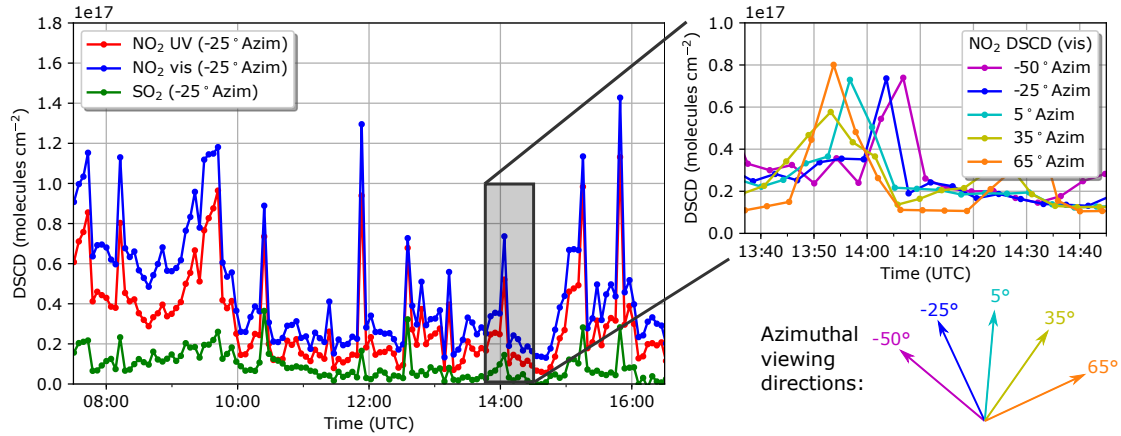
Figure 6. NO_2 (UV and visible) and SO_2 differential slant column densities measured in $0.5°$ elevation and the $-25°$ viewing azimuth angle (approximately NNW direction) on Neuwerk on Wednesday, 23 July 2014. The excerpt on the right shows for one example peak the NO_2 (vis) measurements in different azimuth viewing directions.
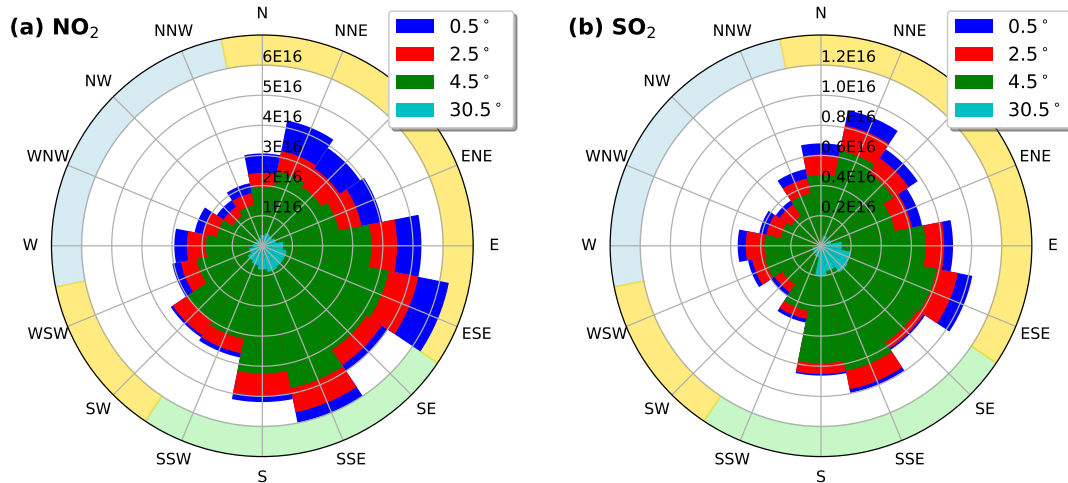

Figure 7. Overlayed wind roses for different elevation angles showing the wind direction distribution of the UV NO_2 **(a)** and SO_2 **(a)** differential slant column densities measured in the main viewing direction in $0.5°$, $2.5°$, $4.5°$ and $30.5°$ elevation in the years 2013 and 2014. The wind roses are plotted on top of each other, i. e. the highest values were measured in the lowest elevation angle (blue bars). The colored sectors show directions with wind from land (green), open North Sea (blue) and mixed origin (yellow).

over the two light paths as they probe different parts of the NO_2 field. Such differences can be identified in the figure by looking at the peaks.

The light path in the visible spectral range is longer than in the UV because of more intensive Rayleigh scattering in the UV. The difference between UV and visible peak values depends on the exact location of the plume within the light paths.

A short distance of the plume to the instrument and its complete coverage by the shorter UV path leads to higher values in the UV since the part of the light path probing the higher NO_2 values has a larger relative contribution to the signal than for the longer visible path.

If the plume is further away from the instrument and only in the visible path or close to the UV scattering point, one will retrieve a higher volume mixing ratio in the visible. This relationship contains information on the horizontal distribution of the absorber and will be further investigated in a second manuscript.

4.3 Statistical evaluation of UV and visible NO_2 data

To investigate quantitatively the relationship between the NO_2 slant column densities measured simultaneously in the UV and visible spectral range, all single pairs of DSCD mea-
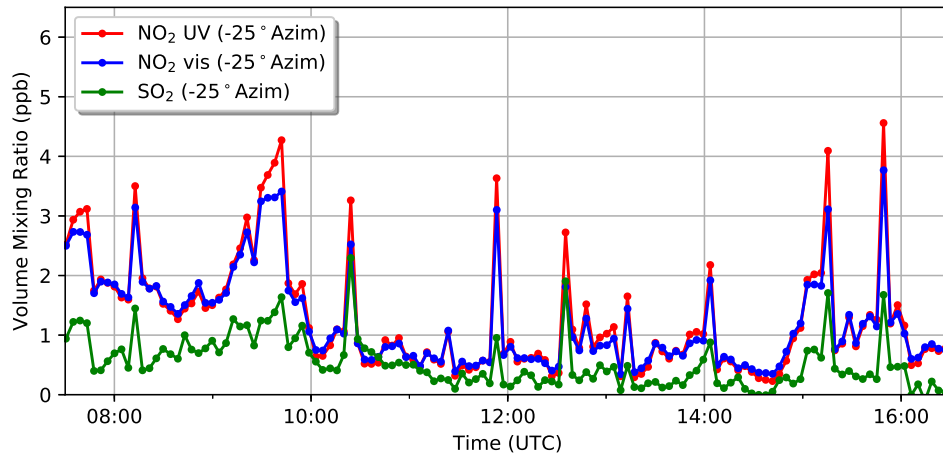
Figure 8. NO_2 (UV and visible) and SO_2 path-averaged volume mixing ratios measured in $0.5°$ elevation angle and $-25°$ viewing azimuth angle (approximately NNW direction) on Neuwerk on Wednesday, 23 July 2014.

surements with an RMS better than 1×10^{-3} are plotted into a scatter plot, shown in Panel (a) of Fig. 9.

As can be seen from the figure, NO_2 DSCDs in UV and visible are strongly positively correlated with a Pearson correlation coefficient of 0.983. Because of the difference in the horizontal light path lengths in both spectral regions (due to more intense Rayleigh scattering in the UV), the slope of the regression line is 1.30 corresponding to a 30 % longer light path in the visible. The intercept of the regression line is small. Panel (b) of Fig. 9 shows a histogram of the ratios between both slant column densities. The distribution peaks for ratios of 1.3, in good agreement with the retrieved slope from the scatter plot.

When converting the slant column densities to mixing ratios using the O_4-scaling, the dependence on light path should be removed and quantitative agreement is expected between the UV and visible VMRs. A scatter plot for the horizontal path averaged volume mixing ratios is shown in Panel (c) of Fig. 9. It is clearly visible that the points scatter symmetrically along the 1:1 identity line. Comparing this plot with the plot in Panel (a) shows that the difference in light path lengths is in fact corrected for by the O_4-scaling approach. The slope of the regression line is close to unity and the intercept is very small. The Pearson correlation coefficient has further increased to 0.984. The histogram (Panel d of Fig. 9) peaks at 1.0.

As discussed above, differences are still expected not only as a result of measurement uncertainties but also due to different averaging volumes in case of inhomogeneous NO_2 distributions (which is especially the case for ship plumes under certain wind directions). For the horizontal light path lengths, a mean value of 9.3 km with a standard deviation of 2.3 km was retrieved in the UV, and a mean value of 12.9 km with a standard deviation of 4.5 km was retrieved in the visi-

ble. On days with optimal measurement conditions (clear sky days), typical horizontal light paths are around 10 km in the UV and 15 km in the visible spectral range.

4.4 Allocation of ship emission peaks to ships using wind and AIS data

The detailed information on passing ships transmitted via the *Automatic Identification System* (AIS) and the acquired weather and wind data can be used to allocate the measured pollutant peaks to individual ships.

Measurements from Wednesday, 9 July 2014 are shown in Fig. 10. Panel (a) shows the MAX-DOAS differential slant column density of NO_2. Panel (b) includes various information about passing ships: The vertical bars indicate when a ship was in the line-of-sight of the MAX-DOAS instrument. Solid bars represent ships coming from the left and going to the right (from west to east, i. e. sailing into the river Elbe), dashed bars vice versa. The colors of the bars indicate the ship length, with small ships shown in blue and very large ships (> 350 m) in red. Panel (c) displays the wind speed and direction.

On this day, the wind was coming from northern directions, directly from the shipping lane, with moderate wind speeds of 10 to 35 km/h, resulting in low background pollution values ($1\text{–}2 \times 10^{16}$ molec/cm^2) as well as sharp and distinct ship emission peaks (up to 1.2×10^{17} molec/cm^2) of NO_2. By comparing the ship emission peak positions to the vertical bars (representing times when ships crossed the MAX-DOAS line-of-sight) in the schematic representation below it can be seen that most of the peaks can be allocated to individual ships. In some cases, when two or more ships simultaneously cross the line-of-sight, the single contributions can not be separated. Large ships (orange and red bars) tend to exhaust more NO_2 while the contribution of small ships
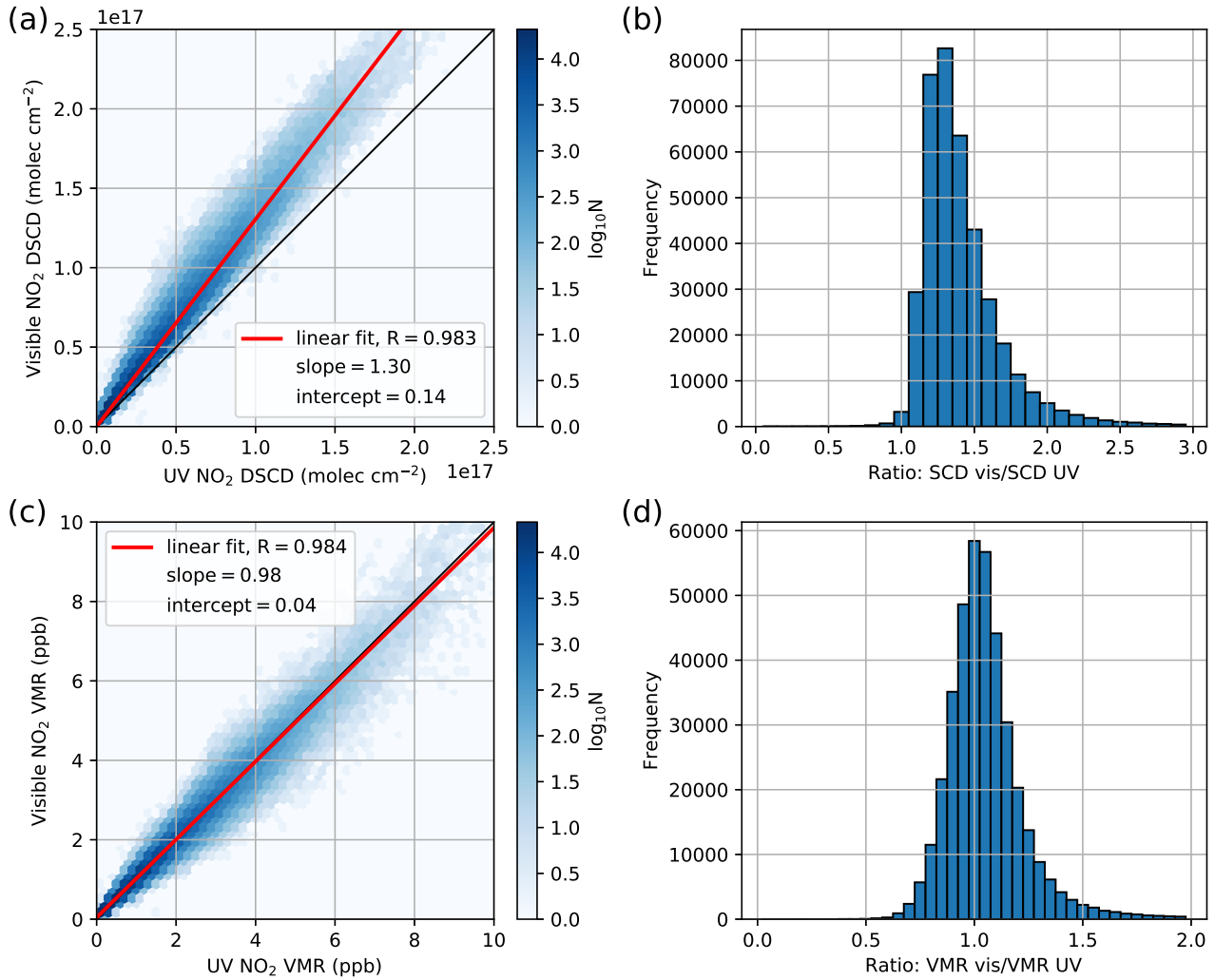
Figure 9. (a) Scatter plot: NO_2 slant column density retrieved in the visible vs. UV measured in all azimuth angles at $0.5°$ elevation for solar zenith angles smaller than $75°$. The parameters derived from the linear fit by orthogonal distance regression (Deming regression) are also shown. **(b)** Histogram of the ratio of the two NO_2 slant column densities (visible/UV). **(c)** As (a), but for volume mixing ratios. **(d)** Histogram of the ratio of the two NO_2 volume mixing ratios (visible/UV).

(length $< 30\,m$) represented by the dark blue bars is usually not measurable.

4.5 Comparison of MAX-DOAS VMR to in-situ measurements

The fact that our measurement site is also equipped with an in-situ device (see Section 3.5 for a description), makes it possible to compare the MAX-DOAS VMRs of NO_2 and SO_2 to our simultaneous in-situ measurements. The differences of both measurement techniques need to be considered for such a comparison: The MAX-DOAS averages over a long horizontal light path, while the in-situ device measures at a single location inside the plume. Since ship plumes usually never cover the whole light path but rather a small fraction of it, very high concentration peaks are usually underestimated in the MAX-DOAS VMR.

Figure 11 shows the horizontal path averaged NO_2 volume mixing ratio retrieved from the differential slant column densities shown in Fig. 10 as well as the in-situ NO_2 volume mixing ratio (Panel a) in combination with ship data (Panel b) and wind data (Panel c).

Ship emission peaks measured by the in-situ instrument are both higher and broader than the corresponding MAX-DOAS peaks, leading to a considerably larger integrated peak area, showing the systematic underestimation of the NO_2 concentrations inside ship plumes by the MAX-DOAS instrument due to the averaging along the horizontal light path.
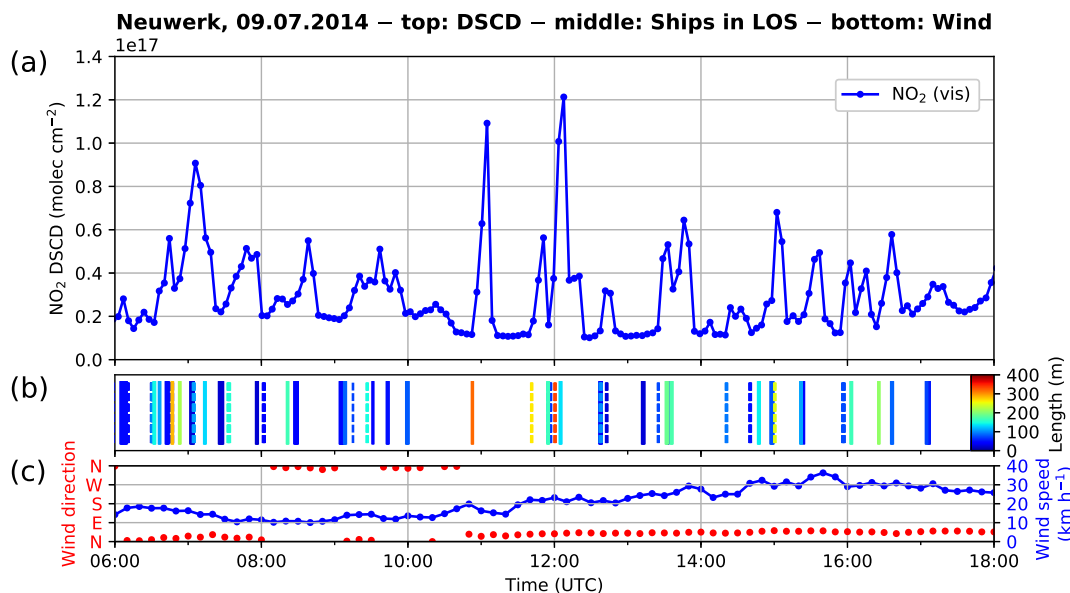
Figure 10. NO$_2$ differential slant column densities, AIS and wind data for Neuwerk on Wednesday, 9 July 2014.
(a) NO$_2$ DSCD in 0.5° elevation for the 35° azimuth viewing direction
(b) Vertical bars indicating that a ship is in the line-of-sight of the instrument, solid bars: ship moves from left to right (west to east), dashed vice versa, colors representing ship length
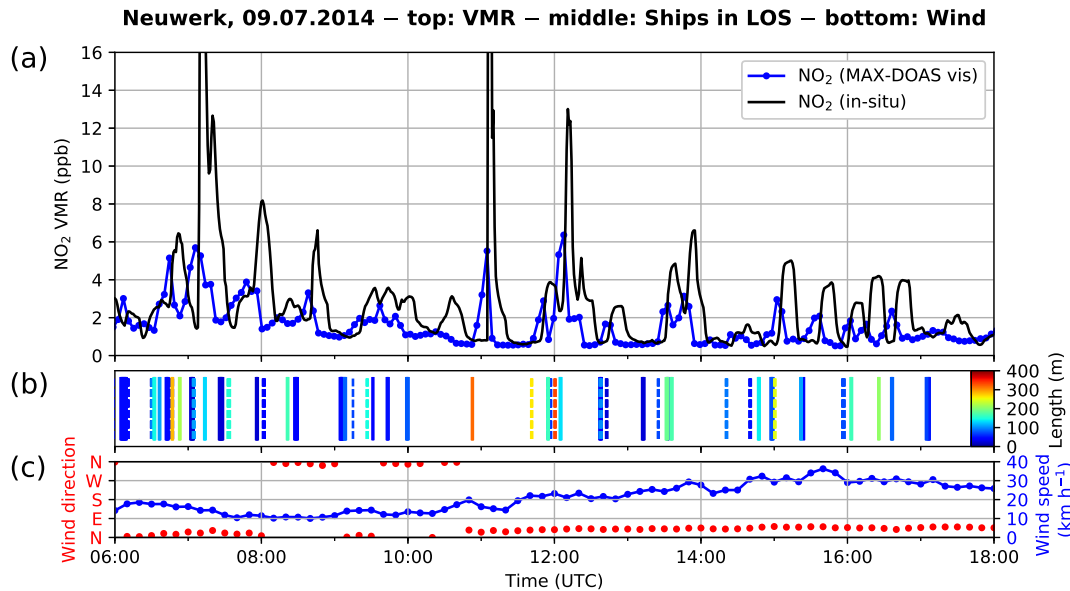**(c)** Wind speed and direction measured on Scharhörn (HPA)

Figure 11. MAX-DOAS and in-situ NO$_2$ volume mixing ratio, AIS and wind data on Wednesday, 9 July 2014:
(a) MAX-DOAS (visible) and in-situ NO$_2$ VMR
(b) Vertical bars indicating that a ship is in the line-of-sight of the instrument, solid bars: ship moves from left to right (west to east), dashed vice versa, colors representing ship length
(c) Wind speed and direction measured on Scharhörn (HPA)

Normally, a time-shift between MAX-DOAS and in-situ peaks exists, which is due to the long distance of about 6–7 km to the shipping lane, that the plumes have to travel until they reach the radar tower. This time-shift depends on the wind velocity and gets smaller for higher wind speeds. In the figure, this dependency can be seen when comparing the magnitude of the time delay for measurements in the morning (low wind speeds) and evening (higher wind speeds) This travel time also explains the broader peaks in the in-situ measurements, since the emitted plume spreads and dilutes on its way to the radar tower.

However, if the pollution is horizontally well-mixed in the measured air mass, which is approximately the case for background pollution coming from the coast but not for ship plumes, MAX-DOAS and in-situ instrument should in principle measure the same values. However, as discussed in Section 3.4, correction factors need to be applied to the MAX-DOAS VMRs to account for the different profile shapes of O_4 and the investigated pollutants NO_2 and SO_2, but in our case cannot be determined because no measurements of the height of the NO_2 and SO_2 layer exist. The uncorrected VMRs shown here can be strongly underestimated (up to a factor of 3), because they have been calculated with an overestimated path length. This is the case for background pollution as well as shipping emission measurements.

Since the lack of comparability between both instruments for individual measurements, for a meaningful comparison and the computation of a correlation coefficient at this measurement site an averaging over longer time spans was applied to reduce the impact of the differences between both measurement methods. The fact that MAX-DOAS averages over a large horizontal distance should therefore cancel out on temporal average when comparing to in-situ measurements.

Figure 12 shows in Panel (a) three months of daily mean NO_2 VMRs from the in-situ and MAX-DOAS UV instrument in summer 2014 and in Panel (b) due to instrumental problems with the in-situ SO_2 device (see Fig. 4) six weeks of SO_2 daily mean VMRs from summer 2013. To have comparable conditions, for the in-situ instrument all measurements between the start of the MAX-DOAS measurements in the morning (with sunrise) and the end of measurements in the evening (with sunset) have been averaged. The shaded areas show the corresponding standard deviation and indicate the variability during the single days.

The long gap in the SO_2 time series was caused by a power outage.

It is clearly visible that the in-situ NO_2 VMRs are systematically higher than the uncorrected MAX-DOAS VMRs. The scaling factors which would be needed to bring both time series into agreement differ from day to day. A closer look into the individual days shows that these scaling factors also vary over the course of the day, even when wind direction and speed do not change. The scatter plot for this time-series of NO_2 measurements in Fig. 13 Panel (a) shows a good cor-

relation between MAX-DOAS and in-situ daily means, but a slope strongly deviating from one and also some scatter.

The most important reason for the systematic differences is certainly the non-consideration of the correction factors arising from the different profile shapes of O_4 and NO_2, leading to a systematic underestimation of the VMRs from the MAX-DOAS instrument (see Section 3.4 for a more detailed discussion). But also "light dilution", i.e. light scattered into the line-of-sight between the instrument and the trace gas plume (Kern et al., 2010) might play a role reducing the measured off-axis SCDs .

For SO_2, the daily mean VMRs from MAX-DOAS and in-situ instrument in Fig. 12 Panel (b) show a much better agreement. The scatter plot in 13 Panel (b) confirms this with a slope much closer to unity, but more scatter around the fitted line.

The difference in scaling factors for NO_2 and SO_2 can be attributed to plume chemistry. During combustion, mainly nitric oxide (NO) is produced. This has to be converted to NO_2 (through reaction with tropospheric ozone) before it can be measured by the MAX-DOAS instrument. Since the MAX-DOAS instrument sees the ship plumes in an earlier state, the fraction of NO_2 should be lower than in the in-situ measurements, explaining at least a part of the difference.

Although MAX-DOAS and in-situ VMRs show systematic deviations in the absolute values, a very good agreement of the shape (the course) of the curves is found for NO_2 as well as SO_2. This illustrates that MAX-DOAS can determine day-to-day trends as in-situ measurements, even though no correction factors have been applied.

4.6 Diurnal and weekly variability of NO_2

Although our measurement station is located on a small island in the German Bight close to the mouths of the Elbe and Weser river, our measurements are strongly influenced by air pollution from traffic and industry on land, depending on the prevailing wind direction. As can be seen from Fig. 1 (a) and 3, wind coming from northeasterly, easterly, southerly and southwesterly directions will blow polluted air masses from the German North Sea Coast and hinterland to our site. In Figure 14 the average diurnal variation of the measured NO_2 volume mixing ratios is shown as hourly mean values. Solid curves show the respective curve for all measurements (with all wind directions), dashed lines show the subset of measurements with wind coming only from the open North Sea with no coastal background pollution. Looking at the diurnal variation in all measurements, the typical daily cycle for road-traffic-influenced air masses with enhanced values in the morning and in the late afternoon during rush hour can be seen. If we restrain the data to periods with wind from the open North Sea (dashed curves), this diurnal cycle vanishes and values are more or less constant over day and also considerably lower. This result is in accordance with the ex-
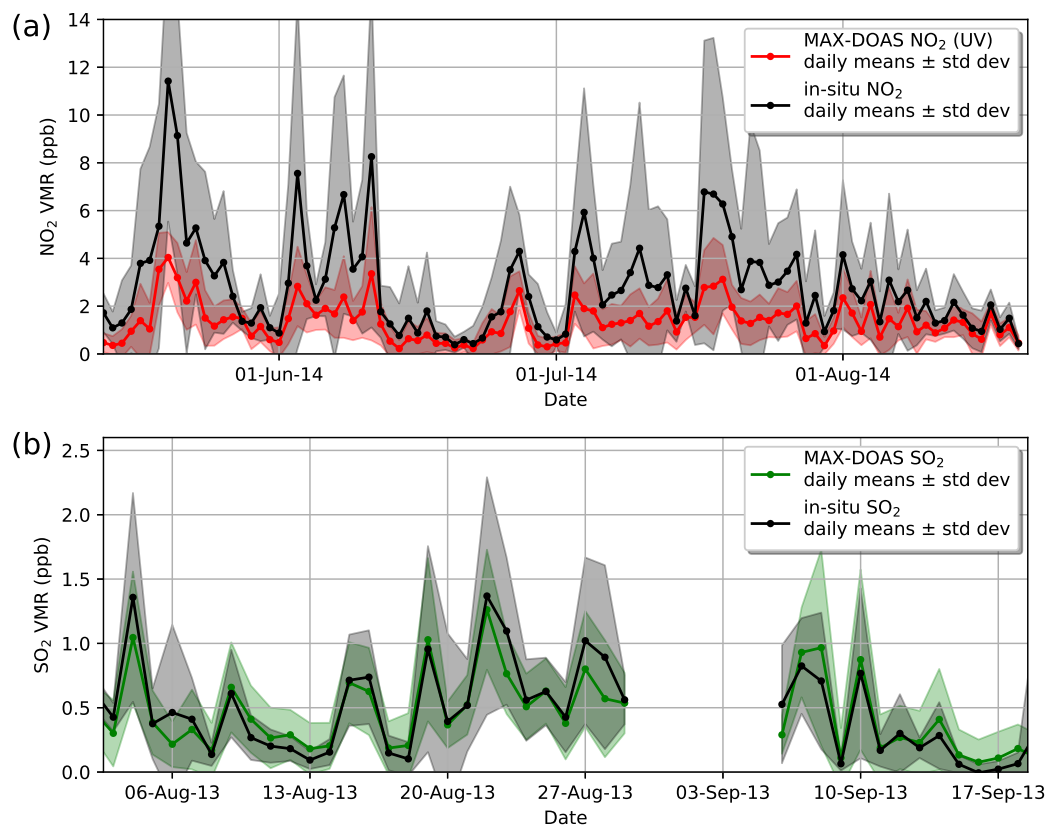
Figure 12. Comparison of MAX-DOAS (UV) and in-situ daily mean VMRs of NO_2 **(a)** during summer 2014 and SO_2 **(b)** during summer 2013. Shaded areas show the standard deviation for each daily mean value.
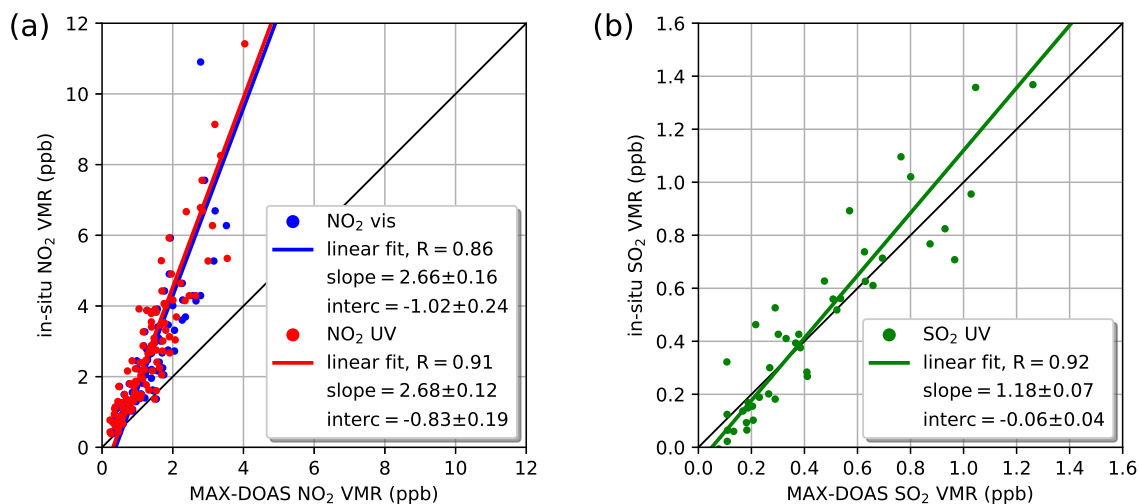

Figure 13. Scatter plot of **(a)** NO_2 VMR and **(b)** SO_2 VMR from MAX-DOAS vs. in-situ. For NO_2 daily means from summer 2014, for SO_2 daily means from summer 2013 are shown. For the MAX-DOAS instrument, to get a better statistic, all measurements in all azimuth viewing directions have been averaged. For the in-situ instrument, the mean of all measurements during the daily MAX-DOAS measurement periods (sunrise till sunset) has been taken. The linear fits were calculated with orthogonal distance regression (Deming regression), parameters are shown in the figures.
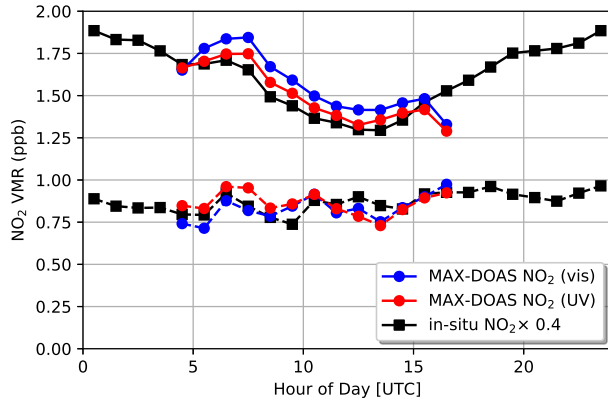
Figure 14. Average diurnal cycle of MAX-DOAS (UV and visible) and in-situ NO$_2$ volume mixing ratios for all measurements (solid lines) and for a subset of measurements with wind from the open North Sea (dashed lines). For a better visual comparability the in-situ values are scaled by a factor of 0.4.
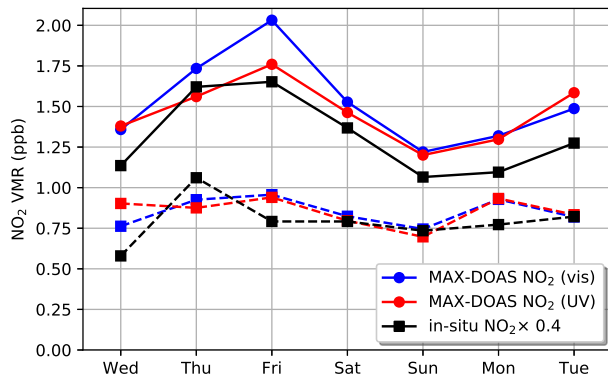

Figure 15. Average weekly cycle of MAX-DOAS (UV and visible) and in-situ NO$_2$ volume mixing ratios for all measurements (solid lines) and for a subset of measurements with wind from the open North Sea (dashed lines). For a better visual comparability the in-situ values are scaled by a factor of 0.4.

pectations that the amount of ship traffic should be almost independent from the time of day.

The mean NO$_2$ volume mixing ratios for each weekday shown in Fig. 15 illustrate again the influence of land-based road traffic. If we consider the whole time series (solid lines), lowest values are measured on Sundays, when road traffic is less intense. There is only little weekly cycle for air masses coming from the open North Sea (dashed lines). Measurements are more or less constant and again considerably lower. Such a weekly cycle for NO$_2$ in polluted regions has been observed and discussed several times before, for example in Beirle et al. (2003), Kaynak et al. (2009), Bell et al. (2009) and Ialongo et al. (2016).

It is also remarkable that except for a scaling factor of approximately 0.4, the shape of the diurnal and weekly cycle retrieved from MAX-DOAS and in-situ measurements agrees very well for both instruments.

4.7 Dependence of NO$_2$ and SO$_2$ pollution levels on wind direction

As already mentioned in Sect. 1, on the 1st of January 2015, the sulfur content of marine fuels allowed inside the North and Baltic Sea Emission Control Areas (ECA) has been substantially decreased from 1.0 % to 0.1 %. Therefore, one would expect lower sulfur dioxide (SO$_2$) values in 2015 compared to the years before, especially when the wind is blowing from the open North Sea, where shipping emissions are the only source of SO$_2$. This expectation is confirmed by the measurements. In the data since 2015, no distinct ship emission peaks are visible anymore (for an example day see Section 4.9 below). For a more detailed analysis, mean values over the whole time series before and after 1 January 2015 have been investigated, separated according to the prevailing wind direction.

Two days of SO$_2$ measurements (20 and 30 October 2014) showing very high values over several hours have been excluded from the time-series. Comparisons with our simultaneous in-situ measurements and measurements from the German Umweltbundesamt at the coast of the North Sea in Westerland/Sylt and at the coast of the Baltic Sea on the island Zingst showing a similar behavior as well as HYSPLIT backward trajectories suggest that on both days SO$_2$ plumes of the Icelandic volcano Bárdarbunga have influenced the measurements in northern Germany.

Figure 16 shows the wind direction distribution of the mean NO$_2$ and SO$_2$ path averaged volume mixing ratios for all measurements before and after the change in fuel sulfur limit regulations.

For SO$_2$, a significant decrease is found, particularly for wind directions from West to North with wind from the open North Sea. For this sector, values in 2015 are close to zero. This shows that the new and more restrictive fuel sulfur content limits lead to a clear improvement in coastal air quality. For wind directions with mainly land-based sources, no or only a small decrease is observed.

The typical average SO$_2$ concentrations measured by the German Federal Environmental Agency (Umweltbundesamt, 2017) in 2016 for rural stations in Northern Germany are around 0.5–1 µg m^{-3}, corresponding to 0.2–0.4 ppb (Conversion factor: 1 ppb $\widehat{=}$ 2.62 µg m^{-3} for SO$_2$). Measurements in cities and especially close to industrial areas show higher values. Bremerhaven, which is the station closest to our instrument, has a mean concentration of 1.77 µg m^{-3}, corresponding to 0.67 ppb. The reported values for rural stations are in good agreement with our measurements of 0.3–0.4 ppb for wind directions with mainly land-based pollution sources (green sector in Fig. 16 Panel b) since January 2015.

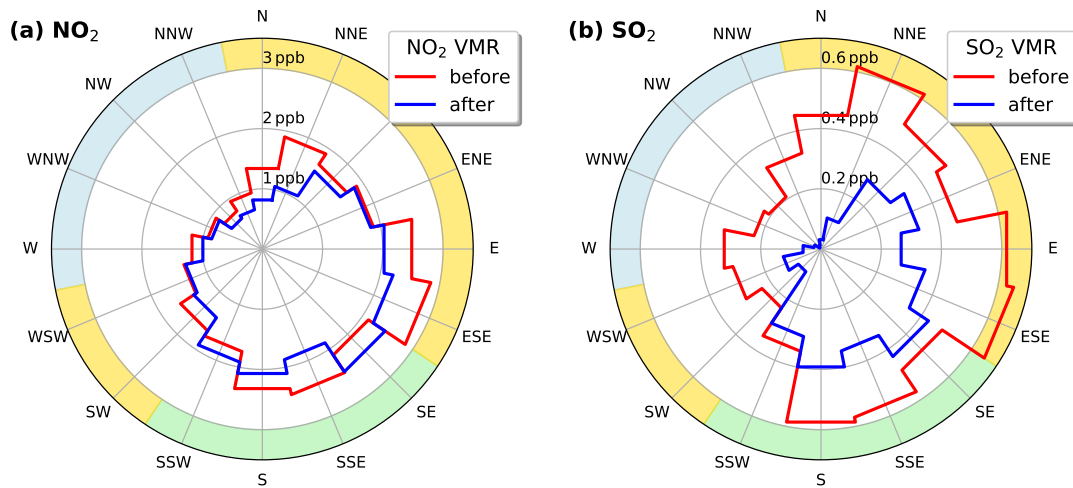**Figure 16.** Wind direction distribution of the measured NO_2 **(a)** and SO_2 **(b)** volume mixing ratio in $0.5°$ elevation before and after the change in fuel sulfur limit regulations on 1 January 2015. The colored sectors show directions with wind mainly from land (green), open North Sea (blue) and mixed origin (yellow).

For NO_2 on the other hand, both the directional distribution and the absolute values are nearly identical for both time periods, implying no considerable changes in NO_x emissions. This result meets the expectations, since no NO_x emission limits have been set into force up to now for the North and Baltic Sea emission control area.

4.8 Contributions of ships vs. land-based pollution sources on coastal air quality on Neuwerk

The distribution of measured NO_2 and SO_2 volume mixing ratios depending on the wind direction shown in Fig. 16 can be used to estimate the contributions of ships and land-based sources to coastal air pollution levels. To trade ship emissions off against land-based emissions (e.g. industry, road transport), two representative sectors of wind directions have been chosen, both 90 degrees wide: A north-westerly sector ($258.75°$ to $348.75°$) with wind from the open North Sea and ships as the only local source of air pollution and a south-easterly sector ($123.75°$ to $213.75°$) with wind mainly coming from land and almost no ship traffic. Air masses brought by wind from the other directions, for example from the mouth of the river Elbe in the East of Neuwerk, can contain emissions from land-based pollution sources as well as ship emissions. These remaining directions will be called "mixed" in the following. It is now assumed, that trace gas concentrations measured during periods with wind from one of these sectors have their source in the according sector. For getting a good statistic, measurements in all azimuth angles have been included. Figure 17 shows the results in several pie charts.

For both NO_2 and SO_2, more than half (around 50–60 %) of all measurements have been taken while wind was coming from either the assigned sea or land sector. This implies that

not only a small sample, but the majority of measurements can be used for the estimation of source contributions, making the assumption of using these sectors as representative samples for ships and land-based source regions a reasonable approximation. There are differences in the time series of NO_2 and SO_2 coming from the fact that the SO_2 fit delivers realistic values only up to $75°$ solar zenith angle and the NO_2 was fitted until $85°$ SZA, leading to less measurements for SO_2 than for NO_2, especially pronounced in winter times. Despite this, the general distribution pattern of wind direction frequency for NO_2 and SO_2 is quite similar, with wind coming from the sea 32–42 % of the time and from the land sector 18–24 % of the time.

For NO_2 (upper row in Fig. 17), more than half of the total NO_2 measured on Neuwerk can be attributed to wind from either of both sectors, with 21 % coming from ships and 31 % coming from land.

If we consider only the two sectors, for which we can identify the primary sources and take theses as representative, we can say that 40 % of the NO_2 on Neuwerk is coming from shipping emissions, but with 60 %, the majority, is coming from land. One reason for that is that the island Neuwerk is relatively close to the coastline (around $10\,km$) and is obviously still impacted by polluted air masses from land, which has also been observed in the diurnal and weekly cycle analysis shown in Figures 14 and 15. This might also give us a hint that in coastal regions in Germany land-based sources like road traffic and industry are, despite the heavy ship traffic, the strongest source of air pollution and ship emissions come in second.

For SO_2 the whole time series of measurements from 2013 to 2016 was divided into two periods of nearly the same length: The first period is 2013 and 2014, which was before
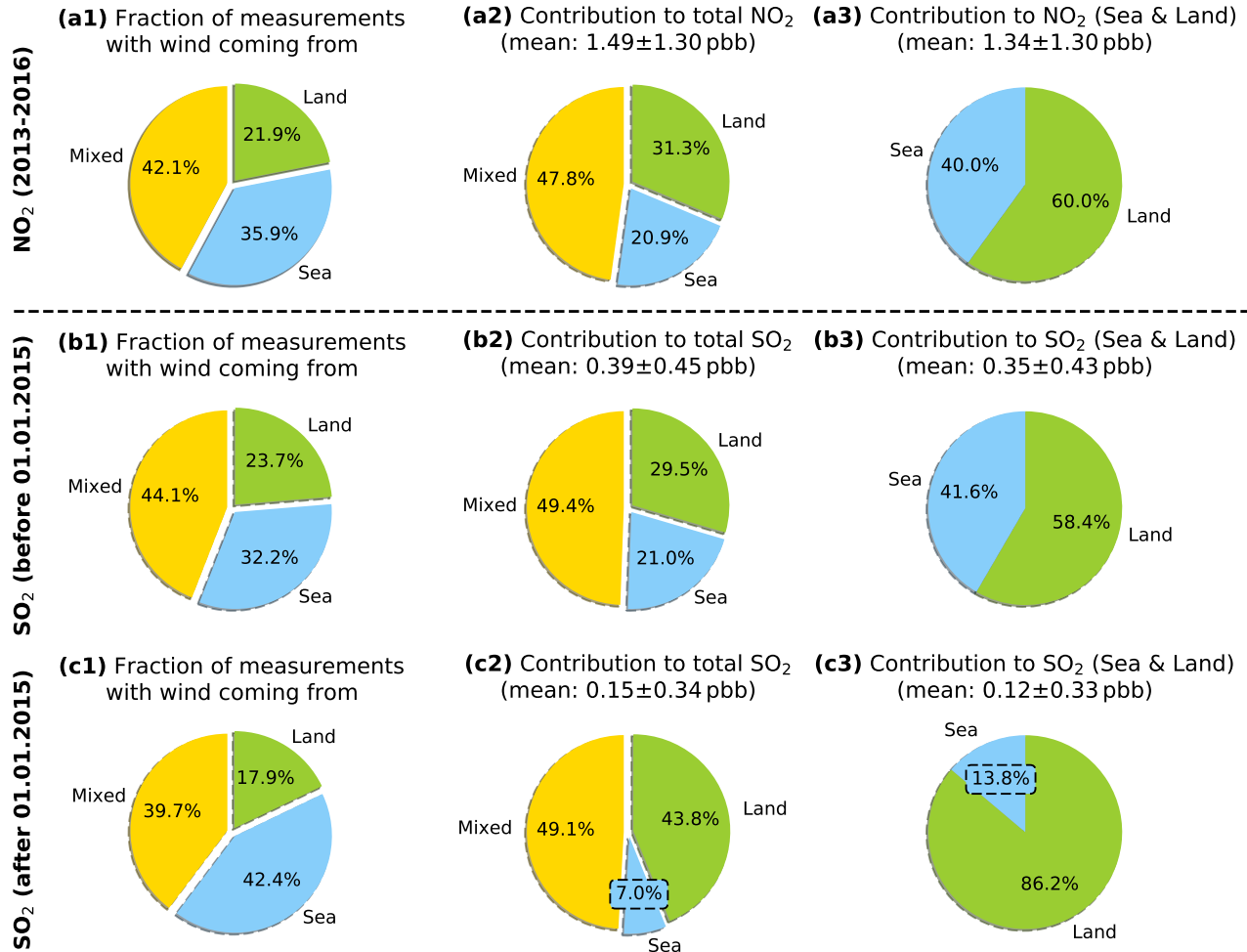
Figure 17. Contributions of ships and land-based pollution sources to measured NO_2 and SO_2 levels on Neuwerk:
(a1), (b1) and (c1): Percentage of measurements with wind coming mainly from land (green), only from sea (blue) and from directions with mixed contributions (yellow) for all NO_2 data **(a1)**, SO_2 data before (b1) and after the change in fuel sulfur content limits **(c1)**.
(a2), (b2) and (c2): Contributions to the integrated volume mixing ratios of NO_2 **(a2)** and SO_2 **(b2, c2)** from the source regions in percent.
(a3), (b3) and (c3): Contributions to the integrated volume mixing ratios when considering only the land and sea sector. It can clearly be seen that the lower fuel sulfur limit lead to a strong decrease in the SO_2 contribution from shipping since 2015.

the introduction of stricter sulfur limits for maritime fuels in the North Sea on 1 January 2015. The according statistics to this period are shown in the middle row in Fig. 17. The second time period, after the change in fuel sulfur limits, includes all measurements from 2015 and 2016, with the corresponding pie plots in the bottom row of Fig. 17.

Before the change, 32 % of the measurements were taken when the wind was coming from the sea sector and about 24 % when it was blowing from the dedicated land sector. After the change, the wind was coming a bit more often from sea (42 %) and less often from land (18 %), but in general the situation was quite similar.

The contributions of the three sectors (land, sea and mixed) to the total integrated SO_2 with 21 % coming from

ships, 30 % from land and 49 % from the mixed sector for the time before the change in sulfur limits are very similar to those of NO_2, too. After the change, the contribution from the sea sector shrinks significantly from 21 to 7 %, while the relative contribution from the land sector increased from 29 to 44 %, the contribution from the mixed sector staying the same as around 49 %. This increase for the land source sector is only a relative increase while the absolute contributions slightly decreased, as can be seen from Fig. 16. The relative contribution from the sea sector (shipping only source) decreased by a factor of 3 while the absolute contribution from this sector decreased by a factor of 8, even though the wind was coincidentally blowing more often from the open sea in this time period.

The overall mean SO_2 volume mixing ratio before 2015 is 0.39 ± 0.45 ppb (mean $\pm$ standard deviation). For 2015 and 2016, the total mean value declined by two-thirds to 0.15 ± 0.34 ppb (mean $\pm$ standard deviation).

These results show clearly that the stricter limitations on the fuel sulfur content are working and significantly improved air quality in the North Sea coastal regions with respect to SO_2. This is in good agreement with other studies such as Kattner et al. (2015), who found that around 95 % of the ships are sticking to the new limits. This implies that the cheaper high sulfur heavy oil fuel is no longer in use in the region of measurement.

If again the two selected sectors are considered as representative for both land and sea sources, the shares of the contributions from sea/land changed from 42 % : 58 % (which is very similar to those of NO_2) to 14 % : 86 %. This again shows that since 2015, the vast majority of SO_2 emissions can be attributed to land sources and ships play only a negligible role. Prior to 2015, shipping emissions have been a significant source for SO_2 in coastal regions.

One aspect which is neglected in the source allocation to wind sectors is that in situations with good visibility and low wind speeds even for wind coming from southern directions, the MAX-DOAS instrument can measure ship emissions peaks in the north of the island, but being typically very small. Compared to the often strongly enhanced background pollution in cases with southerly winds, the contribution from these peaks is negligible (around 1–3 %), but certainly leads to a small overestimation of land sources.

4.9 Determination of SO_2 to NO_2 ratios in ship plumes

A monitoring of emissions from single ships requires the analysis of individual plume peaks in the NO_2 and SO_2 data sets. It is difficult to derive the absolute amounts (e.g. in mass units) of the emitted gaseous pollutants by our MAX-DOAS remote sensing technique. The height and width of the measured peaks does not only depend on the amount of emitted pollutants), but also strongly on the geometry, while getting the highest values when measuring alongside the plumes, and much smaller values when the plume moves orthogonal to the line-of-sight of our instrument. In addition to that, also the time span between emission and measurement plays a role for the height of the NO_2 peaks because of NO to NO_2 titration.

To determine the mixing ratio inside the plumes, additional information on the length of the light path inside the plume would be needed, which cannot be retrieved from our measurements. This means that without further assumptions, we cannot determine emission factors for the emitted gases (e.g for emission inventories, which are used as input for model simulations).

Although emission factors cannot be measured by MAX-DOAS directly, the NO_2 and SO_2 signals yield the ratio of both. These ratios can then be compared to ratios of emission factors reported in other studies as well as measurements on other sites or with different instruments, bearing in mind possible deviations due to NO to NO_2 titration.

By comparing SO_2 to NO_2 ratios from different ships it is possible to roughly distinguish whether a ship is using fuel with high or low sulfur content (giving a high or low SO_2 to NO_2 ratio). Beecken and Mellqvist from Chalmers University (Sweden) use this relationship for airborne DOAS measurements of ship exhaust plumes on an operational basis in the CompMon project (Compliance monitoring pilot for MARPOL Annex VI) (Van Roy, 2016). Following the ships and measuring across the stack gas plume they can discriminate between low (0.1 %) and high (1 %) fuel sulfur content ships with a probability of 80–90 % (Van Roy, 2016).

From the spectra measured by our MAX-DOAS UV instrument both SO_2 and NO_2 columns can be retrieved at once. The two columns are measured at the exact same time along nearly the same light path. To calculate SO_2 to NO_2 ratios for the measured pollutant peaks simply the ratio of the measured differential slant column densities has to be computed.

In order to separate ship related signals from smooth background pollution, first a running median filter was applied to the time series of NO_2 and SO_2 measurements with a large kernel size (e.g. over 21 points). If too many broad peaks are contained in the time series this is not sufficient and the resulting median might be systematically higher than the actual baseline. In this case, on the values in the lower 50 % quantile again a running median with a smaller kernel size (e.g. 5) was applied, giving a good approximation of the real baseline.

In the next step, this baseline is subtracted from the raw signal. A simple peak detection algorithm was used to identify the peaks in the baseline-corrected NO_2 signal. Then the corresponding peaks in the SO_2 were assigned, thus accounting for cases when no SO_2 enhancement is measured. In a final manual checkup, all the identified peaks were looked through, filtering out for example all the cases when peaks are too close together to be separated and fine-tuning the baseline detection algorithm parameters if necessary.

To achieve a better signal-to-noise ratio, the integrals over both the NO_2 and SO_2 peak are calculated and the ratio of both values is computed in the last step.

Figure 18 shows the approach as well as the results for an example day in summer 2014, before the stricter fuel sulfur content limits were introduced. Both the NO_2 and SO_2 signal show high and sharp peaks, originating from ship plumes. Most of the peaks are of similar shape in NO_2 as well as SO_2 signal. The measured SO_2 to NO_2 ratios lie in the range from 0.17 to 0.41. The SO_2 to NO_2 ratio can vary strongly for different ships. For example, the plume of the ship passing the line-of-sight around 12:00 UTC has a high NO_2 content, but is low in SO_2, whereas the opposite is true for the ship passing at 12:30 UTC, indicating that the second ship was

using fuel with a considerably higher sulfur content than the first one.

Figure 19 shows one example day in summer 2015, after the establishment of stricter sulfur limits. For better comparison to Fig. 18, the y-axis limits are the same. High NO2 peaks also occur on this day. However, the SO_2 signal shows no clearly distinguishable peaks anymore, a result of much less sulfur in the fuel. Consequentially, the measured SO_2 to NO_2 ratios are much smaller on this day and range from 0 to 0.09. There might be some small peaks in the SO_2 signal, but for most of them it cannot be determined if these are real enhancements or just noise fluctuations. The two peaks at 10:40 and 14:00 UTC, slightly above noise level but still very small, might be real SO_2 signals from ships with a higher than average fuel sulfur content.

For a statistically meaningful comparison of both time periods two representative samples of ship emission peaks have been selected by hand for days with good measurement conditions, which were identified by using the solar radiation measurement data of our weather station. One sample of more than 1000 peaks, measured in 2013 and 2014 representing the state before introduction of stricter fuel sulfur content limits, and another equally-sized sample of more than 1000 peaks measured in 2015 and 2016, representing the situation afterwards, were analyzed in a semi-automatic way. It has to be noted that it cannot be ruled out that a certain fraction of ships were measured repeatedly on different days. It is also highly probable that the plume from some individual ships was measured multiple times at different locations in the different azimuth directions while the ship was passing the island.

The distributions of the SO_2 to NO_2 ratios derived from the peak integrals for the two samples are shown in a histogram in Fig. 20. It can be seen that SO_2 to NO_2 ratios were considerably higher before 2015, with a mean of 0.30, a standard deviation of 0.13 and a median value of 0.28. After the change in fuel sulfur content limits, the SO_2 to NO_2 ratios became much lower with a mean of 0.007, a standard deviation of 0.089 and a median value of 0.013, a drastic reduction. A Welch's t-test (unequal variances t-test) shows that the reduction is statistically highly significant. These results can be compared to the overall average SO_2 to NO_2 ratios on all days with good measurement conditions from which the peaks have been selected: For the time before 2015, this gives a mean value of 0.10 and a median of 0.17 and for 2015 and 2016, one gets a mean value of 0.024 and a median of 0.058. As expected, these values are significantly lower than the SO_2 to NO_2 ratios obtained from the ship plumes which do not include background pollution.

It is also interesting to compare our results with those from other studies, bearing in mind possible systematic differences due to different measurement geometries, techniques and sites and therefore different NO to NO_2 titration in the plumes.

McLaren et al. (2012) measured NO_2 to SO_2 emission ratios in marine vessel plumes in the Strait of Georgia in summer 2005. In a sample of 17 analyzed plumes, a median molar NO_2/SO_2 ratio of 2.86 was found. Translated into a SO_2/NO_2 ratio this yields a value of 0.35 which is, considering the small sample size, in good agreement with our findings for the time before 2015.

Another study was carried out by Diesch et al. (2013) measuring gaseous and particulate emissions from various marine vessel types and a total of 139 ships on the banks of the river Elbe in 2011. SO_2 to NO_2 emission ratios can also be derived from from their reported SO_2 and NO_2 emission factors: For small ships ($< 5\,000$ tons) a ratio 0.13 and an average fuel sulfur content (FSC) of $0.22 \pm 0.21\,\%$ was found, for medium size ships ($5\,000$–$30\,000$ tons) a ratio of 0.24 and a FSC of $0.46 \pm 0.40\,\%$ and for large ships ($> 30\,000$ tons) a ratio of 0.28 and a FSC of $0.55 \pm 0.20\,\%$. Especially the values for medium size and large ships fit quite well to our results while plumes from very small vessels (if measurable at all) have often not been taken into account for the statistic because of the low signal-to-noise ratio.

When assuming that the dependency of SO_2 to NO_2 ratio to fuel sulfur content is also applicable to our dataset, we can roughly estimate that the ships measured by us before 2015 used an average sulfur content of 0.5–0.7 %, in good agreement with the results of Kattner et al. (2015), which since 2015 decreased drastically with 0.1 % as an upper limit.

5 Conclusions

In this study, three years of MAX-DOAS observations of NO_2 and SO_2 taken on the island of Neuwerk close to the shipping lane towards the harbor of Hamburg, Germany were analyzed for pollution emitted from ships. Using measurements taken at $0.5°$ elevation and different azimuthal directions, both background pollution and plumes from individual ships could be identified. Using simultaneously retrieved O_4 columns, path averaged volume mixing ratios for NO_2 and SO_2 could be determined. Comparison of NO_2 measurements in the UV and visible parts of the spectrum showed excellent agreement between mixing ratios determined from the two retrievals, demonstrating consistency in the results.

MAX-DOAS measurements were also compared to co-located in-situ observations. High correlation was found between mixing ratios derived with the two methods on average, in-situ measurements showing systematically larger values, in particular during ship emission peaks. These deviations can be understood by the difference in measurement volume, the MAX-DOAS measurements averaging over light paths of several kilometers and a systematic underestimation of MAX-DOAS VMRs due to different profile shapes of O_4 and the pollutants NO_2 and SO_2. For NO_2, the difference is larger than for SO_2, probably because of conversion of NO to NO_2 during the transport from the ship where the signal is
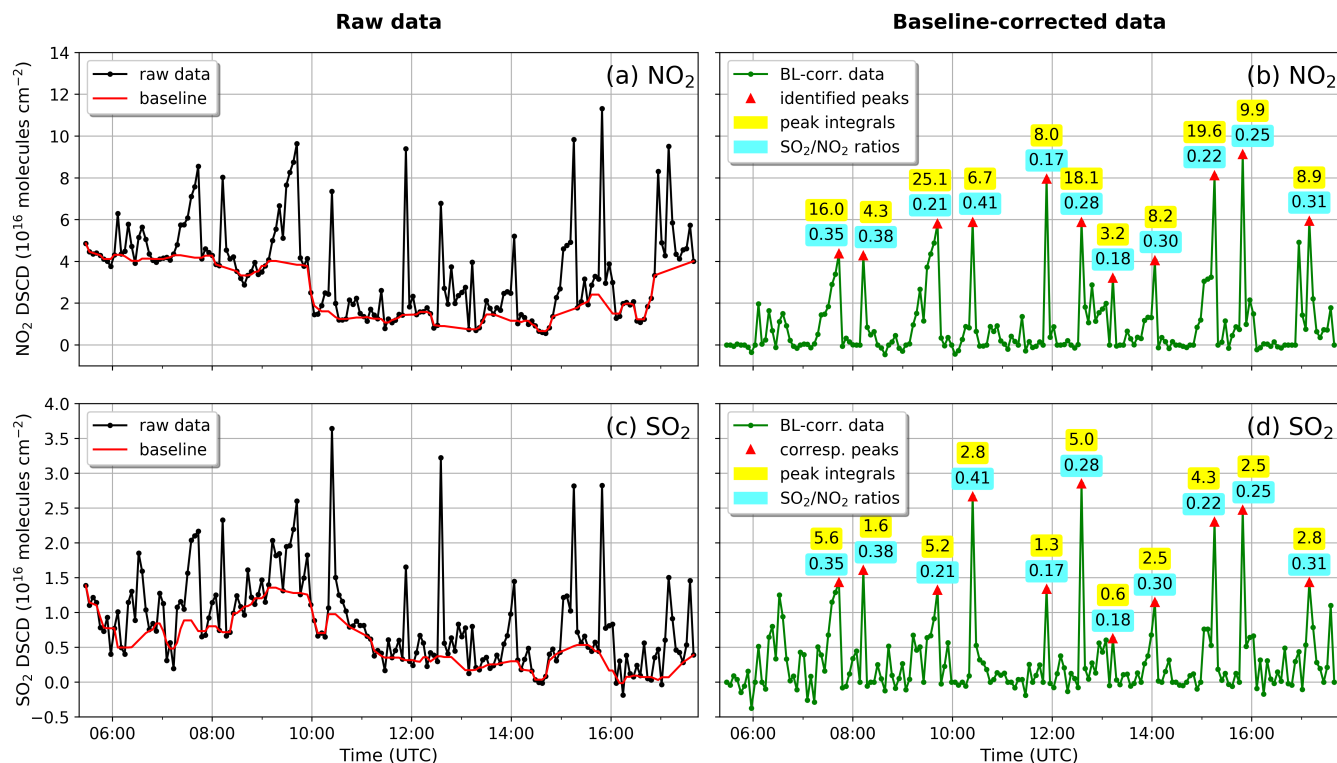
Figure 18. Calculation of SO_2 to NO_2 ratios for ship emission peaks for one example day (23 July 2014) before the change in sulfur emission limits. Panel **(a)** shows the UV NO_2-DSCD raw data for $0.5°$ elevation and $-25°$ azimuth and the determined baseline. Panel b shows the baseline-corrected NO_2 data for which the automatically identified peaks are highlighted with red triangles. Numbers close to the peaks denote the peak integrals in 10^{16} molecules/cm^2 (marked in yellow) and the SO_2 to NO_2 ratios (marked in blue). Panels **(c)** and **(d)** show the corresponding plots for SO_2.

detected by MAX-DOAS to the measurement site where the in-situ instrument was located.

Although the measurement site is within a few kilometers from one of the main shipping lanes, it is influenced by land based pollution depending on wind direction. Comparing measurements taken under wind direction from the shipping lane and from land, systematic differences in the diurnal and weekly cycles of NO_2 are found. While NO_2 from land shows high values in the morning and evening and lower values around noon and on weekends, NO_2 levels from sea are more or less constant over time as expected from continuous shipping operations. These results are found in both MAX-DOAS and in-situ observations. Both NO_2 and SO_2 levels are often higher when wind is coming from land, indicating that land based sources contribute significantly to pollution levels on the island in spite of its vicinity to the shipping lanes. Analyzing the wind dependence of the signals in more detail, and excluding data with mixed air mass origin, the contribution of shipping sources to pollution on Neuwerk could be estimated to be 40 % for NO_2 and 41 % for SO_2 in the years 2013 and 2014. As nearly half of the measurements were taken under wind coming from mixed directions, this is only a rough estimate but is still a surprisingly small fraction.

Although the MAX-DOAS measurements cannot be used to directly determine NO_x or SO_2 emissions from individual ships due to the measurement geometry, the ratio of SO_2 to NO_2 column averaged mixing ratios gives a good estimate of the SO_2 to NO_x emission ratio. Using the data from Neuwerk, more than 2000 individual ship emission plumes were identified and the ratio of SO_2 to NO_2 computed after subtraction of the background values. The results varied between ships but on average yielded values of about 0.3 for the years 2013/2014, in good agreement with results from other studies.

Since January 2015, much lower fuel sulfur content limits of 0.1 % apply in the North and Baltic Sea. This resulted in large changes in SO_2 levels in the MAX-DOAS measurements when the wind is coming from the shipping lanes. In fact, ship related SO_2 peaks are rarely observed anymore since 2015. Applying the same analysis as for the period before the change in legislation, no significant changes were found for NO_2 in terms of ratio between ship and land contribution or absolute levels. For SO_2 in contrast overall levels were reduced by two-thirds, and the relative contribution of shipping sources was reduced from 41 % to 14 %. It is interesting to note that a reduction in SO_2 levels was also
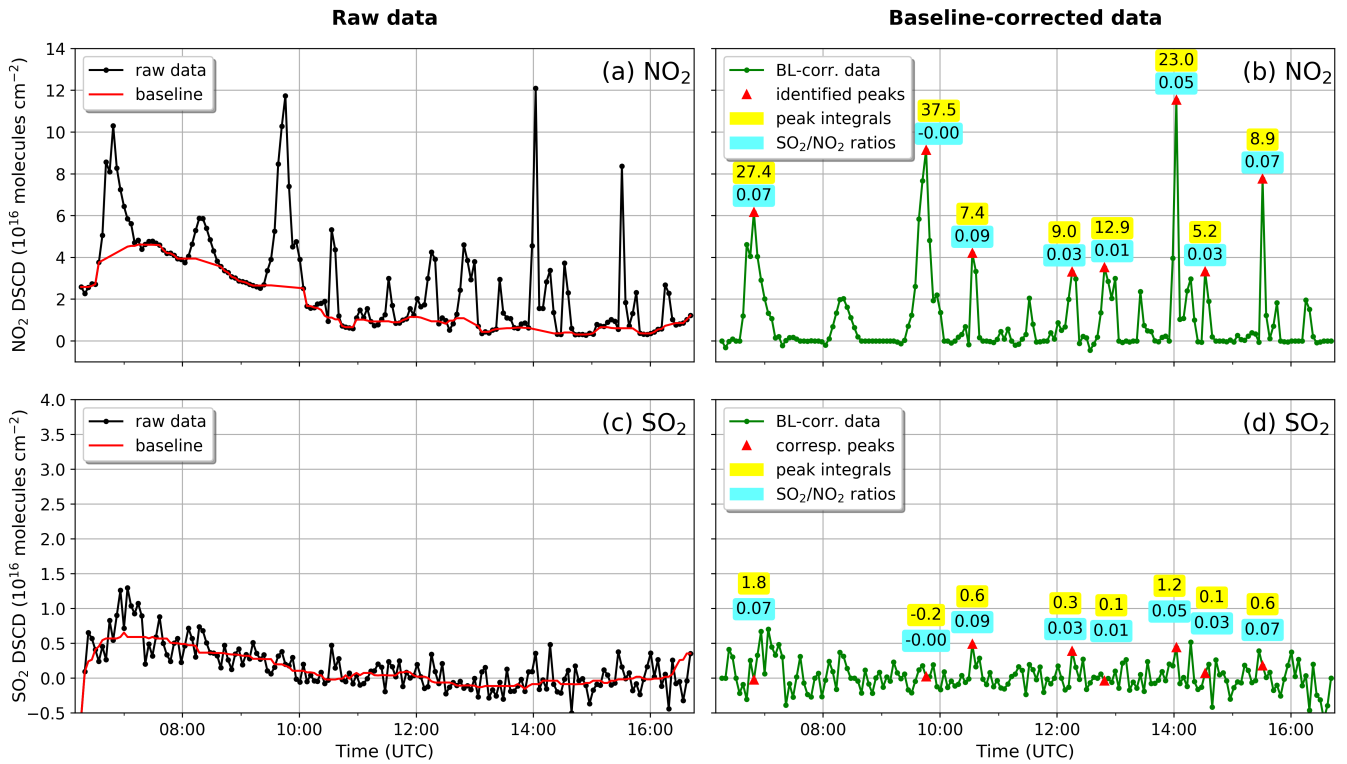
Figure 19. As Figure 18 but for an example day (3 July 2015) after the introduction of stricter fuel sulfur content limits. Measurements in $0.5°$ elevation and $65°$ azimuth are shown. Peak integrals are given in 10^{16} molecules/cm^2.
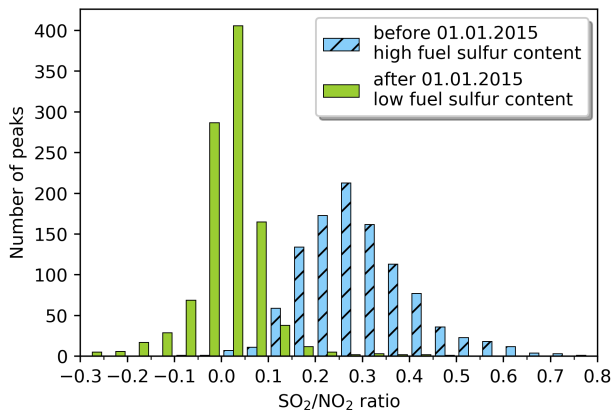

Figure 20. Histogram showing the distribution SO_2 to NO_2 ratios in two samples ($N = 1055$ for each) of ship emission peaks measured in $0.5°$ elevation and all azimuth angles for the time before (blue) and after (green) the change in fuel sulfur content regulation on the 1st of January 2015.

In summary, long-term measurements of NO_2 and SO_2 using a MAX-DOAS instrument demonstrated the feasibility of monitoring pollution originating from ships remotely. Pollution signals from individual ships can be identified and path averaged mixing ratios can be determined, which on average correlate well with in-situ observations, reproducing day-to-day trends. MAX-DOAS measurements do not provide emission estimates for individual ships but allow statistical analysis of signals from thousands of ships at a distance and even under unfavorable wind conditions. Implementation of stricter sulfur limits in shipping fuel lead to a large reduction in SO_2/NO_x ratios in shipping emissions and a significant reduction in SO_2 levels at the German coast. The amounts of NO_2 are as expected not significantly impacted by the change of sulfur content in the fuel. This implies that combustion temperatures were probably not significantly changed. The overall contribution of ship emissions to pollution levels at the measurement site is large but land based sources still dominate, even in the immediate vicinity of shipping lanes.

observed in most wind directions coming from land, presumably because shipping emissions also contributed to SO_2 levels in coastal areas.

References

Alföldy, B., Lööv, J. B., Lagler, F., Mellqvist, J., Berg, N., Beecken, J., Weststrate, H., Duyzer, J., Bencs, L., Horemans, B., Cavalli, F., Putaud, J. P., Janssens-Maenhout, G., Csordás, A. P., Van Grieken, R., Borowiak, A., and Hjorth, J.: Measurements of air pollution emission factors for marine transportation in SECA, Atmospheric Measurement Techniques, 6, 1777–1791, doi:10.5194/amt-6-1777-2013, 2013.

Aulinger, A., Matthias, V., Zeretzke, M., Bieser, J., Quante, M., and Backes, A.: The impact of shipping emissions on air pollution in the greater North Sea region – Part 1: Current emissions and concentrations, Atmospheric Chemistry and Physics, 16, 739–758, doi:10.5194/acp-16-739-2016, http://www.atmos-chem-phys.net/16/739/2016/, 2016.

Balzani Lööv, J. M., Alfoldy, B., Gast, L. F. L., Hjorth, J., Lagler, F., Mellqvist, J., Beecken, J., Berg, N., Duyzer, J., Westrate, H., Swart, D. P. J., Berkhout, A. J. C., Jalkanen, J. P., Prata, A. J., Van Der Hoff, G. R., and Borowiak, A.: Field test of available methods to measure remotely SOx and NOx emissions from ships, Atmospheric Measurement Techniques, 7, 2597–2613, doi:10.5194/amt-7-2597-2014, 2014.

Beecken, J., Mellqvist, J., Salo, K., Ekholm, J., and Jalkanen, J. P.: Airborne emission measurements of SO2, NOx and particles from individual ships using a sniffer technique, Atmospheric Measurement Techniques, 7, 1957–1968, doi:10.5194/amt-7-1957-2014, 2014.

Beecken, J., Mellqvist, J., Salo, K., Ekholm, J., Jalkanen, J. P., Johansson, L., Litvinenko, V., Volodin, K., and Frank-Kamenetsky, D. A.: Emission factors of SO2, NOx and particles from ships in Neva Bay from ground-based and helicopter-borne measurements and AIS-based modeling, Atmospheric Chemistry and Physics, 15, 5229–5241, doi:10.5194/acp-15-5229-2015, 2015.

Beirle, S., Platt, U., Wenig, M., and Wagner, T.: Weekly cycle of NO2 by GOME measurements: a signature of anthropogenic sources, Atmospheric Chemistry and Physics, 3, 2225–2232, doi:10.5194/acpd-3-3451-2003, 2003.

Beirle, S., Platt, U., von Glasow, R., Wenig, M., and Wagner, T.: Estimate of nitrogen oxide emissions from shipping by satellite remote sensing, Geophysical Research Letters, 31, 4–7, doi:10.1029/2004GL020312, 2004.

Bell, T. L., Rosenfeld, D., and Kim, K. M.: Weekly cycle of lightning: Evidence of storm invigoration by pollution, Geophysical Research Letters, 36, 1–5, doi:10.1029/2009GL040915, 2009.

Berg, N., Mellqvist, J., Jalkanen, J. P., and Balzani, J.: Ship emissions of SO 2 and NO 2: DOAS measurements from airborne platforms, Atmospheric Measurement Techniques, 5, 1085–1098, doi:10.5194/amt-5-1085-2012, 2012.

Bobrowski, N. and Platt, U.: SO2/BrO ratios studied in five volcanic plumes, Journal of Volcanology and Geothermal Research, 166, 147–160, doi:10.1016/j.jvolgeores.2007.07.003, 2007.

Bogumil, K., Orphal, J., Homann, T., Voigt, S., Spietz, P., Fleischmann, O. C., Vogel, A., Hartmann, M., Kromminga, H., Bovensmann, H., Frerick, J., and Burrows, J. P.: Measurements of molecular absorption spectra with the SCIAMACHY preflight model: instrument characterization and reference data for atmospheric remote-sensing in the 230-2380 nm region, Journal of Photochemistry and Photobiology A: Chemistry, 157, 167–184, doi:10.1016/S1010-6030(03)00062-5, http://linkinghub.elsevier.com/retrieve/pii/S1010603003000625, 2003.

Bollmann, M., Bosch, T., Colijn, F., Ebinghaus, R., Körtzinger, A., Latif, M., Matthiessen, B., Melzner, F., Oschlies, A., Petersen, S., Proelß, A., Quaas, M., Requate, T., Reusch, T., Rosenstiel, P., Schrottke, K., Sichelschmidt, H., Siebert, U., Soltwedel, R., Sommer, U., Stattegger, K., Sterr, H., Sturm, R., Treude, T., Vafeidis, A., van Bernem, C., van Beusekom, J., Visbeck, M., Wahl, M., Wallmann, K., and Weinberger, F.: Living With the Oceans, World Ocean Review: Living with the oceans, 1, 236, 2010.

Brasseur, G. P.: Atmospheric chemistry and global change: [a textbook prepared by scientists at the National Center for Atmospheric Research, Boulder], Topics in environmental chemistry, Oxford Univ. Press, New York, NY [u.a.], 1999.

Chen, G., Huey, L. G., Trainer, M., Nicks, D., Corbett, J., Ryerson, T., Parrish, D., Neuman, J. A., Nowak, J., Tanner, D., Holloway, J., Brock, C., Crawford, J., Olson, J. R., Sullivan, A., Weber, R., Schauffler, S., Donnelly, S., Atlas, E., Roberts, J., Flocke, F., Hübler, G., and Fehsenfeld, F.: An investigation of the chemistry of ship emission plumes during ITCT 2002, Journal of Geophysical Research D: Atmospheres, 110, 1–15, doi:10.1029/2004JD005236, 2005.

Corbett, J. J. and Koehler, H. W.: Updated emissions from ocean shipping, Journal of Geophysical Research, 108, 4650, doi:10.1029/2003JD003751, http://doi.wiley.com/10.1029/2003JD003751, 2003.

Corbett, J. J., Fischbeck, P. S., and Pandis, S. N.: Global nitrogen and sulfur inventories for oceangoing ships, Journal of Geophysical Research, 104, 3457–3470, doi:10.1029/1998JD100040, 1999.

Corbett, J. J., Winebrake, J. J., Green, E. H., Kasibhatla, P., Eyring, V., and Lauer, A.: Mortality from ship emissions: A global assessment, Environmental Science and Technology, 41, 8512–8518, doi:10.1021/es071686z, 2007.

Diesch, J. M., Drewnick, F., Klimach, T., and Borrmann, S.: Investigation of gaseous and particulate emissions from various marine vessel types measured on the banks of the Elbe in Northern Germany, Atmospheric Chemistry and Physics, 13, 3603–3618, doi:10.5194/acp-13-3603-2013, 2013.

DNV: Marpol 73/78 Annex VI - Regulations of Air Polution from Ships - Technical and Operational implications, Fuel, pp. 1–32, 2008.

Endresen, Ø., Sørgard, E., Sundet, J., Dalsøren, S., Isaksen, I., and Berglen, T.: Emission from international sea transportation and

environmental impact, Journal of Geophysical Research, 108, 1–22, doi:10.1029/2002JD002898, 2003.

EU: Directive 2005/33/EC of the European Parliament and of the Council, Official Journal of the European Union, pp. 59–69, doi:10.3000/17252555.L_2009.140.eng, http://eur-lex.europa.eu/LexUriServ/LexUriServ.do?uri=OJ:L:2005:191:0059:0069:EN:PDF, 2005.

EU: Directive 2008/50/EC of the European Parliament and of the Council of 21 May 2008 on ambient air quality and cleaner air for Europe, Official Journal of the European Communities, 152, 1–43, http://eur-lex.europa.eu/LexUriServ/LexUriServ.do?uri=OJ:L:2008:152:0001:0044:EN:PDF, 2008.

EU: Air Quality Standards, http://ec.europa.eu/environment/air/quality/standards.htm, 2016.

Eyring, V., Köhler, H. W., Lauer, A., and Lemper, B.: Emissions from international shipping: 2. Impact of future technologies on scenarios until 2050, Journal of Geophysical Research, 110, D17 306, doi:10.1029/2004JD005620, http://doi.wiley.com/10.1029/2004JD005620, 2005a.

Eyring, V., Köhler, H. W., van Aardenne, J., and Lauer, A.: Emissions from international shipping: 1. The last 50 years, Journal of Geophysical Research, 110, D17 305, doi:10.1029/2004JD005619, http://doi.wiley.com/10.1029/2004JD005619, 2005b.

Eyring, V., Bovensmann, H., Cionni, I., Dall'Amico, M., Franke, K., Khlystova, I., Klinger, C., Lauer, A., Paxian, A., Righi, M., and Schreier, M.: Impact of Ship Emissions on Atmosphere and Climate, SeaKLIM Final Report, Tech. rep., DLR, http://www.pa.op.dlr.de/SeaKLIM/SeaKLIM_Nachwuchsgruppe_Schlussbericht_FINAL.pdf, 2010a.

Eyring, V., Isaksen, I. S., Berntsen, T., Collins, W. J., Corbett, J. J., Endresen, O., Grainger, R. G., Moldanova, J., Schlager, H., and Stevenson, D. S.: Transport impacts on atmosphere and climate: Shipping, Atmospheric Environment, 44, 4735–4771, doi:10.1016/j.atmosenv.2009.04.059, http://linkinghub.elsevier.com/retrieve/pii/S1352231009003379, 2010b.

Galle, B., Johansson, M., Rivera, C., Zhang, Y., Kihlman, M., Kern, C., Lehmann, T., Platt, U., Arellano, S., and Hidalgo, S.: Network for Observation of Volcanic and Atmospheric Change (NOVAC) - A global network for volcanic gas monitoring: Network layout and instrument description, Journal of Geophysical Research Atmospheres, 115, 1–19, doi:10.1029/2009JD011823, 2010.

Galloway, J. N., Aber, J. D., Erisman, J. W., Seitzinger, S. P., Howarth, R. W., Cowling, E. B., and Cosby, B. J.: The Nitrogen Cascade, American Institute of Biological Sciences, 53, 341, doi:10.1641/0006-3568(2003)053[0341:TNC]2.0.CO;2, http://www.jstor.org/stable/1314367, 2003.

Gomez, L., Navarro-Comas, M., Puentedura, O., Gonzalez, Y., Cuevas, E., and Gil-Ojeda, M.: Long-path averaged mixing ratios of O3 and NO2 in the free troposphere from mountain MAX-DOAS, Atmospheric Measurement Techniques, 7, 3373–3386, doi:10.5194/amt-7-3373-2014, 2014.

Grainger, J. F. and Ring, J.: Anomalous Fraunhofer Line Profiles, Nature, 193, 762, 1962.

Greenblatt, G. D., Orlando, J. J., Burkholder, J. B., and Ravishankara, A. R.: Absorption measurements of oxygen between 330 and 1140 nm, Journal of Geophysical Research, 95, 18 577, doi:10.1029/JD095iD11p18577, http://doi.wiley.com/10.1029/JD095iD11p18577, 1990.

Hönninger, G., von Friedeburg, C., and Platt, U.: Multi axis differential optical absorption spectroscopy (MAX-DOAS), Atmos. Chem. Phys., 4, 231–254, 2004.

Ialongo, I., Hakkarainen, J., Hyttinen, N., Jalkanen, J. P., Johansson, L., Boersma, K. F., Krotkov, N., and Tamminen, J.: Characterization of OMI tropospheric NO2 over the Baltic Sea region, Atmospheric Chemistry and Physics, 14, 7795–7805, doi:10.5194/acp-14-7795-2014, 2014.

Ialongo, I., Herman, J., Krotkov, N., Lamsal, L., Boersma, F., Hovila, J., and Tamminen, J.: Comparison of OMI NO2 observations and their seasonal and weekly cycles with ground-based measurements in Helsinki, Atmospheric Measurement Techniques Discussions, pp. 1–13, doi:10.5194/amt-2016-212, http://www.atmos-meas-tech-discuss.net/amt-2016-212/, 2016.

IEA/OECD: Transport, Energy and CO2 – moving towards sustainability., International Energy Agency, Paris, 2009.

International Air Transport Association (IATA): IATA Annual Review 2015, p. 62, http://www.iata.org/about/Documents/iata-annual-review-2015.pdf, 2015.

Irie, H., Takashima, H., Kanaya, Y., Boersma, K. F., Gast, L., Wittrock, F., Brunner, D., Zhou, Y., and Van Roozendael, M.: Eight-component retrievals from ground-based MAX-DOAS observations, Atmospheric Measurement Techniques, 4, 1027–1044, doi:10.5194/amt-4-1027-2011, 2011.

Jonson, J. E., Tarrason, L., and Bartnicki, J.: Effects of international shipping on European pollution levels. 2000, Tech. rep., The Norwegian Metrorological Institute, Oslo, Norway, 2000.

Kattner, L., Mathieu-Üffing, B., Burrows, J. P., Richter, A., Schmolke, S., Seyler, A., and Wittrock, F.: Monitoring compliance with sulfur content regulations of shipping fuel by in situ measurements of ship emissions, Atmospheric Chemistry and Physics, 15, 10 087–10 092, doi:10.5194/acp-15-10087-2015, http://www.atmos-chem-phys.net/15/10087/2015/, 2015.

Kaynak, B., Hu, Y., Martin, R. V., Sioris, C. E., and Russell, a. G.: Comparison of weekly cycle of NO2 satellite retrievals and NOx emission inventories for the continental United States, Journal of Geophysical Research: Atmospheres, 114, 1–10, doi:10.1029/2008JD010714, 2009.

Kern, C., Deutschmann, T., Vogel, L., Wöhrbach, M., Wagner, T., and Platt, U.: Radiative transfer corrections for accurate spectroscopic measurements of volcanic gas emissions, Bulletin of Volcanology, 72, 233–247, doi:10.1007/s00445-009-0313-7, 2010.

Lack, D. A., Cappa, C. D., Langridge, J., Bahreini, R., Buffaloe, G., Brock, C., Cerully, K., Coffman, D., Hayden, K., Holloway, J., Lerner, B., Massoli, P., Li, S. M., McLaren, R., Middlebrook, A. M., Moore, R., Nenes, A., Nuaaman, I., Onasch, T. B., Peischl, J., Perring, A., Quinn, P. K., Ryerson, T., Schwartz, J. P., Spackman, R., Wofsy, S. C., Worsnop, D., Xiang, B., and Williams, E.: Impact of fuel quality regulation and speed reductions on shipping emissions: Implications for climate and air quality, Environmental Science and Technology, 45, 9052–9060, doi:10.1021/es2013424, 2011.

Lampel, J., Pohler, D., Tschritter, J., Frieß, U., and Platt, U.: On the relative absorption strengths of water vapour in the blue wavelength range, Atmospheric Measurement Techniques, 8, 4329–4346, doi:10.5194/amt-8-4329-2015, 2015.

Lauer, a., Eyring, V., Hendricks, J., Jöckel, P., and Lohmann, U.: Global model simulations of the impact of ocean-going ships on aerosols, clouds, and the radiation budget, Atmospheric Chem-

istry and Physics Discussions, 7, 9419–9464, doi:10.5194/acpd-7-9419-2007, 2007.

Lawrence, M. G. and Crutzen, P. J.: Influence of NOx emissions from ships on tropospheric photochemistry and climate, Nature, 402, 167–170, doi:10.1038/46013, 1999.

Lee, C., Richter, A., Lee, H., Kim, Y. J., Burrows, J. P., Lee, Y. G., and Choi, B. C.: Impact of transport of sulfur dioxide from the Asian continent on the air quality over Korea during May 2005, Atmospheric Environment, 42, 1461–1475, doi:10.1016/j.atmosenv.2007.11.006, 2008.

Masieri, S., Premuda, M., Bortoli, D., Kostadinov, I., Petritoli, A., Ravegnani, F., and Giovanelli, G.: Cruise ships flow rate emission evaluated by means of a passive DOAS instrument, SPIE Europe Remote Sensing, 7478, 74 781S—-74 781S—-10, doi:10.1117/12.830309, http://dx.doi.org/10.1117/12.830309, 2009.

Matthias, V., Aulinger, A., Backes, A., Bieser, J., Geyer, B., Quante, M., and Zeretzke, M.: The impact of shipping emissions on air pollution in the greater North Sea region-Part 2: Scenarios for 2030, Atmospheric Chemistry and Physics, 16, 759–776, doi:10.5194/acp-16-759-2016, 2016.

McLaren, R., Wojtal, P., Halla, J. D., Mihele, C., and Brook, J. R.: A survey of NO2:SO2 emission ratios measured in marine vessel plumes in the Strait of Georgia, Atmospheric Environment, 46, 655–658, doi:10.1016/j.atmosenv.2011.10.044, http://linkinghub.elsevier.com/retrieve/pii/S135223101101123X, 2012.

Meller, R. and Moortgat, G. K.: Temperature dependence of the absorption cross sections of formaldehyde between 223 and 323 K in the wavelength range 225-375 nm, Journal of Geophysical Research: Atmospheres, 105, 7089–7101, doi:10.1029/1999JD901074, http://dx.doi.org/10.1029/1999JD901074, 2000.

Pandya, R. J., Solomon, G., Kinner, A., and Balmes, J. R.: Diesel exhaust and asthma: Hypotheses and molecular mechanisms of action, Environmental Health Perspectives, 110, 103–112, doi:10.1289/ehp.02110s1103, 2002.

Peters, E.: Improved MAX-DOAS measurements and retrievals focused on the marine boundary layer, Ph.D. thesis, University of Bremen, 2013.

Platt, U. and Perner, D.: Direct measurements of atmospheric CH2O, HNO2, O3, NO2, and SO2 by differential optical absorption in the near UV, Journal of Geophysical Research: Oceans, 85, 7453–7458, doi:10.1029/JC085iC12p07453, http://dx.doi.org/10.1029/JC085iC12p07453, 1980.

Platt, U. and Stutz, J.: Differential optical absorption spectroscopy, Physics of Earth and Space Environments, Springer, Berlin ; Heidelberg, 2008.

Prata, A. J.: Measuring SO2 ship emissions with an ultraviolet imaging camera, Atmospheric Measurement Techniques, 7, 1213–1229, doi:10.5194/amt-7-1213-2014, 2014.

Premuda, M., Masieri, S., Bortoli, D., Kostadinov, I., Petritoli, A., and Giovanelli, G.: Evaluation of vessel emissions in a lagoon area with ground based Multi axis DOAS measurements, Atmospheric Environment, 45, 5212–5219, doi:10.1016/j.atmosenv.2011.05.067, http://dx.doi.org/10.1016/j.atmosenv.2011.05.067, 2011.

Richter, A.: Absorptionsspektroskopische Messungen stratosphärischer Spurengase über Bremen, 53° N, Phd thesis, Universität Bremen, Göttingen, 1997.

Richter, A., Eyring, V., Burrows, J. P., Bovensmann, H., Lauer, A., Sierk, B., and Crutzen, P. J.: Satellite measurements of NO2 from international shipping emissions, Geophys. Res. Lett., 31, L23 110, doi:10.1029/2004GL020822, 2004.

Richter, A., Begoin, M., Hilboll, A., and Burrows, J. P.: An improved NO2 retrieval for the GOME-2 satellite instrument, Atmospheric Measurement Techniques, 4, 1147–1159, doi:10.5194/amt-4-1147-2011, 2011.

Roscoe, H. K., Van Roozendael, M., Fayt, C., Du Piesanie, A., Abuhassan, N., Adams, C., Akrami, M., Cede, A., Chong, J., Clémer, K., Friess, U., Gil Ojeda, M., Goutail, F., Graves, R., Griesfeller, A., Grossmann, K., Hemerijckx, G., Hendrick, F., Herman, J., Hermans, C., Irie, H., Johnston, P. V., Kanaya, Y., Kreher, K., Leigh, R., Merlaud, A., Mount, G. H., Navarro, M., Oetjen, H., Pazmino, A., Perez-Camacho, M., Peters, E., Pinardi, G., Puentedura, O., Richter, A., Schönhardt, A., Shaiganfar, R., Spinei, E., Strong, K., Takashima, H., Vlemmix, T., Vrekoussis, M., Wagner, T., Wittrock, F., Yela, M., Yilmaz, S., Boersma, F., Hains, J., Kroon, M., Piters, A., and Kim, Y. J.: Intercomparison of slant column measurements of NO2 and O4 by MAX-DOAS and zenith-sky UV and visible spectrometers, Atmospheric Measurement Techniques, 3, 1629–1646, doi:10.5194/amt-3-1629-2010, 2010.

Rozanov, V. V., Rozanov, A. V., Kokhanovsky, A. A., and Burrows, J. P.: Radiative transfer through terrestrial atmosphere and ocean: Software package SCIATRAN, Journal of Quantitative Spectroscopy and Radiative Transfer, 133, 13–71, doi:10.1016/j.jqsrt.2013.07.004, http://dx.doi.org/10.1016/j.jqsrt.2013.07.004, 2014.

Schreier, S. F., Richter, A., Wittrock, F., and Burrows, J. P.: Estimates of free-tropospheric NO2 and HCHO mixing ratios derived from high-altitude mountain MAX-DOAS observations in the mid-latitudes and tropics, Atmospheric Chemistry and Physics, 16, 2803–2817, doi:10.5194/acp-16-2803-2016, 2016.

Seinfeld, J. H. and Pandis, S. N.: Atmospheric chemistry and physics: from air pollution to climate change, Wiley, Hoboken, NJ, 2. ed. edn., 2006.

Serdyuchenko, A., Gorshelev, V., Weber, M., Chehade, W., and Burrows, J. P.: High spectral resolution ozone absorption cross-sections – Part 2: Temperature dependence, Atmospheric Measurement Techniques, 7, 625–636, doi:10.5194/amt-7-625-2014, 2014.

Singh, H. B.: Reactive nitrogen in the troposphere, Environmental Science & Technology, 21, 320–327, doi:10.1021/es00158a001, 1987.

Sinreich, R., Merten, A., Molina, L., and Volkamer, R.: Parameterizing radiative transfer to convert MAX-DOAS dSCDs into near-surface box-averaged mixing ratios, Atmospheric Measurement Techniques, 6, 1521–1532, doi:10.5194/amt-6-1521-2013, 2013.

Statistische Ämter des Bundes und der Länder (Statistikamt Nord): Anzahl der Ankünfte von Kreuzfahrtschiffen im Hamburger Hafen in den Jahren 2005 bis 2014., http://de.statista.com/statistik/daten/studie/29729/umfrage/ankuenfte-von-kreuzfahrtschiffen-in-hamburg/, 2015.

Thalman, R. and Volkamer, R.: Temperature dependent absorption cross-sections of O2-O2 collision pairs between 340 and 630

nm and at atmospherically relevant pressure., Physical chemistry chemical physics, 15, 15 371–15 381, doi:10.1039/c3cp50968k, http://www.ncbi.nlm.nih.gov/pubmed/23928555, 2013.

Umweltbundesamt: Aktuelle Luftdaten, https://www. umweltbundesamt.de/daten/luftbelastung/aktuelle-luftdaten, 2017.

UNCTAD: Review of Maritime Transport 2014, http://unctad.org/ en/PublicationsLibrary/rmt2014_en.pdf, 2014.

UNCTAD: Review of Maritime Transport 2015, October, http:// unctad.org/en/PublicationsLibrary/rmt2015_en.pdf, 2015.

Van Roy, W.: Best Practices Airborne MARPOL Annex VI Monitoring, https://www.trafi.fi/filebank/a/1482762219/ d80cdd7de80e58885ce5a4dd0af86c02/23541-Best_Practices_ Airborne_MARPOL_Annex_VI_Monitoring.pdf, 2016.

Vandaele, A. C., Hermans, C., Simon, P. C., Roozendael, M. V., Guilmot, J. M., Carleer, M., and Colin, R.: Fourier Transform Measurement of NO2 Absorption Cross-Section in the Visible Range at Room Temperature, J. Atmos. Chem., 25, 289–305, 1996.

Vinken, G. C. M., Boersma, K. F., van Donkelaar, A., and Zhang, L.: Constraints on ship NOx emissions in Europe using GEOS-Chem and OMI satellite NO2 observations, Atmospheric Chemistry and Physics, 14, 1353–1369, doi:10.5194/acp-14-1353-2014, http://www.atmos-chem-phys.net/14/1353/2014/ acp-14-1353-2014.html, 2014.

Wagner, T., Dix, B., Friedeburg, C. V., Frieß, U., Sanghavi, S., Sinreich, R., and Platt, U.: MAX-DOAS O4 measurements: A new technique to derive information on atmospheric aerosols - Principles and information content, Journal of Geophysical Research D: Atmospheres, 109, 1–19, doi:10.1029/2004JD004904, 2004.

Wang, T., Hendrick, F., Wang, P., Tang, G., Clémer, K., Yu, H., Fayt, C., Hermans, C., Gielen, C., Müller, J. F., Pinardi, G., Theys, N., Brenot, H., and Van Roozendael, M.: Evaluation of tropospheric SO2 retrieved from MAX-DOAS measurements in Xianghe, China, Atmospheric Chemistry and Physics, 14, 11 149–11 164, doi:10.5194/acp-14-11149-2014, 2014a.

Wang, Y., Li, A., Xie, P. H., Wagner, T., Chen, H., Liu, W. Q., and Liu, J. G.: A rapid method to derive horizontal distributions of trace gases and aerosols near the surface using multi-axis differential optical absorption spectroscopy, Atmospheric Measurement Techniques, 7, 1663–1680, doi:10.5194/amt-7-1663-2014, 2014b.

Wayne, R. P.: Chemistry of atmospheres: an introduction to the chemistry of the atmospheres of earth, the planets, and their satellites, Oxford Univ. Press, Oxford [u.a.], 3. ed., re edn., 2006.

WHO: Air Quality Guidelines: Global Update 2005 : Particulate Matter, Ozone, Nitrogen Dioxide, and Sulfur Dioxide, A EURO Publication, World Health Organization, 2006.

Wittrock, F., Oetjen, H., Richter, A., Fietkau, S., Medeke, T., Rozanov, A., and Burrows, J. P.: MAX-DOAS measurements of atmospheric trace gases in Ny-Ålesund - Radiative transfer studies and their application, Atmos. Chem. Phys., 4, 955–966, 2004.

WSV: Verkehr und Güterumschlag, http://www.ast-nordwest.gdws. wsv.de/schifffahrt/verkehr_gueterumschlag/index.html, 2013.

WSV: Schiffsverkehr und Güterumschlag, http://www. wsd-nord.wsv.de/Schiff-WaStr/Schifffahrt/Schiffsverkehr_ und_Gueterumschlag/index.html, 2014.

Yang, M., Bell, T. G., Hopkins, F. E., and Smyth, T. J.: Attribution of atmospheric sulfur dioxide over the English Channel to dimethyl sulfide and changing ship emissions, Atmospheric Chemistry and Physics, 16, 4771–4783, doi:10.5194/acp-16-4771-2016, 2016.

Zhang, F., Chen, Y., Tian, C., Lou, D., Li, J., Zhang, G., and Matthias, V.: Emission factors for gaseous and particulate pollutants from offshore diesel engine vessels in China, Atmospheric Chemistry and Physics, 16, 6319–6334, doi:10.5194/acp-16-6319-2016, 2016.